A characterisation of the integumentary skeleton of lizards (Reptilia: Squamata)

Alexander Charles Kirby

DEPARTMENT OF MEDICAL PHYSICS

UNIVERSITY COLLEGE LONDON (U.C.L.)

A thesis submitted in accordance with the requirements for the partial fulfilment of the Doctor of Philosophy degree

21/06/2020

London, United Kingdom

Signed Declaration of Originality

"I, Alexander Charles Kirby confirm that the work presented in this thesis is my own. Where information has been derived from other sources, I confirm that this has been indicated in the thesis."

Abstract

Osteoderms (ODs) are present within the dermis of 14 families of squamates although snakes and Sphenodontidae lack ODs. The expression of ODs within squamates has been described as highly variable and diverse since they were first reported. Some examples of squamate OD expression are as compound structures, fused together into overlapping, imbricating plates (as in Scincidae); as distorted, bent cylinders, partially overlapping one another (as in Varanidae), or as discrete, regularly tessellated, non-overlapping, polygonal beads (as in Helodermatidae), but this is not an exhaustive list. Currently, our understanding of OD structure-to-function relationships, general anatomy and internal composition remains limited. In this study, using histological staining, computed tomography, polarised light microscopy and electron microscopy, the microstructure of materials comprising ODs from multiple families of lizards is revealed. The results show that ODs are comprised of different proportions of numerous biomaterials including osteodermine, a highly mineralised, dense capping tissue on the apical surface of the osteoderm; lamellar bone rich in secondary osteons (haversian bone tissue), Sharpey-fibred bone, woven bone and parallel-fibred bone. These results are an indication that ODs of closely related families can differ substantially in terms of their overall anatomy, the structural composition of material elements and consequently their function and ontogeny. Histological variation within the biomineralised tissues is shown to relate to differences in overall OD architecture; these data provide insights into the mechanism of formation of ODs from different families and afford a direct comparison of the histological properties between the ODs of the multiple species. Attempts are made to elucidate the relationship between OD expression and other variables, such as function and phylogeny. Finally, the varied assortment of biomaterials found within ODs manifesting in diverse hierarchical structures are shown to be valuable in future translational applications, including the creation of bioinspired materials.

Impact Statement

This research presents data on the histology of the osteoderms of lizards, both extinct and extant, from multiple families. Benefits of this research to academia are that this work contributes towards our understanding of the micro- and macro-structure of the dermal skeleton of lizards and in turn, broadens our understanding of function and development of the reptilian skeletal system and integument. I used characterisation methods more modern than those been used previously, including novel techniques using polarised light. The areas in which the research is likely to have the clearest impact are in understanding the evolutionary history and relationships of squamates and the micro or nanofabrication of bioinspired materials and protective armours.

The first two chapters present results on the osteoderms of a Gila monster (*Heloderma suspectum*). An unusual, non-osseous tissue, osteodermine, was described here for the first time as were implications for metaplastic development of the basal Sharpey-fibred bone region. These data formed the basis of a poster presentation at the international congress on vertebrate morphology (ICVM2019). The analysis presented could be used as leverage in reptile conservation efforts, as it highlights how natural biological materials are a source of both phylogenetic data and novel materials for material characterisation and bioinspiration. Conservation is very important as habitat destruction threatens populations of *Heloderma* throughout most of its range and currently helodermatid lizards inhabit a small fraction of what was once suitable habitat. During the last 150 years, thousands of square miles of desert and tropical dry forest habitats have been cleared for agriculture and/or residential development in their natural habitat of seasonally dry scrub in North America. This research therefore underscores the importance of the conservation of natural habitats for lizards to protect from climate change and/or habitat destruction.

In subsequent chapters, similar materials, including osteodermine, are described in the osteoderms of other families of lizards, as well as in fossil osteoderms. Data concerning implications for osteoderm development in two separate lizards, *Heloderma suspectum* and *Varanus komodoensis* were published as an article in Journal of Anatomy (Kirby et al., 2020). Information on bone development in reptiles has been shown to be a useful model for human diseases, and thus the impact of knowing more about bone formation in lizards helps us to make models for medical applications as well.

This research will likely bring about impact through the various disseminating outputs used during the project, including publications made in scholarly journals, presentation of the research at international conferences, and collaboration with both academics and non-academics.

Acknowledgements

Table of Contents

List of Tables

List of Figures

3.9: BSE-SEM imaging of *H. suspectum* OD, sagittal section, resin embedded, ground and polished.

3.10: Histological overview of *Heloderma suspectum* post-cranial, dorsal OD.

4.1: Polarised light micrograph of *Heloderma suspectum* OD.

4.2: Parasagittal sections of *H. suspectum* OD stained with toluidine blue visualised with standard black and white polarised light microscopy and multi-rotation polarised light microscopy.

4.3: µ-CT scan data and Z-projection analysis of *Heloderma suspectum* OD.

4.4: High magnification 3D surface reconstruction of µ-CT data from the osteodermine region, BSE-SEM micrograph displaying all three separately structured materials, FIB-TEMs of all three materials.

4.5: BSE-SEM micrographs of *Heloderma suspectum* OD, ground, polished sections from dorsum, side of neck, forearm and tail, depicting OST. region.

4.6: BSE-SEM Micrograph of *Heloderma suspectum* OD, ground, polished sections from dorsum, side of neck, forearm and tail, depicting S.F.B. region.

4.7 BSE-SEM micrographs of *Heloderma suspectum* OD, ground, polished sections from dorsum, side of neck, forearm and tail, depicting L.B. region.

4.8: TEM micrographs of localised clusters of 500nm-1µm diameter dense spherical particles.

4.9: BSE-SEM micrograph and corresponding EDX mapping of elements present in *Heloderma suspectum* OD.

5.1: Tree of lizard relationships based on molecular evidence showing cranial OD arrangement.

5.2: Typical scientific illustration of OD from the mid-dorsal trunk of *Mabuya gravenhorstii.*

5.3: Comparative X-ray plate imaging of *Heloderma suspectum, Timon lepidus*, *Tiliqua rugosa*, *Crocodylus niloticus*, *Salvator merianae*, *Tarentola annularis, Corucia zebrata*, *Elgaria multicarinata, Egernia stokesii, Varanus niloticus, Ophisaurus*

ventralis juvenile, *Ophisaurus ventralis* adult, *Varanus komodoensis juvenile, Varanus komodoensis* adult and *Gekko gecko* skin samples.

5.4: Comparative H&E histological staining of *Heloderma suspectum, Timon lepidus*, *Tiliqua rugosa*, *Crocodylus niloticus*, *Salvator merianae, Tarentola annularis, Corucia zebrata*, *Elgaria multicarinata, Egernia stokesii, Varanus niloticus, Ophisaurus ventralis juvenile*, *Ophisaurus ventralis* adult, *Varanus komodoensis juvenile, Varanus komodoensis* adult and *Gekko gecko* skin samples.

5.5: Comparative Masson's Trichrome histological staining of *Heloderma suspectum, Timon lepidus*, *Tiliqua rugosa*, *Crocodylus niloticus*, *Salvator merianae, Tarentola annularis, Corucia zebrata*, *Elgaria multicarinata, Egernia stokesii, Varanus niloticus, Ophisaurus ventralis juvenile, Ophisaurus ventralis* adult, *Varanus komodoensis juvenile, Varanus komodoensis* adult and *Gekko gecko* skin samples.

5.6: Comparative Alcian blue histological staining of *Heloderma suspectum, Timon lepidus*, *Tiliqua rugosa*, *Crocodylus niloticus*, *Salvator merianae, Tarentola annularis, Corucia zebrata*, *Elgaria multicarinata, Egernia stokesii, Varanus niloticus, Ophisaurus ventralis juvenile, Ophisaurus ventralis* adult, *Varanus komodoensis juvenile, Varanus komodoensis* adult and *Gekko gecko* skin samples.

5.7: Comparative view of three-dimensional, false colour surface reconstructions of OD meshes, segmented from HRXCT data of post-cranial, dorsal squamate skin samples.

5.8: Comparative view of three-dimensional, false colour surface reconstructions of single ODs, segmented from HRXCT data of post-cranial, dorsal squamate skin samples.

5.9: Comparative BSE-SEM microscopy of squamate ODs. Low magnification BSE-SEM micrographs of ODs.

5.10: Photograph of adult *Tarentola annularis* dorsal skin and corresponding x-ray plate image.

5.11: Histological staining of *Tarentola annularis* dorsal skin sample, parasagittal sections stained with Masson's trichrome, H&E and Alcian blue.

5.12: Parasagittal sections of *T. annularis* OD stained with Alcian blue and visualised with multi-rotation polarised light microscopy.

5.13: Photograph of adult *Tarentola annularis* skin sample, corresponding volume rendering of HRXCT data in dorsal view.

5.14: Photograph of adult *Gekko gecko* dorsal skin and corresponding x-ray plate image.

5.15**:** Histological staining of *Gekko gecko* dorsal skin sample, parasagittal sections stained with Masson's trichrome, H&E and Alcian blue.

5.16: Three-dimensional, false colour surface reconstruction of OD mesh, segmented from HRXCT data of post-cranial, dorsal, adult *Gekko gecko* skin.

5.17: BSE-SEM imaging of *Gekko gecko* OD parasagittal sections, resin embedded, ground and polished.

5.18: photograph of adult *Varanus komodoensis* dorsal skin and corresponding x-ray plate image.

5.19: Three-dimensional false-colour surface reconstruction of OD mesh, segmented from HRXCT data of post-cranial, dorsal *Varanus komodoensis* skin.

5.20: Three-dimensional false-colour surface reconstruction of OD mesh in dorsal view, segmented from HRXCT data of adult *Varanus komodoensis* dorsal skin and single OD.

5.21: Histological staining of *Varanus komodoensis* dorsal skin sample stained with Alcian blue in parasagittal and coronal section, stained with Masson's trichrome in parasagittal and coronal section; and stained with Haematoxylin and Eosin in parasagittal section and coronal section.

5.22**:** *Varanus komodoensis* dorsal skin sample stained with H&E and visualised with multi-rotation polarised light microscopy in parasagittal section and coronal section.

5.23**:** BSE-SEM imaging of adult *Varanus komodoensis* OD coronal sections, resin embedded, ground and polished.

5.24: Photograph of juvenile *Varanus komodoensis* dorsal skin sample and corresponding x-ray plate image.

5.25**:** Histological staining of *V. komodoensis* dorsal skin sample stained with Masson's trichrome in coronal section, H&E in parasagittal section and stained with Alcian blue in parasagittal section.

5.26: Photograph of adult *Varanus niloticus* dorsal skin sample and corresponding x-ray plate image.

5.27: Histological staining of *Varanus niloticus* dorsal skin, parasagittal section stained with Masson's Trichrome, H&E, and Alcian blue.

5.28: Parasagittal section of *Varanus niloticus* dorsal skin, stained with Masson's Trichrome and visualised with multi-rotation polarised light microscopy.

5.29: Volume rendering of HRXCT data of *Lanthanotus borneensis* cranium.

5.30: Photograph of adult *Ophisaurus ventralis* post-cranial skin sample and corresponding x-ray plate image.

5.31: Photograph of adult *Ophisaurus* ventralis post-cranial skin sample and corresponding three-dimensional false-colour surface reconstruction of OD mesh, in dorsal view, segmented from HRXCT data of the same sample.

5.32: Three-dimensional false-colour volume rendering of OD mesh, generated from HRXCT data of adult *Ophisaurus ventralis* post-cranial, skin sample and three-dimensional false-colour surface reconstruction of single OD, generated from HRXCT data of the same sample.

5.33: Histological staining of adult *Ophisaurus ventralis* dorsal skin sample sectioned parasagittally, stained with Masson's trichrome, stained with H&E and stained with Alcian blue.

5.34: Parasagittal sections of adult *Ophisaurus ventralis* post-cranial dorsal skin stained with Alcian blue and visualised with multi-rotation polarised light microscopy.

5.35: Photograph of juvenile *Ophisaurus ventralis* post-cranial skin sample and corresponding x-ray plate image.

5.36: Photograph of juvenile *Ophisaurus ventralis* post-cranial skin sample cut in the ventral midline and corresponding three-dimensional false-colour surface reconstruction of OD mesh, in dorsal view, segmented from HRXCT data of the same sample.

5.37: Three-dimensional false-colour surface reconstruction of single OD, segmented from HRXCT data of juvenile *Ophisaurus ventralis* post-cranial dorsal skin.

5.38: Histological staining of juvenile *Ophisaurus ventralis* dorsal skin, sectioned parasagittally and stained with Masson's trichrome, stained with H&E and stained with Alcian blue.

5.39: Parasagittal sections of juvenile *Ophisaurus ventralis* dorsal skin stained with Alcian blue and visualised with multi-rotation polarised light microscopy.

5.40: Photograph of *Elgaria multicarinata* dorsal skin sample at time of imaging and corresponding x-ray plate image.

5.41: Three-dimensional, false colour surface reconstruction, segmented from HRXCT data of post-cranial, dorsal *Elgaria multicarinata* skin.

5.42: Histological staining of *Elgaria multicarinata* skin, parasagittal sections stained with Masson's trichrome, stained with H&E and stained with Alcian blue.

5.43**:** Parasagittal section of *Elgaria multicarinata* dorsal skin, stained with Masson's Trichrome and visualised with multi-rotation polarised light microscopy.

5.44**:** BSE-SEM imaging of *Elgaria multicarinata* OD coronal sections, resin embedded, ground and polished.

5.45: Photograph of *Tiliqua rugosa* dorsal single OD and corresponding x-ray plate image.

5.46: Three-dimensional, false colour surface reconstructions, segmented from HRXCT data of post-cranial, dorsal *Tiliqua rugosa* skin.

5.47: Histological staining of *Tiliqua rugosa* skin sample sectioned parasagittally stained with Masson's trichrome, stained with H&E and stained with Alcian blue.

5.48: Parasagittal sections of *Tiliqua rugosa* dorsal skin, stained with Masson's Trichrome and visualised with multi-rotation polarised light microscopy.

5.49: BSE-SEM imaging of *Tiliqua rugosa* OD parasagittal sections, resin embedded, ground and polished.

5.50: Photograph of *Corucia zebrata* dorsal skin sample at time of imaging and (b) corresponding x-ray plate image.

5.51: Three-dimensional, false colour surface reconstruction of OD mesh, segmented from HRXCT data of post-cranial, dorsal *Corucia zebrata* dorsal skin sample.

5.52: Three-dimensional, false colour surface reconstruction of single OD, segmented from HRXCT data of post-cranial, dorsal *Corucia zebrata* skin.

5.53: Histological staining of *Corucia zebrata* dorsal skin sample sectioned parasagittally, stained with Masson's trichrome, stained with Masson's trichrome, stained with H&E and stained with Alcian blue.

5.54: Parasagittal sections of *Corucia zebrata* dorsal skin, stained with Masson's Trichrome and visualised with multi-rotation polarised light microscopy.

5.55: Photograph of *Egernia stokesii* dorsal skin sample at time of imaging and corresponding x-ray plate image.

5.56: Histological staining of *Egernia stokesii* dorsal skin sectioned transversely, stained with Masson's trichrome, stained with H&E and stained with Alcian blue.

5.57: Photograph of *Egernia stokesii* tail skin sample at time of imaging and corresponding x-ray plate image.

5.58: Histological staining of *Egernia stokesii* tail skin sectioned transversely, stained with Masson's trichrome, stained with H&E and stained with Alcian blue.

5.59: Parasagittal sections of *Egernia stokesii* post-cranial dorsal skin, and tail skin, stained with Masson's Trichrome and visualised with multi-rotation polarised light microscopy.

5.60: Photograph of *Timon lepidus* cranial skin sample at time of imaging and corresponding x-ray plate image.

5.61: Histological staining of *Timon lepidus* cranial skin, sectioned parasagittally, stained with Masson's trichrome, stained with H&E, and stained with Alcian blue.

5.62: Photograph of *Salvator merianae* dorsal skin sample and corresponding x-ray plate image.

5.63: Histological staining of *Salvator merianae* dorsal skin sample sectioned parasagittally stained with Masson's trichrome, stained with H&E and stained with Alcian blue.

5.64: Parasagittal sections of *Salvator merianae* dorsal skin, stained with Masson's Trichrome and visualised with multi-rotation polarised light microscopy.

5.65: Photograph of *Crocodylus niloticus* ventral skin sample and corresponding x-ray plate image.

5.66: Histological staining of *Crocodylus niloticus* ventral skin sectioned parasagittally, stained with Masson's trichrome, stained with H&E and stained with Alcian blue.

5.67: Parasagittal section of *Crocodylus niloticus* ventral skin, stained with Masson's Trichrome and visualised with multi-rotation polarised light microscopy.

5.68: Timetree of lizard relationships among clades as understood at time of print, with annotations depicting taxa in which osteodermine expression has been confirmed in this thesis.

6.1 Geological stratifications of the Isle of Wight, U.K.

6.3.1: Morphotype 1 ODs from layer 15 of the Bembridge Limestone Formation visualised with light microscopy.

6.3.2: Morphotype 1 ODs from layer 16/17 of the Bembridge Limestone Formation visualised with light microscopy.

6.3.3: Morphotype 2 and Morphotype 1 ODs from layer 1 of the Headon Hill Formation visualised with light microscopy.

6.3.4: Three-dimensional, false colour surface reconstructions of Morphotype 1 ODs from layer 15 of the Bembridge Limestone Formation, segmented from HRXCT data.

6.3.5: Three-dimensional, false colour surface reconstructions of Morphotype 1 ODs from layer 17 of the Bembridge Limestone Formation, segmented from HRXCT data.

6.3.6: Three-dimensional, false colour surface reconstructions of Morphotype 2 and Morphotype 1 ODs from layer 1 of the Headon Hill Formation, segmented from HRXCT data.

6.3.7: Transverse, ground section through a Morphotype 1 OD (BL.15.2), visualised with multi-rotation polarised light microscopy at 10x magnification and 20x magnification.

6.3.8: Transverse, ground section through a Morphotype 1 OD (BL.17.3), visualised with multi-rotation polarised light microscopy at 20x magnification and 40x magnification.

6.3.9: Transverse, ground section through a Morphotype 2 OD(HH.1.1) visualised with multi-rotation polarised light microscopy at 10x magnification and 20x magnification.

6.3.10: Ground, polished, transverse section of BL.15.2 imaged with BSE-SEM.

6.3.11: Ground, polished, transverse section of a Morphotype 1 OD (BL.17.3) imaged with BSE-SEM.

6.3.12: Ground, polished, transverse section of HH.1.1 imaged with BSE-SEM.

7.1.1: Finite-element simulations of four mechanical loading scenarios applied to a *Heloderma suspectum* OD, hypothetically composed of L.B., Sharpey-fibred bone, osteodermine, and the actual composition. Stiffness values measured by atomic force microscopy (A.F.M.) were used to test distribution of strain and stress under application of force or displacement obtained by finite element analysis.

List of Abbreviations

AFM	Atomic Force Microscopy
BSE	Backscattered electrons
C	Carbon
Ca	Calcium
CA	California
CCD	Charge-coupled device
CT	Computed Tomography
EDX	Energy dispersive X-ray spectroscopy
FL	Florida
HA	Hydroxyapatite
H&E	Haematoxylin and Eosin
HRXCT	High resolution X-ray Computed Tomography (μ-CT)
LAG(s)	Line(s) of Arrested Growth
LB	Lamellar Bone
MRPLM	Multi-rotation polarised light microscopy
MA	Massachusetts
NY	New York
NL	Netherlands
NSW	New South Wales
O	Oxygen
OD(s)	Osteoderm(s)

ODite(s)	Osteodermite(s)
OST	Osteodermine
P	Phosphorus
PBS	Phosphate Buffered Saline
PFB	Parallel-fibred bone
SC	Stratum compactum
SEM	Scanning Electron Microscopy
SE	Secondary Electrons
SFB	Sharpey-fibred bone
SS	Stratum superficiale
TEM	Transmission Electron Microscopy
UK	United Kingdom
USA	United States of America
VVG	Verhoeff van Gieson

Glossary of bone terminology

Intramembranous:

The direct conversion of layers of mesenchymal tissue into bone, without a cartilaginous precursor. This produces cortical and cancellous bone, with a periosteum (a layer of vascular connective tissue enveloping the bone) (Hall, 2005).

Endochondral:

Any bone that develops in and replaces hyaline cartilage. The cartilage is then either completely or partially resorbed (reabsorbed), leaving bone in its place (Hall, 2005).

Cortical:

The dense outer surface of an endochondral bone that forms around the internal cavity of trabecular bone. Also known as compact bone (Warshaw et al., 2017).

Cancellous:

Cancellous bone, also called trabecular bone or spongy bone, light, porous bone enclosing numerous large spaces that give a honeycombed or spongy appearance. The bone matrix, or framework, is organized into a three-dimensional latticework of bony processes, called trabeculae, arranged along lines of stress (Warshaw et al., 2017).

Metaplastic:

Bone that forms without a cartilaginous precursor, forming directly from the mineralisation of pre-existing fibrous connective tissue, by osteoblasts differentiating from fibroblasts, and without a periosteum (Haines and Mohuiddin, 1968).

Lamellar:

A microstructure of bone that exhibits regular, repeating sheets of collagen fibres (lamellar bone). Secondary reconstructions result in specific structures observable in thin sections, including scalloped borders of secondary osteons and reconstruction lamellae. Lamellar bone is characterised by this distinctive scalloped border as a result of remodelling and is only found on the endosteal surfaces of secondary osteons (Warshaw et al., 2017).

Woven:

Also known as fibrous bone, this microstructure is characterised by a random organisation of collagen fibres without any clear pattern or arrangement (Warshaw et al., 2017).

Parallel-fibred:

Parallel-fibred bone refers to a microstructure containing parallel-fibres of mineralised collagen. Unlike lamellar bone, these do not manifest on the endosteal surfaces of secondary osteons and do not display a "scalloped border" around the periphery of the tissue. Parallel-fibred bone exhibits an arrangement of collagen fibres that do not mirror the surrounding soft tissue (Warshaw et al., 2017).

Sharpey-fibred:

A microstructure of a collagenous fibre arrangement that mirrors the surrounding connective, soft tissue. This is due to a metaplastic formation; hence collagen fibres can be observed seamlessly entering the mineralised tissue from the surrounding soft tissue (these are known as Sharpey's fibres) (Jones and Boyde, 1974).

Glossary References

Haines R. W. and Mohuiddin A. (1968) Metaplastic Bone. *Journal of Anatomy* **103**:527–38.

Hall B. K. (2005) Chapter 2 – Bone. In: *Bones and Cartilage.* Editor: Hall B. K. Publisher: Academic Press, Cambridge, Massachusetts, USA. Pp. 13-32.

Jones S. J. and Boyde A. (1974) The organization and gross mineralization patterns of the collagen fibrils in Sharpey fibre bone. *Cell and Tissue Research* **148**:83-96.

Warshaw J., Bromage T. G., Terranova C. J. and Enlow D. H. (2017) Collagen fiber orientation in primate long bones. *The Anatomical Record* **300**:1189–1207.

Copyright Declaration

1 CHAPTER 1 Introduction to mineralised tissues

1.1 Outline of thesis structure

This thesis is divided into six chapters:

1. The first chapter begins with an outline of the thesis, then describes our current knowledge of the mineralised tissues present in vertebrates, focusing on the integumentary skeletal system of tetrapods, then specifically on osteoderms. An overview of the published research into osteoderms is presented, highlighting the holes in our understanding.

2. The second chapter introduces the techniques and methodology used to characterise lizard osteoderms in this study.

3. In the third chapter, experimental results are introduced and the elucidation of *Heloderma suspectum* osteoderm tissue structure is presented.

4. The fourth chapter presents results that attempt to characterise the micro and nanostructure of the material components in the *Heloderma suspectum* osteoderm, highlighting the important of nanoanalytical techniques for full materials characterisation.

5. The fifth chapter explores the use of modern techniques to elucidate osteoderm composition in other taxa. Other samples of squamate osteoderms are analysed and compared to *Heloderma suspectum.*

6. The sixth chapter analyses fossil osteoderms and compares these results with the results presented in earlier chapters for extant taxa.

7. The seventh and final chapter is a discussion chapter that also includes the overall conclusions, limitations, project outcomes, recommendations and future outlook.

1.2   Introduction to mineralised tissues

Mineralised tissues are essential for life in all vertebrates, as they underpin the formation of various adaptive phenotypes, such as armour for protection, teeth for consuming prey, and the endoskeleton for biomechanical support and motion (Weiner and Wagner, 1998). The range of mineralised tissues that can be formed is very diverse - each having a unique structure that corresponds to an evolved working function (Hall, 2005). Many different terms have been applied to the process of mineral development by different authors (Bauer and Russell, 1989; Liu et al., 2011), with ossification, mineralisation and calcification all being used to describe the same or similar processes. Some mineralised tissues, including bone, are constantly remodelled after minerals are deposited, as part of the normal function of the animal, through two continuous processes known as resorption (removal) and deposition (construction) of the intercellular matrix (Weiner and Wagner, 1998).

Previously, attempts to characterise mineralised tissues have focused on four major fields: structural-mechanical relationships, growth and remodelling, histological features and the chemical composition of the sample. Initial attempts to study hard tissues included the creation of hierarchal tables of structures – from first order, at higher, macro scales to fourth order, at more microscopic scales (Vickaryous and Sire, 2009). On the first order, the overall anatomical level, general morphology, vascular orientation etc. are used to characterise the tissue. The second order relates to the histological level – the orientation, size and number of bone trabeculae, the structure of extracellular matrices and fibre orientation. Third order corresponds to the cytological level – details of cells and extracellular matrix, and finally the fourth order is the molecular level (the nano-scale) or the chemical and biophysical organisation of both mineral and organic components (Francillon-Vieillot et al., 1989). Recently, there has been relatively more emphasis on elucidating the gene expressions that are responsible for forming these structures (Nilsson et al., 2007), rather than on examining and characterising the structures themselves at microscopic scales (Bai et al., 2015).

In Mammalia, endoskeletal bones have been well characterised on the first order down to the fourth order, in various studies and experiments, across multiple species (Clarke, 2008). For example, the femur is known as a long bone, which is defined anatomically as having two bulbous ends with a shaft running between them (Hall, 2005). Long bones of mammals have a characteristic outer cortical layer of dense mineralised material, which surrounds an inner trabecular layer described as 'spongy'

as it is much more porous than the cortical layer. Cortical bone is composed of concentric lamellae of mineralised material surrounding canals of blood and lymph vessels and/or nerves. A singular canal is called an osteon or a "Haversian system" (Fratzl and Weinkamer, 2007). Bone producing cells called osteocytes are spaced consistently, within spaces in the bone matrix called lacunae, which are connected to each other by small capillary-like channels called canaliculi. Located in the core of the long bone, trabecular bone is much less dense and contains a network of trabeculae with marrow-filled non-mineralised holes (Weiner and Wagner, 1998). Each trabecula contains concentric lamellae, osteocytes, lacunae and canaliculi, but no central canal. This description is a standard definition of endoskeletal bone on the first order, but an overriding problem in the correct characterisation and description of mineralised tissues is that many mineralised tissues have not been studied in this way or have not been fully investigated down to the fourth order, the nanoscale.

At the nanoscale, it is accepted that long bones consist of two basic components: the mineral (inorganic) crystals making up roughly 65% of bone's weight, and the organic matrix making up the remainder (Dorozhkin, 2007). Hydroxyapatite is the most common phosphate mineral in bones, but in some cases, for example, in the femoral head, magnesium whitlockite has been discovered using X-ray diffraction (Lagier and Baud, 2003). In order to investigate hard tissues on the molecular level, electron microscopy (EM) is one technique that can be used to determine the size, morphology and composition of the mineral crystals, as well as providing insight into the organisation of crystals in relation to collagen (McNally et al., 2012). Previous EM studies of mouse endoskeletal bone have found that collagen fibrils lie parallel to each other and in layers held together by cross-links between the proteins (Pasteris et al., 2008). The exact 3D relationship between the mineral crystals and collagen fibrils is debated but consensus is that the crystals are found as 70-90nm long globular structures, spaced in an alternating formation approximately 50nm apart (Bertazzo and Bertran, 2006; McNally et al., 2012). The main school of thought is that the gap region within the fibril is where the first crystals of HA are formed and then it eventually spreads within the interior (Nudelman et al., 2010). On the molecular level, the actual process of apatite crystal deposition can be achieved through either inotropic mineralisation, where the crystals are orientated in the gap region parallel to the collagen fibrils, or spheritic mineralisation where one nucleating centre produces a radial arrangement of crystals (Liu et al., 2011).

As shown above, obtaining detailed information on the fourth order such as the organic and mineral structure, crystallinity and chemical composition can help researchers understand the ontogeny, function and biological importance of these tissues as well as help to classify them correctly. Fourth order data acquisition can provide a comprehensive insight into the physical arrangement and nanostructures of atoms and molecules in the materials, for example the identification of elements in crystals and their phase (Bertazzo and Bertran, 2006). Unlike the higher orders, which can be analysed using simple light microscopes, data pertaining to the fourth order can only be obtained through modern physical-chemical methods including scanning and transmission electron microscopy (SEM/TEM) as well as computational tomography (CT). These techniques are employed in this report in an attempt to classify the mineralised tissues found in the lizard integument down to the fourth order.

Many researchers have tried to describe mineralised tissues as all having one common modular building block – the mineralised collagen fibril (Francillon-Vieillot et al., 1989). This is erroneous as many vertebrate mineralised tissues – for example, enamel or ganoine – are actually completely void of collagen and instead display non-collagenous matrix scaffolds (Vickaryous and Sire, 2009). "Bone" is herein defined as mineralised tissue containing a structural motif of mineralised collagen fibres and "atypical mineralised tissues" are herein defined as materials containing a structural motif of mineralised non-collagenous matrices.

Possibly the most well-known atypical mineralised tissue is enamel, found on the surface of the teeth of chordates, which caps a tissue within the tooth known as dentine (Teaford et al., 2000). Enamel is a highly mineralised (up to 96% by mass) material layer deposited by ectodermal ameloblasts after dentine formation has started (Dorozhkin, 2013). Enamel mineral crystals are orientated perpendicular to the depositional surface and this is thought to increase the overall strength and/or stiffness of the tissue (Daculsi et al., 1984). Interestingly, enamel forms the superficial surface of scales of lobe-finned fish Sarcopterygii (Song et al., 2011; Rücklin et al., 2012). Clearly the presence of this atypical mineralised tissue on the surface of teeth and scales has an important functional role. There has been continuous, unresolved debate on the evolutionary origin of armour and teeth in the earliest ancestors of tetrapods (Smith et al., 1996). All extant tetrapods are classified within Sarcopterygii, and extant non-tetrapods (i. e fish) are known to produce odontogenic tissues in the dermis (such as dermal denticles in the skin of sharks). However modern tetrapods

are thought to only produce odontogenic tissues in the oral cavity and the existence of odontogenic tissue in other anatomical areas of the body has not been investigated sufficiently.

Many names exist for various modified versions of enamel. Another tissue thought to be a kind of 'stratified' enamel is called ganoine, a hyper-mineralised capping tissue covering the dermal skeleton of polypterids and lepisosteids, which are primitive actinopterygian fishes (Francillon-Vieillot et al., 1989). Ganoine was first defined as the dense, homogenous enamel-like substance covering the exterior part of ganoid fish scales (Sire, 1995). Ganoine was previously considered to be a type of enamel as it contains amelogenin-like proteins as well as a similar mineral content to tooth enamel (Zylberberg et al., 1997). The fact that these previous authors describe it as "enamel-like" provides insight into the enigmatic nature of such atypical mineralised tissues. Indeed, the formation or origin of ganoine has been the subject of much controversy. Ganoine may be directly produced by inner epidermal layer cells, ameloblasts, after dentine has formed at the scale surface and a new layer of ganoine is deposited with each new growth stage of the scale (Francillon-Vieillot et al., 1989). The contribution from the epidermis would mean that this atypical mineralised tissue is not produced through typical osteogenic mechanisms and instead is odontogenic in origin, as the placoid scales of sharks and rays are homologous to "dermal denticles", also known as odontodes, and are composed of odontogenic tissues (Sire et al., 2009). Teeth and denticles may share structural similarities but are very different, being formed by different cell arrangements and showing different patterning. The diversity of odontogenic tissues, in particular dentine, is indeed highly diverse.

Dentine caps the innermost tissue (pulp) of the vertebrate tooth. Pulp is a soft tissue comprised mostly of water and containing all the blood vessels and nerves needed to support the tooth. Dentin makes up the majority of the mass of teeth and is made by a layer of odontoblasts lining the pulp cavity (Teaford et al., 2000). Despite dentine and enamel being well documented and commonly identified there is still much debate over their expressed structures, with some authors reporting vascularised 'vasodentin', "enamel-like" 'vitrodentin' and compact 'orthodentine' (Kerebel et al., 1978). Many extinct and living fish have been observed to display a greater degree of diversity of dentine architecture than do living tetrapods, but it is not known why (Fraser et al., 2010). Dentine can be cellular or acellular and the main types of dentinous tissues are mesodentine and semidentine (Teaford et al., 2000).

Mesodentine is known to have cell spaces as well as branching tubules, whereas semidentine has been defined as having single dentinal tubules, joined to cell spaces containing odontoblasts. Mesodentine occurs in the in odontodes (also known as dermal teeth) of the early vertebrates ("fish") such as Osteostraci Heterostraci and Acanthodii (Fraser et al., 2010).

It can be concluded from the above information that dentine and enamel cannot be accurately expressed using a first to fourth order hierarchal system of classification as the tissue manifests across a broad spectrum of anatomical, histological, cytological and molecular ranges. Rather they exist more as a range of different physical materials that have characteristics incorporating a spectrum of expression. The more datasets that can be obtained across all of the four orders for all mineralised tissues, the easier it will be to characterise the ranges of tissues expressed.

Given the fact that there are a multitude of often overlapping terms for enamel-derived tissues and dentine-derived tissues, for example, it can be reasoned that "bones", "teeth" and "scales" should not be viewed as separate anatomical entities but rather organs composed of a spectrum of mineralised tissues with both overlapping and discrete features, formed by many different cells via many separate processes, transformations and interactions. As discussed, many of the materials present in these anatomical entities appear as modifiable moieties. Vertebrate evolution is not characterised by the progressive appearance and refinement of new components of skeletal tissues (Francillon-Vieillot et al., 1989). Instead, the earliest vertebrates had already evolved the basic components of skeletal tissues, and later vertebrates seemingly kept these components but evolutionary pressures caused them to adapt and thus form new hard tissue structures. Components therefore do not appear in a linear, progressive pattern of increasing complexity, but in many different forms, each corresponding with precise adaptations, which compounds the problem of hard tissue classification (Francillon-Vieillot et al., 1989). Complete anatomical classification of the broad variety of hard materials is not yet achieved and will arise from further fundamental measurements and observations of natural hard tissues. Thus, the need for further sampling is made clear.

Jawed vertebrates are known as gnathostomes, and create two types of bone through two separate processes. The first and most well-known is "endochrondral bone" which first manifests as cartilage and is later mineralised in a process known as endochondral perichondral ossification (Hall, 2005). Endochrondral bone includes the vertebrae and ribs, derived from somitic sclerotome as well as the bones of the limbs

arising from lateral plate mesoderm. Secondly, there is "dermal bone". As the name suggests, dermal bone consists of "bony" structures that can develop in the dermis. There is no cartilaginous intermediate when dermal bones are produced. They form initially as W.B. either via intramembranous ossification, or bone metaplasia, not endochondral ossification (Patterson, 1977). Intramembranous ossification is also an essential process during the natural healing of bone fractures (Hall, 2005). Metaplastic ossification, also known as bone metaplasia, occurs when one type of fully developed tissue is directly ossified (Haines and Mohuiddin, 1968). The armour of early jawless and jawed fish, the scales of sharks, as well as the dermatocranium and the clavicle in humans are also composed of dermal bone. Dermal bone is thought to originate as a more ancient and rudimentary system of ossification (Forey, 1995; Porter, 2006). Additionally, complete elements of the vertebrate skeleton may be compound structures made of both of these types of bone - for example the vertebrate cranium is actually a complex structure of both endochondral and dermal bone.

1.3 The vertebrate integumentary skeleton

Mineralised tissues located within the skin are known as the integumentary skeleton, In both non-tetrapod and tetrapod vertebrates, the integumentary skeleton contains a diversity of hard tissues within the dermal layers that have previously been categorised as either odontogenic (for example, hyper-mineralised tissues or dentine) or osteogenic (bone) tissues, which can occur either separately (e.g. carapaces) or can be combined in a same element (e.g. ganoid scales) (Sire et al., 2009; Vickaryous and Sire, 2009). The integumentary skeleton of vertebrates is best described by distinguishing between that of the tetrapods and the non-tetrapods. In both, the integumentary skeletal elements are relatively structurally diverse. In tetrapods, they are widely understood to be derivatives of the once all-encompassing dermal skeleton of early stem gnathostomes, originating more than 500 million years ago. In almost all of the modern taxa, the integumentary skeleton has seen an extensive decrease in expression and a reduction when expressed, over geological timescales, meaning that the relationships between these materials are frequently confused and uncertain and a full characterisation has not been accomplished. As with other dermal bones in vertebrates, the tetrapod integumentary skeleton forms through either direct ossification of the skin, which is named bone metaplasia, or via intramembranous ossification (Vickaryous and Sire, 2009).

Taxon	Distribution and adult morphology of ODs	Skeletally mature tissue type within ODs	Organisation	Skeletogenesis	References
Stem tetrapods	Dorsal and ventral surfaces, rhombic and scale-like	Cellular bone (lamellar and Sharpey-fibred bone)	cortex of compact bone surrounding an inner cancellous core	uncertain	Ørvig, 1957; Dias and Richter, 2002
Anura	Mostly dorsal surface, usually small polygonal	Cellular bone, parallel-fibred and/or lamellar bone	non-stratified compact bone	uncertain	Ruibal and Shoemaker, 1984
Synapsida	Dorsal body surface: polygonal and rectangular	Cellular bone (parallel-fibred, lamellar, Sharpey-fibred bone)	cortex of compact bone surrounding an inner cancellous core	Intramembranous ossification	Hill, 2006; Vickaryous and Hall, 2006
Archosauria	mostly dorsal body surface but may develop within virtually any portion of the dermis (e.g. eyelids, cheeks); often plate-like shapes	cellular bone (woven-fibred, parallel-fibred, lamellar); calcified and unmineralised fibrous connective tissue	cortex of compact bone surrounding an inner cancellous core	Fibrous connective tissue mineralisation (bone metaplasia)	Moss, 1969; Scheyer and Sander, 2004; Main et al., 2005; Vickaryous and Hall, 2008
Lepidosauria	Sometimes restricted to head and/or dorsal body surface but may encase the entire body; granular, bead-like, vermiform, compound and imbricating	cellular bone (woven-fibred, parallel-fibred, lamellar); calcified fibrous connective tissue; and (in some taxa) an enigmatic collagen-poor capping tissue	often stratified into two distinct layers of which the basal portion is always bone (parallel-fibred or lamellar); superficial layer is variable and may consist of woven-fibred bone or an enigmatic collagen poor tissue	Evidence suggests both bone metaplasia and intramembranous ossification	Moss, 1969; Zylberberg and Castanet, 1985; Levrat-Calviac et al., 1986; Levrat-Calviac and Zylberberg, 1986

Table 1.1: List of osteoderm expressing tetrapods with information on skeletogenesis, tissue types, organisation, morphology and references for each (adapted from Vickaryous and Sire, 2009).

The modern-day integumentary skeleton of tetrapods is classified into three different types of structures (Vickaryous and Sire, 2009). Firstly, the carapace (shell) of tortoises, turtles and terrapins is a skeletal complex of the ribs and vertebrae, that are formed from both perichondral ossification as well as 'multiple fused bony elements', which are thought to form intramembranously (Chen et al., 2015). Carapaces from extant and extinct species are composed of cellular bone with a cancellous core (Scheyer and Sánchez-Villagra, 2007), thought to be osteogenic in origin. Turtles, tortoises and terrapins also exhibit ODs in addition to this carapace. "Dermal scales", seen in caecilians (legless amphibians), are observed to contain elasmodine, similar to elasmoid scales (Zylberberg and Wake, 1990), thought to be odontogenic in origin (Zylberberg et al., 1980). Lastly, osteoderms (ODs) are components of the dermal skeleton of stem-tetrapods, Anura (frogs), Synapsida (mammals and their ancestors), Archosauria (birds, crocodiles and extinct relatives) and Lepidosauria (lizards, snakes, amphisbaenians, and tuatara) (Vickaryous and Sire, 2009). Table 1.1 lists the variety of OD expression in these different taxa, contributing to the integumentary skeleton of tetrapod vertebrates.

As the table shows, ODs are considered to contain various types of bone, thus are currently considered to be osteogenic. ODs represent the most frequently acknowledged element of the tetrapod integumentary skeleton, yet as shown in Table 1.1, many facets of their formation, composition and anatomy are unknown. Therefore, this study was designed to focus on ODs, as there is a clear need for further research into these vertebrate hard tissues.

1.4   Osteoderms

Osteoderms (ODs), derived from Greek words, literally meaning bone skin, are classically defined as a structural category of mineralised organ embedded into the dermis (Camp, 1923; Romer, 1957; Francillon-Vieillot et al., 1989).

ODs are classified as dermal bones, and form part of the integumentary skeleton of tetrapods (Vickaryous and Sire, 2009). They are also occasionally described as a type of scute - the term scute being used to encompass any horny, keratinous or bony element located within the skin of an animal (Main et al., 2005). However, the term scute should be restricted to the non-mineralised, cornified (keratinised) structure in the uppermost epidermal layer of the skin, which is a separate anatomical entity to the mineralised scales that form part of the integumentary skeleton of fish.

ODs show a range of diverse expressions. They are patterned either as overlapping, imbricating elements or as a single layer with regularly repeating, individual units. They can fuse together to create large, compound articulated mosaics; or, at the other extreme, can be found sparsely distributed, singular, reduced and seemingly unimportant. Much of the discrepancy between the size, shape, and geometry of OD expression remains structurally and functionally enigmatic and many ODs in many species remain completely undescribed.

Unlike that of archosaurs or mammals, the lepidosaur integument is separated into distinct layers, starting from the superficial surface and moving deep into the body, the order of these is as follows: the epidermis is the upper layer of skin, containing the superficial stratum corneum and beneath that the regenerative stratum germinativum, then below that there is the dermis, divided into the stratum superficiale, stratum compactum and stratum laxum. The stratum laxum and the compactum are combined to form the stratum profundum (deep dermis). This arrangement allows for the periodic shedding of the stratum corneum, with large areas of skin being shed as single sheets. Below the skin is the hypodermis, and under that is the deep fascia, overlying smooth muscle or bone. ODs share a common feature as forming within the dermis (forming either in the stratum compactum, in the stratum superficiale, or the interface between the two) and are composed primarily of osseous (bone) tissue.

1.4.1 Evolution

The bony scales of the earliest tetrapods are structurally consistent with ODs, pushing back the origin of these integumentary elements to the late Devonian, when the stem tetrapods appeared (Vickaryous and Sire, 2009). In many cases, the fossilised ODs of extinct animals are the only direct evidence of the skin, given their mineralised composition and the non-mineralised composition of the surrounding dermal tissues; they are the only preserved characters. Thus, they are very important to account for when classifying fossilised taxa but are often overlooked. ODs can disappear and reappear from the fossil record across geological timescales, but due to a sparse fossil record, it is not known if the appearance of ODs in some lineages is a real event, an artefact due to a lack of specimens, or an artefact due to loss of the skin during the fossilisation process.
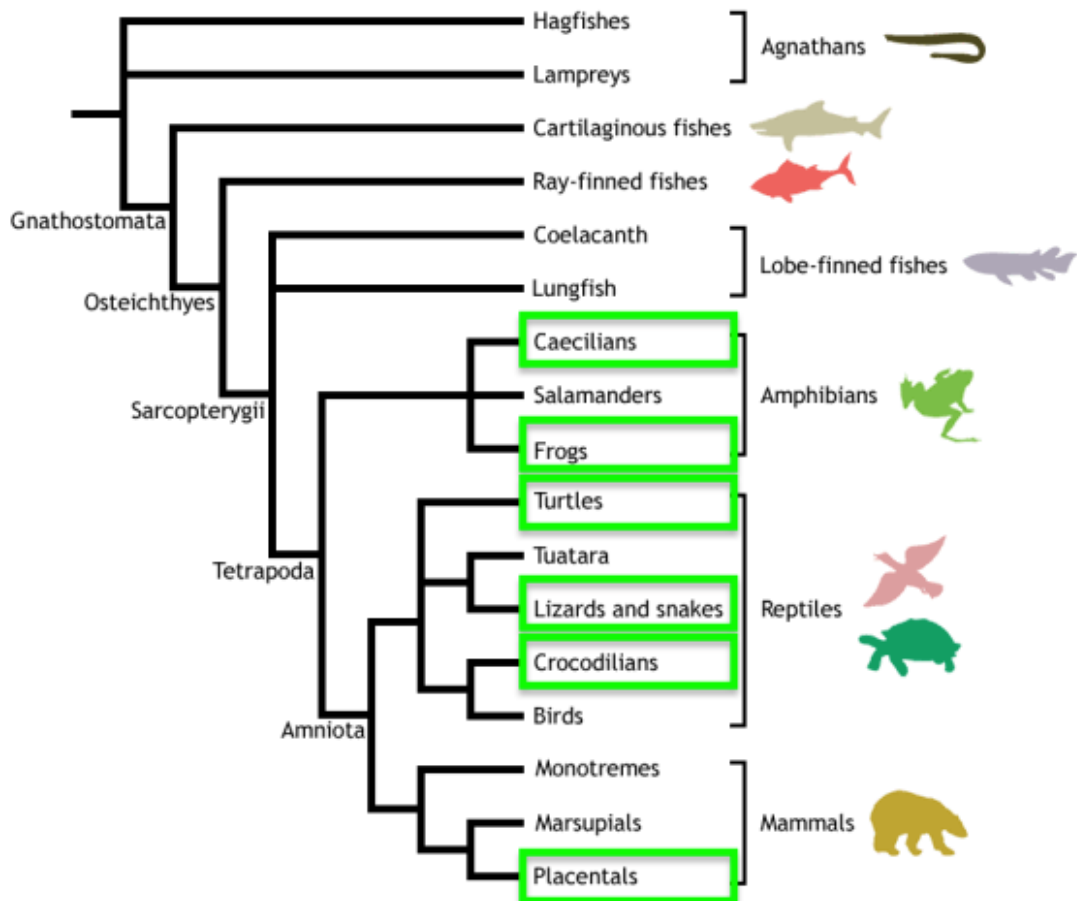
Figure 1.1: Phylogenetic tree of vertebrates, with highlighted extant taxa expressing ODs (adapted from Vickaryous and Sire, 2009).

In the extant amniotes, ODs occur in almost all major lineages (Fig 1.1). They are found in amphibians, anurans, lepidosaurs (exclusive of snakes), archosaurs (exclusive of birds and pterosaurs), placodonts (a group of extinct aquatic reptiles

[Sauropterygia]), and some synapsids (for example, armadillos) (Moss, 1969; Ruibal and Shoemaker, 1984; Barrett et al., 2002; Hill, 2005; Vickaryous and Sire, 2009; Chen et al., 2011). The occurrence of ODs is highly irregular – appearing only in Xenarthrans among mammals but in almost all post-Triassic crocodilians other than metriorhynchids. Most ODs are expressed in reptiles. Reptiles with two temporal openings in the skull (diapsids) are generally divided into two groups – the Lepidosauria and the Archosauria.

In terms of their palaeontological history, ODs have been recorded in many diverse fossil taxa. They are commonly identified in herbivorous Dinosauria (D'Emic et al., 2009; de Buffrénil et al., 2010) as well as in taxa such as in *Elliotsmithia longiceps*, a basal synapsid (Reisz et al., 1998), and many parareptiles, for example, *Sclerosaurus armatus* (Sues and Reisz, 2008). Although turtles develop carapaces as dermal armour, some fossil testudines have been found to exhibit ODs as well, for example, *Proganochelys quenstedti* (Gaffney, 1990)*.

The group with the highest number of taxa expressing ODs, along with some of the most diverse OD expressions, is Lepidosauria. Lepidosauria (originally diagnosed as reptiles with overlapping scales) includes Rhynchocephalia (with only one living genus, *Sphenodon* and fossil relatives) and the sister group Squamata (lizards, snakes and amphisbaenians) (Estes, 1983; Evans, 1984; Benton, 1985). Despite some lineages expressing dramatic ODs in the fossil record, there are only a few unambiguous fossils of stem-lepidosaurs that are represented by articulated skeletons, but there is currently no evidence that stem-Lepidosaurs expressed ODs (S. E. Evans, pers. comm.). Today, Rhynchocephalia comprises only the New Zealand genus *Sphenodon*, with no OD expression. Fossil rhynchocephalians also lack ODs, with one exception - a fossil rhynchocephalian from the Tlayúa Formation in Puebla, Mexico (Early Cretaceous) *Pamizinsaurus tlayuaensis*, which is covered in small, rounded ODs (Reynoso, 1997). The genus name is based on the word for corn-cob, and reflects the appearance of the ODs that covered this small reptile.

Despite this finding in an early rhynchocephalian, there are no records of ODs in the ancestors of squamates nor are they present in the rare UK fossil deposits containing the earliest known squamates (during the Middle Jurassic, ~170 mya). However, Middle Jurassic deposits in the Junggar valley of north-west China have yielded an OD covered lizard (Conrad et al., 2013) that is, as yet, not fully described or named. ODs are also recorded in several in Late Jurassic (~164-145 mya) and Early Cretaceous (~145-100 mya) lizard fossils from almost every continent. Some Late

Jurassic and Early Cretaceous OD-bearing squamates include lizards of the family Paramacellodidae (e.g. Evans and Chure, 1998), as well as the phylogenetically indeterminate genera *Jucaraseps* (Bolet and Evans, 2012), *Scandensia* (Evans and Barbadillo, 1998; Bolet and Evans, 2011) and the monstersaurian (=stem-helodermatid) genus *Primaderma* (Nydam, 2000).

There are numerous examples of Late Cretaceous (~100-65 mya) OD-bearing squamates including: the Chinese monstersaur (*Heloderma* relative) *Chianghsia nankangensis,* with rounded cranial ODs (Mo et al., 2012); the indeterminate Mongolian lizard *Myrmecodaptria microphagosa* which has thick, round ODs on the cranium and spine (Gao and Norell, 2000); the Chinese and Mongolian stem-scincoid *Parmeosaurus scutatus* which was covered in rectangular, overlapping bipartite ODs on the cranial, dorsal and ventral surfaces (Gao and Norell, 2000); and the Madagascan cordyliform *Konkasaurus* (Krause et al., 2003). The possession of both dorsal and ventral body ODs is a character attributed to Scincidae and Cordylidae, as well as the stem-scincoid Paramacellodidae (Evans and Chure, 1998). *Parmeosaurus* fossils extend to the Mesozoic era (84.9 to 70.6 Ma) (Dong et al., 2018). Their ODs have been illustrated and described macroscopically, but have not had their histological appearance, microstructure or nanostructure studied (Richter, 1994).

Paleogene fossil squamates bearing ODs include helodermatids from the Eocene-Oligocene (~34 mya) of France and the USA (Mead et al., 2012). The anguid glyptosaurines are a well-documented example of OD-bearing anguimorph squamates recorded from the Cretaceous to the Palaeogene. Their ODs are rectangular, overlapping with a smooth articular surface on one part of the dorsal surface, and an ornamented surface of raised, individual tubercles on the other part. It was in these tubercles that the hyper-mineralised tissue osteodermine (OST.) was first described (de Buffrénil et al., 2011).

In conclusion, some Scincoidea, Anguimorpha, and Gekkota, as well as indeterminate early fossil squamates express a wide diversity of ODs, with multiple morphotypes and expression patterns, from the Middle Jurassic onwards.

1.4.2 Phylogenetic information

Squamate phylogeny is currently controversial because of disagreements between hypotheses based on analyses of either morphological or molecular/combined datasets (Figs 1.2, 1.3) - the main problem is the classification of Iguania. When using morphological characters to assess phylogeny, key characters in iguanians are

inferred to represent the retained ancestral state. However, when using molecular data to assess phylogeny, the iguanians are placed "higher" in the tree, and their ancestral characters are attributed to evolutionary reversal (Losos et al., 2012). However, based on an analysis of OD distribution in tetrapods, Hill (2005) concluded ODs have been lost and regained independently at least five times around the Permian and Triassic periods, making up a significant yet understudied area of the evolutionary history of the tetrapod skeleton.

Although ODs are taxonomically widespread within lizards, their phylogenetic distribution in extant taxa is highly sporadic, as is also the case in the fossil record, being expressed in some closely related taxa and not in other similarly related taxa (for example, in some *Varanus* species but not in others). Although some groups of squamates, for example all iguanians apart from the Marine Iguana *Amblyrhynchus cristatus (*Avery and Tanner, 1971) and *Brookesia perarmata* (Schucht et al., 2020) lack ODs, they are considered an original trait (plesiomorphy) in tetrapods (Francillon-Vieillot et al., 1989; Vickaryous and Sire, 2009; Mead et al., 2015).
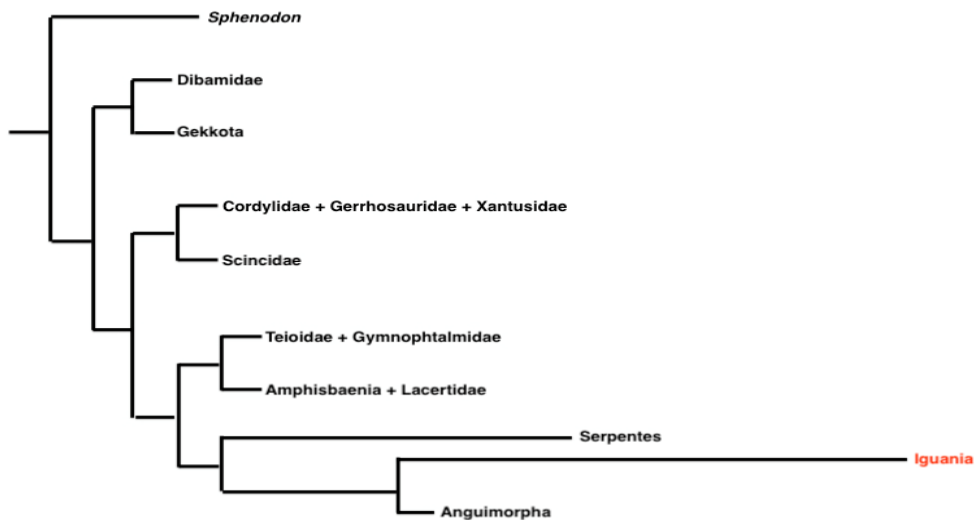
Figure 1.2 Phylogenetic tree of squamates based on molecular analyses (adapted from Losos et al., 2012).
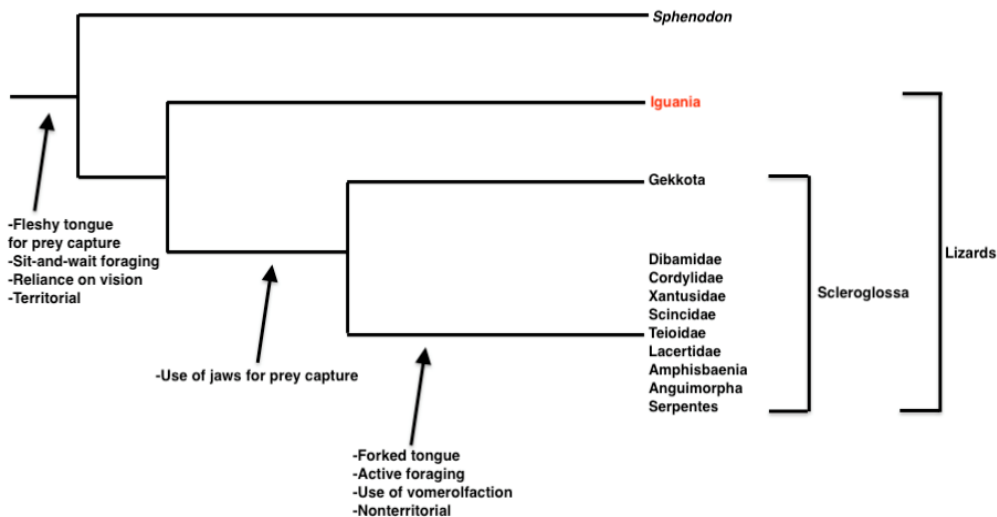
Figure 1.3 Phylogenetic tree of squamates based on morphological analyses (adapted from Losos et al., 2012).

1.4.3 Expression

As briefly mentioned earlier, tetrapod ODs exhibit a wide morphological diversity and vary in abundance, shape, relative and absolute size, aspect ratio, presence or absence of ornamentation such as keels or pits as well as location on the body and articulation pattern.

Within squamates, ODs are found in most (but not all of) the lizard taxa, but with very diverse anatomies, localisations and distributions. Among Squamata, ODs are absent from all snakes and amphisbaenians but are well-represented in lizards including anguids, anniellids, cordyliforms, helodermatids, scincids, shinisaurids, xantusiids, xenosaurids, lacertids, varanids, and gekkonids (Camp, 1923; Estes et al., 1988; Barrett et al., 2002).

In the lizards that express them, ODs see variable distribution. In some taxa, the ODs are confined to the head (e.g. *Timon lepidus*, [Camp, 1923; Estes et al., 1988]), in others they form a continuous covering of overlapping plates (e.g. in anguids, gerrhosaurids, a few gekkonids, scincids), are present in localised clusters (e.g. *Gekko*), or are present as regularly patterned, separate elements that may cover the whole body (e.g. *Varanus, Tarentola* [Vickaryous et al. 2015; Maisano et al. 2019]) Occasionally, they cover just the dorsal surface but not the ventral one (e.g. Helodermatidae [Moss, 1969]). ODs are greatly reduced in varanoids, but are still present as small "vermiform" bones (Erickson et al., 2003). As *Varanus* is such a diverse genus, differences between OD expression and morphotype or ecotype within

the genus are readily apparent. In larger species, such as *V. komodoensis*, ODs are expressed ubiquitously, in four different shapes and as a thick covering (Maisano et al., 2019). In smaller species such as *V. salvator*, they are absent (Erickson et al., 2003; Maisano et al. 2019) Where ODs are expressed they are highly polymorphic: they can be compound structures, consisting of small plates fused together (herein osteodermites [ODites]) into overlapping, imbricating structures (as in Scincidae, Camp, 1923); bent cylinders, partially overlapping one another (as in *Varanus* species, Maisano et al., 2019); branching processes (as in *Anniella spp.,* Bhullar and Bell, 2008) or as discrete, regularly tessellated, non-overlapping, polygonal beads (as in *Tarentola* species, Vickaryous et al., 2015), but this is not an exhaustive list. As well as this varied representation, the problem of characterising OD expression is compounded by the fact they are often unpredictably expressed within the same genus (e.g. *Varanus*, Erickson, 2003; Maisano et al., 2019; and *Gekko*, Vickaryous et al., 2015). It is currently not known if these specific expression types are correlated with the phylogenetic groups to which the species belong. Indeed, intraspecific, interspecific and intrafamilial variation as well as variation through ontogeny, has not been thoroughly documented and analysed in a way that can be controlled for. OD expression has also been shown to be influenced by changes in lifestyle such as starvation or gestation (Dacke et al., 2015).

Otto (1909) was the first to investigate the comparative morphology and histology of ODs among lizards. He proposed that the condition found in geckos is the most advanced stage of expression, and that of *Zonurus* the most primitive, with all other expressed structures lying in a range between these two extremes. The ideas that some families of lizards exhibit the same gross OD anatomy and that some families express more complex and advanced ODs than others, were expanded by Camp (1923), who argued that ODs of Anguimorpha should be regarded as on a "higher plane of development" than those of scincomorphs. He stated that ODs of Anguimorpha appear never to be compound, whereas in Scincomorpha, they are always compound and that the most highly specialised anguimorph ODs are those from the Glyptosauridae and Helodermatidae. The most recent phylogeny of the Amniota by Hill, (2005) demonstrated that the incorporation of characters from the integument resolved relationships that other "traditional" anatomical characters could not.

At the time of writing, the overriding consensus is that OD gross morphology is taxonomically informative (Camp, 1923; Read, 1986; Estes et al., 1988; Conrad,

2008). For example, varanid ODs are renowned for having a worm-like or vermiform shape (McDowell and Bogert, 1954; Erickson et al., 2003), whereas those of most anguids resemble flat, imbricating shingles (Zylberberg and Castanet, 1985) and those of gekkotans appearing as discrete, non-overlapping and irregular shapes (Levrat-Calviac and Zylberberg, 1986). The ODs of scincids and cordyliforms differ from the above in having a distinctive fractured appearance (compound ODs) (Otto, 1909; Camp, 1923; Estes et al., 1988; Zylberberg et al.,1992; Greer, 2007). Broeckhoven et al., 2017, found that *Hemicordylus capensis* displayed significant sexual dimorphism in OD expression, as males showed a greater OD volume than females, regardless of their position on the body, but there is a distinct lack of similar studies in other lizards. Although OD expression has long been regarded a result of natural selection, some of these recent findings suggest that these structures might instead be indirectly sexually selected, as a result of intraspecific conflict (Broeckhoven et al., 2017).

1.4.4 Function

An overriding theme in biology is the theory of structure-function relationship. This theory can be summarised in the following way: function dictates structure and vice versa, structure dictates function. Thus ODs, having variable expression of many diverse anatomies, are likely to have variable function. Dermal ossifications have high nutrient and energy cost of formation (Giles, 1983; Spence et al., 2012), therefore any function that they serve must warrant this cost.

The most commonly hypothesised function of ODs is as defensive armour against predators (Moss, 1972; Seidel, 1979; Vickaryous and Sire, 2009; Vickaryous et al., 2015) so much so that the terms 'osteoderms' and 'armour' are sometimes used as synonyms (Huxley, 1859; Chen et al., 2011; Yang et al., 2012). While it is probably true that many ODs exist to reinforce the structural rigidity and mechanical toughness of the skin, restraint should be exercised when using the term armour to avoid any oversimplification that may be misleading. In crocodilians for example, the ODs are expressed ubiquitously in adults while being absent in hatchlings, despite the fact that adults rarely experience predation (Vickaryous and Sire, 2009). This means that in this example, OD expression is inversely correlated to predation - exactly the opposite of what is expected if the function of all ODs were to protect from predation.

Many dinosaur taxa, such as *Stegosaurus*, have ossifications that were initially presumed to function as defence, but after examining the gross anatomy and microstructural histology of the bone, have been shown to be structurally inadequate

to act as armour (de Buffrénil et al., 1986; Main et al., 2005). Both authors considered that a species recognition or calcium storage function was more likely, although they cautioned that this was a tentative suggestion given the limited evidence on which is was based. Other authors (e.g. Marinho, 2007) arrived at similar conclusions, for example ODs in titanosaurs have been postulated as being too small macroscopically and too spongy microscopically to provide any real defensive advantage to an adult. However, the function of ODs in dinosaurs and indeed other taxa may be dependent on the soft tissue covering, be it epidermis or horn-like material. These "soft" tissues are often in fact very rigid and as such would be able to confer mechanical properties not dissimilar to those of the hard tissues beneath. This factor is important to bear in mind when considering the functions of ODs.

Alongside protective amour, several additional or alternative hypotheses of OD function have been proposed for various taxa, including thermoregulation (de Buffrénil et al., 1986; Farlow et al., 2010; Hayashi et al., 2010; Yang et al., 2012; Broeckhoven et al., 2015; Clarac et al., 2017), homeostasis (Main et al., 2005; Janis et al., 2012; Mead et al., 2012), structural support of the vertebral column (Frey, 1988; Buchwitz et al., 2012), social display (Main et al., 2005; Hayashi et al., 2010;), metabolic or mineral regulation and reserve (Seidel, 1979; Jackson et al., 2003; Marinho, 2007; Farlow et al., 2010; Dacke et al., 2015), defence in intraspecific aggression (Broeckhoven et al., 2017), as intraspecific display structures (Main et al., 2005; Saitta, 2015), as exoskeletal attachment for tendons (Seidel, 1979), as electro-receptive elements as is hypothesised in odontodes (Fraser et al., 2010), or as camouflage (Albertson et al., 2009, Schucht et al., 2020). It has been suggested that the ODs of *Alligator spp.* may play a role in calcium storage as the X-ray density of ODs was shown to be greater in females with ripe ovarian follicles compared to those that had recently laid eggs (Dacke et al., 2015) although Laver et al., (2019) argue that the enlarged endolymphatic sacs in *Gekko gecko* means that ODs act as structures that require rather than provide calcium resources. ODs have been shown to reduce flexibility during locomotion (Frey, 1988; Losos et al., 2002), although some authors have suggested that ODs can stabilise the vertebral column, alleviating some stress on muscles and joints during locomotion on land (Frey, 1988). The absence of OD expression in some lizard taxa has been associated with burrowing (Camp, 1923). Coe and Kunkel (1906), observed that the ODs of the Anniellidae have been greatly reduced, apparently by vacuolisation and concluded that this was due to their subterranean life. However, this explanation is countered by the presence of substantial ossification of the dermis of other lizards that are habitual burrow-dwellers

(for example, in helodermatids). In these examples, burrowing has thus been proposed as being both positively and negatively related to OD expression, highlighting the conflicting reports regarding the relationship between OD expression and function in the literature.

The variety of OD structure, arrangement, and distribution in Squamata make them a very favourable group in which to examine their macrostructure, histology and micro/ultrastructure, to assess their phylogenetic significance and to understand their development and function. The rest of the skeleton is multifunctional, acting as support for soft tissues whilst also being the location of cell differentiation in the bone marrow. ODs are likely to be comparable to the rest of the skeleton in this respect and therefore likely exhibit multiple functions.

1.4.5   Material Components

The most recent review of the integumentary skeleton of tetrapods highlights the gaps in our current knowledge of the skeletogenesis and subsequent material composition of OD skeletal elements in Squamata and calls for further investigation (Vickaryous and Sire, 2009).

ODs are not homogenous mineralised elements and have been described as incredibly heterogeneous in their composition. ODs have previously been described as containing either cancellous bone (Vickaryous and Sire, 2009), compact bone (Scheyer, 2007), parallel-fibred bone (P.F.B.) (Vickaryous and Hall, 2006), lamellar bone (L.B.) (de Buffrénil et al., 2010), Sharpey-fibred bone (S.F.B.) (Moss, 1969) and even containing enigmatic materials that cannot be described as bone (Moss, 1969). The latter author described the bulk of the *Heloderma* OD as comprising a dome of perpendicularly alternating (cross-hatched), mineralised, thick collagen fibres (Moss, 1969), capped by a non-osseous tissue.

Corucia zebrata ODs have previously been observed as containing a "sclerification… intermediate between calcified tendon and bone'' (Moss, 1969). The same tissue was also found to occur in *Tarentola mauritanica*, a gekkonid species, in which Levrat-Calviac and Zylberberg (1986) described long, parallel and densely-packed Sharpey's fibres that deeply enter the peripheral (equatorial) regions of the ODs and make a strong bond between neighbouring elements.

A capping tissue named osteodermine (OST.) was described in a fossil anguid (de Buffrénil et al., 2011). and then in ODs of the extant gecko *Tarentola* (Vickaryous et

al., 2015). These authors characterised OST. as hyper-mineralised and virtually acellular, with no collagen matrix, leading to comparisons with other hyper-mineralised tissues like ganoine (fish scales) or enamel (de Buffrénil et al., 2011). In fact, OST. had been described earlier by Moss (1969) in ODs of *Heloderma horridum*, but as an "enigmatic" capping tissue (Fig 1.4), of an unknown type, with a non-collagenous matrix that is highly mineralised and mostly avascular (Moss, 1972). Like de Buffrénil et al., (2011), he noted that this tissue bore a 'superficial resemblance to ganoine-enamel spectrum" (Moss, 1969, fig.1.1). If tissues such as these can be found capping tetrapod ODs, it may indicate that ODs, as a component of the tetrapod integument, may be more similar to odontogenic organs like odontodes, dermal denticles, or perhaps placoid and ganoid fish scales than previously thought. It has thus become quite clear that squamate OD material diversity is greater than previously thought and can include materials that cannot be classified as bone. Elucidating the structure of the materials present within ODs can provide answers for questions concerning the mechanical behaviour, function and formation of the materials present (Kerebel et al., 1978; Sun and Chen, 2013). This is because the processes that form mineralisations leave behind signatures of their mechanism of formation in their resultant structure. For example, initial metaplasia of an OD will result in indicative structures such as fibrous primary features and subsequent remodelling of this initial tissue will appear as secondary reconstructions (SRs). Secondary reconstructions result in specific structures observable in thin sections, including scalloped borders of secondary osteons and reconstruction lamellae (L.B.) (de Buffrénil et al., 2011; Horner et al., 2016). L.B. is characterised by this distinctive scalloped border as a result of remodelling and is only found on the endosteal surfaces of secondary osteons (Bromage et al., 2003; Schucht et al., 2020).

A comparative study of the ODs in *Tarentola mauritanica* and *Tarentola annularis* (Bauer and Russell, 1989) showed that each consists of two layers, a basal mineralised layer with abundant collagen and an outer mineralised layer with minimal collagen and mineral granules (Levrat-Calviac and Zylberberg, 1986; Bauer and Russell, 1989). The ODs of *Anguis fragilis* contained similar tissues (Zylberberg and Castanet, 1985).

1.4.6 OD Development in extant taxa

There has been relatively little work on OD development in reptiles (squamates and crocodilians). However, existing studies suggest that OD development in reptiles is remarkably different to that of mammals (Vickaryous and Sire, 2009; de Buffrénil et

al., 2010). In reptiles, there is reportedly no condensation of cells with osteoblastic phenotype (Moss, 1969) and no periosteum is observed (Vickaryous and Sire, 2008). This contrasts directly with mammalian OD development (i.e. in armadillos), which occurs via intramembranous ossification (Vickaryous and Hall, 2006).

Metaplastic ossification is a process whereby pre-existing, fully-developed soft connective tissue is transformed into bone (Haines and Mohuiddin, 1968). Development of mineralised tissue within the otherwise fully formed dermis, and in the absence of a cell condensation or cartilaginous precursor, is consistent with metaplastic ossification. Previous studies proposed a role for osseous metaplasia in the formation of ODs in at least 10 genera (12 species) of lizards (Moss, 1969; Zylberberg and Castanet, 1985; Levrat-Calviac and Zylberberg, 1986; Vickaryous and Sire, 2009), one crocodilian (Vickaryous and Hall, 2008), and an ankylosaurian dinosaur (de Ricqlès et al., 2001).

Vickaryous et al., (2015) argued that fibroblast-like cells are initially associated with the OD primordia, although they are not particularly abundant nor do they coalesce to form discrete cell condensations. Gradually, osteoblasts become associated with these centres of mineralisation, and osteoid begins to be deposited (Vickaryous et al., 2008, Fig. 6). Although the exact origin of these osteoblasts remains unclear, the two most likely sources are resident populations of latent osteoprogenitors (or possibly their mesenchymal stem cell precursors) or redifferentiated fibroblasts. Continued osteoid deposition incorporates collagen fibres of the surrounding dermis, creating Sharpey's fibres that firmly anchor the elements within the integument and to one another. Thus, the presence of integrated Sharpey's fibres into the peripheral surfaces of the ODs likely corresponds to metaplastic formation of the OD. The term "parallel-fibred bone" as used by Vickaryous et al., (2015) to describe the parallel orientation of Sharpey's fibre's in *Tarentola* ODs is synonymous with S.F.B. used here to describe the same tissue (after Jones and Boyde, 1974). Parallel-fibred bone refers here to parallel-fibres of mineralised collagen in the basal regions of some ODs, that does not manifest on the endosteal surfaces of secondary osteons and does not display a "scalloped border" around the periphery of the tissue (as is the case in L.B.). S.F.B. was only identified here where continuous fibres enter the basal and peripheral portions of ODs, from the surrounding soft tissue (Sharpey's fibres), whereas P.F.B. does not contain these Sharpey's fibres. In P.F.B. the collagen is self-contained within the OD. S.F.B. is only located in the periphery or basal regions of ODs, due to the deep location of dermal collagen fibres of the stratum compactum (S.C.) that comprise

the Sharpey's fibres. The microstructural nature of S.F.B. is such that it would afford a strong anchor to the dermis, yet would remain quite flexible due to the large diameter of the collagen fibres. The definition of S.F.B. outlined above is synonymous with "mineralised structural fibres" (Haines and Mohuiddin, 1968; Moss, 1969; Scheyer and Sander, 2004).

ODs have been described as having a postponed development compared to the rest of the skeleton, since they do not appear until after hatching (Vickaryous and Hall, 2008). However, the exact pattern of onset of OD formation varies across taxa. For example, while geckos tend to develop ODs first across the head and cervical regions (Vickaryous et al., 2015; Laver et al., 2020), in cordylids they first appear across the tail and along the caudal margins of the head (Stanley et al., 2016). Their development is often associated with underlying bones, for example, within Crocodylomorpha, ODs are typically rectangular, arranged in parallel rows aligned along the anteroposterior axis where each row of ODs corresponds to a single vertebra (Vickaryous and Hall, 2008). ODs have been shown to fuse to the underlying bones of the skull in more mature adult specimens of the Komodo dragon (*Varanus komodoensis*) and Gila monster (*Heloderma*), highlighting the plasticity of the mineralised tissues they are formed from and their ability to merge with separately formed mineralisations (Moss, 1969; Mead et al., 2012). A lack of detailed cranial osteological data on many gerrhosaurid and cordylid lizards is due to ODs being found fused to the bones of the skull, rendering osteological features like bone-to-bone contacts and sutures difficult, if not impossible, to see in articulated specimens (Losos et al., 2002). In some cases, each OD is associated with one epidermal reptilian scale, highlighting the importance of dermal and epidermal interactions during their development.

Embryonically, knowledge of the cellular origins of ODs as components of the vertebrate integumentary skeleton remains inadequate, but a substantial role for the neural crest has been proposed (Moss, 1969; Smith and Hall, 1990). This is likely because ectomesenchymal cells are known to play a role in the formation of the teeth and craniofacial bone elements of the dermal skeleton of humans and when considering the almost universal expression of integumentary elements in many early stem gnathostomes, this conveys the idea that neural crest populations contributed to the formation of these mineralised tissues in ancestors and thus is likely to be the same in living species (Smith and Hall, 1990). By extension, it is hypothesised that cephalic and trunk neural crest cell populations of basal actinopterygian fish and basal sarcopterygians retained the ability to form both odontogenic and osteogenic tissues,

giving rise to the expression of these tissues in the modern-day ganoid and cosmoid scales, respectively. These data support the idea (Vickaryous and Sire, 2009) that all ODs as elements of the dermal skeleton are derivatives of a neural crest-derived osteogenic cell population (with possible matrix contributions from the overlying epidermis) and share a deep homology related to the skeletogenic competence of the dermis. It has been proposed that the early stage OD (known as 'osteoderm primordia') forms in some species, for example *Alligator mississippiensis* and *Heloderma horridum,* via direct metaplasia of the stratum compactum without osteoblast condensations (Moss, 1969). This hypothesis is usually adopted due to the striking similarities between the orientation of the collagen in the soft dermis and the ultimate orientation of the collagen within the mineralised OD. Additionally, bundles of collagen fibrils in the basal part of the OD continue into the surrounding dermis, anchoring the OD within the dermis, linking it to both the dermal-epidermal junction and to neighbouring ODs via a soft, flexible yet fastened connection (Moss, 1969; Vickaryous and Hall, 2008; de Buffrénil et al., 2010, 2011). This metaplasia is similar to how tendons ossify as part of a normal developmental feature of birds (Dubansky and Dubansky, 2018).

After metaplasia of existing fibres, resorption of the OD materials during remodelling is well characterised in many fossil and extant taxa (Witzmann, 2009; de Buffrénil et al., 2011; Buchwitz et al., 2012; Dacke et al., 2015). Resorption involves remodelling the metaplastic bone to form secondary structures, which resemble primary or secondary osteons. L.B. is deposited during this time. Interestingly recent studies have highlighted the resemblance that some OD development shows to pathogenic ossifications in humans such as Fibrodysplasia ossificans progressiva (Dubansky and Dubansky, 2018). This highlights the importance of a greater understanding of OD structure, function and ontogeny, as they can be used in healthcare models that benefit our understanding of pathogenic ossification.

As previously addressed, like the controversy surrounding the question of cellular origins of dentinous tissues there is also debate as to the cellular origins of ODs, notably whether the epidermis makes any contribution to OD formation, and if the mechanism of formation is bone metaplasia, intramembranous ossification and/or both. Moss (1972) was the first to describe the histology of the ODs of the venomous lizard *Heloderma suspectum,* which he described as containing an 'enigmatic tissue' of unknown composition and origin. It seems that Moss was likely to have been referring to the recently described tissue OST. (de Buffrénil et al., 2011) on the surface

of the *Heloderma* OD, but was ahead of his time in this description and did not perform the necessary techniques to fully characterise it.

It has been postulated that the basal epidermal cells or scleroblasts might contribute to the upper layers of OD capping tissues so that the *Heloderma* OD might be a compound product from mesodermal cells and epidermal cells along with neural crest cells playing a role in induction of the epidermis (Levrat-Calviac and Zylberberg, 1986). Indeed, the capping tissues present on the ODs of lizards have been described as similar to ganoine and/or enamel (de Buffrénil et al., 2011) and both of these require contribution from the epidermis to form (Sire et al., 2009).

ODs of *Heloderma* have also been described as containing a dome of perpendicularly alternating (cross-hatched), metaplastically mineralised, thick collagen fibres (Moss, 1969). Mature *Heloderma* ODs are formed from these mineralised interlacing collagen bundles, capped by OST., a non-collagenous matrix that is highly mineralised and mostly avascular (Moss, 1972). Moss makes a clear distinction between calcification and ossification in his work, noting that calcification is process by which hyper-mineralised tissues can form on sulphated mucopolysaccharide matrices, and ossification is the normal process of bone formation. No studies have been published that attempt to determine the cellular origins of the metaplastic formation of ODs. Studies attempting to determine the role of osteoblasts in OD formation are needed, perhaps utilising an ontogenetic series of specimens, cell-surface markers, transcription factors and other molecular markers to target osteoblasts and fibroblasts (posited by Vickaryous et al., 2015, to be responsible for OST. formation).

In the majority of tetrapods, little is known about OD structure and development, particularly at the molecular level as current understanding of their ultrastructure is dated and/or incongruous and not sufficient to completely answer these questions in a broader context (Vickaryous and Sire, 2009). The ultrastructure and mode of development of ODs in mammals, for example in *Dasypus novemcinctus* the nine-banded armadillo, has been examined and is comparable with intramembranously derived elements of the skull (Vickaryous and Sire 2009; Chen et al., 2011), unlike that described for squamate osteoderms, which are thought to arise from within the dermis (or epidermis/dermis interface) by mineralisations that form metaplastically around dense collagen networks (Moss, 1972). *Alligator mississippiensis* ODs also form via metaplasia – where they were suggested to arise from a population of fibroblast-like cells that transformed into osteoblast-like cells, but this could only be

confirmed by work using in-situ hybridisation and immunohistochemistry (Vickaryous and Hall, 2008).

Irregularities in the patterns of mineralised collagen fibres in regions of ODs with metaplastically formed bone, as well as changes to the fibre patterns near to vascular channels, appear to represent where the previous collagen fibre pattern has been eroded and remodelled. Several studies have described patterns of resorption and replacement in various ODs, which implies involvement from osteoclasts and osteoblasts in their formation (de Buffrénil et al., 2010, 2011). Many authors have recorded the absence of a periosteum (bone outer membrane) and no cartilaginous intermediate for squamate ODs. In the absence of this membrane, the lower limit of mineralisation spread is determined by a basophilic histological layer (meaning it will stain positive with a basic dye like haematoxylin or eosin), but little is known regarding the process by which the mineralisation front is halted (Moss, 1972; Vickaryous and Sire, 2009). It is unclear whether or not bone metaplasia requires the use of osteoblasts - in gekkotan ODs (Vickaryous et al., 2015) it has been argued that metaplasia occurs in the presence of osteoblasts, but the origin of the osteoblasts is still unclear as there is no distinct cellular condensation during formation.

1.4.7   OD Development in extinct taxa

Developmental aspects of OD formation among extinct taxa may not be homologous. Metaplastic ossification is the direct ossification of pre-existing structural collagen fibres. A metaplastic origin has been deduced for the ODs of some extinct taxa (e.g. the ankylosaurids *Saichania chulsanensis, Pinacosaurus grangeri, Ankylosauridae indet*), based on the presence of interwoven bundles of mineralised collagen fibres with a well-ordered fibre bundle arrangement ('mineralized structural fibres' Scheyer and Sander, 2004.). According to Vickaryous and Hall (2008) and also Vickaryous and Sire (2009), this material is homologous with S.F.B. and is herein synonymous with S.F.B..

Metaplastic development has also been proposed as the mechanism of OD formation in anamniote tetrapods (Witzmann and Soler-Gijón, 2010; Buchwitz et al., 2012), thyreophoran and sauropod dinosaurs (Dodson et al., 1998; Scheyer and Sander, 2004; Main et al., 2005), Archosauriformes (Cerda et al., 2015), some xenarthran mammals (Hill, 2006), as well as for the dermal bones of turtles (Scheyer and Sánchez-Villagra, 2007) and Placodontia (Scheyer, 2007). It remains uncertain if glyptosaurine ODs developed via osseous metaplasia (de Buffrénil et al., 2011). However, metaplastic ossification in the absence of osteoblasts ceases to be an

acceptable explanation for subsequent OD growth in glyptosaurine ODs because bone remodelling is a histological feature of these ODs and this requires the involvement of osteoblasts (Erickson et al., 2003; de Buffrénil et al., 2010).

During intramembranous ossification, the newly-formed osseous tissue displaces the preformed soft tissue structures instead of incorporating them. Based on the absence of mineralised structural fibres (S.F.B.), this kind of ossification has been proposed for some extinct taxa, including some basal tetrapods (Buchwitz et al., 2012), pareiasaurs (Scheyer and Sander, 2009) and ''aetosaurine'' aetosaurs (Cerda and Desojo, 2010). In the latter case, the particular distribution of the primary bone tissues was also interpreted as independent evidence for an intramembranous origin. The lack of mineralised structural fibres and the presence of "woven-fibred" and "fibrolamellar bone" in the internal core of the rauisuchian ODs studied by Scheyer and Desojo (2011) were interpreted as evidence of intramembranous ossification in at least some members of this group. However, the bone microstructure of rauisuchian ODs led other authors to conclude that they originated through a mechanism that involves both intramembranous and metaplastic ossifications (Cerda et al., 2013). Despite the observations made by Scheyer and Sander, 2004, regarding a possible metaplastic origin of ankylosaurian dinosaur ODs, these ODs have also been reported to be formed from intramembranous ossification without metaplasia due to the presence of "primary fibrolamellar bone", assumed to only be deposited intramembranously (Burns et al., 2013). Further exploration of OD development in extinct taxa occurs in Chapter 6. These discrepancies in the literature highlight the uncertainty surrounding OD development and show how ODs are currently thought to form in drastically different ways.

1.4.8   Conclusions

Given the limited data available on the topics discussed above, obtaining more comprehensive data on squamate ODs from the first order, the anatomical level, down to the fourth order, the molecular level, will allow insight into the structures of the tissues present. More species and samples need to be examined in order to elucidate the facts regarding the tissues that can appear in these odd mineralisations. Given the outcomes of other studies, it is clear that there is much to learn from studying ODs but a lack of research into their origin is harming our understanding of these enigmatic mineralisations.

Consequently, effectively characterising the histological and ultra-structural material compositions of ODs will yield information that can be used to inform the debate

around topics including their formation, development, evolution, function and cellular origins. The mineralised tissues present in ODs may appear structurally similar or completely different to previously characterised mineralised tissues of endoskeletal bones, dental tissues, etc. so analysis of their ultrastructure and histology is fundamental to the aim of classifying them accurately. Beyond this, the information gleaned may potentially prove valuable in future translational applications, including the creation of biomimetic and/or bioinspired materials with special properties for use in various medical and non-medical applications (Huang et al., 2011). This is because it is becoming apparent from research into the mechanical properties of ODs and other dermal armours such as fish scales that, despite some dramatic differences in cellular origins, material compositions and structures, seem to exhibit a similar strategy of merging a soft internal base with a more firm, tougher external part. This coevolved pattern across multiple integumentary elements expressing a universal compound material protection emphasises how the most suitable systems of armour for preservation of life are selected for in evolutionary environments and also how such methods can be exploited for our own use when designing protective armours (Huang et al., 2011; Sun and Chen, 2013).

As explained, many studies show that vertebrate dermal bone exhibits multiple functionalities - consequently there are structural compromises given these different functionalities. Hence, despite the fact that natural body armour might serve as bio-inspiration for the development of artificial protective materials, focussing on model systems in which body armour serves a primary protective function is important. Therefore, conclusive data on the function(s) of ODs are important for our own reverse engineered applications and many OD-bearing taxa require examination for the collection of these data.

1.5 Gaps in our knowledge

The above review highlights the gaps in our knowledge regarding how ODs form from cell populations, what materials are present to help ODs act as multifunctional armour, which mineralised materials manifest in different taxa and also basic histological definitions of the materials present. This is not just because of the diversity of OD expression and material composition in Squamata; it is also compounded by a lack of research into this area.

In order to understand how ODs relate to other mineralisation apparatuses, we need to know more about their composition, how ODs fit into the local systems of the dermal environment, how they are related across taxa and where they come from, both in terms of their evolution and their ontogeny. This information is important as not only can we learn more about the evolution of lizards and their dermal apparatus, but also because the knowledge can be applied to our own understanding of how armour can be used to protect living things from harm.

As shown above, previous authors have identified superficial resemblances between unknown materials in ODs to other previously defined materials present in non-tetrapods such as ganoine. Therefore, enigmatic tissues present within ODs need to be imaged, characterised, compared and discussed, using modern-day techniques to obtain comprehensive data sets which can be used to inform our understanding of the materials present and thus their relationships to other materials.

A major limitation is the sheer number of specimens required to assess all squamate species – >9400 known extant species. This limitation was addressed by ensuring that the lizards chosen were representative of all major families.

1.6 Aims and objectives of the thesis

Given this introduction to the subject, there are obvious areas where further research is required and these form the basis of the thesis. My main aims are to answer the following questions:

- Do all squamate osteoderms have the same microstructural composition?
- Is osteodermine the dense capping tissue present in *Heloderma suspectum* ODs and is osteodermine a more widespread material than previously thought?
- Does the macrostructure of ODs provide clues as to their function and/or development?
- Does the microstructure of ODs provide clues as to their function and/or development?

1.7 References

Albertson R. C., Cresko W., Detrich H. W. and Postlethwait J. H. (2009) Evolutionary mutant models for human disease. *Trends in Genetics* **25**:74-81.

Avery D. F. and Tanner W. W. (1971) Evolution of the iguanine lizards (Sauria, Iguanidae) as determined by osteological and myological characters*. Brigham Young University Science Bulletin* **12**:1-79.

Bai I.-C., McMullan G. and Scheres S. H. W. (2015) How cryo-EM is revolutionizing structural biology. *Trends in Biochemical Sciences* **40**:49-57,

Barrett O. M., Clarke J. B., Brinkman D. B., Chapman S. D. and Ensom P. C. (2002) Morphology, histology, and identification of the 'granicones' from the Purbeck Limestone Formation (Lower Cretaceous: Berriasian) of Dorset, southern England. *Cretaceous Research* **23**:279-295.

Bauer A. M. and Russell A. P. (1989) Supraorbital ossifications in geckos (Reptilia: Gekkonidae). *Canadian Journal of Zoology* **67**:678–684.

Benton M. J. (1985) Classification and phylogeny of the diapsid reptiles. *Zoological Journal of the Linnean Society* **84**:97-164.

Bertazzo S. and Bertran C. A. (2006) Morphological and dimensional characteristics of bone mineral crystals. *Key Engineering Materials* **309**:3–6.

Bhullar B.-A. S. and Bell C. J. (2008) Osteoderms of the California legless lizard *Anniella* (Squamata: Anguidae) and their relevance for considerations of miniaturization. *Copeia* **4**:785–793.

Bolet A. and Evans S.E. (2011) New material on the enigmatic Scandensia, an Early Cretaceous lizard from the Iberian Peninsula. *Special Papers in Palaeontology* **86**:99-108.

Bolet A. and Evans S. E. (2012). A tiny lizard (Lepidosauria, Squamata) from the Lower Cretaceous of Spain. *Palaeontology* **55**:491–500.

Broeckhoven C., Diedericks G. and Mouton P. L. F. N. (2015) What doesn't kill you might make you stronger: functional basis for variation in body armour. *Journal of Animal Ecology* **84**:1213–21.

Broeckhoven C., de Kock C. and Mouton P. L. F. N. (2017) Sexual dimorphism in osteoderm expression and the role of male intrasexual aggression. *Biological Journal of the Linnean Society* **122**:329-339.

Bromage T. G., Goldman H. M., McFarlin S. C., Warshaw J., Boyde A. and Riggs C. M. (2003) Circularly polarized light standards for investigations of collagen fiber orientation in bone. *Anatomical Record - Part B New Anatomist* **274**:157-168.

Buchwitz M., Witzmann F., Voigt S. and Golubev V. (2012) Osteoderm microstructure indicates the presence of a crocodylian-like trunk bracing system in a group of armoured basal tetrapods. *Acta Zoologica* **93**:260–280.

Burns M. E., Vickaryous M. K. and Currie P. J. (2013) Histological variability in fossil and recent alligatoroid osteoderms: Systematic and functional implications. *Journal of Morphology* **274**:676-686.

Camp C. L. (1923) Classification of the Lizards. *Bulletin of the American Museum of Natural History* **48:**289-481.

Cerda I. A. and Desojo J. B. (2010) Dermal armour histology of aetosaurs (Archosauria: Pseudosuchia), from the Upper Triassic of Argentina and Brazil. *Lethaia*, **44**:417-428.

Cerda I. A., Desojo J. B, Scheyer T. M. and Schultz C. L. (2013) Osteoderm microstructure of "rauisuchian" archosaurs from South America. *GeoBios* **46**:273-283*.*

Cerda I. A., Desojo J. B., Trotteyn M. J. and Scheyer T. M. (2015) Osteoderm histology of *Proterochampsia* and *Doswelliidae* (Reptilia: Archosauriformes) and their evolutionary and paleobiological implications. *Journal of Morphology* **276**:385–402.

Chen I. H., Kiang J. H., Correa V., Lopez M. I., Chen P-Y., Mc Kittrick J. and Meyers M. A. (2011) Armadillo armor: mechanical testing and micro-structural evaluation. *Journal of Mechanical Behaviour Biomedical Materials* **4**:713–22.

Chen I. H., Yang W. and Meyers M. A. (2015) Leatherback sea turtle shell: a tough and flexible biological design. *Acta Biomaterialia* **28**:2–12.

Clarac F., Goussard F., Teresi L., de Buffrénil V., and Sansalone V. (2017) Do the ornamented osteoderms influence the heat conduction through the skin? A finite element analysis in Crocodylomorpha. *Journal of Thermal Biology* **69**:39-53.

Clarke B. (2008) Normal bone anatomy and physiology. *Clinical Journal of the American Society of Nephrology : CJASN* **3:**131-139.

Coe W. R. and Kunkel B. W. (1906) Studies on the California limbless lizard, *Anniella*. *Transactions of the Kansas Academy of Science* **12**:349–403.

Conrad J. L. (2008) Phylogeny and systematics of Squamata (Reptilia) based on morphology. *Bulletin of the American Museum of Natural History* **310**:1–182.

Conrad J. L., Wang Y., Xu X., Pyron A. and Clark J. (2013) Skeleton of a heavily armored and long-legged Middle Jurassic lizard (Squamata, Reptilia). *Supplement to the online Journal of Vertebrate Paleontology* 73rd Annual Meeting, Abstracts. Pp. 108.

Dacke C. G., Elsey R. M., Trosclair P. L., Sugiyama T., Nevarez J.G. and Schweitzer M. H. (2015) Alligator osteoderms as a source of labile calcium for eggshell formation. *Journal of Zoology* **297**:255-264.

Daculsi G., Menanteau J., Kerebel L. M. and Mitre D. (1984) Length and shape of enamel crystals. *Calcified Tissue International* **36:**550–55.

De Buffrénil V., Farlow J. O. and de Ricqlès A. (1986) Growth and function of *Stegosaurus* plates: evidence from bone histology. *Paleobiology* **12**:459-473.

De Buffrénil V., Dauphin Y., Rage J-C. and Sire J-Y. (2011) An enamel-like tissue, osteodermine, on the osteoderms of a fossil anguid (Glyptosaurinae) lizard. *Comptes Rendus de l'Academie des Sciences Palevol* **10:**427-437.

De Buffrénil V., Sire J. Y. and Rage J. C. (2010) The histological structure of glyptosaurine osteoderms (Squamata: Anguidae), and the problem of osteoderm development in squamates. *Journal of Morphology* **271**:729–737.

D'Emic M. D., Wilson J. A. and Chatterjee S. (2009) The titanosaur (Dinosauria: Sauropoda) osteoderm record: review and first definitive specimen from India. *Journal of Vertebrate Paleontology* **29**:165–77.

De Ricqlès A., Pereda-Suberbiola X., Gasparini Z. and Olivero E. B. (2001) Histology of dermal ossifications in an ankylosaurian dinosaur from the Late Cretaceous of Antarctica. *Asociación Paleontológica Argentina, Publicación Especial* **7:**171–174.

Dias E. V. and Richter M. (2002) On the squamation of *Australerpeton cosgriffi* Barberena, a temnospondyl amphibian from the Upper Permian of Brasil. *Anais da Academia Brasileira de Ciências* **74**:477–490.

Dodson P., Krause D. W., Forster C. A., Sampson S. D. and Ravoavy F. (1998) Titanosaurid (Sauropoda) osteoderms from the Late Cretaceous of Madagascar. *Journal of Vertebrate Palaeontology* **18**:563–568.

Dong L., Xu X., Wang Y. and Evans S. E. (2018) The lizard genera *Bainguis* and *Parmeosaurus* from the Upper Cretaceous of China and Mongolia. *Cretaceous Research* **85:**95-108.

Dorozhkin S. V. (2007) A hierarchical structure for apatite crystals. *Journal of Materials Science: Materials in Medicine* **18**:363–66.

Dorozhkin S. V. (2013) Calcium orthophosphates in dentistry. *Journal of Materials Science: Materials in Medicine* **24**:1335–63.

Dubansky B. H. and Dubansky B. D. (2018) Natural development of dermal ectopic bone in the american alligator (*Alligator mississippiensis*) resembles heterotopic ossification disorders in humans. *The Anatomical Record* **301**:56–76.

Erickson G. M., Ricqlès A. de, Buffrénil V. de, Molnar R. E. and Bayless M. K. (2003) Vermiform bones and the evolution of gigantism in *Megalania* — How a reptilian fox became a lion. *Journal of Vertebrate Palaeontology* **23**:966-970.

Estes R. (1983) The fossil record and early distribution of lizards. In: *Advances in Herpetology and Evolutionary Biology: Essays in Honor of Ernest E. Williams*. Editors: Rhodin A. G. J. and Miyata K. Publisher: Museum of Comparative Zoology, Cambridge, MA, USA. Pp. 725.

Estes R., De Queiroz K. and Gauthier J. (1988) Phylogenetic relationships within Squamata. In: *Phylogenetic Relationships of the Lizard Families: Essays Commemorating Charles L. Camp*. Editors: Estes R. and Pregill G., Publisher: Stanford University Press, Redwood City, CA, USA. Pp. 119-281.

Evans S. E. (1984) The Classification of the Lepidosauria. *Zoological Journal of the Linnean Society* **82**:87-100.

Evans S. E. and Barbadillo L.J. (1998) An unusual lizard (Reptilia: Squamata) from the Early Cretaceous of Las Hoyas, Spain*. Zoological Journal of the Linnean Society* **124**:235-265.

Evans S. E. and Chure D. (1998) Paramacellodid lizard skulls from the Jurassic Morrison Formation at Dinosaur National Monument, Utah. *Journal of Vertebrate Paleontology* **18**:99-114.

Farlow J. O., Hayashi S. and Tattersall G. J. (2010) Internal vascularity of the dermal plates of *Stegosaurus* (Ornithischia, Thyreophora). *Swiss Journal of Geoscience*s **103**:173-185.

Forey P. L. (1995) Agnathans recent and fossil, and the origin of jawed vertebrates. *Reviews in Fish Biology and Fisheries* **5**:267–303.

Francillon-Vieillot H., de Buffrénil V., Castanet J., Géraudie J., Meunier F. J., Sire J-Y., Zylberberg L. and de Ricqlès A. (1989) Microstructure and mineralization of vertebrate skeletal tissues. *Skeletal Biomineralization: Patterns, Processes and Evolutionary Trends* **5**:175–234.

Fraser G. J., Cerny R., Soukup V., Bronner-Fraser M. and Streelman J. T. (2010) The odontode explosion: the origin of tooth-like structures in vertebrates. *BioEssays: news and reviews in molecular, cellular and developmental biology* **32**:808-17.

Fratzl P. and Weinkamer R. (2007) Nature's hierarchical materials. *Progress in Materials Science* **52**:1263–1334.

Frey E. (1988) The crocodile support system - a biomechanical and phylogenetic analysis. *Stuttgart Contributions to Natural History Series A (Biology)* **426**:1-60.

Gaffney E. S. (1990) The comparative osteology of the Triassic turtle *Proganochelys. Bulletin of the American Museum of Natural History* **194**:263.

Gao K-Q. and Norell M. (2000) Taxonomic composition and systematics of Late Cretaceous lizard assemblages from Ukhaa Tolgod and adjacent localities, Mongolian Gobi Desert. *Bulletin of the American Museum of Natural History* **249**:1-118.

Giles N. (1983) The possible role of environmental calcium levels during the evolution of phenotypic diversity in outer hebridean populations of the three-spined stickleback, *Gasterosteus Aculeatus*. *Journal of Zoology* **199**:535-544

Greer A. (2007) The Biology and Evolution of Scincid Lizards. Online at: https://www.academia.edu/35305801/The_Biology_and_Evolution_of_Scincid_Lizar ds.doc Accessed: 02/05/2020.

Haines R. W. and Mohuiddin A. (1968) Metaplastic Bone. *Journal of Anatomy* **103**:527–38.

Hall B. K. (2005) Chapter 2 – Bone. In: *Bones and Cartilage.* Editor: Hall B. K. Publisher: Academic Press, Cambridge, Massachusetts, USA. Pp. 13-32.

Hayashi S., Carpenter K., Scheyer T. M., Watabe M. and Suzuki D. (2010) Function and evolution of ankylosaur dermal armor. *Acta Palaeontologica Polonica*, **55**:213–228.

Hill R. V. (2005) Integration of morphological data sets for phylogenetic analysis of Amniota: the importance of integumentary characters and increased taxonomic sampling. *Systematic Biology* **54**:530–547.

Hill R. V. (2006) Comparative anatomy and histology of xenarthran osteoderms. *Journal of Morphology* **267**:1441-1460.

Horner J. R., Woodward H. N. and Bailleul A. M. (2016) Mineralized tissues in dinosaurs interpreted as having formed through metaplasia: A preliminary evaluation. *Comptes Rendus – Palevol* **15**:183–203.

Huang J., Durden H. and Chowdhury M. (2011) Bio-inspired armor protective material systems for ballistic shock mitigation. *Materials and Design* **32**:3702–3710.

Huxley T. H. (1859) On the dermal armor of *Crocodilus hastingsiae Quarterly Journal of the Geological Society of London* **15**:678-680.

Jackson D. C., Andrade D. V. and Abe A. S. (2003) Lactate sequestration by osteoderms of the broad-nose caiman, *Caiman latirostris*, following capture and forced submergence. *Journal of Experimental Biology* **206**:3601-3606.

Janis C. M., Devlin K., Warren D. E. and Witzmann F. (2012) Dermal bone in early tetrapods: a palaeophysiological hypothesis of adaptation for terrestrial acidosis. *Proceedings of the Royal Society B: Biological Sciences* **279**:3035–3040.

Jones S. J. and Boyde A. (1974) The organization and gross mineralization patterns of the collagen fibrils in Sharpey fibre bone. *Cell and Tissue Research* **148**:83-96.

Kerebel B., Le Cabellec M. T., Daculsi G. and Kerebel L. M. (1978) Osteodentine and vascular osteodentine of *Anarhichas Lupus* (L.). *Cell and Tissue Research* **187**:135–46.

Krause D.W., Evans S. E. and Gao K.-Q. (2003) First definitive record of Mesozoic lizards from Madagascar. *Journal of Vertebrate Paleontology* **23**:842-856.

Lagier R. and Baud C.-A. (2003) Magnesium Whitlockite, a Calcium Phosphate Crystal of Special Interest in Pathology. *Pathology - Research and Practice* **199**:329–335.

Laver R. J., Morales C. H., Heinicke M. P., Gamble T., Longoria K., Bauer A. M. and Daza J. D. (2019) The development of cephalic armor in the tokay gecko (Squamata: Gekkonidae: *Gekko gecko*). *Journal of Morphology* **281**:213-228.

Levrat-Calviac V. and Zylberberg L. (1986) The structure of the osteoderms in the gekko: *Tarentola mauritanica. American Journal of Anatomy* **446**:437–446.

Liu Y., Young-Kyung K., Dai L., Li N., Khan S. O., Pashley D. H., and Tay F. R. (2011) Hierarchical and non-Hierarchical mineralisation of collagen. *Biomaterials* **32**:1291–1300.

Losos J. B., Hillis D. M. and Greene H. W. (2012) Who speaks with a forked tongue? *Science* **338**:1428–1429

Losos J. B., Mouton P. L. F. N., Bickel R., Cornelius I. and Ruddock L. (2002) The effect of body armature on escape behaviour in cordylid lizards. *Animal Behaviour* **64**:313-321.

Maisano J. A., Laduc T. J., Bell C. J. and Barber D. (2019) The cephalic osteoderms of *Varanus komodoensis* as revealed by high-resolution X-ray computed tomography. *The Anatomical Record* **302**:1675–1680.

Main R. P., de Ricqlès A., Horner J. R. and Padian K. (2005) The evolution and function of thyreophoran dinosaur scutes: implications for plate function in *Stegosaurus. Paleobiology* **31**:291-314.

Marinho T. D. S. (2007) Functional aspects of titanosaur osteoderms. *Anuario Do Instituto de Geociencias* **30**.

McDowell S. M. Jr and Bogert C. M. (1954) The systematic position of *Lanthanotus* and the affinities of the anguinomorphan lizards. *Bulletin of the American Museum of Natural History* **105**:1–142.

McNally E. A., Schwarcz H. P., Botton G. A., and Arsenault A. L. (2012) A model for the ultrastructure of bone based on electron microscopy of ion-milled sections. *PLoS ONE* **7**:1–12.

Mead J. I., Schubert B. W., Wallace S. C. and Swift S. L. (2012) Helodermatid lizard from the Mio-Pliocene oak-hickory forest of Tennessee, Eastern USA, and a review of monstersaurian osteoderms. *Acta Palaeontologica Polonica* **57**:111-121.

Mead J. I., Holte S., White R. S. and McCord R (2015) Early Pleistocene (Blancan) helodermatid lizard from Arizona, USA. *Journal of Herpetology* **49**:295–301.

Mo J.Y., Xu X. and Evans S. E. (2012) A large predatory lizard (Platynota, Squamata) from the Late Cretaceous of South China. *Journal of Systematic Palaeontology* **10**:333-339.

Moss M. L. (1969) Comparative histology of dermal sclerifications in reptiles. *Acta Anatomica* **73**:510–533.

Moss M. L. (1972) The vertebrate dermis and the integumental skeleton. *American Zoologist* **12**:27–34.

Nilsson O., Parker E., Hegde A., Chau M., Barnes K. and Baron J. (2007) Gradients in bone morphogenetic protein-related gene expression across the growth plate. *Journal of Endocrinology* **193**:75-84

Nudelman F., Pieterse K., George A., Bomans P. H. H., Friedrich H., Brylka, L. J., Hilbers P. A. J., Gijsbertus de W. and Sommerdijk N. A. J. M. (2010) The role of collagen in bone apatite formation in the presence of hydroxyapatite nucleation inhibitors. *Nature Materials* **9**:1004–1009.

Nydam R. L. (2000) A new taxon of helodermatid-like lizard from the Albian–Cenomanian of Utah. *Journal of Vertebrate Palaeontology* **20**:285-294.

Otto H. (1909) Die Beschuppung der Brevilinguier und Ascalaboten. *Jena Z Naturwiss* **44**:193–252.

Ørvig T. (1957) Remarks on the vertebrate fauna of the Lower Upper Devonian of Escuminac Bay, P.Q., Canada, with special reference to the porolepiform crossopterygians. *Arkiv för Zoologi* **10**:367–426.

Pasteris J. D., Wopenka B. and Valsami-Jones E. (2008) Bone and tooth mineralization: why apatite? *Elements* **4**:97–104.

Patterson C. (1977) Cartilage bones, dermal bones and membrane bones, or the exoskeleton versus the endoskeleton. In: *Problems in Vertebrate Evolution: Essays Presented to Professor T S Westoll*, *Linnean Society symposium series 4* Editors: Westoll S., Andrews S. M., Miles R. S. and Walkerpp A. D. Publisher: Linnean Society of London, London, UK. Pp. 77–122.

Porter M. E. (2006) Material properties and biochemical composition of mineralized vertebral cartilage in seven Elasmobranch species (Chondrichthyes). *Journal of Experimental Biology* **209**:2920–28.

Read R. (1986) Osteoderms in the Lacertilia: an investigation into the structure and phylogenetic implications of dermal bone found under the skin of lizards. PhD Thesis, Department of Biological Sciences, California State University, Fullerton, CA. Pp. 142.

Reisz R., Dilkes D. and Berman D. (1998) Anatomy and relationships of *Elliotsmithia longiceps* Broom, a small synapsid (Eupelycosauria: Varanopseidae) from the Late Permian of South Africa. *Journal of Vertebrate Paleontology* **18**:602-611.

Reynoso V. H. (1997) A "beaded" sphenodontian (Diapsida: Lepidosauria) from the Early Cretaceous of central Mexico. *Journal of Vertebrate Palaeontology* **17**:52–59.

Richter A. (1994) Lacertilia aus der Unteren Kreide von Uña und Galve (Spanien) und Anoual (Marokko). *Berliner geowissenschaftliche Abhandlungen* **14**:1-147.

Romer A. S. (1957) Osteology of the reptiles. *The Quarterly Review of Biology* **32**:406-406.

Ruibal R. and Shoemaker V. (1984) Osteoderms in anurans. *Journal of Herpetology* **18**:313–328

Rücklin M., Donoghue P., Johanson Z., Trinajstic K., Marone F. and Stampanoni M. (2012) Development of teeth and jaws in the earliest jawed vertebrates. *Nature* **491**:748–751.

Saitta E. T. (2015) Evidence for sexual dimorphism in the plated dinosaur *Stegosaurus mjosi* (Ornithischia, Stegosauria) from the Morrison Formation (Upper Jurassic) of Western USA. *PLoS ONE* **10**:e0123503.

Scheyer T. M. (2007) Skeletal histology of the dermal armor of Placodontia: the occurrence of 'postcranial fibro-cartilaginous bone' and its developmental implications. *Journal of Anatomy* **211**: 737–53.

Scheyer T.M. and Desojo J. (2011) Palaeohistology and external microanatomy of Rauisuchian osteoderms (Archosauria: Pseudosuchia). *Palaeontology* **54**:1289-1302.

Scheyer T.M. and Sánchez−Villagra M.R. (2007) Carapace bone histology in the giant pleurodiran turtle *Stupendemys geographicus*: Phylogeny and function. *Acta Palaeontologica Polonica* **52**:137–154.

Scheyer T. M. and Sander P. M. (2004) Histology of ankylosaur osteoderms: implications for systematics and function. *Journal of Vertebrate Palaeontolog*y **24**: 874-893.

Scheyer T. M. and Sander P. M. (2009) Bone microstructures and mode of skeletogenesis in osteoderms of three pareiasaur taxa from the Permian of South Africa. *Journal of Evolutionary Biology* **22:**1153-1162.

Schucht P. J., Rühr P. T., Geier B., Glaw F. and Lambertz M. (2020) Armored with skin and bone: The integumentary morphology of the Antsingy leaf chameleon *Brookesia perarmata* (Iguania: Chamaeleonidae). *Journal of Morphology* **280**:214–244.

Seidel M. R. (1979) The osteoderms of the American alligator and their functional significance. *Herpetologists' League* **35**:375-380.

Sire J-Y. (1995) Ganoine formation in the scales of primitive actinopterygian fishes, lepisosteids and polypterids. *Connective Tissue Research* **33**:213–22.

Sire J-Y., Donoghue P. C. J. and Vickaryous M. K. (2009) Origin and evolution of the integumentary skeleton in non-tetrapod vertebrates. *Journal of Anatomy* **214**:409–40.

Smith M. M. and Hall B. K. (1990) Developmental and evolutionary origins of vertebrate skeletogenic and odontogenic tissues. *Biological Reviews of the Cambridge Philosophical Society* **65**:277–374.

Smith M. M., Sansom I. J. and Smith M. P. (1996) 'Teeth' before armour: the earliest vertebrate mineralized tissues. *Modern Geology* **20**:303–3.

Song J., Ortiz C. and Boyce M. C. (2011) Threat-protection mechanics of an armored fish. *Journal of the Mechanical Behavior of Biomedical Materials* **4**:699–712.

Spence R., Wootton R. J., Przybylski M., Zieba G., MacDonald K., and Smith C. (2012). Calcium and salinity as selective factors in plate morph evolution of the three-spined stickleback (*Gasterosteus aculeatus*). *Journal of Evolutionary Biology* **25**:1965-1974.

Stanley E., Ceríaco L., Bandeira S., Valerio H., Bates M. and Branch W. (2016) A review of *Cordylus machadoi* (Squamata: Cordylidae) in southwestern Angola, with the description of a new species from the Pro-Namib desert. *Zootaxa* **4061**:201–226.

Sues H-D. and Reisz R. R. (2008) Anatomy and phylogenetic relationships of *Sclerosaurus armatus* (Amniota: Parareptilia) from the Buntsandstein (Triassic) of Europe. *Journal of Vertebrate Paleontology* **28**:1031-1042.

Sun C-Y. and Chen P-Y. (2013) Structural design and mechanical behavior of Alligator (*Alligator mississippiensis*) osteoderms. *Acta Biomaterialia* **9**:9049–64.

Teaford M. F., Smith M. M., Ferguson M. W. J. (editors) (2000) *Development, Function and Evolution of Teeth*. Publisher: Cambridge University Press, New York City, NY, USA. Pp. 314.

Vickaryous M. K. and Hall B. K. (2006) Osteoderm morphology and development in the nine-banded armadillo, *Dasypus novemcinctus* (Mammalia, Xenarthra, Cingulata). *Journal of Morphology* **267**:1273-1283.

Vickaryous M. K. and Hall B. K. (2008) Development of the dermal skeleton in *Alligator mississippiensis* (Archosauria, Crocodylia) with comments on the homology of osteoderms. *Journal of Morphology* **269**:398–422.

Vickaryous M. K. and Sire J-Y. (2009) The integumentary skeleton of tetrapods: origin, evolution, and development. *Journal of Anatomy* **214**:441–64.

Vickaryous M. K., Meldrum G. and Russell A. P. (2015) Armored geckos: A histological investigation of osteoderm development in *Tarentola* (Phyllodactylidae) and *Gekko* (Gekkonidae) with comments on their regeneration and inferred function. *Journal of Morphology* **276**:1345–1357.

Weiner S. and Wagner H. D. (1998) The material bone: structure-mechanical function relations. *Annual Review of Materials Science* **28**:271–98.

Witzmann F. (2009) Comparative histology of sculptured dermal bones in basal tetrapods, and the implications for the soft tissue dermis. *Palaeodiversity* **2**:233–70.

Witzmann F. and Soler-Gijón R. (2010) The bone histology of osteoderms in temnospondyl amphibians and in the chroniosuchian *Bystrowiella*. *Acta Zoologica* **91**:96–114

Yang W., Chen I. H., McKittrick J. and Meyers M. A. (2012) Flexible dermal armor in nature. *Journal of Morphology* **64**:475-285

Zylberberg L., Castanet J. and de Ricqlès A. (1980) Structure of the dermal scales in Gymnophiona (Amphibia). *Journal of Morphology* **165**:41-54.

Zylberberg L. and Castanet J. (1985) New data on the structure and the growth of the osteoderms in the reptile *Anguis fragilis* (Anguidae, Squamata). *Journal of Morphology* **186**:327–342.

Zylberberg L. and Wake M. H. (1990) Structure of the scales of *Dermophis* and *Microcaecilia* (Amphibia: Gymnophiona), and a comparison to dermal ossifications of other vertebrates. *Journal of Morphology* **206**:25–43.

Zylberberg L., Geraudie J., Meunier F., Sire J-Y. (1992) Biomineralization in the integumental skeleton of the living lower vertebrates. In: *Bone, Vol. 4: Bone Metabolism and Mineralization.* Editor: Hall, B.K. Publisher: CRC Press, Boca Raton, FL, USA. Pp. 171–224.

Zylberberg L., Sire J-Y. and Nanci A. (1997) immunodetection of amelogenin-like proteins in the ganoine of experimentally regenerating scales of *Calamoichthys calabaricus*, a primitive actinopterygian fish. *The Anatomical Record* **249**:86–95.

2 CHAPTER 2 Techniques, materials and methods

2.1   Introduction to Techniques

Publication information			Techniques employed					
Taxa	First Author	Year	Histological staining	Polarised light	SEM	TEM	CT	Sample preparation method
Heloderma suspectum	M. Moss	1969	✓	✗	✗	✗	✗	Fixed wet
Corucia zebrata	M. Moss	1969	✓	✗	✗	✗	✗	Fixed wet
Egernia kingii	M. Moss	1969	✓	✗	✗	✗	✗	Fixed wet
Anguis fragilis	L. Zylberberg	1985	✓	✗	✓	✓	✗	Fixed wet and dried
Tarentola mauritanica	V. Levrat-Calviac	1986	✓	✗	✓	✓	✗	Fixed wet
Lanthanotus borneensis	J. Maisano	2002	✗	✗	✗	✗	✓	Not fixed
Varanus salvator	G. Erickson	2003	✓	✓	✗	✗	✗	Fixed wet
Shinisaurus crocodilurus	G. S. Bever	2005	✗	✗	✗	✗	✓	Not fixed
Alligator mississippiensis	M.K. Vickaryous	2008	✓	✗	✗	✗	✗	Fixed wet
Glyptosaurinae	V. de Buffrénil	2010 and 2011	X	✓	✓	✗	✗	Dried

Tarentola mauritanica	M. K. Vickaryous	2015	✓	✗	✗	✗	✗	Fixed wet
Tarentola annularis	M. K. Vickaryous	2015	✓	✗	✗	✗	✗	Fixed wet
Geckolepis maculata	D. Paluh	2017	✓	✗	✗	✗	✓	Fixed wet and not fixed
Alligator mississippiensis	B. Dubansky	2018	✓	✓	✗	✗	✓	Fixed wet and not fixed
Varanus komodoensis	J. Maisano	2019	✗	✗	✗	✗	✓	Not fixed

Table 2.1: List of techniques employed in the study of osteoderms from various reptilian taxa, with first author names, years and sample preparation method for each species.

In this chapter, techniques employed in this study are outlined and a brief description of the background to each technique used is presented. Specific explanations of how the results were obtained using these techniques are described in the materials and methods section. Classical techniques are introduced first, then more recently developed techniques, with reference to the authors that pioneered studies using these techniques to elucidate the structures present within the ODs of various taxa.

As can be seen in Table 2.1, it is clear that most older papers have applied the use of histological staining methods to elucidate the composition of ODs, whereas more modern papers have applied the use of 3D data using CT. This is likely because histological techniques are historically utilised, are relatively cheap and quick to perform, and result in a basic understanding of the nature of the tissue present. Further techniques that are more modern, such as CT, SEM or TEM correspond to finer scales of the tissue that may not be required for a basic understanding and involve more hazardous reagents, take more time to perform, require the use of expensive equipment, and often cost more money to undertake. The table shows that these more modern techniques have been used infrequently in the available literature

and thus highlight an area of research that can be addressed by the study presented herein.

2.2 Materials and Methods

2.2.1 Sampling locations

In most cases, ODs were prepared and examined from middorsal, midlateral, and midventral portions of the body, but some specimens were complete enough to also afford a comparison of the dermis from the dorsum of the tail, including *Heloderma suspectum* and *Egernia stokesii.*

2.2.2 Osteoderm tissue samples

For the purposes of this study, samples of reptile skin from different anatomical locations were obtained and analysed. The skin was dissected from the underlying bone and muscle with a pair of fine dissection scissors and stored at -20°C until required. All species had skin samples taken from the post-cranial dorsum. Where further samples were taken, these were dissected from the dorsal part of the left forearm, the right side of the neck, and the dorsal part of the tail where possible. The majority of samples were provided by ZSL London Zoo Pathology Department, through Prof. Susan Evans (Department of Cell and Developmental Biology, UCL, U.K.), with additional material from Dr. Eraqi Khannoon (Fayoum University, Egypt: *Tarentola*) and Dr. Ryoko Matsumoto (Kanagawa Prefectural Museum Natural History, Japan: CT scan of *Lanthanotus borneensis*)

List of all species analysed:

*Heloderma suspectum (*Gila monster)

Elgaria multicarinata (Southern alligator lizard)

Ophisaurus ventralis (Glass lizard)

Varanus komodoensis (Komodo dragon)

*Varanus niloticus (*Nile monitor)

Lanthanotus borneensis (Earless monitor)

Gekko gecko (Tokay gecko)

Tarentola annularis (White-spotted wall gecko)

Tiliqua rugosa (Shingle-back lizard)

Egernia stokesii (Gidgee skink)

Corucia zebrata (Solomon Islands skink)

Salvator merianae (Argentine black and white tegu)

Crocodylus niloticus (Nile crocodile)

2.2.3 Fixation

Fixation is a method of chemically treating a biological sample to stop biochemical reactions, preserve tissue components and protect from decay. When any of the samples listed above were removed from -20°C, they were allowed to defrost at room temperature, then fixed in a solution of 4% formaldehyde in phosphate buffered saline (PBS) for at least 24 hours, using at least 20x the volume of the tissue to be fixed. This is a cross-linking fixative, whereby the fixation process produces covalent bonds between macromolecules such as protein and DNA in the sample. This prevents any degradation of the sample, either from microbial action or microstructural damage.

2.2.4 Decalcification

When working with mineralised tissues, one of the most significant obstacles to overcome is the fact that tissues often need to be sectioned very thinly for microscopy, but the tissues themselves are very brittle and hard due to their natural, intrinsic mineralised state. The mineral crystals present in the material mean that the sample must be demineralised prior to sectioning, otherwise the sample will tear significantly and the section will be unusable. Another problem is that the microtomes used to section the sample sometimes utilise diamond blades for sectioning. These diamond blades are very expensive due to a complicated manufacturing process and may become damaged when sectioning if the sample is not sufficiently demineralised. This obstacle was overcome by the use of glass knives, and/or when required, complete decalcification whenever the samples were to be sectioned, however, this process had to be optimised first to ensure no equipment was broken and also to ensure no part of the precious skin sample was lost. Often, the result of insufficient decalcification was a torn section, thus a lot of time was spent optimising the demineralisation process. A solution of 0.15M EDTA, in 0.06M sodium cacodylate buffer, adj. 7.4pH at 4°C for 4 weeks was eventually found to be sufficient to demineralise the OD, but each specimen required different incubation times in this

solution due to differences in OD size and surface area to volume ratio. EDTA is the active ingredient in this solution, acting to chelate Ca2+ ions in the tissue and washing with fresh solution removes these ions from the tissue. Thus, many washes in this solution act to slowly remove the calcium from the crystals within the sample, until none remains. After this process was optimised, the thin sections could be used in microscopy techniques. Decalcification was not used for BSE-SEM or EDX sample preparation as the presence of mineral was required for these techniques.

2.2.5 Histology

Histology is the study of the microscopic structures of cells and tissues. In order to differentiate biological structures more accurately, stains are often used to colour certain types of biological structures depending on their biochemical composition and inherent molecular electrical charges. Histological methods allow the researcher to view both mineralised and non-mineralised tissues within a sample.

Histochemical stain	Utility	Colour results
H&E (Haematoxylin and eosin)	Shows general nuclear and cytoplasmic morphology.	Nuclei: Blue Cytoplasm, collagen: Pink
Masson's Trichrome	Shows collagen and keratin	Collagen: Green/Blue Nuclei: Black Muscle, cytoplasm, keratin: Red
E.V.G./V.V.G. (Elastic/Verhoeff Van Gieson)	Shows elastic fibres	Collagen: Red Elastic fibres: Black
Alcian Blue	Shows acid mucosubstances/ carboxylated glycosaminoglycans and acid mucins	Acid mucosubstances: Blue; Nuclei: Red; Cytoplasm: Pink
Toluidine Blue	Standard Light: Shows general morphology/ mineralisation of bone matrix Polarised light: Arrangement, orientation of collagen	Acidic tissue compounds (incl. DNA, RNA): Blue Collagen: Birefringent (doubly refracting)

Table 2.2: A list of included histological stains, a description of their general characteristics and colour interpretation of the results.

Samples were embedded in paraffin wax and then sectioned either coronally or parasagittally, at 5µm thickness, with an HM Microm 355S automatic rotary microtome (Thermo Fisher Scientific). These sections were stained with haematoxylin and eosin (H&E; Kiernan et al., 2010), Alcian blue (Klymkowsky and Hanken, 1991), Masson's trichrome (Calvi et al., 2012) or Elastic Verhoeff van Gieson (V.V.G.; Puchtler and Waldrop, 1979) (Table 2.2). The slides were scanned using a Leica SCN400 scanner to create a digital image.

2.2.6 Polarised Light Microscopy

In non-polarised beams of light, the waveform vector of the electric field oscillates with equal distribution in all planes. Polarisers act to block any plane of light other than that allowed through the polariser, resulting in the production of polarised light when a non-polarised beam is shone through the polariser.

The polarised light microscope is designed to exploit the nature of polarised light and allows enhanced contrast of birefringent (doubly-refracting) samples when compared to techniques such as brightfield illumination. The microscope is fitted with a polariser and also a second polariser known as an analyser. These are placed in the optical pathway between the light source, the sample, and the lenses. Image contrast arises from the interaction of plane-polarised light with the specimen to produce two individual wave components that are each polarised in mutually perpendicular planes. The velocities of these components are different and vary with the propagation direction through the specimen. After exiting the specimen, the light components become out of phase, but interfere and are recombined when they pass through the analyser.

For this technique, decalcified, fixed samples were embedded in paraffin wax, sectioned either coronally or parasagittally, at 5-µm thickness, collected on glass slides, stained with 0.5% aqueous toluidine blue on a heating block at 70ºC for 15s and washed with 70% ethanol. The resultant metachromatic stain was observed through bipolarised (crossed polarised) light with a lambda compensator on a 510 Zeiss LSM 510 Meta Confocal Laser scanning microscope at 10x and 20x magnifications. 20x magnification images were stitched together in Photoshop CS6 (Abode) and then cropped.

2.2.7 Multi-rotation polarised light microscopy

Multi-rotation polarised light microscopy is achieved by rotating crossed-polarising filters around a stationary sample, a new approach to increase the information content in polarised light microscopy of all tissues, introduced by Boyde et al., (2019). In the present study, the overwhelming polarised light microscopy signal is attributable to the positive form birefringence of collagen. By sampling at close rotation intervals of 15°, the signal due to collagen fibre orientation was constant (to within 96.7%: cos 15° = 0.9659), irrespective of its axis in the plane of section. For the present study, we (i.e. Alex Kirby and Alan Boyde) used automated rotation of the polarising and analysing filters at six 15° intervals, with linearly polarised light images recorded at

each orientation. For reference, the objectives used were 4/0.13, 10/0.30, 20/0.50 and 40/0.75. The images were merged using ImageJ in the colour circular sequence red (R), yellow (Y), green (G), cyan (C), blue (B), magenta (M; importantly, ensuring that the intensities generated by the intermediate Y, C, M colours matched those of the three primary colours, RGB). Colour in the composite image shows the orientation within the section plane, with four repeat cycles in 360°. Brightness was proportional to the cosine of the strike angle with respect to section plane, being brightest in plane, and black when perpendicular to that plane, i.e. parallel to the optic axis. For the present study, we used H&E- and Masson's trichrome-stained sections. Prior staining makes some difference to the light absorption, but this did not contribute to the output colour in the combined images.

2.2.8 Dehydration and resin embedding for EM

Organic resins are used for embedded samples for use in electron microscopy. These samples are not decalcified so that any mineral present can be visualised. Because samples are in aqueous solution of PBS following fixation, the organic resin will not infiltrate the sample if water present due to the hydrophobicity of the resin. Thus, aqueous solutions must be removed and the sample resuspended in a purely organic solution that contains no water. This is done through dehydration with an ethanol concentration gradient as follows: fixed samples were dehydrated by submerging in an ethanol/distilled water series of gradients 20, 30, 40, 50, 60, 70, 80, 90, 100%, for 1 hour each. Then the samples were then infiltrated with "EMbed 812" (EMS catalogue number 13940) epoxy resin or Ultra Bed Low Viscosity Epoxy Kit (EMS Catalogue number 14310) diluted with absolute ethanol in the ratios 3:1, 2:1, 1:1, 1:2, 1:3, for 4 hours at each concentration. The 1:3 ratio was replaced with 100% epoxy resin, and then this was replaced again with fresh 100% epoxy resin. Samples submerged in 100% epoxy resin were placed in plastic moulds then cured to form a solid block by heating at 60°C for 48 hours.

2.2.9 Sample preparation for EM

Following dehydration and resin embedding, subsequent solid resin blocks were removed from the plastic mould and cut into 1mm thick sections using a Buehler Isomet low speed saw at 100rpm with a diamond blade. These sections were then polished using sand paper with a grit series of 1250, 2500 and 5000 and a Buehler MetaServ 250 grinder-polisher, under flowing water, for 5-10mins per grade at 250RPM. Next, polishing diamond compounds with 3µm, 1µm and finally 0.25µm

diameter bead size were used at 250RPM, for 5-10mins, to create an increasingly fine polished face.

ODs were also prepared by freeze fracturing. A single OD was dissected from a frozen sample, fixed but not decalcified, then completely immersed in liquid nitrogen for 5mins to increase the brittleness of the sample. After the OD was sufficiently cooled, it was removed from the liquid nitrogen, placed on a metal tray, and then shattered into many pieces by hand, with a wooden mallet. These pieces were then prepared for SEM the same as for cut and polished sections as outlined below.

2.2.10 Scanning Electron Microscopy (SEM)

SEM was used in this study to provide high resolution images - theoretically down to 3nm- of the detailed structure of the mineralised tissue. This allowed the collection of data that pertains to the fourth order in species that have not been examined in this way previously. The basic concept of SEM is that the stained sample scatters electrons, and different types of electrons are released. Electron microscopy can produce higher resolution images than light microscopy because of the use of electrons. Two different modes of SEM imaging were utilised in this report: secondary electron (SE) and backscatter electron (BSE). Each mode uses its own detector, as shown in figure 2.1, and each produce unique and characteristic images with different use cases.
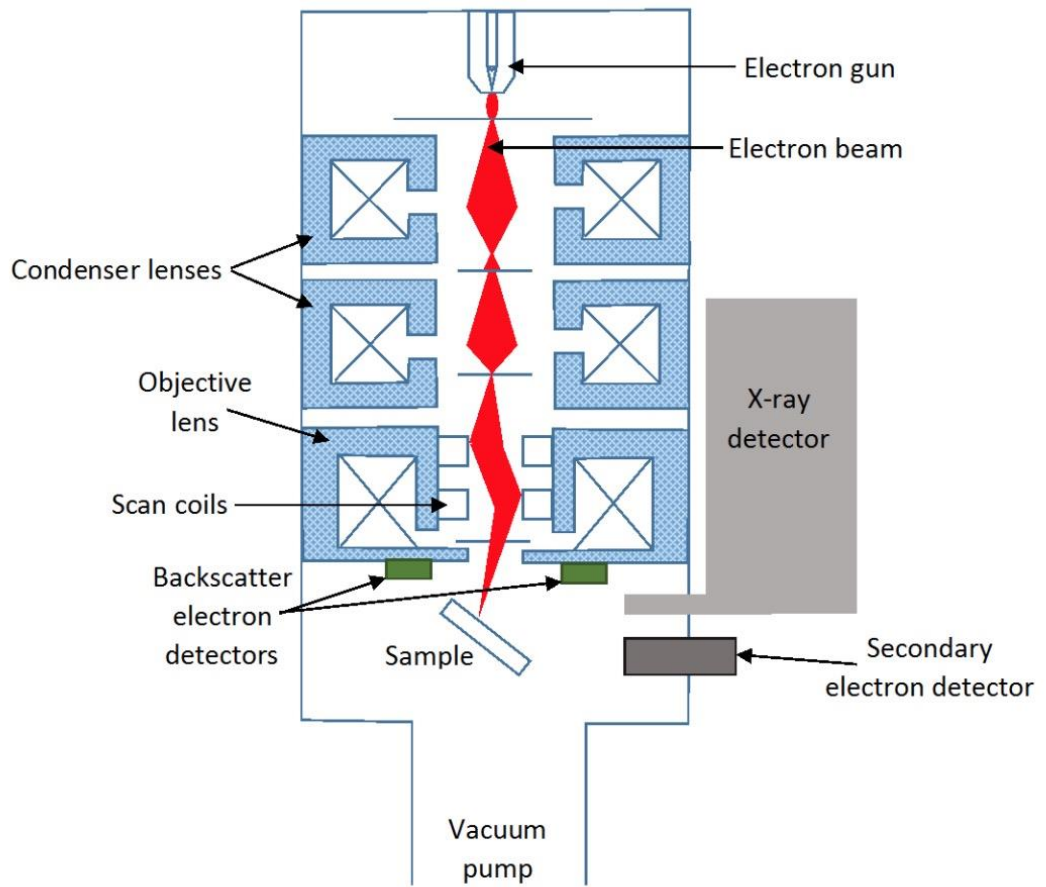
Figure: 2.1 SEM schematic

Figure 2.1 depicts a schematic representation of an SEM. The electron gun generates a beam of electrons and accelerates them through a series of condenser lenses, resulting in a focused electron beam on the sample surface. When the sample is struck by these high-energy electrons, electromagnetic radiation is emitted, which is then detected by either the Secondary electron (SE), In-lens (IL) or the back scattered electron (BSE) detector, and the signal is converted into an image on the computer monitor via the computing unit.

SE are low energy scattered electrons emitted close to the sample surface. These electrons are released from the atoms in the sample when enough energy is absorbed for an electron to escape from the electron shell. The resolution of the SE mode tends to be better than the other modes because of the small escape depth of the electrons, however the contrast is poorer and there is no way of differentiating different densities of materials in the samples when using this mode.

The BSE mode detects high-energy electrons that have been scattered elastically from a larger sample depth than the electrons in SE mode. By placing the BSE detector above the sample, only electrons that have been scattered as a result of the sample's composition will be detected. BSE imaging results in much more contrast in the final image when compared to SE mode. The intensity of the signal is proportional to the difference in average atomic number between areas. This is why regions of highly mineralised tissue, composed primarily of Ca and P elements (with relatively high atomic numbers of 20 and 16 respectively) will appear brighter than the surrounding non-mineralised tissue, which is composed of primarily H, C, N and O (with low atomic numbers of 1, 6, 7 and 8) elements. For these reasons, the BSE mode was used for the mineralised samples in this study.

Cut and polished sections as outlined under the "sample preparation" heading were attached to SEM specimen stubs with carbon tape and carbon paste, painted with silver paint, coated with carbon using a Quorum K975X Carbon coater and imaged using a Zeiss Sigma VP scanning electron microscope at 10-20KV, an aperture of 30µm working distance 9-11mm, using the back-scattered electron detector. The SE detector was also used and this was combined within the same image for red/green stacked density dependant images (Bertazzo et al., 2013). Additionally, a Hitachi S-3400N scanning electron microscope was used with a voltage of 10kV, aperture of 30µm and a working distance of 7mm-10mm depending on the calibration of the

microscope for acquisition of the best quality images. BSE detectors allowed for the visualisation of the relative density (based on atomic number) of elements in the sample.

2.2.11 Transmission Electron Microscopy

TEM is very similar to SEM, utilising a beam of electrons to image a sample, instead of detecting radiation emitted from a sample, a beam of electrons is transmitted through a thin section of the sample to form an image on a screen. Historically this has been a fluorescent plate but in modern times the microscope is usually fitted with a retrograde CCD and linked to a computer. As in SEM, there are many electromagnetic lenses that focus and adjust the beam according to the operator's intent. The electrons in the sample interfere with the electron beam as both are negatively charged and thus the image forms from differences in electron density in the sample section.

Sectioned, resin-embedded, decalcified and fixed samples were transferred to a TEM in order to observe the internal structure and for electron diffraction patterns to be obtained. A JEOL JEM 2100Plus Transmission Electron Microscope with a consolidated EDX Oxford Instrument at Imperial College London, and a JOEL 1010 TEM at the Institute of Ophthalmology at UCL were used. The information obtained with the TEM allowed for a resolution down to 50nm. For the TEM imaging the software used was TEM centre for JEM 2100Plus and Gatan Digital Micrograph. An operation voltage of 200kV was used for the electron diffraction to be obtained. For the analysis of the electron diffraction, the Gatan Microscopy Suite software was used for the processing of the image, as well as the Crystal Maker, Single Crystal and Crystal Diffract software for the identification of the chemical properties. Samples were embedded in resin as outlined except occasionally araldite resin was used instead of Epon812. The resulting resin block was then sectioned using a Leica ultracut EM FC7 on an ultracut UC7 chassis, into ultra-thin, 80nm sections, mounted on copper grids, stained with Reynold's lead citrate adjusted to pH12 for 15mins and then stained with Uranyl acetate 1% for 15mins and imaged on the Jeol 1010 TEM at 80kv.

For etched TEM and SEM sections, 1 μm sections were placed onto coverslips, etched with sodium methoxide solution 0.5M in methanol (Sigma Aldrich) for 1 hour. Then washed with methanol twice, then HMDS hexamethyldisilzane twice to remove residual water, carbon coated in a Cressington Scientific High Vacuum Carbon Coater

208 and imaged using the methods outlined above for Transmission and Scanning Electron Microscopy.
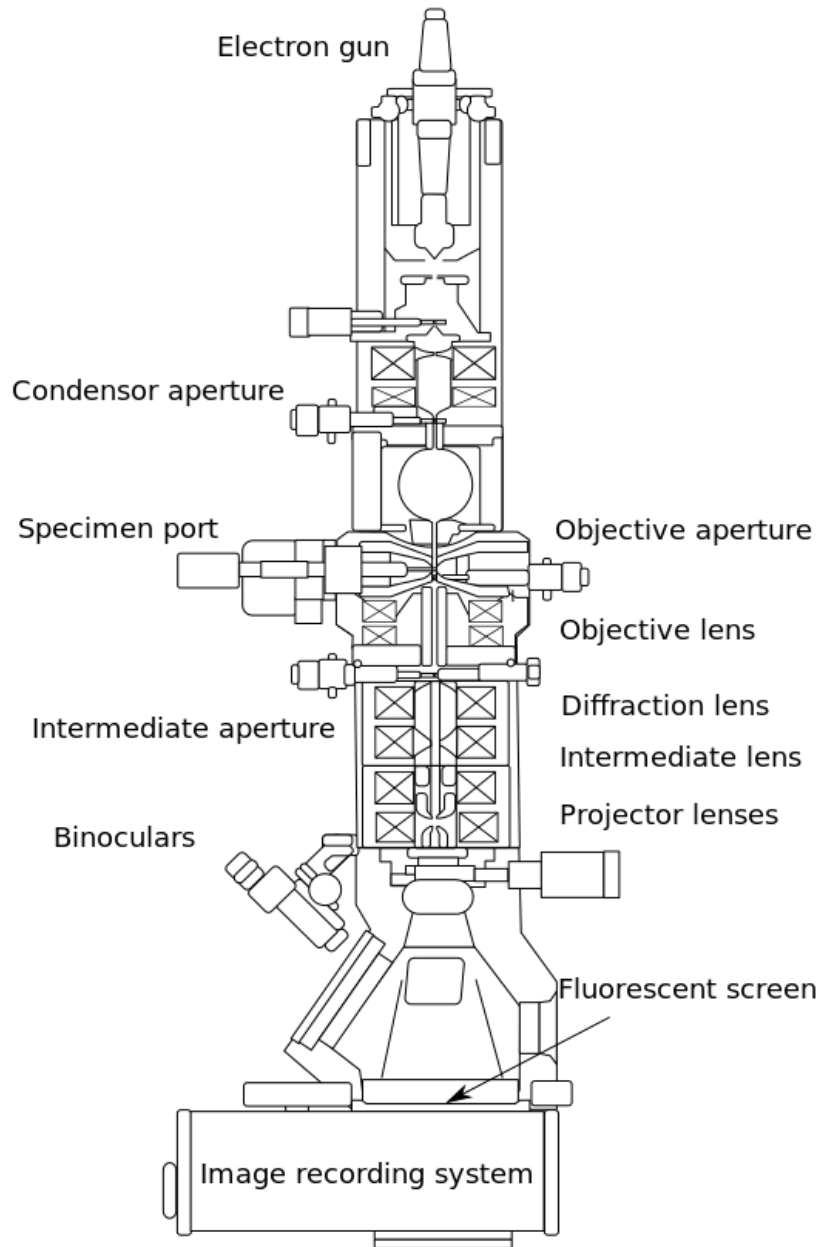
Figure 2.2:

TEM schematic

2.2.12 Energy Dispersive X-ray Spectroscopy

Energy dispersive X-ray spectroscopy (EDX) measures the X-rays that are generated when the electron beam of the electron microscope hits the sample. This occurs because an electron (SE) is knocked out from the inner shell of the sample's atom, and an electron from a higher energy level falls down to fill the now empty inner shell, emitting energy in the form of an X-ray. This X-ray has an energy that is equal to the difference between the outer and inner energy levels, making it unique to each specific element. EDX therefore measures this X-ray energy in order to determine the element that it came from, and so can create a spectrum of all the elements found in a selected region of a sample, as shown in figure 2.4. This provides compositional information across the surface of the sample, in this case Energy Dispersive X-ray (EDX) function was used for elemental mapping of the mineralisation.
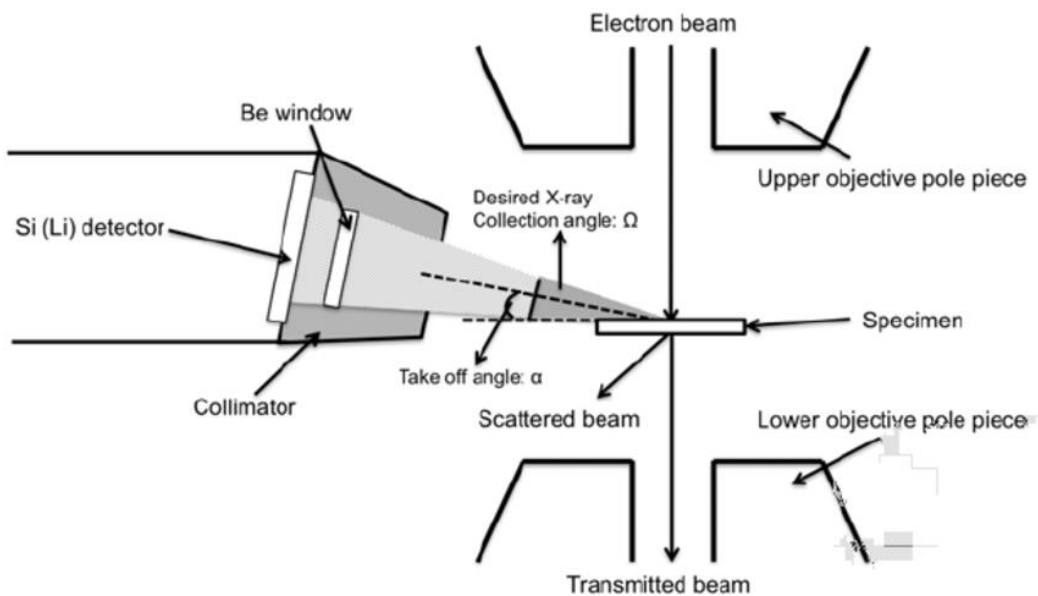
Figure 2.3: EDX schematic
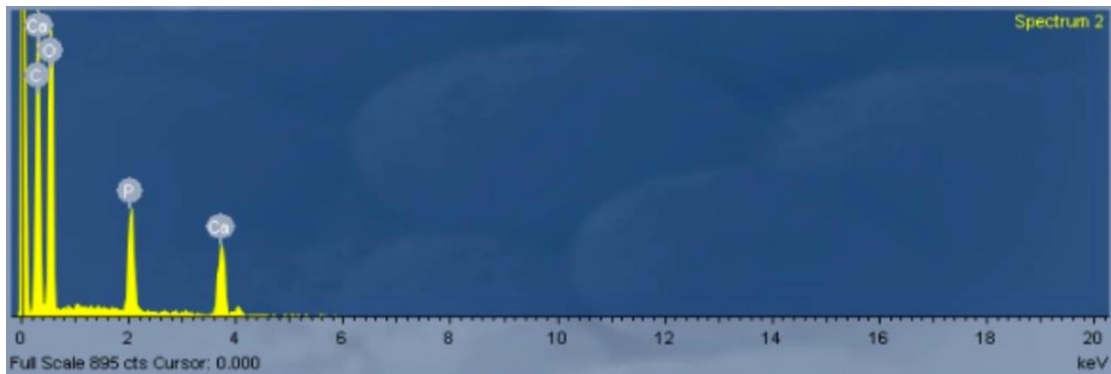
Figure 2.4: An example of an EDX spectrum

For the EDX analysis, the INCA Energy Software suite was used, with an acquisition time of 15-25 seconds per reading. The EDX spectra obtained were semi-quantitative, thus it was not possible to compare quantitative elemental composition between samples, but afforded the ability to understand the distribution of the elements within the tissue, and to obtain data on the density of the mineral content, by element, in each individual sample.

2.2.13 Computed tomography

Computed tomography scanning involves directing an X-ray beam at a rotating sample, and then detecting the X-ray beam on a sensor and processing the data produced form the sensor in a computer. The measurements taken from the different angles are then processed to produce cross-sectional tomographic virtual "slices" of the scanned object, appearing in black and white. Because differences in sample density will affect differences in X-ray transparency, CT can be used to compare the densities of materials in the same sample. Both soft and hard tissues will appear in the resulting data set, but hard tissues appear bright white on the greyscale histogram due to the crystals present within them having a low X-ray transmission, whereas the soft tissues will appear as a dark grey colour on the histogram, due to absence of crystals and thus their high X-ray transmission.
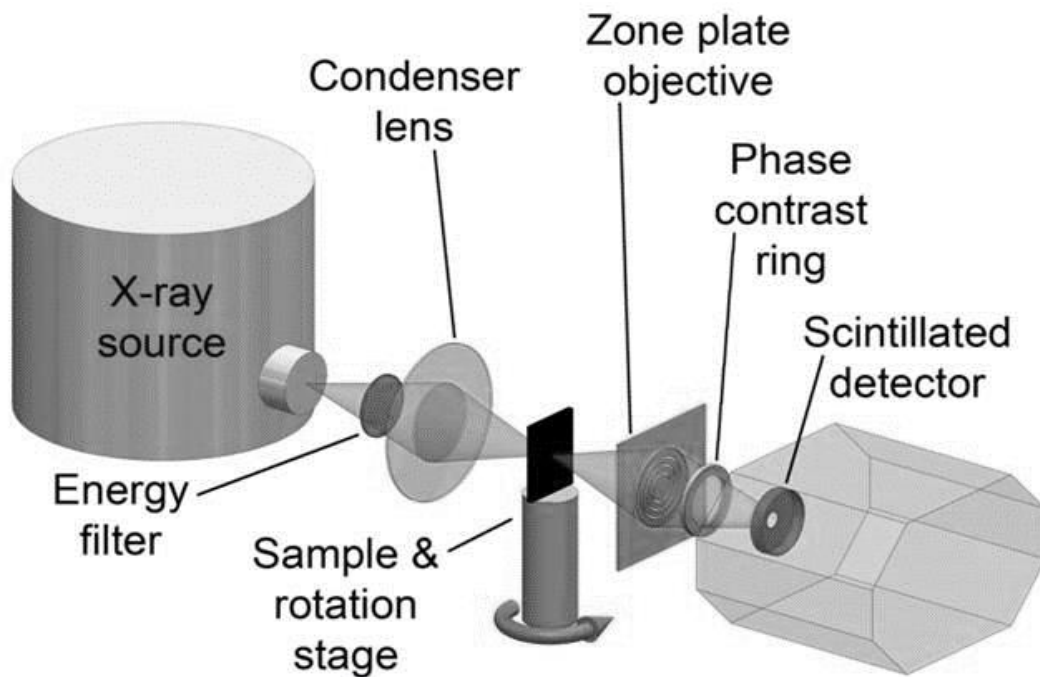
Figure 2.5: CT scanning (rotating sample) schematic

For standard CT HRXCT as shown in Chapters 3 and 6, dorsal skin samples from sampled species and the whole head of an adult Gila monster *(Heloderma suspectum)* was dissected from the body at the base of the skull, wrapped in parafilm and imaged directly in a Nikon XT H 225 Computed tomography (CT) scanner at the Electrochemical Innovation Lab in the Department of Chemical Engineering at UCL for 1601 projections.

For higher magnification (µ-CT) CT scanning as shown in Chapters 3 and 4, OD samples were dissected and washed 5 times in distilled H2O then 5 times in 70% ethanol and left to dry for 48 hours. The non-mineralised soft tissue was removed using a scalpel blade and an A Series Compact LASER micromachining system (Oxford Laser, Oxford, UK) was used to cut out a cylinder 1mm wide, then this cylinder was cut to incrementally smaller cylinders of 500µm diameter, then 100µm diameter, then finally 65µm in diameter. The thinner, upper part of this series of cylinders was imaged using either a ZEISS Xradia 520 Versa (500 and 100µm diameter cylinders) or a ZEISS Ultra 810 X-ray (65 µ-m diameter cylinder) microscopes (Carl Zeiss X-ray Microscopy Inc. Pleasanton, CA, USA). Normal scanning parameters were a working voltage of 80Kv, 7W power and 40x objective, an exposure of 35 seconds and 1601 projections. The raw transmission images from both X-ray CT imaging experiments were reconstructed using a commercial image reconstruction software p packages

(Zeiss XMReconstructor, Carl Zeiss X-ray Microscopy Inc., Pleasanton, CA, and CT Pro 3D, Nikon Metrology, Tring, UK), which employ a filtered backprojection algorithm. The data from all CT scans were volumetrically rendered in three dimensions and manual compartmental tracing and density-dependant data partitioning were performed using FEI Avizo 9.0.1 software (VSG, Visualisation Sciences Group, Burlington, MA, USA) resulting in the final 3D model with transparent flesh and colour-coded density labels. All resulting images were optimised and/or colourised in Photoshop 5.0 (Adobe Systems Inc., San Jose, CA).

A z-series is generally difficult to represent as a 2-D image for publication purposes. A montage will allow the 3-D dataset to be visualised in 2-D, but results in each frame being very small. There are several ways to "flatten" the 3D stack. Z Project is a method of analysing a stack by applying different projection methods to the pixels within the stack. A start and stop slice are chosen, which will determine the range of the stack that will be included in the z projection. The default for these values is the endpoint slices of the stack. There are six different projection types to choose from: average intensity, maximum intensity, minimum intensity, sum slices, standard deviation, and median.

2.2.14 X-ray Plate Imaging

X-ray plate imaging involves placing a sample between an X-ray source and an X-ray sensor. It works in a similar way to CT, but involves just one image capture instead of many, therefore results in a 2D dataset, rather than 3D one. X-ray plate imaging was one of the first methods used for X-ray imaging, being used to diagnose bone fractures or dental pathologies in a clinical setting. It is useful for obtaining a quick depiction of the mineralised tissues within a sample.

Skin samples from sampled taxa were removed from storage (either removed from -20°C to defrost or removed from fixation solution to dry) and placed on a Carestream RVG 6200 sensor, using double-sided adhesive tape. Then a KaVo NOMAD™ Pro 2 handheld x-ray unit was placed facing the sensor, 200mm away. After evacuating the area to be exposed to the beam, the X-rays were emitted at a 30cm of distance from the sensor and the resulting digital image file saved. The settings used for the imaging were 0.12 exposure time, 60kV anode operating potential, 2.5mA anode current, beam profile of 34x45mm, focal spot to sample distance 200mm. The digital file was scaled using Fiji (ImageJ) and a control image of a radiopaque ruler.

2.3   References

Bertazzo S., Gentleman E., Cloyd K. L., Chester A. H., Yacoub M. H. and Stevens M. M. (2013) Nano-analytical electron microscopy reveals fundamental insights into human cardiovascular tissue calcification. *Nature Materials* *12*:576–583.

Bever G. S., Bell C. J. and Maisano J. A. (2005) The ossified braincase and cephalic ODs of *Shinisaurus crocodilurus* (Squamata, Shinisauridae). *Palaeontologia Electronica* **8**:1–36.

Boyde A., Felder A. and Mills D. (2019) New approach to increase infor-mation content in polarised light microscopy of skeletal and dental tissues. Proc Microscience Microscopy Congress. Available at: https://www5.shocklogic.com/scripts/jmevent/programme.php?Client_Id=%27RMS%27&Project_Id=%27MMC2019%27&System_Id=1 [Accessed: 10 October 2019].

Calvi E. N., Nahas F. X. amd Barbosa M. V. (2012) An experimental model for the study of collagen fibers in skeletal muscle. *Acta Cirúrgica Brasileira* **27:**681–686.

De Buffrénil V., Sire J. Y. and Rage J. C. (2010) The histological structure of glyptosaurine osteoderms (Squamata: Anguidae), and the problem of osteoderm development in squamates. *Journal of Morphology* **271**:729–737.

De Buffrénil V., Dauphin Y., Rage J-C. and Sire J-Y. (2011) An enamel-like tissue, osteodermine, on the osteoderms of a fossil anguid (Glyptosaurinae) lizard. *Comptes Rendus de l'Academie des Sciences Palevol* **10:**427-437.

Dubansky B. H. and Dubansky B. D. (2018) Natural development of dermal ectopic bone in the american alligator (*Alligator mississippiensis*) resembles heterotopic ossification disorders in humans. *The Anatomical Record* **301**:56–76.

Erickson G. M., Ricqlès A. de, Buffrénil V. de, Molnar R. E. and Bayless M. K. (2003) Vermiform bones and the evolution of gigantism in *Megalania* — How a reptilian fox became a lion. *Journal of Vertebrate Palaeontology* **23**:966-970.

Kiernan J., Lillie R. and Pizzolato P. (2010) Haematoxylin Eosin (H&E) Staining Protocols Online. Available at: https://www.protocolsonline. com/histology/dyes-and-stains/haematoxylin-eosin-he-staining/ [Accessed: 05 June 2019].

Klymkowsky M.W. and Hanken J. (1991) Whole-mount staining of Xenopus and other vertebrates. In: *Xenopus laevis*: *Practical Uses in Cell and Molecular Biology, Methods in Cell Biology 36.* Editors: Kay B. K. and Peng H. B. Publisher: Elsevier, London, UK. Pp. 419–428.

Levrat-Calviac V. and Zylberberg L. (1986) The structure of the osteoderms in the gekko: *Tarentola mauritanica. American Journal of Anatomy* **446**:437–446.

Maisano J. A., Bell C. J., Gauthier J. A. and Rowe T. (2002) The ODs and palpebral in *Lanthanotus borneensis* (Squamata: Anguimorpha). *Journal of Herpetology* **36**:678–682.

Maisano J. A., Laduc T. J., Bell C. J. and Barber D. (2019) The cephalic osteoderms of *Varanus komodoensis* as revealed by high-resolution X-ray computed tomography. *The Anatomical Record* **302**:1675–1680.

Moss M. L. (1969) Comparative histology of dermal sclerifications in reptiles. *Acta Anatomica* **73**:510–533.

Paluh D. J., Griffing A. H. and Bauer A. M. (2017) Sheddable armour: identification of osteoderms in the integument of *Geckolepis maculata* (Gekkota). *African Journal of Herpetology* **66**:12-24

Puchtler H. and Waldrop F.S. (1979) On the mechanism of Verhoeff's elastica stain: a convenient stain for myelin sheaths. *Histochemistry* **62:**233–247.

Vickaryous M. K. and Hall B. K. (2008) Development of the dermal skeleton in *Alligator mississippiensis* (Archosauria, Crocodylia) with comments on the homology of osteoderms. *Journal of Morphology* **269**:398–422.

Vickaryous M. K., Meldrum G. and Russell A. P. (2015) Armored geckos: A histological investigation of osteoderm development in *Tarentola* (Phyllodactylidae) and *Gekko* (Gekkonidae) with comments on their regeneration and inferred function. *Journal of Morphology* **276**:1345–1357.

Zylberberg L. and Castanet J. (1985) New data on the structure and the growth of the osteoderms in the reptile *Anguis fragilis* (Anguidae, Squamata). *Journal of Morphology* **186**:327–342.

3 CHAPTER 3 Histology of *Heloderma suspectum* osteoderms

3.1 Introduction

The genus *Heloderma* encompasses two extant species in the family Helodermatidae, which are survivors of a group of lizards called the Monstersauria (Nydam, 2000). Monstersaurs belong to the major lizard group Anguimorpha which also includes varanids (e.g. *Varanus komodoensis*) and anguids (e.g. *Elgaria, Ophisaurus*). The Monstersauria clade has been traced back nearly 100 million years, and managed to survive the late Cretaceous extinction that overwhelmed the non-avian dinosaurs 65 million years ago (Conrad, 2008). The genus *Heloderma* has existed since at least the early Miocene (about 23 million years ago) (Pregill et al., 1986), and the two species *H. horridum* and *H. suspectum* are hypothesized to have diverged from a most recent common ancestor in the late Eocene ~35 mya (Douglas et al., 2010). They are thought to have undergone relatively little gross morphological change over this time (Beaman et al., 2006).

Genus *Heloderma:*

- *H. horridum* (Wiegmann, 1829) Mexican beaded lizard

- *H. h. alvarezi* (Bogert and del Campo, 1956) Chiapan beaded lizard

- *H. h. charlesbogerti* (Campbell and Vannini, 1988) Guatemalan beaded lizard

- *H. h. exasperatum* (Bogert and del Campo, 1956) Rio Fuerte beaded lizard

- *H. suspectum cinctum* (Cope, 1869) Banded Gila monster

- *H. suspectum suspectum* (Wiegmann, 1829) Reticulated Gila Monster

Heloderma suspectum can only be found in arid parts of the northern states of Mexico (Sonora and Chihuahua) and southwestern states of the USA (Arizona, Nevada, California, New Mexico, and Utah). In Mexico, *H. horridum* is sympatric with *H. suspectum* in southern Sonora but unlike *H. suspectum* its range continues down the

Pacific coast of Mexico into Guatemala. The rarer subspecies have a much smaller range, found only within the Rio Grijalva valley of Guatemala (Fig. 3.1).
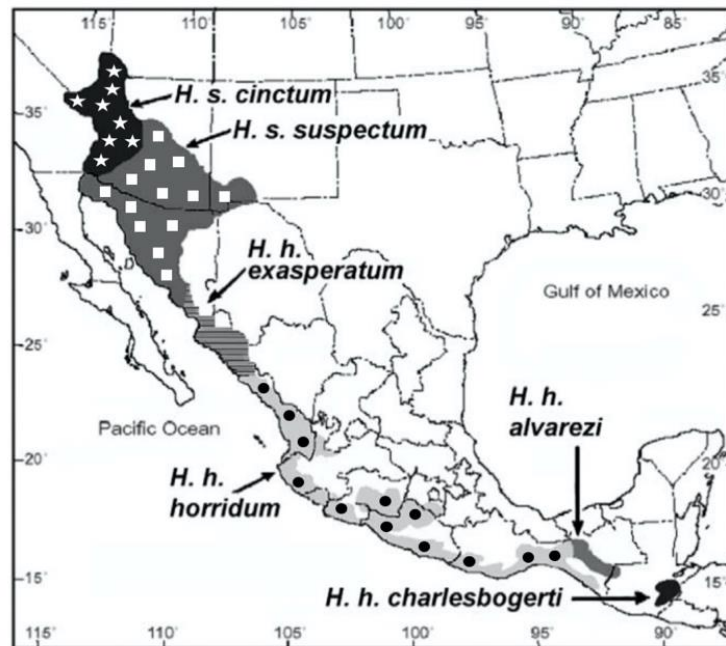
Figure 3.1: Map showing *Heloderma* species distribution, adapted from Douglas et al., (2010). Black with five-pointed stars = H. s. cinctum, grey with squares = *H. s. suspectum*, grey with stripes = *H. h. exasperatum*, grey with circles = *H. h. horridum*, grey = *H. h. alvarezi*, black = *H. h. charlesbogerti.*

There has been debate regarding whether the rare sub species of *H. horridum* should be classified as full species after a molecular study was published by Reiserer et al., (2013). The results of that study even ignited debate as to whether or not *H. suspectum* should be placed in its own genus separate from *Heloderma* (Road and Orchards, 2013), but as consensus has not been reached on either of these suggestions the taxa are named herein as per their classification on the reptile database website (Uetz et al., 2018).

The present study concerns *H. suspectum*, because of the relatively common distribution and large population in the wild and successful breeding in UK zoos (the material used here is from captive bred zoo animals that died of natural causes). Specimens of the rarer subspecies are much harder to acquire and thus are less likely to be studied as a result of this scarcity.

Morphologically, *Heloderma suspectum* appear as large lizards (300–500 mm adult snout-vent length) with a relatively large head, powerful jaw muscles, short limbs with

large toes and long claws for burrowing (Vitt and Caldwell, 2014). They are sedentary nest predators and return annually to the same foraging areas and shelters. Males compete to mate with females through intraspecies combat rituals. Their low base metabolic rate and the ability to eat large meals storing the energy as fat in their thick tails, enables them to offset the energy costs of searching for a widely distributed food source and to survive for extended periods without feeding. These traits make frequent foraging unnecessary and contribute to their ability to feed in a specialised feeding niche – eating almost solely on the contents of vertebrate eggs and young in their nests (Camp, 1923; Bogert and del Campo, 1956).

Coloration of the skin is mostly pink or orange, with black patches. The dorsal scales appear as raised bumps, or as the common name of *H. horridum* suggests, beads, underlain by osteoderms. *H. horridum* its subspecies are often blacker in colour than *H. suspectum*, sometimes totally black. The mottled pattern of colouration in *H. suspectum* and multi-coloured specimens of *H. horridum* can provide camouflage in the desert vegetation, but the bright colours may also work as an aposematic warning to potential predators of the venom contained in glands in the lower jaw (Lindström, 1999).

In regards to their integument, *Heloderma spp.* were initially described as having ODs in 1956 (Bogert and del Campo, 1956). The dermis and ODs were later examined with a light microscope in a comparative histological study of lizards, recorded with black and white photography (Moss, 1969, see fig. 1.1). As well as presenting the first images of sectioned dermal tissue, this study was also the first to propose that the ODs were created through a mechanism of metaplasia, and the first to identify an "enigmatic tissue" on the superficial surface of the OD, different from bone.

Three years later the same author published an extended study of the vertebrate dermal apparatus (Moss, 1972) that included further micrographs of the *H. suspectum* OD. However, since these initial descriptions by Moss, there has been no further study of the *Heloderma* OD. This means nearly half a century of scientific knowledge and technological improvement has not been applied to the study of these unique mineralised organs. It was therefore apparent that further work was required in order to characterise the tissues present effectively, using modern techniques. This is what this chapter aims to address.

3.2   Results

Figure 3.2: *Heloderma suspectum* photograph, right side shown. This adult specimen pictured is not the source of the dermal samples used in this chapter. This photograph was taken by staff at ZSL London Zoo Reptile House for this study.

No scalebar.

A single lizard often develops thousands of individual ODs. They initially appear to the naked eye as smoothly domed, regularly interspaced circular structures (Fig. 3.3a), but beneath the epidermal layer of the cornified scale, the superficial part of the mineralised OD displays a rough ornamented surface, with many grooves and ridges. The ornamentation on the surface of the OD can be seen when viewed using X-ray plate imaging (Fig. 3.4). Often, each OD resides beneath a scale in a 1:1 ratio, but not all scales have ODs beneath them (Fig. 3.4) and the ventral skin exhibits flatter, square scales, devoid of any underlying OD (Fig. 3.3b). The limbs, and flanks of the animal also express fewer ODs when compared to the cranium and the post-cranial dorsum. Sampled ODs were measured at 3mm deep, 3mm wide and 2mm tall, but this sizing can vary. The ODs reach their largest size on the dorsal part of the head,

particularly on the upper cranial area above and between the eyes, while those covering the tail and limb appendages are much smaller. ODs also vary quite dramatically in size in the local vicinity, some appearing as roughly twice the area of the adjacent OD in the X-ray plate image (Fig. 3.4). Although X-ray plate imaging was useful in identifying the locations of OD expression and for an overview of the shape and distribution of the ODs, a CT scan was performed to view the ODs in 3D and with higher resolution.
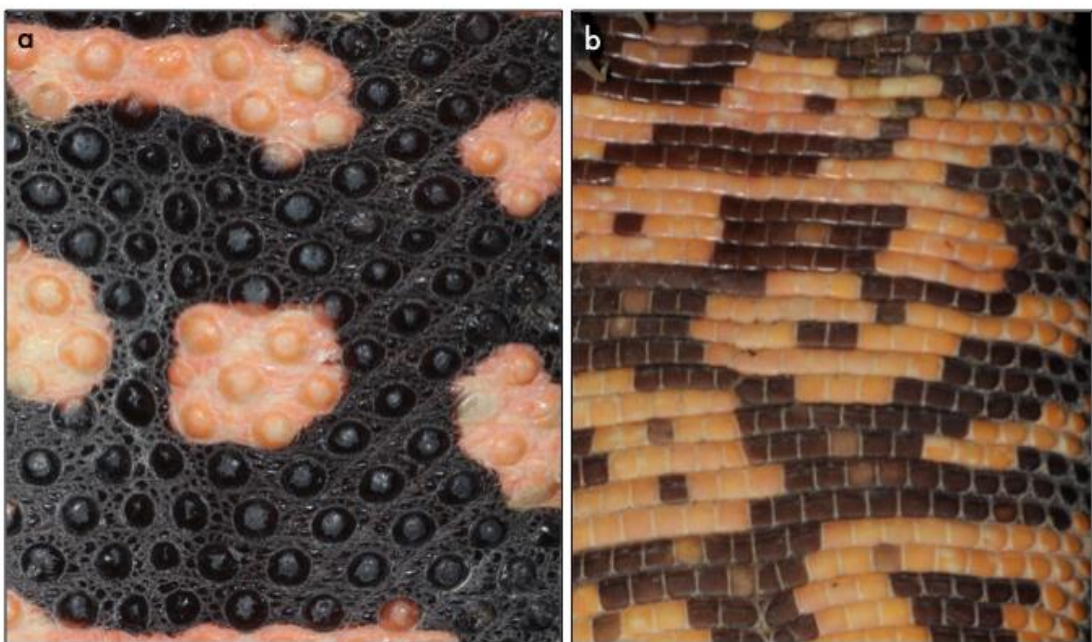
Figure 3.3: Photograph of *Heloderma suspectum* dorsal skin (a) and ventral skin (b). Osteoderms correspond to the domed, bead-like studs in the skin of (a). The ventral skin is void of these features, instead it shows regularly repeating, rectangular, flat scales. On the dorsal surface, (a), the ODs are independent of colour; on the ventral surface, (b), the ODs appear not to be independent of colour.

These photographs were taken by staff at ZSL London Zoo Reptile House for
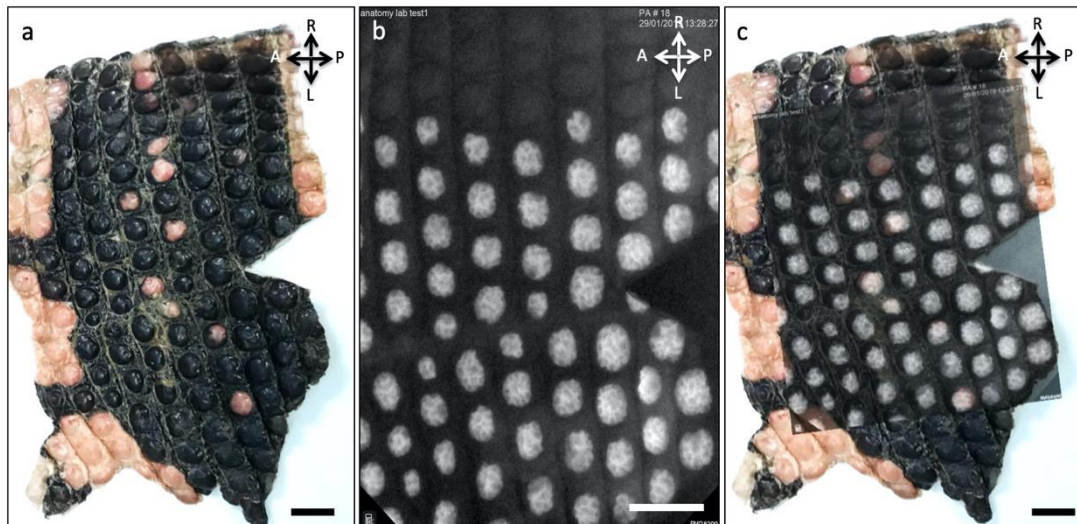
Figure 3.4: Photograph of *Heloderma suspectum* dorsal skin (a), corresponding X-ray plate image of the same sample (b) and a composite of both (a) and (b), with transparency of (b) set to 40% (c). Notice the presence of dense, white (mineralized) tissue underneath some scales in the lower, more dorsal portion of the skin – these are ODs and are absent in the upper, more lateral and ventral portions of the skin.

An initial CT scan of the cranium (with a resolution, or voxel size, of 14 microns) visualised under density-dependant false-colour, showed the individual ODs as tessellated polygons, mainly hexagonal, sometimes pentagonal in shape when viewed from a coronal perspective (Fig. 3.5). The ODs do not overlap; rather tessellate alongside each other as polygonal tiles, with a gap of non-mineralised tissue between each. This gap is approximately a half to a quarter of the length of the average OD, meaning that the majority of the skin surface area surrounding the cranium is underlain by mineralised tissue. The non-mineralised gap may allow for flexibility between the ODs as the skin is stretched and compressed while the animal is moving. This hypothesis is reinforced when one regards the absence of ODs in the skin of the lips and cheeks of the animal as these parts of the skin stretch dramatically when the animal opens the jaws to consume large prey. ODs are mineralised and therefore less flexible than the soft tissue that surrounds them so they cannot be expressed in areas of the skin that stretch substantially.
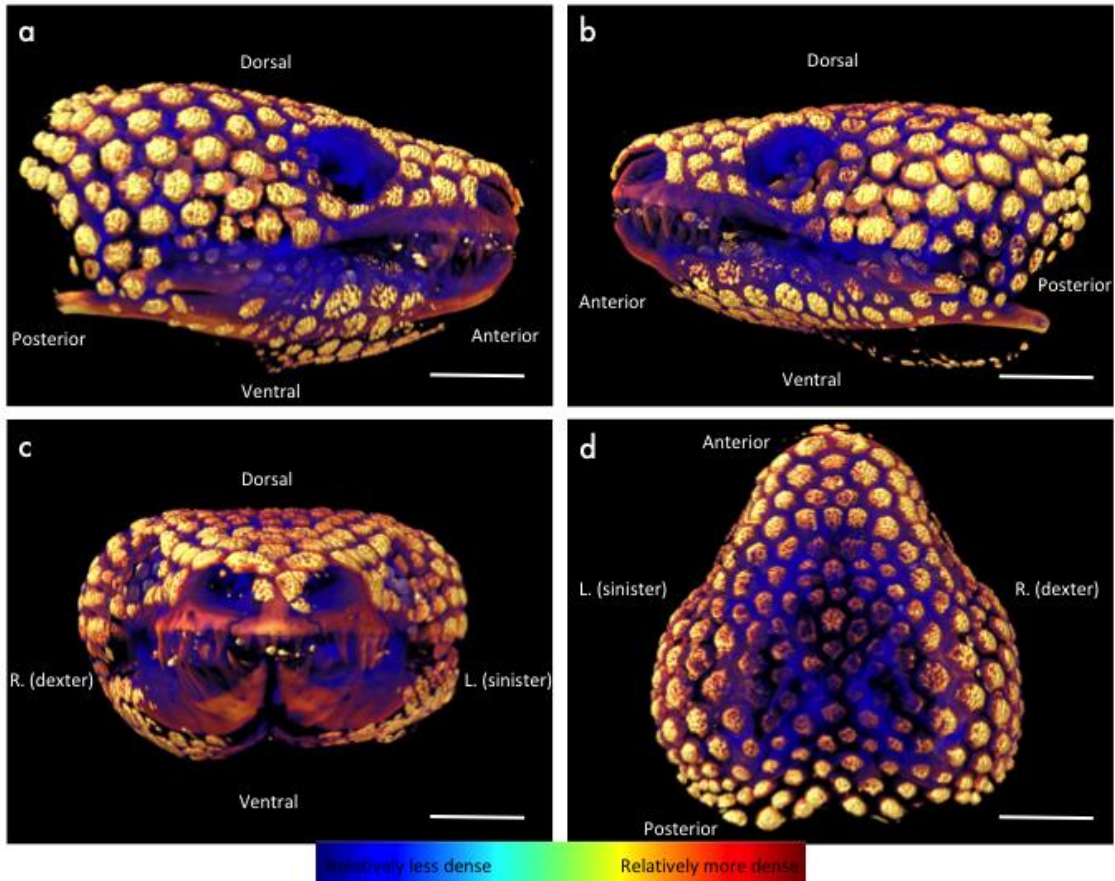
Figure 3.5: Volume rendering of HRXCT data of *H. suspectum* cranium. Density dependent false-colour where blue indicates less dense material, orange indicates more dense material, in (a) right lateral view, (b) left lateral view, (c) anterior view and (d) dorsal view.

Scale bars: 20 mm.

The initial CT scan showed that ODs are found completely covering the skull except for the posterior portion of the ventral side, the lips and cheeks. It also showed that they fuse to the underlying frontal, parietal, nasal, premaxilla, prefrontal, maxilla, jugal and dorsal bones of the skull. Additionally, due to the observed difference in colour of the ODs compared to the cranial bones in the density-dependant volume rendering, they are capped by a material that is relatively denser than that of the underlying bones (Fig. 3.5).

This initial CT scan of the head provided valuable information on the arrangement of ODs in regard to the bones of the skull and the casing of the braincase for protective functions. It is clear the ODs create a comprehensive covering and are composed of a dense material in the central, dorsal area. However, the resolution of this scan was

not sufficient to discern topological features of each individual OD nor was it sufficient to analyse the internal structures of the mineralised tissues within a single OD.
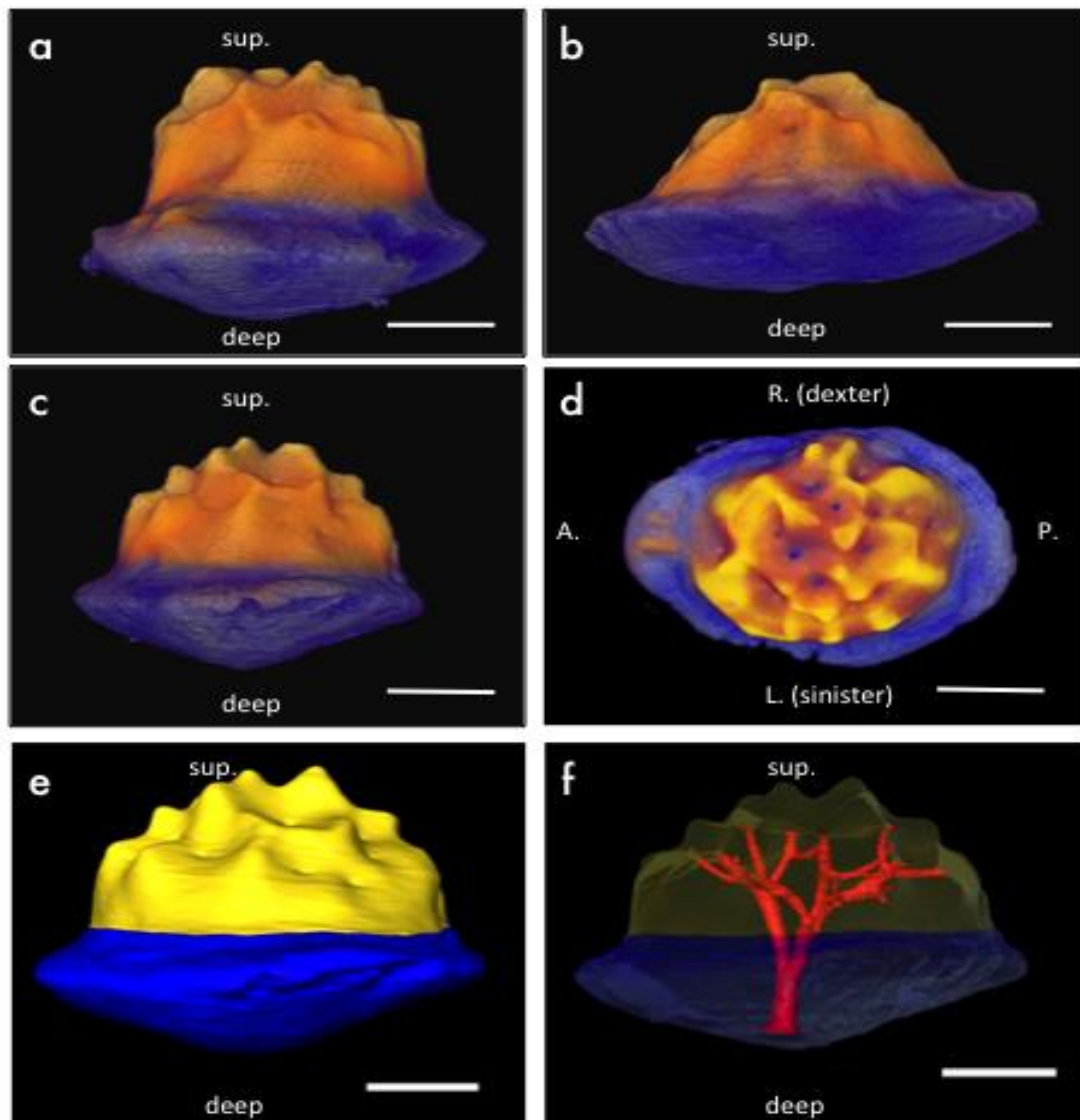
Figure 3.6: Volume rendering of HRXCT data of a whole, dorsal *H. suspectum* OD. Density dependent false-colour - blue indicates less dense material, orange indicates more dense material in right side view (a), left side view (b), anterior view (c) and superficial view (d), segmented, false colour anterior view, yellow corresponds to the superficial material, blue the basal material and red the vasculature within the OD (e), segmented, false colour anterior view with 50% transparency of external surfaces, same colour labels (f).

Scale bars: 600μm.

A higher resolution scan (with a voxel size of 0.1646 microns) of a single OD was performed in order to address these concerns. Micro-computed tomography of a single dorsal OD (Fig. 3.6) was performed and visualised under density-dependant false-colour view in line with the initial scan. Here, the results again display a clear gradient of increasing density from deep to superficial regions, complimenting results shown in the first scan. ODs appear as lozenge-shaped overall, with a deep, peripheral part (a ring extension) that extends out radially past the superficial region. In *H. suspectum,* this extension of the base portion runs along the entire circumference of the OD in a ring around the equatorial plane. The ODs have a convex, spherically curved deep surface, with a rutted, uneven superficial surface exhibiting a vermiculate texture of ridges, peaks and troughs, these troughs often host pits, that lead to channels extending inside the OD (Fig. 3.6b, d, f). Slices obtained from this CT scan were segmented so that voxels that corresponded to the different regions of the OD were assigned labels with a false colour. Fig. 3.6e shows the result of this segmentation and the horizontal partitioning between the basal, in blue, and the dense, central, superficial layer, in yellow, becomes clearer. The vasculature that runs from the base of the OD to the pits in the superficial surface was also segmented and coloured red (Fig. 3.6f), but can only be seen when the transparency of the other regions is reduced, due to its location, residing within an internal location of the OD. In summary, CT scanning afforded high resolution, three-dimensional views of the OD arrangement as a mesh and also afforded a view of the materials that compose a single osteoderm, their relative densities, and a view of the internal vasculature. These results show for the first time, the topology, tomography and density of the cranium and associated ODs as well as the same measures for a single OD and the different internal components that make up the OD organ.

Because the results of these CT scans showed that the ODs were indeed composed of various different materials, to investigate these materials further additional techniques were performed on OD material. This included BSE-SEM imaging of liquid nitrogen freeze- fractured ODs (Fig 3.7).
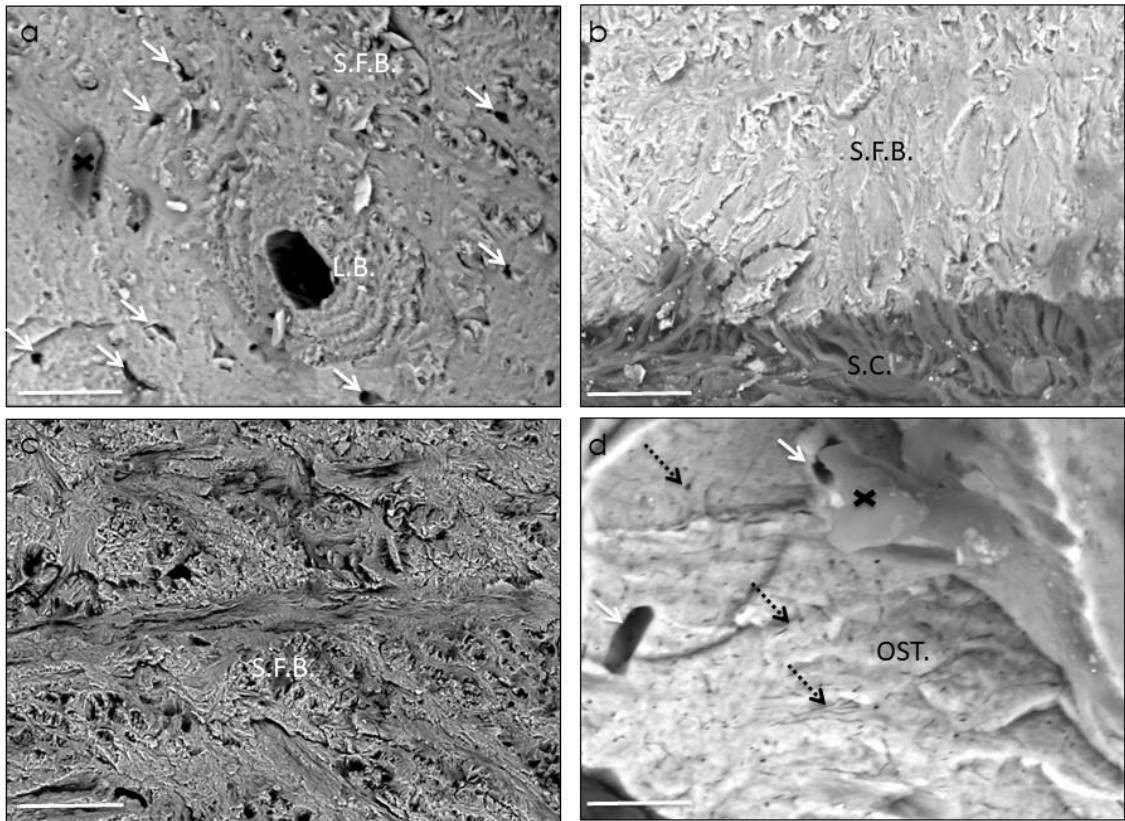
Figure 3.7: BSE-SEM imaging of freeze-fractured *H. suspectum* OD depicting osteon (haversian system) and corresponding lumen (haversian canal) surrounded by lamellar bone (a), mineralized collagen fibres (b, c) and superficial region (d). Black crosses = debris/dust artefacts, dashed black arrows = canaliculi, L.B. = lamellar bone, OST. = osteodermine, S. C. = stratum compactum, S.F.B. = Sharpey-fibre bone, White arrows = lacunae,

Scale bars: (a) = 40µm, (b) = 40µm, (c) = 20µm, (d) = 10µm.

The results showed the OD was composed of mineralised collagen fibrils, exhibiting lacunae (cell spaces, white arrows). The collagen fibrils are regularly but not densely arranged, orthogonally organised relative to each other and inorganic crystals are only partially present, indicating that they were not, or only poorly, mineralised in the living animal (Fig. 3.7c, grey lines). Non-mineralised fibres from the stratum compactum of the dermis (dark grey, labelled S.C.) were observed as travelling continuously into the mineralised (whiter) portions of the OD (Fig. 3.7b). Larger hollow channels presumed
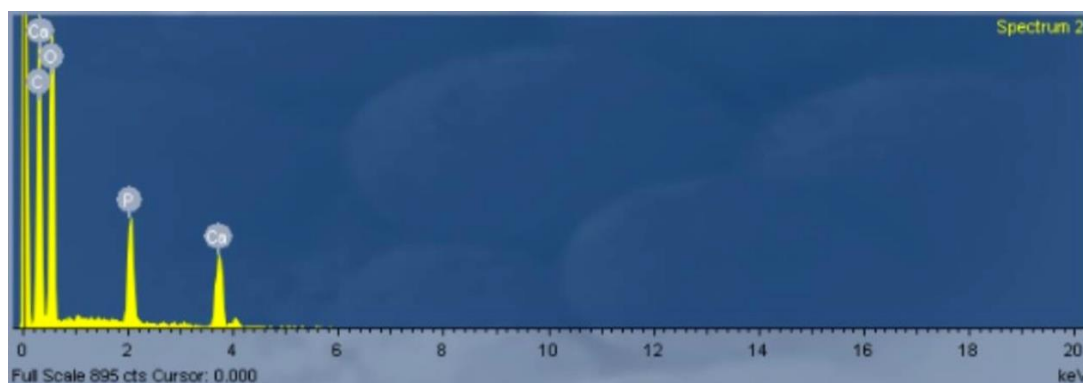
Figure 3.8(a): EDX spectrum taken from mineralized region of *H. suspectum* OD marked S.F.B. on Figure 3.9.

to be vasculature were observed to have parallel fibres circling the lumen (Fig. 3.7a), resembling a Haversian system, also known as an osteon. Surrounding this osteon, small cell spaces were observed (Fig. 3.7a, white arrows). Due to these observed features, these results seem to coincide with Moss's (1969) findings in that the OD is composed of materials resembling L.B. and S.F.B. in the basal portion (Moss, 1969). The dense superficial surface of the OD was found to have a completely different structure, being more highly mineralised, with smaller channels, presumed to be canaliculi, within the mineralised matrix (Fig. 3.7d, dashed black arrows) and almost zero mineralised collagen fibrils (Fig. 3.7d). Fewer oblong cell spaces (lacunae) were observed in this region, but were still present (Fig. 3.7d, white arrows). This region was therefore interpreted as belonging to a different material than the lower portion of bone, and is similar to that of the previously documented OD material, OST. (de Buffrénil et al., 2011).

After detecting these three different materials in the *Heloderma suspectum* OD, it was deemed important to check what mineral was present in each material. This was achieved by using energy dispersive X-ray spectroscopy or EDX. Wherever it was performed on the mineralised tissues of the OD, either on the S.F.B. region, L.B. region or OST. region, EDX analysis resulted in twin peaks of calcium and phosphorus, indicating that the crystals of mineral present within these OD materials are hydroxyapatite (Fig. 3.8). This is the expected outcome as hydroxyapatite is the mineral present in bone; therefore, OST. is composed of the same mineral as the basal bone portion.

To complement the fractured BSE-SEM results, resin embedded, cut and polished sections were imaged under BSE-SEM to gain additional understanding of the internal materials of the OD. Embedding the samples in resin, then sectioning the resin block and polishing the exposed face allows for an image of a flat plane section rather than a rough, jagged break as is the case in the liquid nitrogen freeze-fractured samples. In the images gained from this secondary method, it is again clear that the superficial OST. region appears brighter when compared to the basal part of the OD in BSE-SEM imaging. Due to the fundamentals concerning BSE-SEM as discussed in Chapter 2, this indicated that the OST. region (Fig. 3.9, OST.) is denser than the basal region, complimenting the results seen in liquid nitrogen freeze-fractured SEM and the results seen in volume-rendering of the CT scan data. Growth lines of arrested mineral deposition (LAGs) were visible in the OST. region (Fig. 3.9, black arrows). The OST. region again displayed dramatic reductions in collagen content and the number of lacunae compared to the other materials present, complimenting the results seen in Fig. 3.7. The lamellar fibres of the bone surrounding the internal channels again displayed a different structure to the S.F.B. of the basal cortex, complimenting the findings of the fractured SEM results (Fig. 3.9, L.B.). This sectioning method also afforded a comparison of the ratio of the materials in relation to one another – the capping region of OST. is seen to comprise roughly one quarter to one third of the total surface area of the OD section. The majority of the OD area is composed of the basal bone region and a small (roughly 5-10%) portion of the OD area comprises the L.B. encased internal vasculature channels.

Because every previous technique outlined thus far only produced results that visualised the mineralised components of the OD, histological staining and light microscopy was utilised to visualise both non-mineralised and mineralised tissue components in order to understand how the OD is located in relation to the surrounding soft tissue components of the skin. As explained in Chapter 2, histochemical methods selectively stain tissue components based on their inherent dye affinities and thus their corresponding electric charges. The results of the histological staining gave a clear indication that the three separately structured mineralised materials observed to be present in earlier imaging techniques were again visible as separate entities in the ODs sampled (Fig. 3.10). In these micrographs, the mineralised OD and non-mineralised surrounding tissues are clearly seen in all stained sections. Inherent differences in collagen arrangement between the lower (stratum compactum) and upper (stratum superficiale) dermis can be readily identified, the lower stratum compactum being composed of thicker, more tightly

packed collagen fibrils, the upper stratum superficiale region containing thinner, more loosely packed collagen fibrils. The compact orthogonal arrangement of the large fibres that comprise the stratum compactum of the deep dermis are readily visible in coronal sections void of any OD (Fig. 3.10b, e, h) and subsequently, following mineralisation, the same arrangement is then also clearly visible in coronal sections of mineralised ODs of the same sample (Fig. 3.10c, f, i).
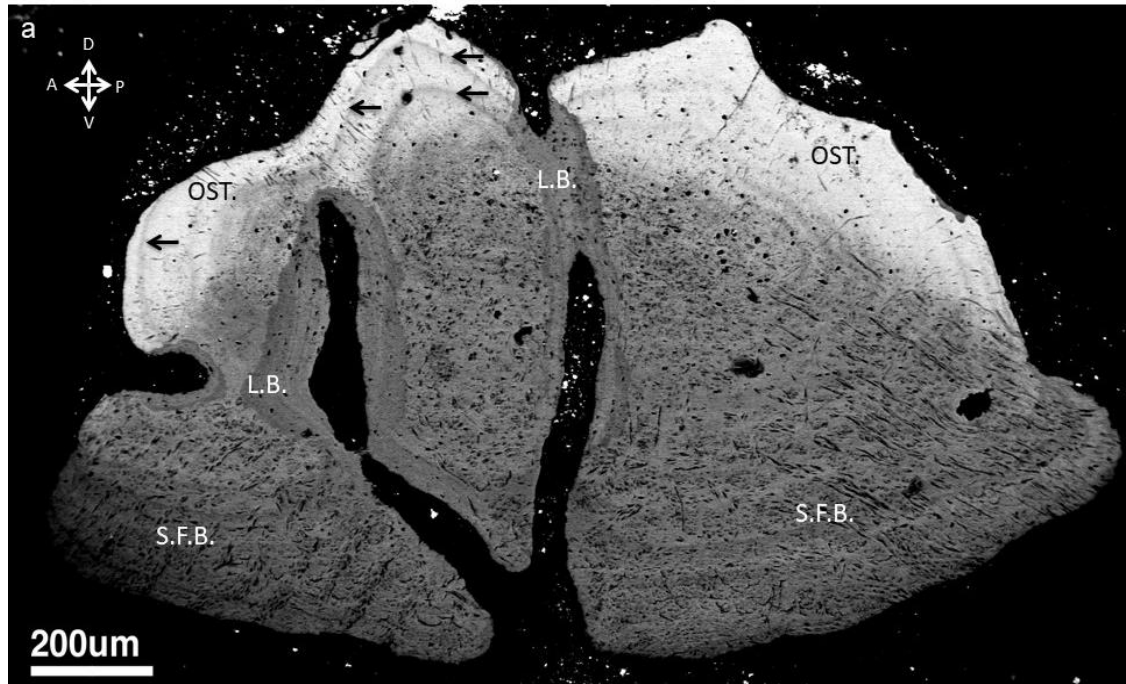
Figure 3.9: BSE-SEM imaging of *H. suspectum* OD, sagittal section, resin embedded, ground and polished. S.F.B. = Sharpey-fibre bone, L.B. = lamellar bone, OST. = osteodermine, black arrows = lines of arrested growth (LAGs).

Scale bar: 200µm.

Because the mineralised material retains the original patterning of the dermis, this may indicate spontaneous mineralisation of the underlying dermal collagen mesh in the creation of this material, another reason for the nomenclature of S.F.B. for these mineralised fibres in the basal, equatorial and central areas of the lower part of the OD. The keratin of the scale located above each OD appears bright red in Masson's Trichrome stained sections (Fig. 3.10d). This staining procedure selectively stains keratin and thus afforded a clear view of where this keratin-rich layer began and ended, as well as allowing for proper measurement of the thickness of the cornified scale region. Combined, the layers of the epidermal scale appeared to be on average 100µm thick, whereas ODs range in height from 2-4mm from superficial to deep surfaces. This highlights the importance of the size of the OD in relation to the

epidermis and shows that the ODs comprise the majority of the height of each "bead" forming a thick, protective, mineralised layer. The same keeled, lozenge shaped transverse profile of the OD that was seen in cut and polished embedded SEM images was observed in these histological sections, as were the alternating ridges and troughs of the superficial OST. layer and convex deep surface, highlighting the uniformity of these features across multiple ODs from the same animal.
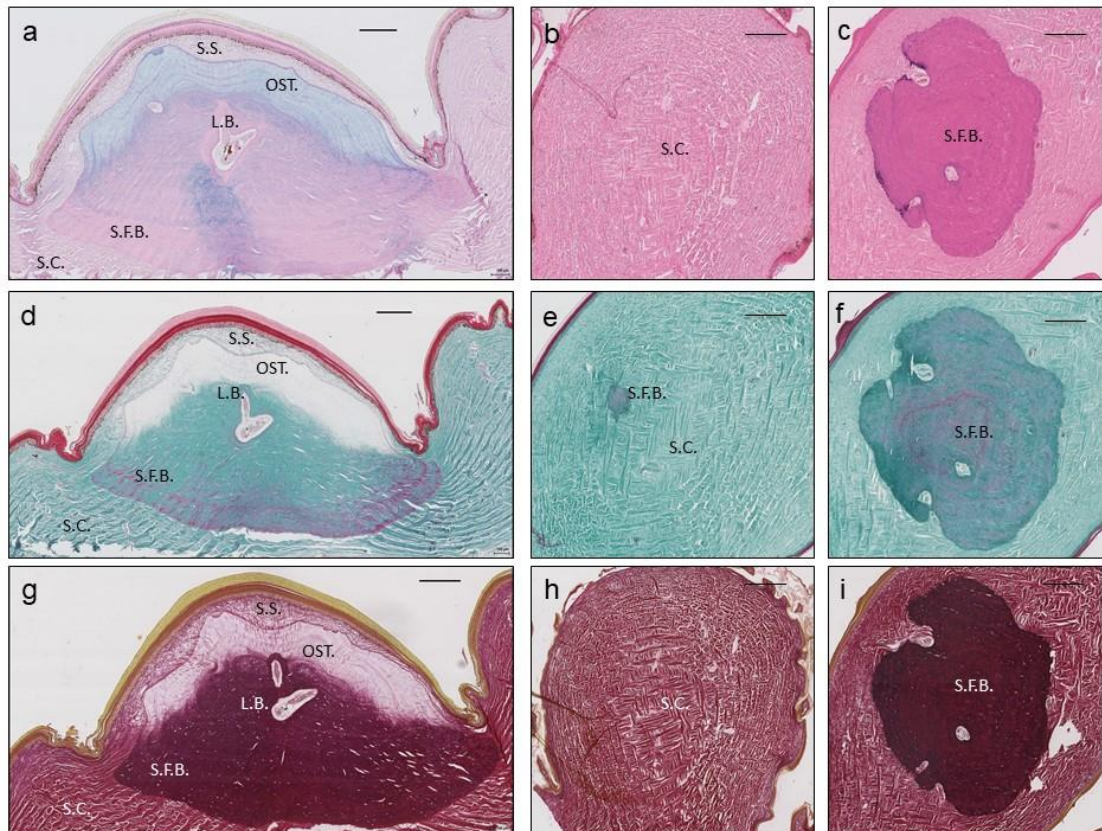
Figure 3.10: Histological overview of *Heloderma suspectum* post-cranial, dorsal OD (a, c, d, f, g) and non-mineralized dermis (b, e, h), paraffin-embedded, 10μm thick sections, in sagittal (a, d, g) and coronal (c, f, i) view stained with Alcian blue (a), H&E (b,c) Masson's Trichrome (d-f), Verhoff van Geison (g-i). L.B. = lamellar bone, OST. = osteodermine, S.C. = stratum compactum, S.F.B. = Sharpey-fibre bone, S.S. = stratum superficiale.

Scale bars: all 200μm.

The three structurally distinct materials exhibited differential staining in histological sections. S.F.B. in the base of the OD stains pink with blue mottling in Alcian blue staining (Fig. 3.10a), indicating small amounts of acid mucosubstances. It stains pink-purple in H&E staining (Fig. 3.10c) indicating collagen, green with red mottling in

Masson's trichrome staining (Fig. 3.10d, f), green indicating collagen and red mottles indicating collagen under tension. The S.F.B. stains red-black in V.V.G. staining (Fig. 3.10g), indicating that collagen fibres are present. This region also displays concentric, repeating lines of staining (Fig. 3.10a, d) delineated by basophilic lines in the deep and peripheral areas. OST. stains blue in Alcian blue staining (Fig. 3.10a), indicating the presence of sulphated mucosubstances, very light green – no stain, in Masson's trichrome (Fig. 3.10d) indicating sparse collagen, and stains very light red in EVG (Fig. 3.10g), again indicating sparse collagen. Complimenting earlier techniques, L.B. regions were identified resembling haversian systems, or primary/secondary osteons, which are often but not exclusively, found surrounding a lumen of internal vasculature channels of the OD (Fig. 3.10a, L.B.). Within this material we observed osteocyte-containing lacunae within collagenous layers displaying concentric lamellae in orientation around the lumen (Fig. 3.10c, d). These features fit the description of L.B.. L.B. stains pink-purple with H&E staining (Fig. 3.10c) indicating collagen, green with red mottling with Masson's trichrome staining (Fig. 3.10d), indicating collagen and collagen under tension and black with E.V.G. staining (Fig. 3.10g), indicating that elastic fibres are present. Along the deep periphery, a basophilic line was observed at the limit of mineralisation in Alcian blue, H&E and Masson's Trichrome staining (Fig. 3.10a, b, d).

3.3   Discussion

The above results show that the sampled ODs of *Heloderma suspectum* are formed of two separately structured bone materials, L.B. and S.F.B., in the basal part of the organ, with OST. identified as the previously enigmatic superficial tissue of *H. suspectum* ODs. *H. suspectum* is therefore the third known extant species to feature this unique mineralised tissue in the OD, after the geckos *Tarentola mauritanica* and *Tarentola annularis* (Vickaryous et al., 2015). The basal and central parts of the ODs of *H. suspectum* were found to be composed of materials that resemble metaplastically mineralised pre-existing dermal fibres and occasionally, materials that resemble L.B. encasing an osteon lumen. The basal portion of the OD was also found to exhibit a basophilic line along the deep periphery, complimenting previous observations (Moss, 1969).

In the superficial region of each OD, the basal bone material gradually changes into a denser, more crystalline material that was observed to display a different nanostructure, with features homologous to that of OST.. Many previously identified features of OST. were also observed in the results presented, including a lack of collagen, fewer cell spaces (lacunae), lines of arrested growth (LAG) and the presence of sulphated mucosubstances (Moss, 1969; Levrat-Calviac and Zylberberg, 1986; de Buffrénil et al., 2011; Vickaryous et al., 2015). The discovery of OST. capping *Heloderma suspectum* ODs shows that OST. as a material is more widely expressed than previously thought and puts an end to the uncertainty regarding the nature of the capping material on their ODs (Moss, 1969; Vickaryous and Sire, 2009).

The presence of osteons as traditional bone-like structures, in direct association and contact with S.F.B. is a finding that may suggest multiple mechanisms of formation during the ontogenesis of *H. suspectum* ODs – with dermal collagen fibres being first metaplastically mineralised, and then remodelled via resorption systems (de Buffrénil et al., 2011). *H. suspectum* ODs may therefore form via a combination of both metaplastic ossification and intramembranous haversian systems, as previously proposed for OD formation in other squamate species, complimenting these hypotheses (Patterson, 1977; de Buffrénil et al., 2010). However, at what stage the OST. is added as a capping material, and how, is currently unresolved.

After identifying the three separate materials in the ODs of *Heloderma suspectum*, further characterisation work was required to define these materials on the nanoscale, as ODs have rarely, if ever, had their mineralised material structures studied down to the ultra-structural level (fourth order). The presence of OST. in the sampled ODs meant there was ample opportunity to study this strange tissue further in order to obtain an accurate definition of OST. ultrastructure, as well as the other bone materials present. The further characterisation work regarding OD material ultrastructure is presented in the next chapter (Chapter 4).

3.4 Conclusions

- The ODs of *Heloderma suspectum* are thick granular structures embedded in the soft tissue of the dermis, underlying single scales, and primarily distributed over the dorsal and lateral sides of the head and the body.
- The ODs of *Heloderma suspectum* are made up of three distinct tissues: S.F.B., L.B. and OST., supplied by neurovasculature.

- This complex structure implies the involvement of multiple mechanisms during OD formation
- *Heloderma suspectum* is the third lizard taxon reported to exhibit OST. as a capping tissue in its ODs

3.5 References

Beaman K. R., Beck D. and MacGurty B. M. (2006) The Beaded lizard (*Heloderma horridum*) and Gila monster (*Heloderma suspectum*):a bibliography of the family Helodermatidae. *Smithsonian Herpetological Information Service* **136**:1-66.

Bogert C. M. and del Campo R. M. (1956) The Gila monster and its allies; the relationships, habits, and behavior of the lizards of the family Helodermatidae. *Bulletin of the American Museum of Natural History* **109**:1-238.

Camp C. L. (1923) Classification of the Lizards. *Bulletin of the American Museum of Natural History* **48:**289-481.

Campbell J.A. and Vannini J.P. (1988) A new subspecies of beaded lizard, *Heloderma horridum*, from the Motagua Valley of Guatemala. *Journal of Herpetology* **22**:457-468.

Conrad J. L. (2008) Phylogeny and systematics of Squamata (Reptilia) based on morphology. *Bulletin of the American Museum of Natural History* **310**:1–182.

Cope, E.D. (1869) Protocol of the March 9, 1869 meeting. *Proceedings of The Academy of Natural Sciences of Philadelphia* **21**:5.

De Buffrénil V., Dauphin Y., Rage J-C. and Sire J-Y. (2011) An enamel-like tissue, osteodermine, on the osteoderms of a fossil anguid (Glyptosaurinae) lizard. *Comptes Rendus de l'Academie des Sciences Palevol* **10:**427-437.

De Buffrénil V., Sire J-Y., and Rage J. C. (2010) The histological structure of glyptosaurine osteoderms (Squamata: Anguidae), and the problem of osteoderm development in squamates. *Journal of Morphology* **271**:729–737.

Douglas M. E., Douglas M. R., Schuett G. W., Beck D. D. and Sullivan B. K. (2010) Conservation phylogenetics of helodermatid lizards using multiple molecular markers and a supertree approach. *Molecular Phylogenetics and Evolution* **55:**153–167.

Levrat-Calviac V. and Zylberberg L. (1986) The structure of the osteoderms in the gekko: *Tarentola mauritanica. American Journal of Anatomy* **446**:437–446.

Lindström L. (1999) Experimental approaches to studying the initial evolution of conspicuous aposematic signalling. *Evolutionary Ecology* **13**:605-618.

Moss M. L. (1969) Comparative histology of dermal sclerifications in reptiles. *Cells Tissues Organs*, **73:**510–533.

Moss M. L. (1972). The vertebrate dermis and the integumental skeleton. *Integrative and Comparative Biology*, **12:**27–34.

Nydam R. L. (2000) A new taxon of helodermatid-like lizard from the Albian–Cenomanian of Utah. *Journal of Vertebrate Palaeontology* **20**:285-294.

Patterson C. (1977) Cartilage bones, dermal bones and membrane bones, or the exoskeleton versus the endoskeleton. In: *Problems in Vertebrate Evolution: Essays Presented to Professor T S Westoll*, *Linnean Society symposium series 4* Editors: Westoll S., Andrews S. M., Miles R. S. and Walkerpp A. D. Publisher: Linnean Society of London, London, UK Pp. 77–122.

Pregill G. K., Gauthier J. A. and Greene H. W. (1986) The evolution of helodermatid squamates, with description of a new taxon and an overview of Varanoidea. *Transactions of the San Diego Society of Natural History* **21:**167–202.

Reiserer R. S., Schuett G. W. and Beck D. D. (2013) Taxonomic reassessment and conservation status of the beaded lizard, *Heloderma horridum* (Squamata: Helodermatidae). *Amphibian and Reptile Conservation* **1**:74-96.

Road P. and Orchards P. (2013) Not in *Heloderma*... A revised taxonomy and new genus for the Gila Monster. *Australasian Journal of Herpetology* **21**:37-40.

Uetz P., Freed P., and Hosek J. (2018) *The Reptile Database*. Accessed: 02/02/2020 URL: http://reptile-database.reptarium.cz/

Vickaryous M. K. and Sire J-Y. (2009) The integumentary skeleton of tetrapods: origin, evolution, and development. *Journal of Anatomy* **214**:441–64.

Vickaryous M. K., Meldrum G. and Russell A. P. (2015) Armored geckos: A histological investigation of osteoderm development in *Tarentola* (Phyllodactylidae) and *Gekko* (Gekkonidae) with comments on their regeneration and inferred function. *Journal of Morphology* **276***:*1345–1357.

Vitt L. J. and Caldwell J. P. (2014) Squamates—Part I. Lizards. In: *Herpetology (4th Edition).* Editors: Gomez K. and Gonzalez P. Publisher: Elsevier, Amsterdam, NL. Pp. 749.

Wiegmann A.F.A. (1829) Über die Gesetzlichkeit in der geographischen Verbreitung der Saurier. *Isis von Oken* **22**:418-428.

4 CHAPTER 4 Extended characterisation of *Heloderma suspectum* osteoderms

4.1 Introduction

In Chapter 3, the presence of OST. as a capping material, S.F.B. in the basal regions and secondary osteons containing L.B. were established within the ODs of *Heloderma suspectum*. These tissues were visualised with X-ray plate imaging, histological staining, CT scanning, SEM and EDX spectroscopy. This chapter shows the results of further SEM and µ-CT scanning techniques at higher magnifications and resolutions, as well as additional techniques such as polarised light microscopy and TEM. The overall aim is to characterise the materials identified in Chapter 3 at a smaller scale and to identify any features that are unique to a single material. A comprehensive definition of structures, features and chemical composition for each material on multiple scales will make definitive identification of these materials easier in the future. A study of ODs from multiple anatomical locations is also presented in order to confirm whether or not the expression of these materials is universal or if their expression is limited to any specific area(s) of the body.

4.2 Results

In order to further characterise these mineralised materials, further light microscopy, utilising polarised light was attempted. Because earlier histology and SEM images showed differences in collagen arrangement between the two materials, this technique was employed, as it is useful for determining collagen arrangement in a sample. Collagen is an anisotropic material (doubly refracting), whereas apatite also has its own optical properties, thus bone exhibits birefringence under polarised light dependent upon the orientation of the collagen composition.
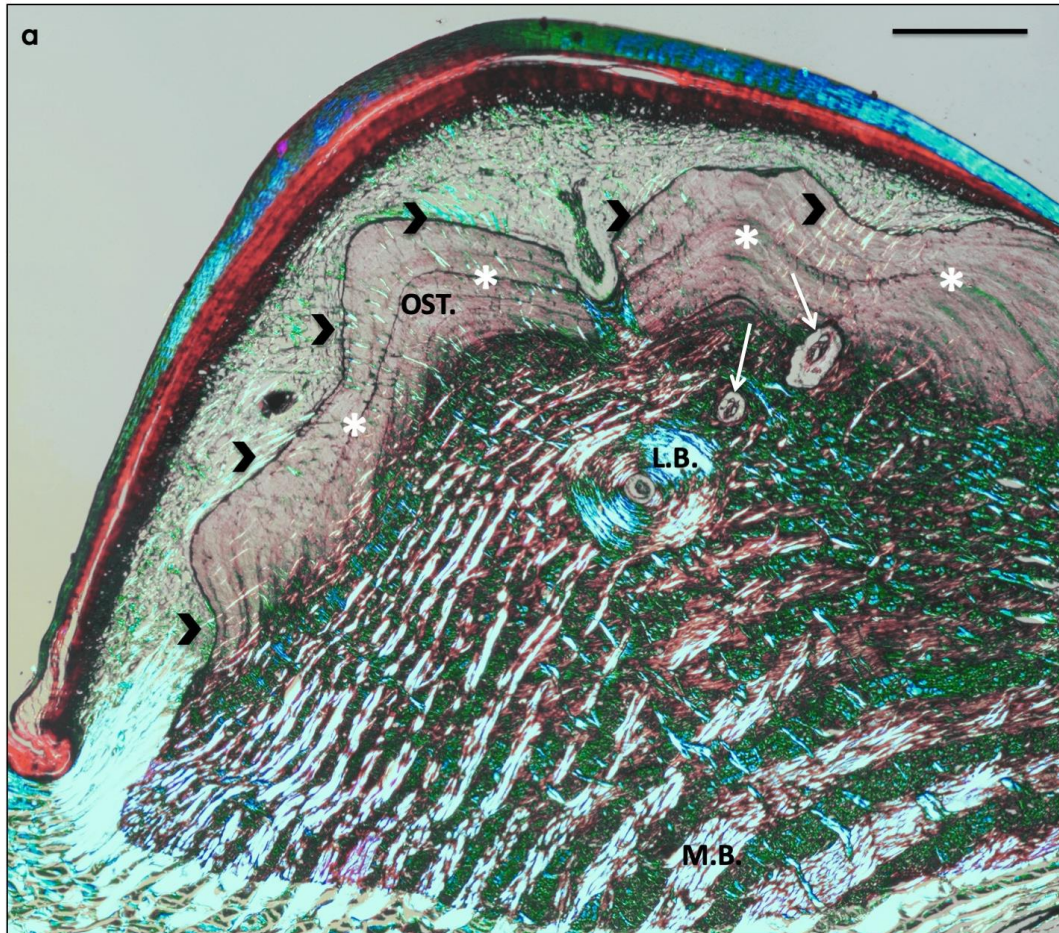
Figure 4.1: Cross polarised light micrograph of paraffin-embedded *Heloderma suspectum* OD, sectioned parasagittally, stained with toluidine blue. Asterisks (white) = lines of arrested growth (LAGs), Black chevrons = Sharpey's fibres, L.B. = lamellar bone, OST. = osteodermine, S.F.B. = Sharpey-fibred bone, White arrows = vasculature not encased by L.B..

Scale bar: 100μm.

The preliminary results of the polarised light microscopy are shown in Fig. 4.1. The OST. region displayed negative toluidine blue staining and was monorefringent, compared to the extensive positive staining and birefringence seen in the basal bone regions (labelled L.B. and S.F.B.). In spite of the lack of a collagen matrix, it was possible to see occasional bundles of collagen fibres within and surrounding the OST. region, which were homologous with Sharpey's fibres (Fig. 4.1, black chevrons) as they were observed as isolated, individual bundles of fibres within the OST. that were located both within the OST. and the surrounding soft tissue, anchoring the apical surface of the OD to the stratum superficiale. Lines of arrested growth (LAGs) are visible in the OST. region as grey-black repeating lines that mirror the shape of the

apical surface (Fig 4.1, asterisks). LAGs could not be identified in other regions using this technique.

A "maltese cross" (a cross-shaped formation of transmitted light) is evident in the L.B. region (Fig. 4.1), indicative of a secondary osteon after bone remodelling has occurred (Bromage et al., 2003). Occasionally, it was possible to identify vascular channels that are not encased by this L.B. and therefore did not show any difference in collagen arrangement and so did not produce a "maltese cross" (Fig. 4.1, white arrows). The regularly repeating, orthogonally arranged collagen fibres of the S.F.B. region appear highly birefringent, and their three-dimensional cross-hatched arrangement is clearly visible, with the red fibres exhibiting a rostrocaudal orientation
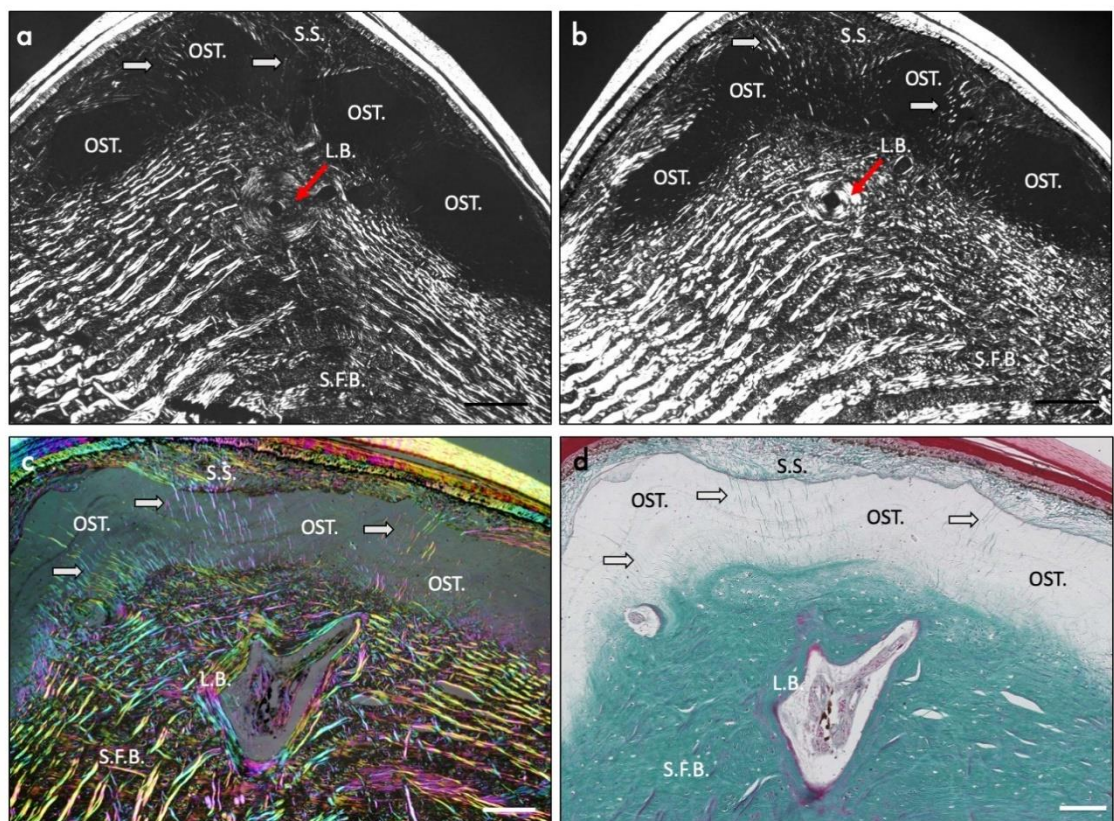
Figure 4.2: (a and b) Parasagittal sections of *H. suspectum* OD stained with toluidine blue visualized with standard black and white polarised light microscopy. (c) *H. suspectum* OD, sagittal section stained with Masson's Trichrome, visualized with Multi rotation polarised light microscopy (MRPLM) and (d) same section as (c), visualized with light microscopy. L.B. and red arrows = lamellar bone, OST. = osteodermine, S.F.B. = Sharpey-fibered bone, S.S. = stratum superficiale, white arrows = Sharpey's fibres.

Scale bars: All 100μm.

and the blue/green fibres exhibiting a dorsoventral orientation. As with the histological sections, it is clear that these collagen fibres originate in the dermis, and are metaplastically mineralised, not only because they exhibit the same structure as the non-mineralised dermis, but also because they can be seen originating in the dermis and seamlessly entering into the mineralised base of the OD.

These results were further confirmed with Multi-rotation polarised light microscopy (MRPLM) (Fig 4.2), where a "maltese cross" were again seen in the L.B. region, in multiple sections and images. Consistent histology was seen for OST., with negative staining and a lack of a birefringent collagen matrix, save for a few Sharpey's Fibres (Fig 4.2c, d, white arrows),

Following polarised light microscopy, samples of *Heloderma suspectum* OD sections were imaged with higher resolution micro-CT (μ-CT) scanning. Using this technique, CT scan data of a dorsal post-cranial OD visualised with density-dependant greyscale volume rendering (Fig 4.3a), again exhibited branching internal channels of vasculature occasionally surrounded by a dark coloured, thus less-dense region (L.B.). When comparing the material in the basal region (S.F.B.) to the superficial region (OST.), there are dramatic differences in density, with the S.F.B. shaded darker, thus less dense, than the OST. which is shaded lighter, thus denser. L.B. is shaded darker than either region, thus is the least dense material present. There is also an obvious reduction in collagen fibre content in the OST. region compared to S.F.B. and local differences in the mineralisation of the OST., that can be observed as alternating grey lines appearing from disparities in X-ray opacity. These lines resemble the lines of arrested growth (LAGs) described in polarising microscope and SEM results and have previously been designated as corresponding to periodic growth of the OST. tissue (de Buffrénil et al., 2010).

The results of the Z-projection (one image that acts as a representation of multiple images in the z plane) complimented findings from density-dependant μ-CT 3D visualisation in that the different materials display clear differences in structural composition and density. OST. (Fig.4.3b) is brighter, thus denser than any of the materials, containing thin bundles of Sharpey's fibres of collagen, whereas S.F.B. appears darker, thus less dense and is composed of thicker, orthogonal fibres of collagen. L.B. also appeared in z-projections of the OD (Fig 4.3c). Z-projections of

S.F.B. and L.B. also show well-developed osteocyte lacunae, (black holes), whereas OST. shows no lacunae.
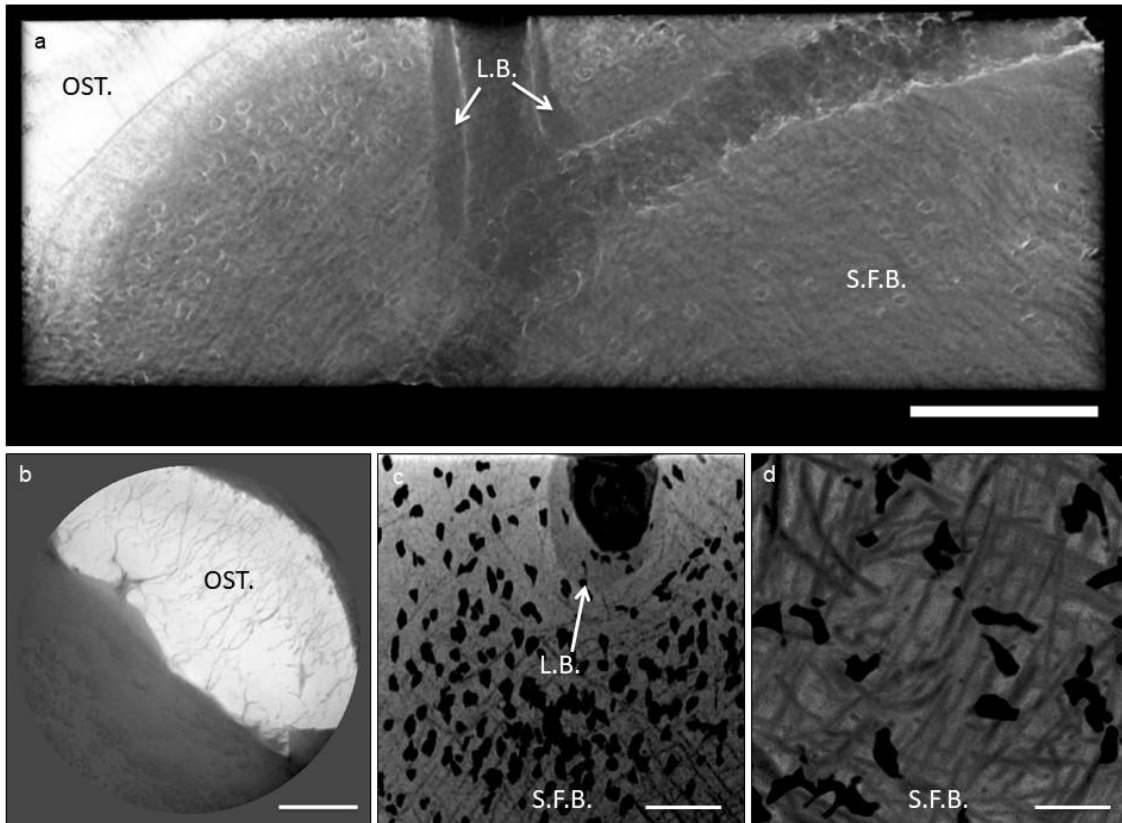
Figure 4.3: µ-CT scan data and Z-projection analysis of *Heloderma suspectum* OD (a) Volume render of CT scan data, density-dependant greyscale view, (b) Z-projection (coronal view) using the minimum pixel brightness of 100 sections from an image sequence of CT scan data in the osteodermine (OST.) region, (c) in the Sharpey-fibred bone (S.F.B.) and lamellar bone regions (L.B.), and (d) in the Sharpey-fibred bone (S.F.B.) region (d).

Scale bars: (a) = 200µm, (b) = 50µm, (c) = 100µm, (d) = 25µm.

Z-projections of OST. and S.F.B. were created from high resolution µ-CT scans of laser-cut pillars of OD, but the z-projection of L.B. is at a lower resolution. Because the expression of L.B. is less common than the other materials, and because it is only found surrounding the walls of foramina within the OD, it was difficult to laser cut a cylinder out of the OD that contained this material for CT scanning. The L.B. is the rarest material within the OD thus is hard to target and the lumen of the foramen made the cylinders structurally unstable. Although µ -CT scans of cylinders that were thought to contain L.B. were attempted, when examined these were found to contain

the more common S.F.B. region rather than L.B. The Z-projection of L.B. (Fig. 4.3c) was created from the lower resolution CT-scan used in Fig 4.3a.
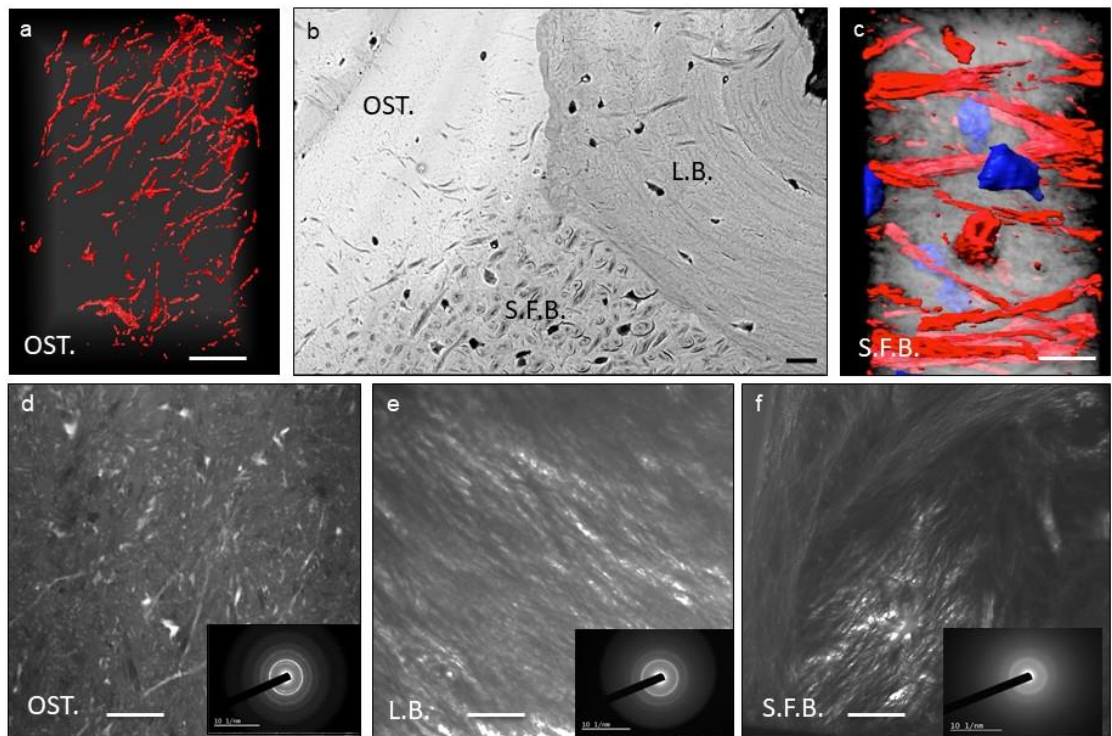
Figure 4.4: (a) High magnification 3D surface reconstruction of **μ**-CT data from the osteodermine region, (b) BSE-SEM micrograph displaying all three separately structured materials, (c) high magnification 3D reconstruction of μ-CT scan data from the S.F.B. region. Red and blue regions relate to specified histogram ranges, white region relates to mineral as brighter voxels represent more dense material. FIB-TEMs with corresponding electron diffraction patterns for (d) osteodermine (OST.), (e) lamellar bone (L.B.) and (f) Sharpey-fibred bone (S.F.B.).

Scale bars: (a) = 50μm, (b) = 20μm, (c) = 20μm, (d-f) = 0.20μm.

3D reconstructions of the higher resolution μ-CT data used to produce the z-projections of OST. (Fig. 4.4a) and S.F.B. (Fig. 4.4c) again highlight differences in the ultrastructural arrangement between the two materials – the fibres are thinner and are parallel in OST. but are thicker and orthogonal in S.F.B. and the material contains no lacunae, whereas S.F.B. displays regularly interspaced bundles of fibres (false-coloured red) with many associated lacunae (false-coloured blue). When viewing a BSE-SEM of all three materials in the same SEM image (Fig.4.4b), the difference in the size and distribution of the mineralised collagen fibres within each material is readily comparable, for example, the average diameter of the collagen in the S.F.B. is greater than the majority of that within the L.B. region or the OST. region. The

differences in pixel brightness (relating to density and mineralisation) are also very apparent in this image, with OST. appearing brightest, thus most dense, then S.F.B., with the L.B. appearing least dense.

Figure 4.4 also depicts FIB-TEM results for the three materials (Fig. 4.4d, e, f). These indicate that the collagen orientation differs between these materials on the nanoscale. The FIB-TEM result for OST. (Fig. 4.4d) did not feature any collagen fibres with banding of 65nm. Collagen fibres and subsequent 65nm banding were observed in L.B. (Fig. 4.3e) and S.F.B. (Fig. 4.4f) results. As expected, the fibres were small and parallel to each other in the L.B. region but in S.F.B. region the collagen is present in thicker bundles and not orientated in parallel. Electron diffraction patterns obtained from the different regions show distinct differences in crystallinity and crystal phase (Fig. 4.4d, e, f, inserts). OST. displays the most crystalline diffraction pattern (with characteristic bright rings of intensity) of a single crystal of hydroxyapatite (HA), whereas the diffraction patterns for L.B. and S.F.B. exhibited a less crystalline pattern (electrons scattered in many directions leading to a widely distributed haze of intensity). This is because in samples that contain single crystals, in a single geometric lattice, the atoms concentrate the electron diffraction into single points, whereas in less crystalline samples, with many different crystals in multiple lattice orientations, the electron diffraction occurs over a wider range of area.

The results presented thus far were all been collected from osteoderms sampled from one anatomical location (post-cranial, dorsal osteoderms). In order to confirm that the materials identified in these ODs where universally expressed throughout the body of *Heloderma suspectum*, it was thought appropriate to sample from more locations around the body. Therefore, four different anatomical locations were sampled using BSE-SEM and the results for all three materials - OST. (Fig. 4.5), S.F.B. (Fig. 4.6) and L.B. (Fig. 4.7) are presented. These results assist with comparisons on the structural composition and density of each material across the body of the animal. They show that all of these materials can be readily identified in multiple sections from multiple anatomical locations around the animal. This confirms that expression of these materials is universal regardless of where on the body the OD is sampled.
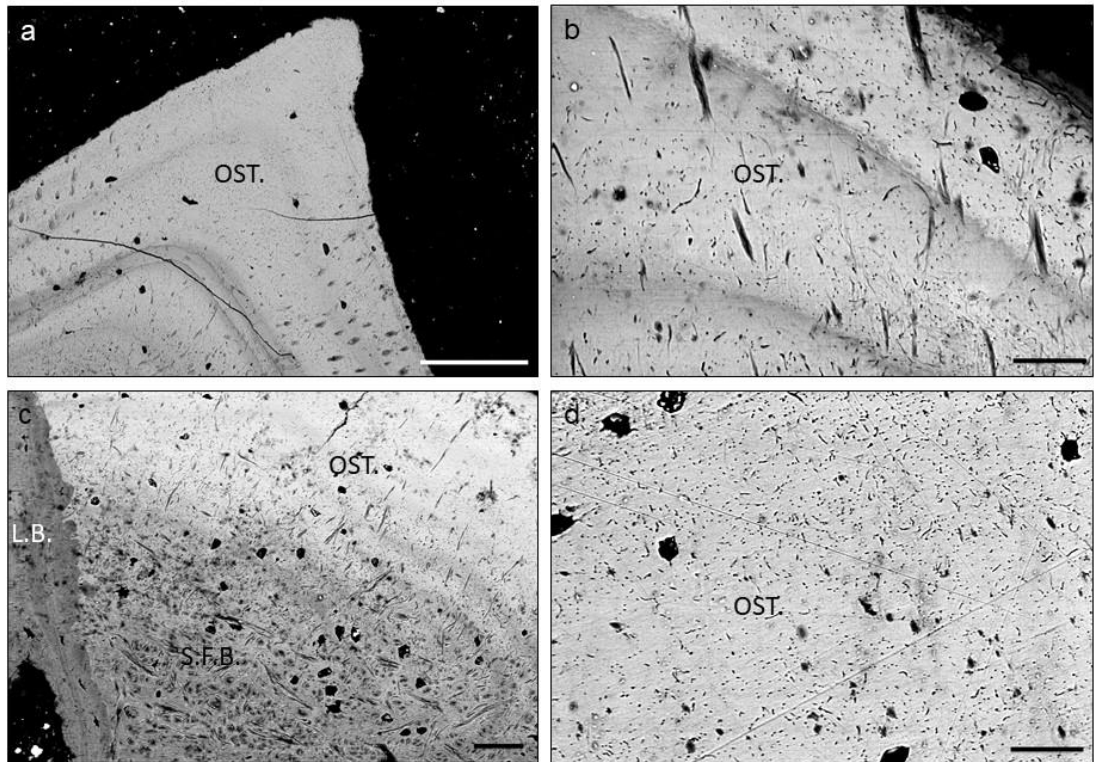
Figure 4.5: BSE-SEM micrographs of *Heloderma suspectum* OD, ground, polished sections from dorsum (a), side of neck (b), forearm (c) and tail (d). These sections afford a direct comparison between the structural composition of osteodermine (OST.) in relation to lamellar bone (L.B.) and Sharpey-fibred bone (S.F.B.)

Scale bars: (a) = 100µm, (b) = 20µm, (c) = 40µm, (d) = 20µm.
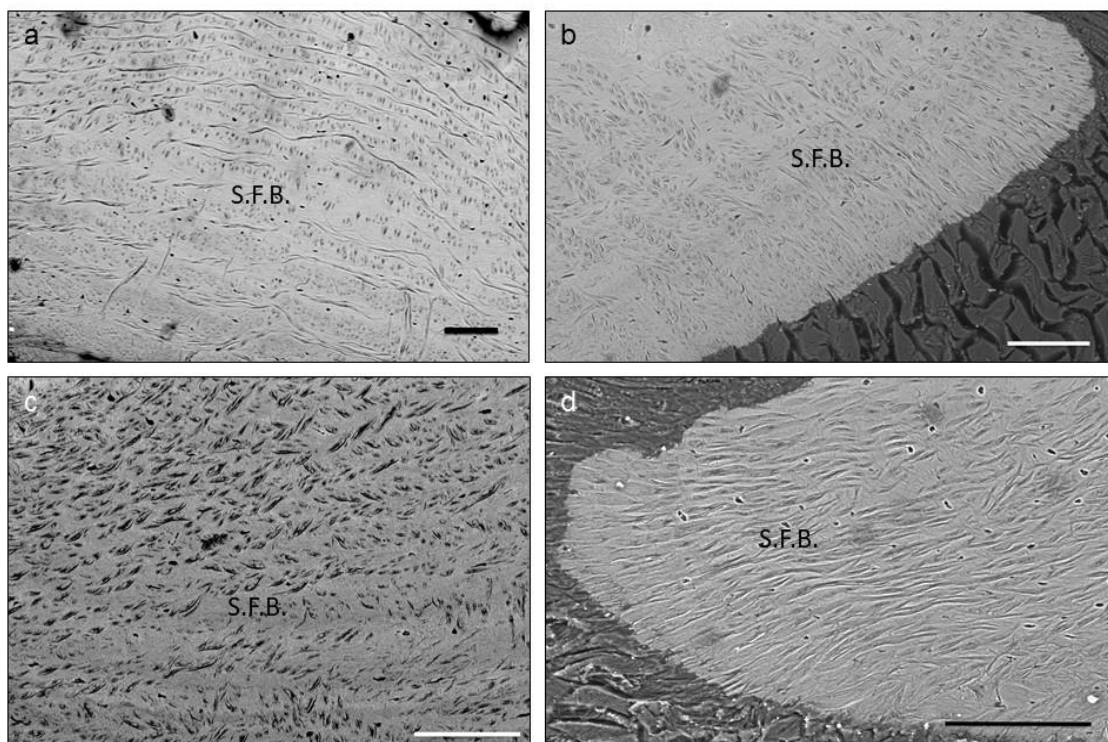
Figure 4.6: BSE-SEM Micrograph of *Heloderma suspectum* OD, ground, polished sections from (a) dorsum, (b) side of neck, (c) forearm and (d) tail. Highlighting the structural composition of Sharpey-fibred bone (S.F.B.).

Scale bars: (a) = 100μm, (b) = 100μm, (c) = 100μm, (d) = 100μm.

Dense, spherical objects were identified in the OST. region in both TEM (Fig. 4.7a and b) and separate SEM results (Fig 4.7c and d). Elemental mapping using EDX was achieved using a sample prepared in the same way for SEM analysis (Fig 4.9). This afforded a 2D view of the distribution of specific elements across the surface of the section. It was possible to identify increased counts of elements present in Hydroxyapatite (HA), including calcium (Ca), phosphorus (P) and oxygen (O), in the OST. region (superficial) compared to the basal S.F.B. and L.B. (basal) regions. The presence of HA was confirmed by comparison of the spectrum obtained from the osteoderm test sample to a hydroxyapatite control sample.
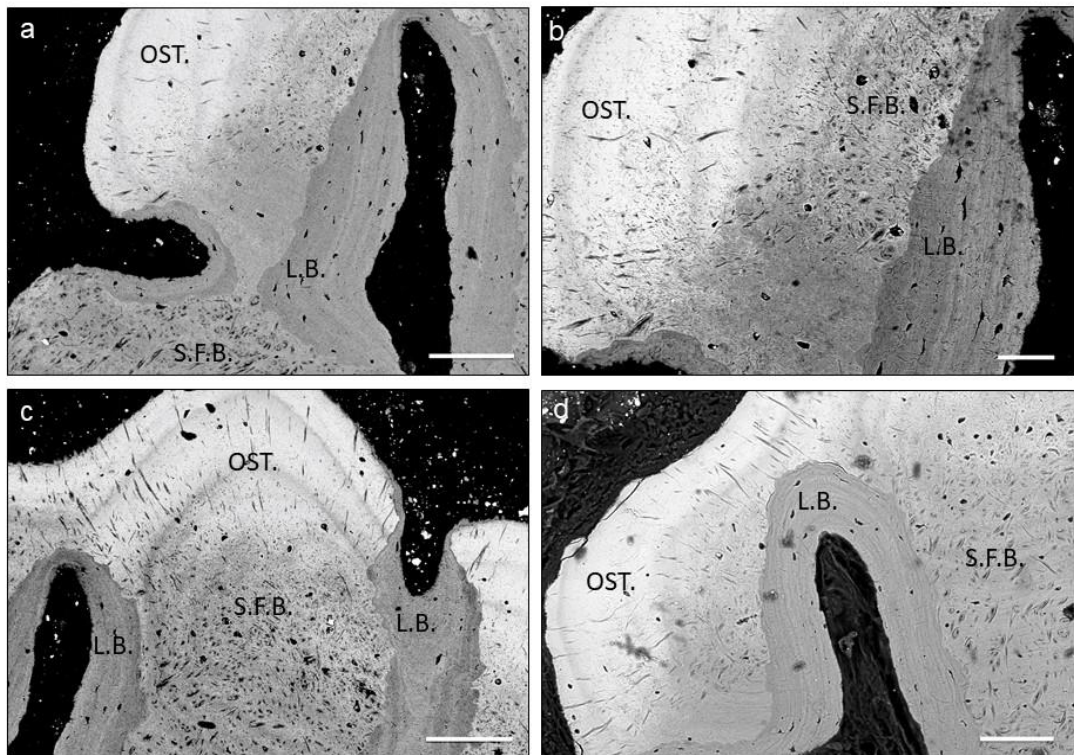
Figure 4.7: BSE-SEM micrographs of *Heloderma suspectum* OD, ground, polished sections from (a) dorsum, (b) side of neck, (c) forearm and (d) tail. These sections afford a direct comparison between the structural composition of lamellar bone (L.B.) in relation to osteodermine (OST.) and Sharpey-fibred bone (S.F.B.).

Scale bars: (a) = 100μm, (b) = 40μm, (c) = 100μm, (d) = 100μm.
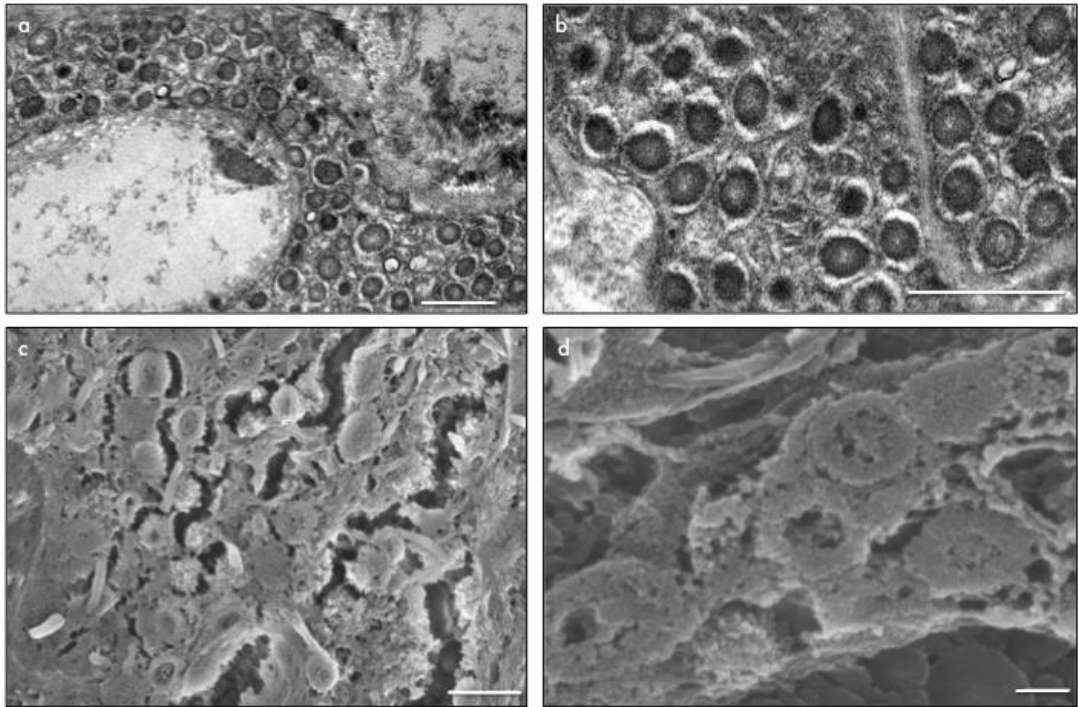
Figure 4.8: TEM micrographs at (a) lower and (b) higher magnification displaying localized clusters of 500nm-1µm diameter spherical particles containing dense, granulated material. These were also identified in SEM micrographs at (c) lower and (d) higher magnification.

Scale bars: a = 2µm, b = 2µm, c = 1µm, d = 200nm.
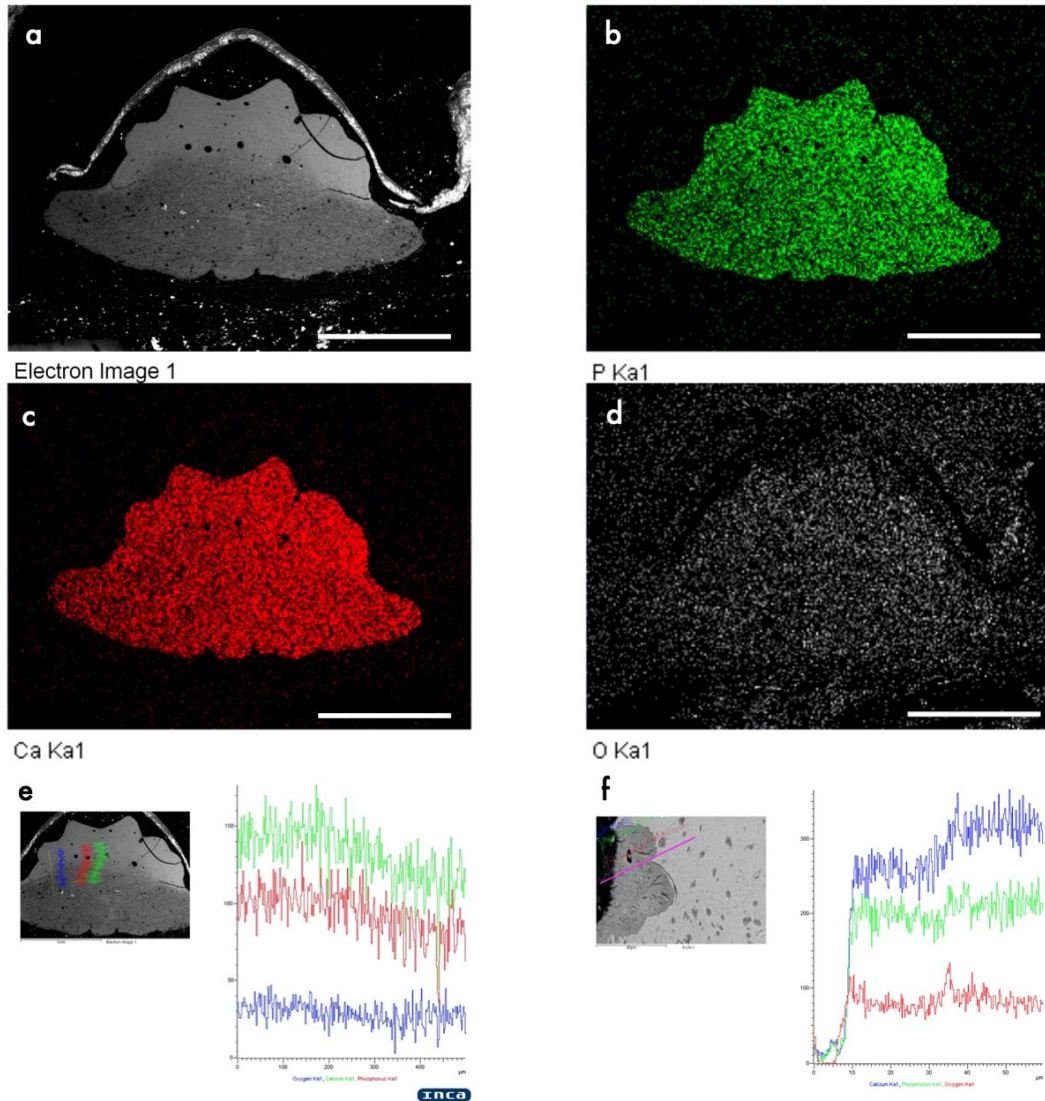
Figure 4.9: (a) SEM BSE micrograph and corresponding EDX mapping of elements present in *Heloderma suspectum* OD. Differences in counts for Phosphorus (P, b), Calcium (Ca, c) and Oxygen (O, d) can be seen between the mineralised OD and surrounding soft tissue. Differences in elemental counts can be better observed when counts are displayed on a graph against a line of distance, as in (e), where the line of sampling moves from the OST. region of the OD, to the M.B. region, and in (f), from the P.F.B. region to the OST region. Increased counts correspond to more highly mineralised areas.

Scale bars: all 1mm.

4.3 Discussion

The techniques that were used in this chapter helped to further characterise the materials in *Heloderma suspectum* ODs. Polarised light microscopy showed that the OST. region was devoid of collagen and the S.F.B. and L.B. materials displayed a different collagen orientation compared to one another. Polarised light microscopy also exhibited a maltese cross in the L.B. region, suggesting this is a secondary osteon, which indicates remodelling occurred during OD formation. The contiguous lamellae show corresponding anisotropic extinction, consistent with an interpretation as a secondary reconstruction of L.B. (Francillon-Vieillot et al., 1989). Within the OD, L.B. was only found surrounding the neurovascular lumen. Occasionally, it was possible to identify proximal vascular channels that were not encased by L.B., meaning that this feature is not an essential component of the composite material and/or that these are primary vascular canals (de Buffrénil et al., 2010). The fact that the L.B. was not always found to encase the lumen adds complexity when considering the presence of osteons as traditional bone-like structures, in direct association to the S.F.B.. This combination of both S.F.B. and traditional haversian systems in squamate ODs is similar to a system that has also been observed in alligators (Vickaryous and Hall, 2008). The vascular channels may either be an artefact of remodelling as hypothesised in glyptosaurine ODs (de Buffrénil et al., 2010) or a vascular structure that was present in the dermis prior to mineralisation. Remodelling of OD materials has been documented many times before, but remains a controversial issue (de Buffrénil et al., 2010; Farlow et al., 2010; Buchwitz et al., 2012; Horner et al., 2016).

The basal cortices of *H. suspectum* ODs contain regularly interspaced bundles of collagen fibres that were observed to weave seamlessly between the mineralised base of the OD and the surrounding dermal collagen mesh of the stratum compactum without any periosteal membrane between the mineralised and non-mineralised areas. These attributes mean that the nascent osteoderm primordia likely becomes spontaneously mineralised along with associated cells of the skin. Previous identification of W.B. , or S.F.B. in the basal part of the OD (Vickaryous and Sire, 2009), must consist of mineralised existing structures, created through a process of bone metaplasia - the direct mineralisation of pre-existing tissue without formation of osteoid and hypothetically without contributions from osteoblasts.

The results in this chapter again proved a lack of collagen matrix in the OST. region (the only collagen present resembles Sharpey's fibres), with this region being the most highly mineralised of the three. Thin sections of OST. also displayed a crystallinity of a single crystal whereas the other materials were amorphous, meaning that large crystals of HA are likely present in OST. in greater proportions to the other materials, probably due to the lack of a collagen matrix. Similar studies comparing the nanostructure, or the crystallinity of the mineral phase between the materials present within ODs could not be found in the literature. Pits and troughs in the apical surface of the OST. are likely to be formed via homologous processes to bone ornamentation (Clarac et al., 2019; de Buffrénil et al., 2015). OST. was also only found on the apical surface of the OD. This is the surface closest to the basal layers of the epidermis and previous authors have alluded to the need for epidermal contribution regarding the mineralisation of OST. given its similarity to other hyper-mineralised tissues such as ganoine (Moss, 1969; de Buffrénil et al., 2010). This also relates to how the inner dental epithelium secretes a protein that interacts with the enameloid matrix (Francillon-Vieillot et al., 1989) in the formation of enamel, another hyper-mineralised tissue. Cell spaces, although rarer than in the other regions, were identified in OST., thus describing this tissue as "acellular" (de Buffrénil et al., 2011) is a misnomer.

Consecutive dark lines were observed in the OST. region under density dependant μ-CT which correspond to de Buffrénil et al.'s (2011) findings of arrested growth lines relating to periodic mineral deposition. These are homologous to the LAGs identified in SEM and histological sections in Chapter 3. Acidic mucosubstances were hypothesised to compose the microfibrillar matrix of OST. in the previous chapter and in *Tarentola* ODs. Levrat-Calviac and Zylberberg (1986) proposed LAGs form due to the accumulation of these mucosubstances during seasonal changes in growth. The origin and developmental prerequisites of this tissue has yet to be identified as further cellular and embryonic studies are required but other authors (de Buffrénil et al., 2011; Vickaryous et al., 2015) have hypothesised that this tissue is odontogenic in origin or at least requires contributions from basal epidermal cells in order to form.

Spherical objects were identified in the OST. region in both TEM and separate SEM results (Fig 4.8). These spherules resemble the calcospherites previously observed in the OST. capping tissue of *Tarentola* ODs (Levrat-Calviac and Zylberberg, 1986) as well as in other mineralised tissues (Boyde and Sela, 1978). This indicates that mineralisation of OST. occurs via spheritic mineralisation as in calcified cartilage (Francillon-Vieillot et al., 1989). Calcified cartilage contains more mineral than bone

and OST. was found to be denser and more highly mineralised compared to the bony basal materials adding weight to this hypothesis. This finding suggests two mineralisation processes occur in OD development in *Heloderma suspectum* – inotropic mineralisation in the basal bone regions and spheritic mineralisation in the capping OST..

The ability to distinguish between the OST. region (superficial) compared to the basal S.F.B. and L.B. (basal) regions using energy dispersive x-ray spectroscopy (EDX) highlights how this technique could be used in the identification of OST. in the future.

4.4   Conclusions

- The three materials that compose the ODs of *Heloderma suspectum* display significant differences in collagen expression, composition, orientation, and thickness on micro and nano scales.
- These materials also exhibit differences in crystallinity of the mineral phase and density of mineral deposited.
- Osteoderms from multiple anatomical locations were observed as being composed of these three materials, suggesting their expression is universal and consistent.
- Spheritic mineralisation may be involved in OST. formation.

4.5　References

Bromage T. G., Goldman H. M., McFarlin S. C., Warshaw J., Boyde A. and Riggs C. M. (2003) Circularly polarized light standards for investigations of collagen fiber orientation in bone. *Anatomical Record - Part B New Anatomist* **274**:157-168.

Boyde A. and Sela J. (1978) Scanning electron microscope study of separate calcospherites from the matrices of different mineralizing systems. *Calcified Tissue Re*search **26**:47-50.

Buchwitz M., Witzmann F., Voigt S. and Golubev V. (2012) Osteoderm microstructure indicates the presence of a crocodylian-like trunk bracing system in a group of armoured basal tetrapods. *Acta Zoologica* **93**:260-280.

Clarac F., Goussard F., de Buffrénil V., and Sansalone V. (2019) The function(s) of bone ornamentation in the crocodylomorph osteoderms: a biomechanical model based on a finite element analysis. *Paleobiology* **45:**182–200.

De Buffrénil V., Clarac F., Fau M., Martin S., Martin B., Pellé E. and Laurin M. (2015) Differentiation and growth of bone ornamentation in vertebrates: A comparative histological study among the Crocodylomorpha. *Journal of Morphology* **276**:425-445.

De Buffrénil V., Sire J-Y. and Rage J-C. (2010) The histological structure of glyptosaurine osteoderms (Squamata: Anguidae), and the problem of osteoderm development in squamates. *Journal of Morphology* **271**:729-737.

De Buffrénil V., Dauphin Y., Rage J-C. and Sire J-Y. (2011) An enamel-like tissue, osteodermine, on the osteoderms of a fossil anguid (Glyptosaurinae) lizard. *Comptes Rendus de l'Academie des Sciences Palevol* **10:**427-437.

Farlow J. O., Hayashi S. and Tattersall G. J. (2010) Internal vascularity of the dermal plates of *Stegosaurus* (Ornithischia, Thyreophora). *Swiss Journal of Geosciences* **103**:173-185.

Francillon-Vieillot H., de Buffrénil V., Castanet J., Géraudie J., Meunier F. J., Sire J.-Y. and de Ricqlès A. (1989) Microstructure and mineralization of vertebrate skeletal tissues. *Skeletal Biomineralization: Patterns, Processes and Evolutionary Trendsiomineralization: Patterns, Processes and Evolutionary Trends*, **5:**175–234.

Horner J. R., Woodward H. N. and Bailleul A. M. (2016) Mineralized tissues in dinosaurs interpreted as having formed through metaplasia: a preliminary evaluation. *Comptes Rendus – Palevol* **15**:183–203.

Levrat-Calviac V. and Zylberberg L. (1986) The structure of the osteoderms in the gekko: *Tarentola mauritanica. American Journal of Anatomy* **446**:437–446.

Moss M. L. (1969) Comparative histology of dermal sclerifications in reptiles. *Cells Tissues Organs*, **73**:510–533.

Vickaryous M. K. and Hall B. K. (2008) Development of the dermal skeleton in *Alligator mississippiensis* (Archosauria, Crocodylia) with comments on the homology of osteoderms. *Journal of Morphology* **269**:398–422.

Vickaryous M. K., Meldrum G. and Russell A. P. (2015) Armored geckos: a histological investigation of osteoderm development in *Tarentola* (Phyllodactylidae) and *Gekko* (Gekkonidae) with comments on their regeneration and inferred function. *Journal of Morphology* **276**:1345–1357.

Vickaryous M. K. and Sire J-Y. (2009) The integumentary skeleton of tetrapods: origin, evolution, and development. *Journal of Anatomy* **214**:441–464.

5 CHAPTER 5 Histology of osteoderms from other lizard families

5.1 Introduction

Chapter 1 contains a review of our current knowledge of the gross anatomy and microstructure of ODs in lizards, but a brief reintroduction follows. The previous chapters examined the overall gross anatomy and micromaterial composition of osteoderms (ODs), focusing on one species of lizard, *Heloderma suspectum*.

Among the other lepidosaurs, ODs are absent from all snakes and amphisbaenians, and all but a single species of rhynchocephalian (the fossil form *Pamizinsaurus tlayuaensis*, Reynoso, 1997), but are well-represented in lizards (Squamata). Among lizards, ODs are common to representative gekkotans (Vickaryous et al., 2015; Laver et al., 2019), scincids (Camp, 1923), cordyliforms including gerrhosaurids (Camp, 1923; Stanley et al., 2016), xenosaurids (Gao and Norell, 1998), helodermatids (Moss, 1969), anguids (Strahm and Schwartz, 1977; Zylberberg and Castanet, 1985), anniellids (Bhullar and Bell, 2008), shinisaurids (Bever et al., 2005), lanthanotids (McDowell and Bogart, 1954; Maisano et al., 2002), varanids (Erickson et al., 2003; Maisano et al., 2019), and the cranium of some lacertids (Read, 1986; Borsuk-Białynicka et al., 1999), xantusiids (Camp, 1923), and iguanians (de Queiroz, 1987; Schucht et al., 2020). A tree outlining how these lizards are related and their corresponding cranial OD anatomy as revealed using HRXCT is shown in Fig. 5.1. The families that contain species sampled in this study are highlighted in this figure with a five-pointed star.
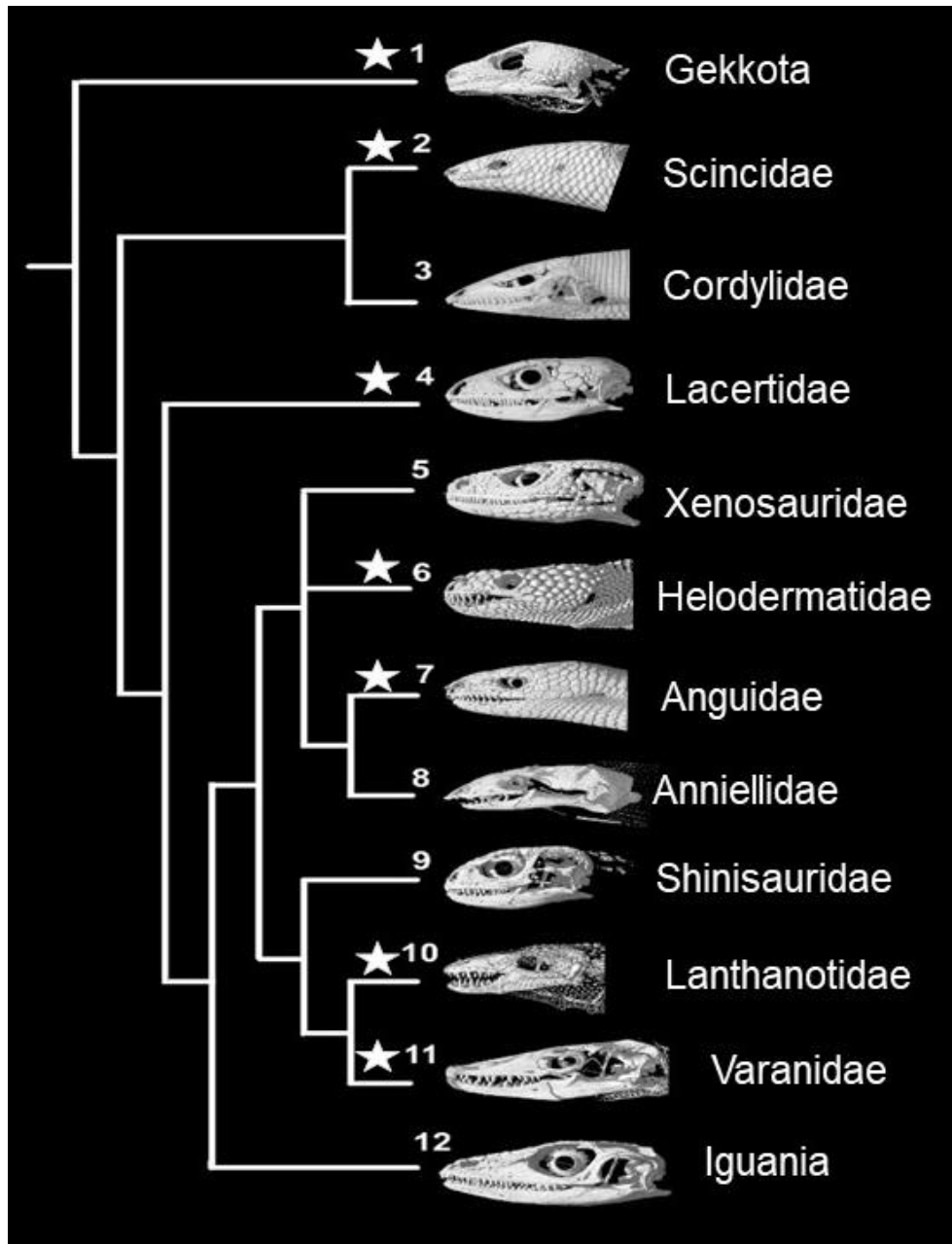
Figure 5.1: Tree of lizard relationships based on molecular evidence showing cranial osteoderm arrangement in the following groups: 1,Gekkota*; 2, Scincidae*; 3, Cordyliformes; 4, Lacertidae*; 5, Xenosauridae; 6, Helodermatidae*; 7, Anguidae*; 8, Anniellidae; 9, Shinisauridae; 10,Lanthanotidae; 11,Varanoidea*; 12, Iguania. * = groups with species targeted in this study.
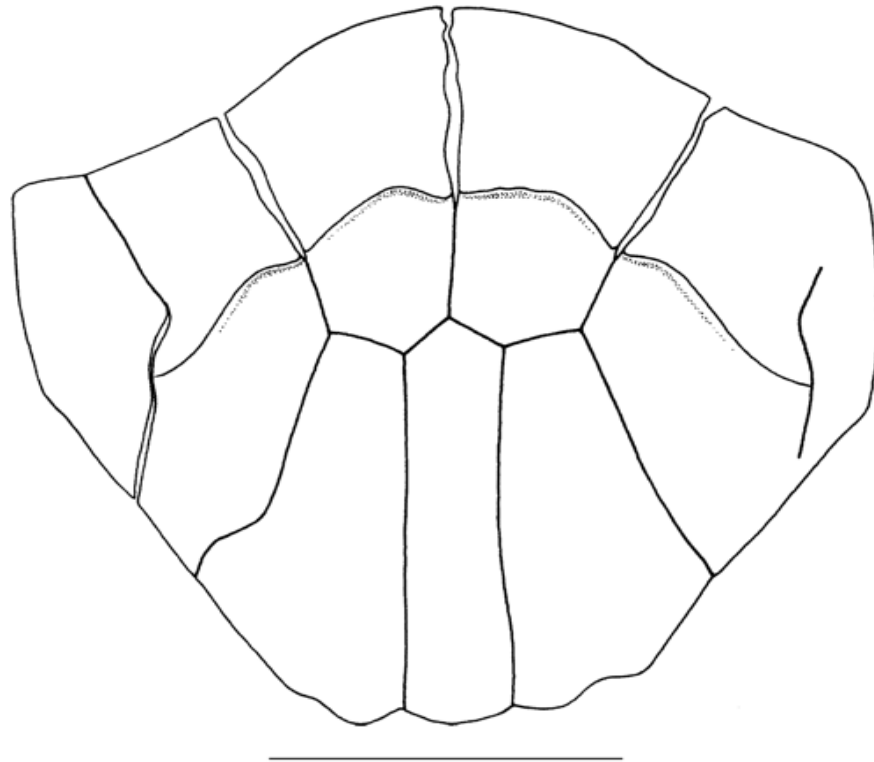
Figure 5.2: Typical scientific illustration of OD from the mid-dorsal trunk of *Mabuya gravenhorstii* depicting many small plates making up a compound arrangement typical of a skink osteoderm. Dorsal view, anterior direction corresponds to the top of the image. (Adapted from Greer, 2007)

Scale bar: 1 mm.

Most early analyses of ODs consist of scientific illustrations drawn by hand. Figure 5.2 shows a typical scientific illustration of a skink OD, from the species *Mabuya gravenhorstii.* The nomenclature "plates" or "units", meaning the multiple modular units that combine to form a single compound OD, is herein synonymous with "osteodermites" or ODites.

Many authors have made observations on the material composition of ODs in various species, but a comprehensive comparison of both OD gross anatomy and microstructure (internal composition), across multiple families of squamates, has yet to be accomplished. Most studies concentrate on documenting OD anatomy and histology in a single species (e.g. *Gekko gecko,* Laver et al., 2019), genus (e.g.

Tarentola, Vickaryous et al., 2015), or family of lizards (e.g. Cordylids, Broeckhoven et al., 2015) and make comparisons to other genera or families based on the available literature This is likely due to a lack of specimen material and perhaps limited access to more sophisticated techniques. Detailed descriptions of internal anatomy have only been made possible with the development, improvement, and wider availability of various techniques in the last 25-50 years. These techniques include electron microscopy (EM) and high-resolution X-ray computed tomography (HRXCT). However, there has been limited application in studying the gross anatomy and micromaterial anatomy of ODs in squamates. On the occasions that internal anatomy has been studied, the composition and microanatomical structure of squamate ODs is documented as being highly variable (Vickaryous and Hall, 2008). Indeed, present day techniques have developed sufficiently to allow us to elucidate the material composition, gross anatomy and general arrangement of ODs very quickly, relatively cheaply and easily (Maisano et al., 2019).

As discussed in Chapter 1, the ODs of squamates have been described as composed of many different types of bone. The names given to materials comprising ODs have included mineralised structural fibres, highly vascularised cancellous bone, compact cortical bone, P.F.B., W.B., L.B., S.F.B. and OST. (Vickaryous and Sire, 2009; Farlow et al., 2010; Sun and Chen, 2013). This chapter aims to address the uncertainty surrounding OD micromaterial composition, by using consistent terminology as outlined in Chapter 1 to characterise the histology of multiple families of extant lizards. Moss (1969) argued that most dermal ossification among reptiles occurs by tendinous and not by periosteal ossification, such that the ODs are metaplastically ossified. Further analysis of how reptiles can initiate such substantial dermal and metaplastic ossification may well contribute to understanding the relationships of modern-day dermal ossifications to the earliest tetrapods and ancient fish. Functional aspects of OD expression were also explored in Chapter 1, this chapter aims to use the data collected in a more comprehensive attempt to develop a hypothesis for function from different structural motifs.

The possible problem of variation due to ontogenetic changes was controlled in this study by obtaining adult specimens whenever possible. However, ontogenetic changes were observed in two species, by sampling one juvenile specimen of *Ophisaurus ventralis* and one juvenile specimen of *Varanus komodoensis*, to compare these results with the adult specimens.

Examples of the following families of squamates were analysed: Helodermatidae, Varanidae, Scincidae, Anguidae, Gekkota (Gekkonidae, Phyllodactylidae), and Lanthanotidae. With the archosaur Crocodylidae used as an outgroup, one of the most important aspects to consider when determining which lizards to sample was the need to sample a broad array of lizards native to many different environments, in a diverse range of ecological niches. This was done with the aim of testing whether it is possible to identify any link between gross OD expression or OD micromaterial composition and the lifestyle/ecology of the lizards concerned (e.g. prey type; predation risk; intraspecies aggression, burrowing or tree living etc.). Essentially, the first step was to characterise the anatomy and material components of the ODs in these lizards and then assess whether any functional aspects of OD expression could be extracted from this data, to compare results in an ecological context using what is known about the habitat and lifestyle that each lizard occupies.

This chapter therefore aims to document both the gross morphology and micromaterial anatomy of the ODs of multiple families of squamates using modern techniques, to firstly address gaps in our knowledge and then to use these results to determine relationships (if any), between expression, gross anatomy, micromaterial composition, function and/or ecology.

5.2   Results

5.2.1   Introduction

As in earlier chapters for *Heloderma suspectum,* an initial investigation into the gross anatomy and organisation of ODs was conducted using X-ray plate imaging. This was performed to obtain a low-magnification, simple overview of any mineralised structures present in the skin. Following this initial overview, after identifying ODs to be targeted, histological staining, multi-rotation polarised light, HRXCT and BSE-SEM were used to investigate the microstructural anatomy of the ODs that were present.
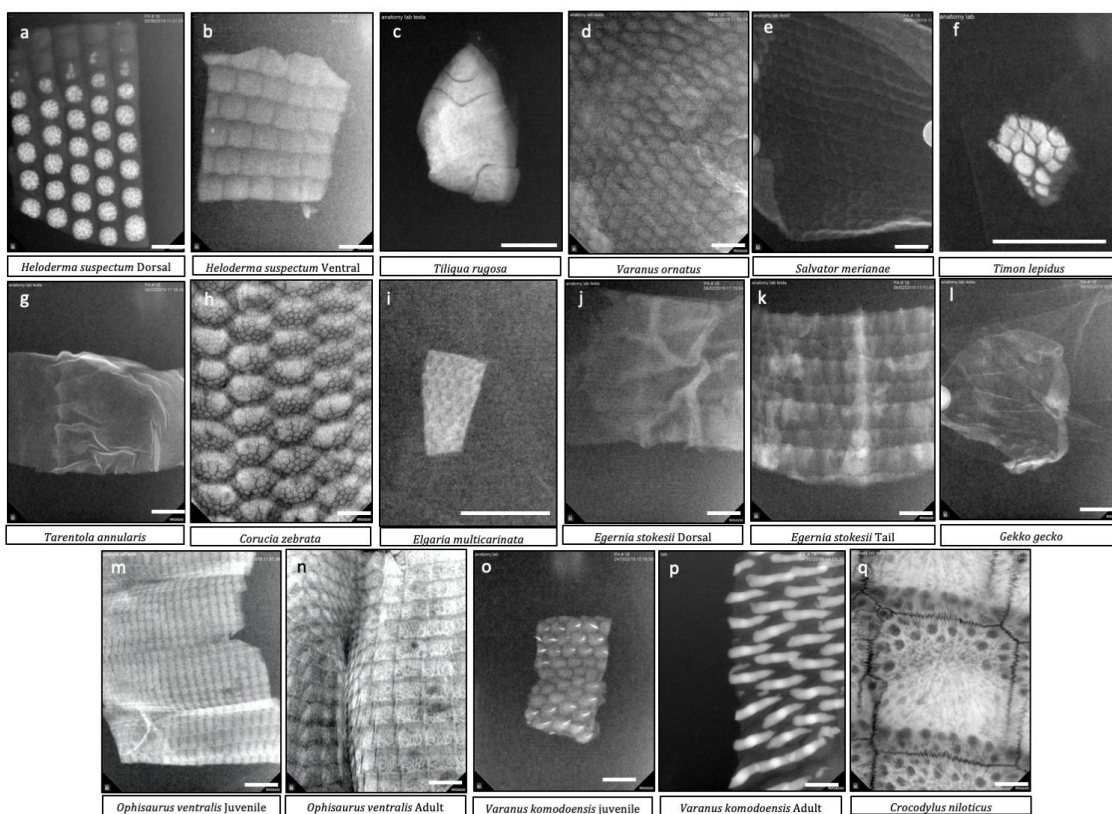
Figure 5.3: Comparative X-ray plate imaging of reptile skin (all are adult unless stated as juvenile, and all except q are squamate). (a) *Heloderma suspectum* dorsal*,* (b) *Heloderma suspectum* ventral, (c) *Tiliqua rugosa*, (d) *Varanus ornatus*, (e) *Salvator merianae*, (f) *Timon lepidus,* (g) *Tarentola annularis,* (h) *Corucia zebrata, (i) Elgaria multicarinata,* (j) *Egernia stokesii* dorsal*,* (k) *Egernia stokesii* tail*,* (l) *Gekko gecko,* (m) *Ophisaurus ventralis juvenile, (n) Ophisaurus ventralis* adult*,* (o) *Varanus komodoensis juvenile, (p) Varanus komodoensis adult and (q) Crocodylus niloticus.*

Scale bars: all = 5mm.

Figure 5.3 presents X-ray plate results for all sampled taxa in this study. Of the 17 (a-q), different images, 11 (a, c, d, f, g, h, i, m, n, o, p) show mineralisations in the skin. The species in which no mineralisation was observed (b, e, j, k, l, q), include *Heloderma suspectum* (ventral skin), *Salvator merianae* (dorsal skin), *Egernia stokesii* (dorsal skin and tail), *Gekko gecko* (dorsal body skin) and *Varanus niloticus* (dorsal skin). Each taxon for which an image is shown in Fig. 5.3 has dedicated figures further on in this section.
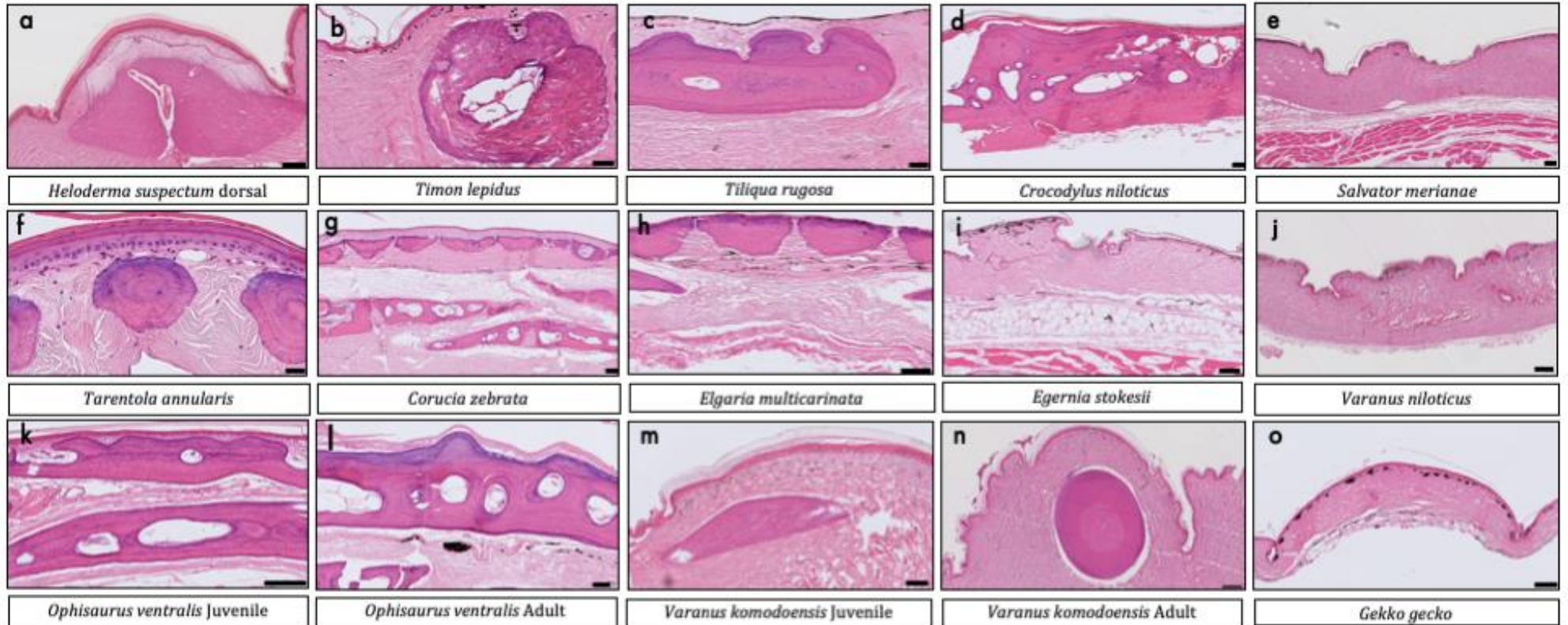
Figure 5.4: Comparative H&E histological staining of reptile skin (all except d are squamate) in (a) *Heloderma suspectum,* (b) *Timon lepidus*, (c) *Tiliqua rugosa*, (d) *Crocodylus niloticus*, (e) *Salvator merianae*, (f) *Tarentola annularis,* (g) *Corucia zebrata*, (h) *Elgaria multicarinata,* (i) *Egernia stokesii,* (j) *Varanus niloticus,* (k) *Ophisaurus ventralis juvenile,* (l) *Ophisaurus ventralis* adult*,* (m) *Varanus komodoensis juvenile,* (n) *Varanus komodoensis* adult*,* (o) *Gekko gecko.*

Scale bars: (a) = 200µm, (b) = 100µm, (c) = 100µm, (d) = 100µm, (e) = 100µm, (f) = 20µm, (g) = 100µm, (h) = 100µm, (i) = 200µm, (j) = 100µm, (k) = 100µm, (l) = 100µm, (m) = 200µm, (n) = 200µm, (o) = 100µm.

Figure 5.4 presents H&E histological staining results for all dorsal skin samples of the taxa in this study. Of the 15 (a-o), different images, 11 (a, b, c, d, f, g, h, k, l, m, n) show mineralisations in the skin. The species in which no mineralisation was observed (e, i, j, o), include *Salvator merianae*, *Egernia stokesii*, *Varanus niloticus* and *Gekko gecko.*
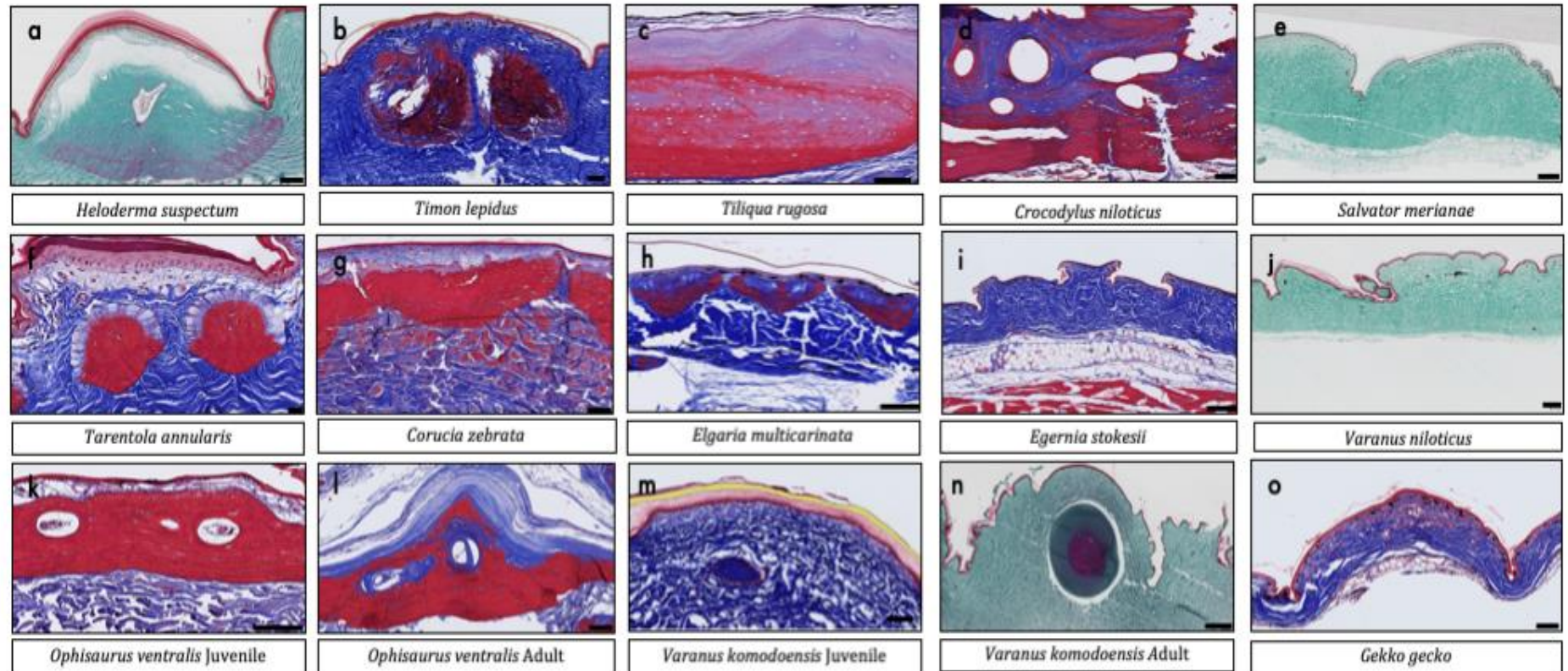
Figure 5.5: Comparative Masson's Trichrome histological staining of reptile skin (all except d are squamate) in (a) *Heloderma suspectum,* (b) *Timon lepidus*, (c) *Tiliqua rugosa*, (d) *Crocodylus niloticus*, (e) *Salvator merianae*, (f) *Tarentola annularis,* (g) *Corucia zebrata*, (h) *Elgaria multicarinata, (i) Egernia stokesii,* (j) *Varanus niloticus,* (k) *Ophisaurus ventralis juvenile,* (l) *Ophisaurus ventralis* adult*, (m) Varanus komodoensis juvenile,* (n) *Varanus komodoensis* adult*, (o) Gekko gecko.* Red staining = keratin, green/blue staining = collagen, yellow/white = no stain.

Scale bars: (a) = 200µm, (b) = 100µm, (c) = 100µm, (d) = 100µm, (e) = 200µm, (f) = 20µm, (g) = 100µm, (h) = 100µm, (i) = 200µm, (j) = 100µm, (k) = 100µm, (l) = 100µm, (m) = 100µm, (n) = 200µm, (o) = 100µm.

Figure 5.5 presents Masson's trichrome histological staining results for all dorsal skin samples of the taxa in this study. Of the 15 (a-o), different images, 11 (a, b, c, d, f, g, h, k, l, m, n) show mineralisations in the skin. The species in which no mineralisation was observed (e, i, j, o), include *Salvator merianae*, *Egernia stokesii*, *Varanus niloticus* and *Gekko gecko.*

Figure 5.6 presents Alcian blue histological staining results for all dorsal skin samples of the taxa in this study. Of the 15 (a-o), different images, 11 (a, b, c, d, f, g, h, k, l, m, n) show mineralisations in the skin. The species in which no mineralisation was observed (e, i, j, o), include *Salvator merianae*, *Egernia stokesii*, *Varanus niloticus* and *Gekko gecko.*
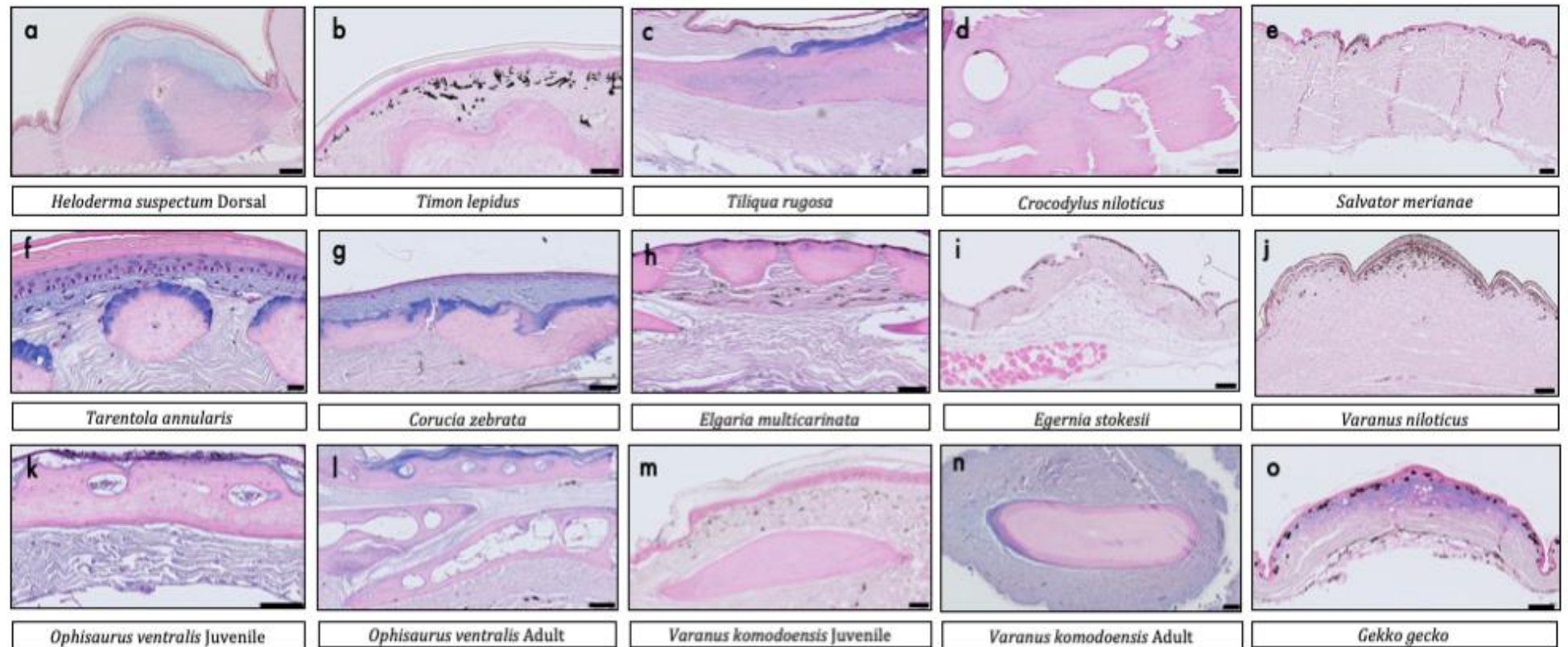
Figure 5.6: Comparative Alcian blue histological staining of reptile skin (all except d are squamate) in (a) *Heloderma suspectum,* (b) *Timon lepidus*, (c) *Tiliqua rugosa*, (d) *Crocodylus niloticus*, (e) *Salvator merianae*, (f) *Tarentola annularis,* (g) *Corucia zebrata*, (h) *Elgaria multicarinata, (i) Egernia stokesii,* (j) *Varanus niloticus,* (k) *Ophisaurus ventralis juvenile,* (l) *Ophisaurus ventralis* adult*,* (m) *Varanus komodoensis juvenile,* (n) *Varanus komodoensis* adult*,* (o) *Gekko gecko.*

Scale bars: (a) = 200µm, (b) = 100µm, (c) = 100µm, (d) = 100µm, (e) = 100µm, (f) = 20µm, (g) = 100µm, (h) = 100µm, (i) = 200µm, (j) = 100µm, (k) = 100µm, (l) = 200µm, (m) = 100µm, (n) = 200µm, (o) = 100µm.

Figure 5.7 presents three-dimensional surface reconstructions of OD meshes from segmented HRXCT results for *Heloderma suspectum, Tiliqua rugosa, Gekko gecko, Tarentola annularis, Corucia zebrata, Elgaria multicarinata*, *Ophisaurus ventralis*, *Ophisaurus ventralis, Varanus komodoensis* dorsal skin samples.
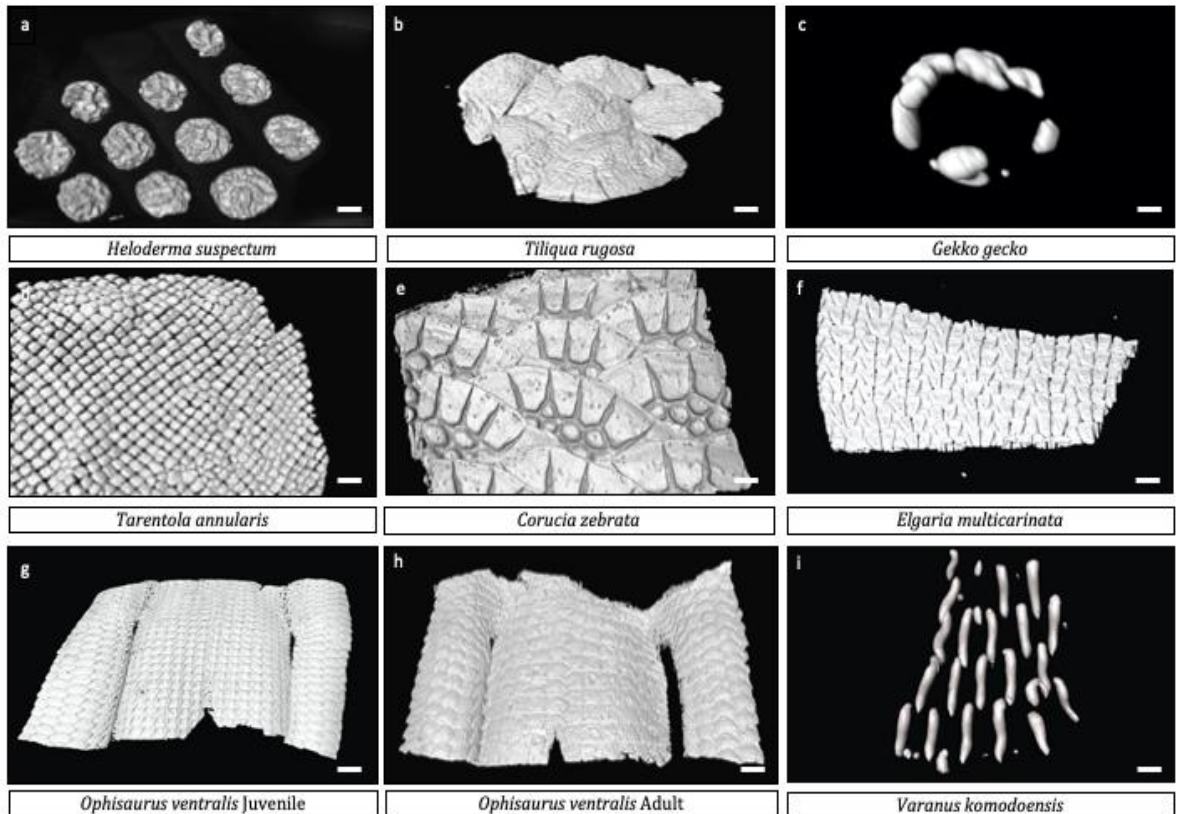
Figure 5.7: Comparative view of three-dimensional surface reconstructions of OD meshes, segmented from HRXCT data of post-cranial, dorsal squamate skin samples. Results shown for the taxa: (a) *Heloderma suspectum,* (b) *Tiliqua rugosa,* (c) *Gekko gecko,* (d) *Tarentola annularis,* (e) *Corucia zebrata,* (f) *Elgaria multicarinata*, (g) *Ophisaurus ventralis* Juvenile, (h) *Ophisaurus ventralis* Adult*,* (i) *Varanus komodoensis.* All dorsal view, apart from (e) and (f), which are ventral view.

Scale bars: (a) = 600µm, (b) = 1000µm, (c) = 50µm, (d) = 250µm, (e) = 25µm, (f) = 50µm, (g) = 500µm, (h) = 1000µm, (i) = 500µm.
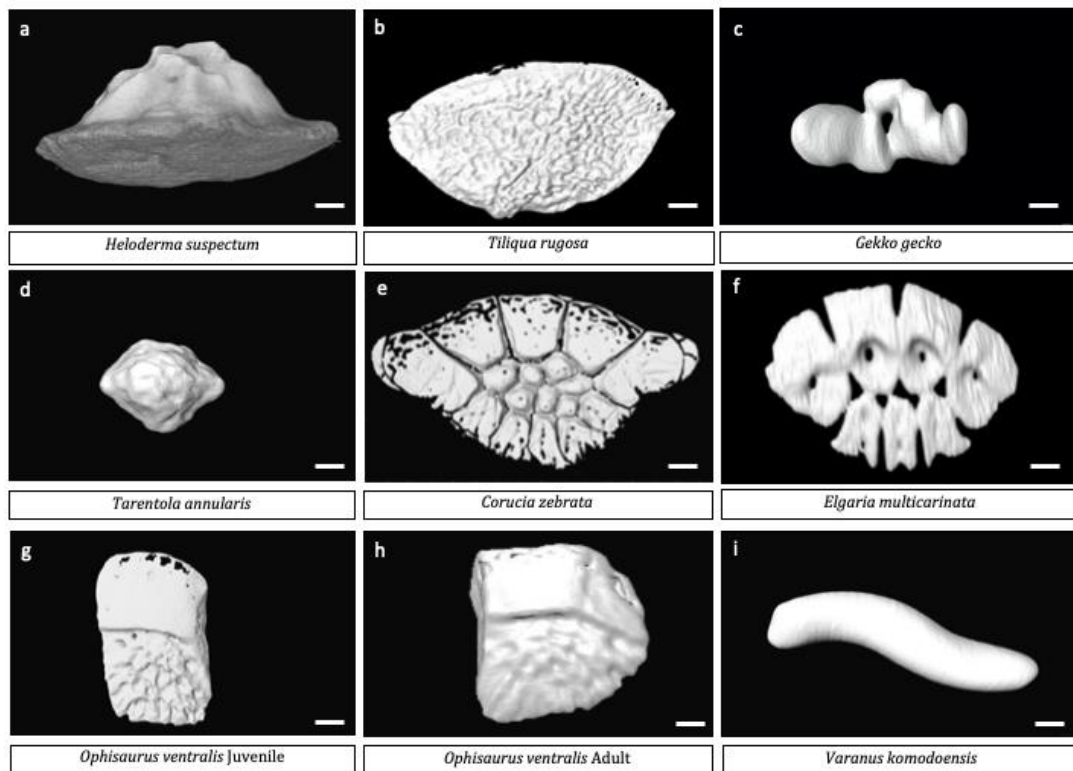
Figure 5.8: Comparative view of three-dimensional surface reconstructions of single ODs, segmented from HRXCT data of post-cranial, dorsal squamate skin samples. Results shown for the taxa: (a) *Heloderma suspectum* in transverse view*,* (b) *Tiliqua rugosa* in dorsal view*,* (c) *Gekko gecko* in transverse view, (d) *Tarentola annularis* in dorsal view, (e) *Corucia zebrata* in ventral view (f) *Elgaria multicarinata* in ventral view, (g) *Ophisaurus ventralis* Juvenile in dorsal view, (h) *Ophisaurus ventralis* Adult in dorsal view*,* (i) *Varanus komodoensis* in transverse view.

 Scale bars: (a) = 100µm, (b) = 500µm, (c) = 20µm, (d) = 25µm, (e) = 50µm, (f) = 20µm, (g) = 50µm, (h) = 20µm, (i) = 100µm.

Figure 5.8 presents three-dimensional surface reconstructions of single OD from segmented HRXCT results for *Heloderma suspectum, Tiliqua rugosa, Gekko gecko, Tarentola annularis, Corucia zebrata, Elgaria multicarinata*, *Ophisaurus ventralis*, *Ophisaurus ventralis, Varanus komodoensis* dorsal skin samples.
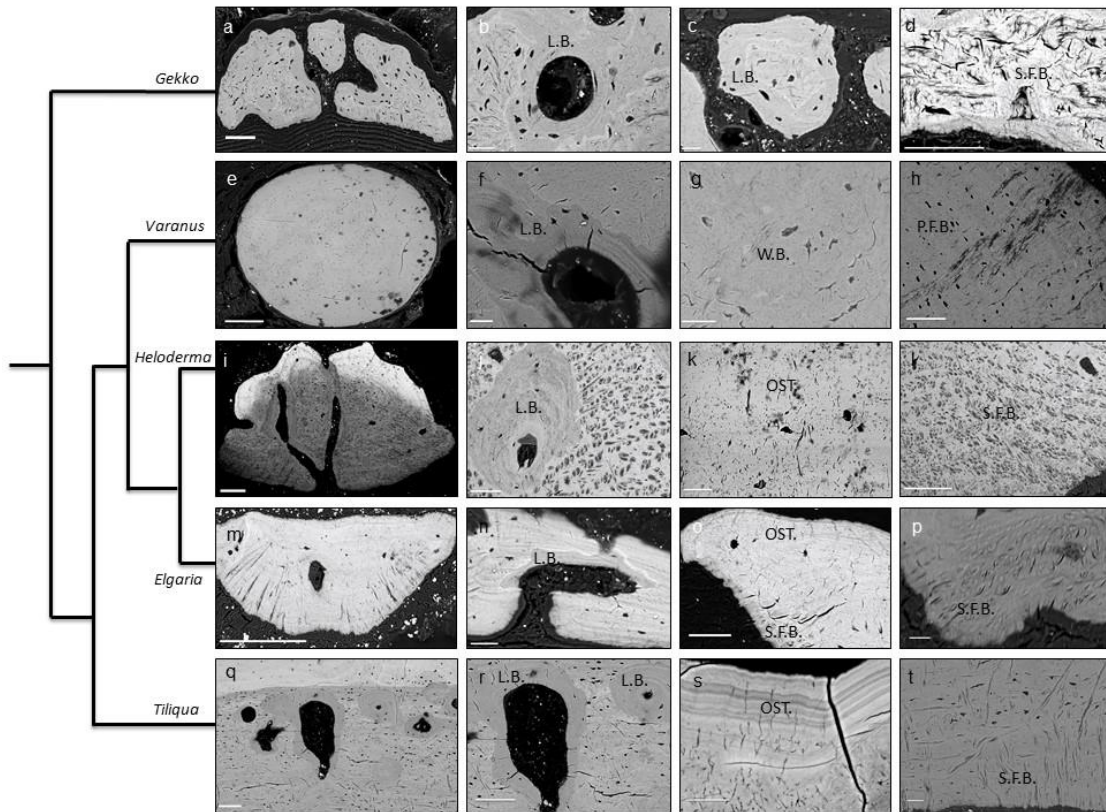
Figure 5.9: Comparative BSE-SEM microscopy of squamate ODs. Low magnification BSE-SEM micrographs of ODs from (a) *Gekko gecko*, (e) *Varanus komodoensis,* (i) *Heloderma suspectum,* (m) *Elgaria multicarinata, (q) Tiliqua rugosa* and higher magnification BSE-SEM micrographs of specific regions of interest. To the left, phylogeny of squamate evolutionary relationships outlined as simplified cladogram (adapted from Vickaryous, Sire 2009). L.B. = lamellar bone, OST. = osteodermine, P.F.B.= parallel-fibred bone, S.F.B. = Sharpey-fibred bone.

Scale bars: (a) = 100µm, (b)= 30µm, (c) = 20µm, (d) = 30µm, (e) = 200µm, (f) = 30µm, (g) = 30µm, (h) = 50µm, (i) = 200µm, (j) = 50µm, (k) = 40µm, (l) = 150µm, (m) = 100µm, (n) = 30µm, (o) = 25µm, (p) = 20µm, (q) = 100µm, (r) = 20µm, (s) = 20µm, (t) = 40µm.

5.2.2 Gekkota

Gekkota is comprised seven families, and contains all geckos and the limbless Pygopodidae. Gekkotans are a highly speciose assemblage of lizards that only include three known OD-bearing genera: *Tarentola* (Otto 1909; Loveridge, 1947; Levrat-Calviac and Zylberberg, 1986; Bauer and Russell, 1989), *Gekko* (Laver et al., 2019) and *Geckolepis* (Scherz et al., 2017; Paluh et al., 2017). Given the variety of

OD expression among these three genera, existing as imbricating, abutting and discrete, Paluh et al., (2017) suggested that ODs have independently evolved at least three times within the Gekkota.

Two gekkotan families are sampled here, Phyllodactylidae (sampled species is *Tarentola annularis*, the Ringed Wall gecko) and Gekkonidae (sampled species is *Gekko gecko* the Tokay gecko).

Phyllodactylidae contains approximately 113 species, distributed throughout the New World, Asia, Africa and Europe. Phyllodactylidae was recognised as a distinct family by Gamble et al., in 2008 based on molecular phylogeny - all members possess a unique single codon deletion in the phosducin (PDC) gene. In *Tarentola*, Otto (1909) found very little correlation between the horny epidermal scales and the small, regularly placed ODs beneath. *Tarentola* are mainly nocturnal but are sometimes active during the day, they hunt insects, can be very aggressive to other members of the same species and express ODs all over the body (Vickaryous et al., 2015).

Gekkonidae is the largest family of geckos, containing over 950 described species in 61 genera. Gekkonid geckos occur globally and are particularly species-rich in tropical areas. Tokay geckos (*Gekko gecko*) are very common in their native habitat of Asia and some Pacific Islands. They are nocturnal and arboreal, with a large size reaching up to 35cm in length with powerful jaws. They express ODs on the head and dorsal surfaces of the shoulders (Laver et al., 2019)
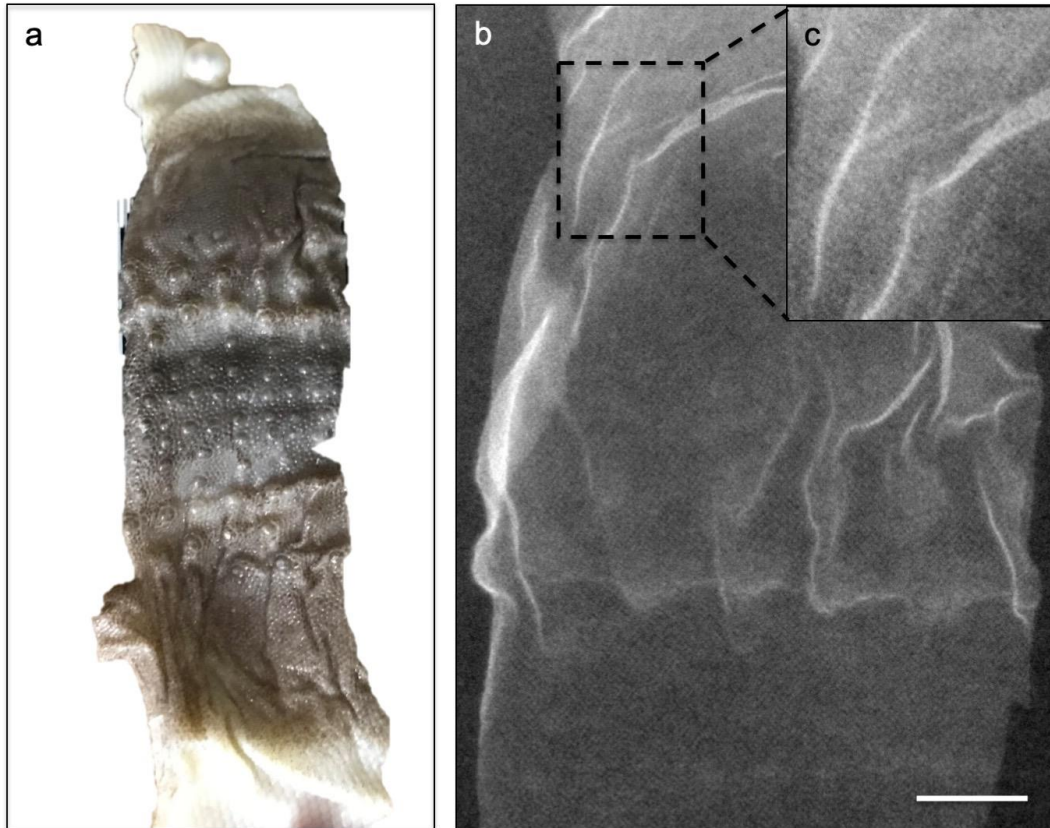
Figure 5.10: (a) photograph of adult *Tarentola annularis* dorsal skin, (b) corresponding x-ray plate image and (c) enlarged view of the dashed square shown in (b). Osteoderms are just visible as white dots in (c).

Scale bars: (b) = 5mm.

Figure 5.10 illustrates X-ray plate imaging for the first target species *Tarentola annularis*. The ODs are visible in the x-ray plate image (Fig. 5.10b) in regularly repeating rows as very small white objects that are just larger than the resolution of the x-ray sensor. ODs are expressed ubiquitously and regularly across the entire sample. A close-up of the x-ray plate result (Fig. 5.10b, c) is included to aid the visual clarity of the ODs.
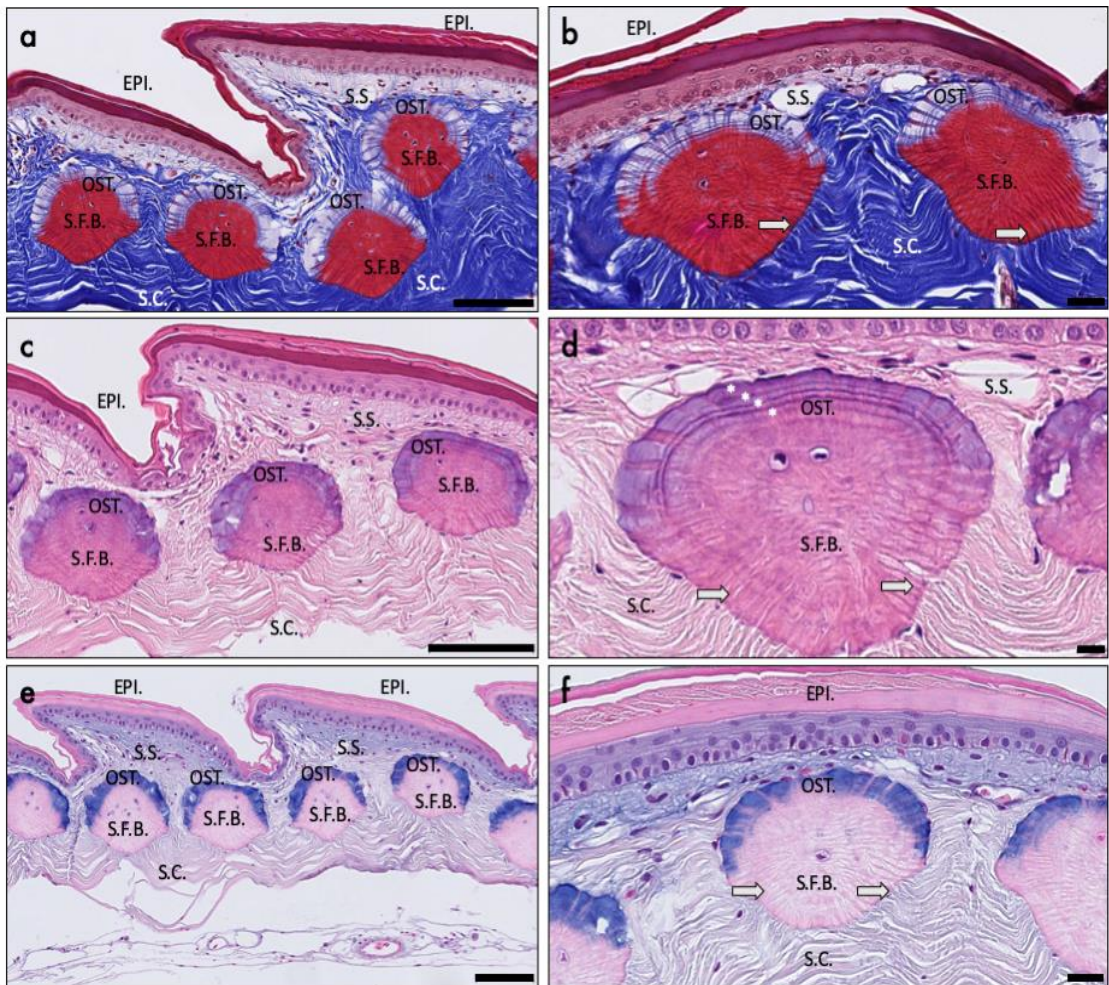
Figure 5.11: Histological staining of *Tarentola annularis* dorsal skin sample, parasagittal sections stained with (a and b) Masson's trichrome, (c and d) H&E and (e and f) Alcian blue. Asterisks = lines of arrested growth, EPI. = epidermis, OST. = osteodermine, S.F.B. = Sharpey-fibre bone, S.C. = stratum compactum, S.S. = stratum superficiale, White arrows = Sharpey's fibres.

Scale bars: (a) = 100μm, (b) = 40μm, (c) = 100μm, (d) = 10μm, (e) = 100μm, (f) = 20μm.

Histological sections showed that *Tarentola annularis* ODs comprise a base of S.F.B. and a cap of OST. (Fig. 5.11). ODs were observed to have a rounded bead shape, roughly 100μm in diameter. Sharpey's fibres were readily observed permeating the basal bone region as well as the OST. region. This result was confirmed with multi-rotation polarised light microscopy (Fig .5.12).
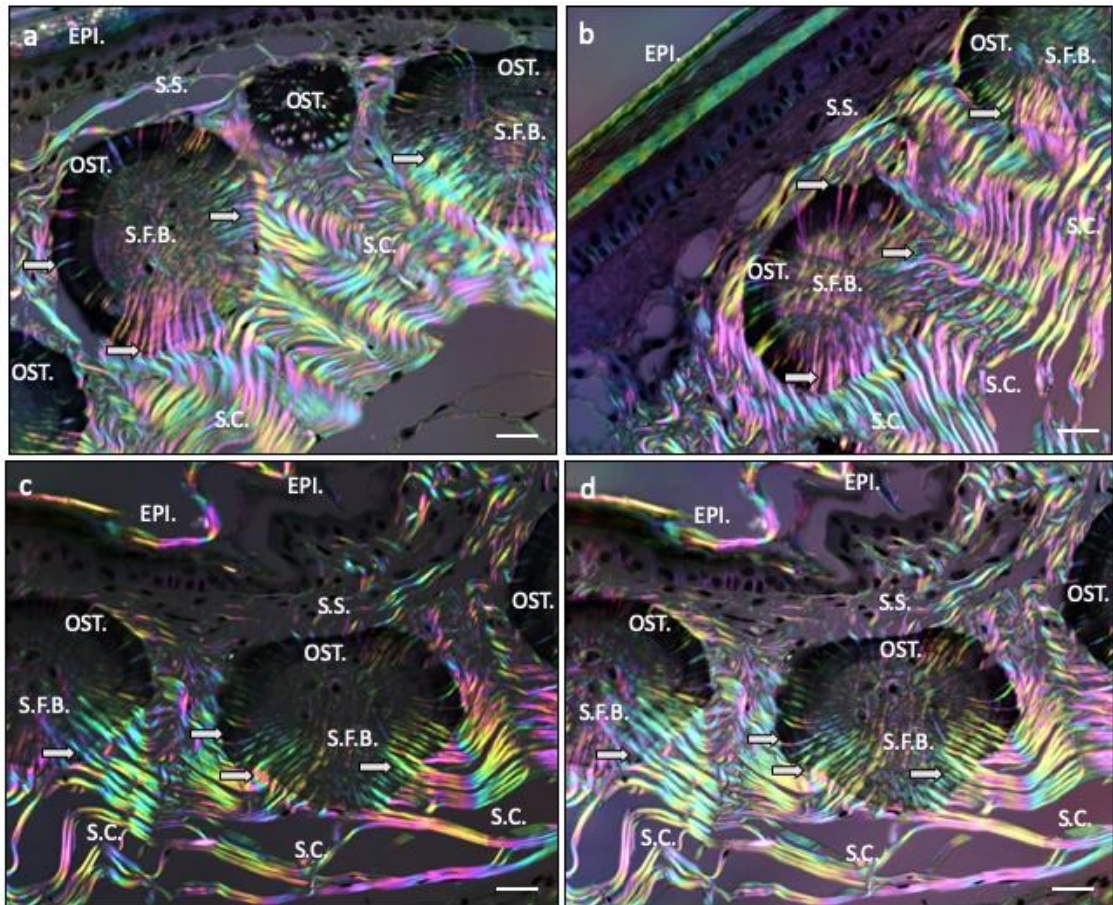
Figure 5.12: (a-d) parasagittal sections of *T. annularis* OD stained with Alcian blue and visualised with multi-rotation polarised light microscopy. The same result is shown in (c and d) however the contrast histogram is equalised in (d) for greater clarity. EPI. = epidermis, S.C. = stratum compactum, S.F.B. = Sharpey-fibred bone, S.S. = stratum superficiale, White arrows = Sharpey's fibres.

Scale bars: (a) = 30μm, (b) = 30μm, (c) = 30μm, (d) = 30μm.

The same fibres that comprise the stratum compactum were found to permeate the basal S.F.B. region of the OD. The S.F.B. region stains red in Masson's Trichrome staining, pink in H&E and pink in Alcian blue. OST. in *Tarentola annularis* ODs does not stain using Masson's Trichrome staining, but stains purple in H&E and blue in Alcian blue, indicating the presence of acid mucosubstances. Lines of growth are readily observed in the OST. region (Fig. 5.11d, asterisks), meaning that periodic growth was involved in OST. formation. The ODs are located very close to the epidermis, with the apical surface residing just below the lower layer of the epidermis. There is no evidence of vascular penetration in any sections taken, which must limit
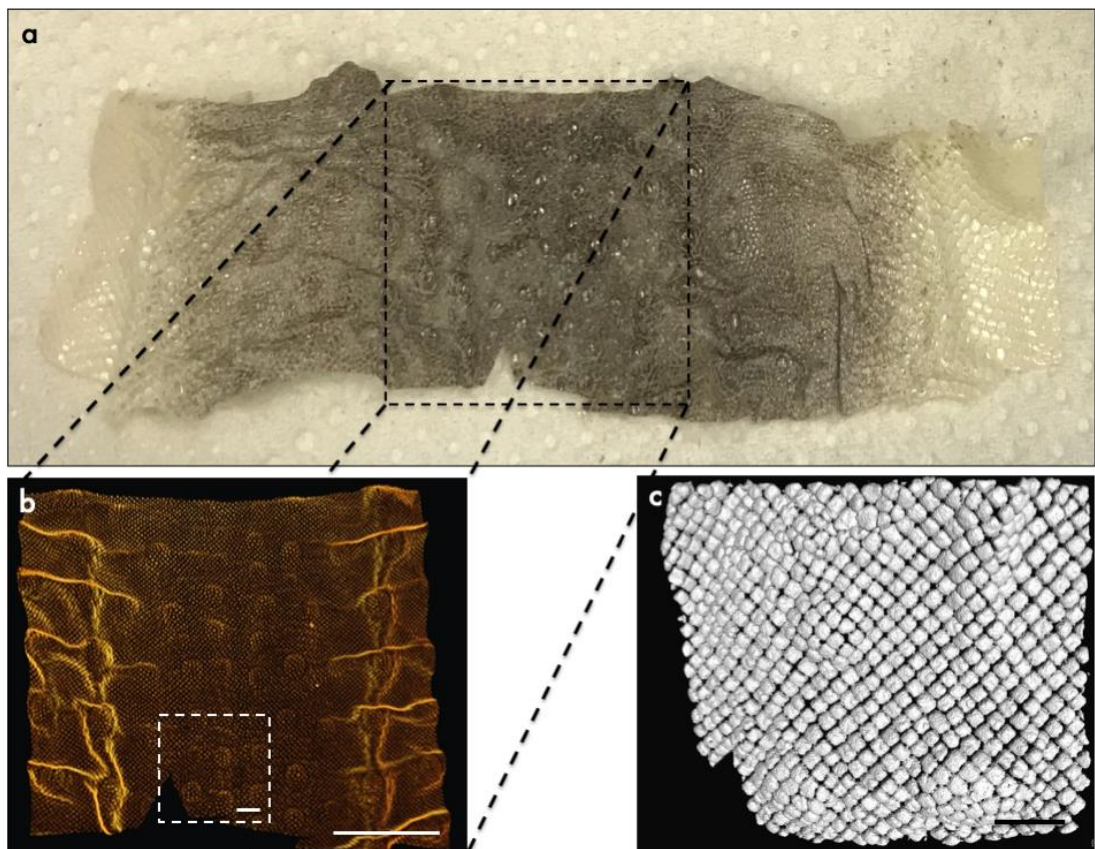
Figure 5.13: (a) photograph of adult *Tarentola annularis* skin sample, dorsal skin is central to the sample, with ventral skin on the left and right side. (b) corresponding volume rendering of HRXCT data in dorsal view and (c) three-dimensional, false colour surface reconstruction segmented from HRXCT data, dorsal view of the dashed square shown in (b). Multiple ODs are observed underneath each epidermal tubercle (scale).

Scale bars: (b) = 5mm, (c) = 500µm.

the size of each OD given this circulation restraint.

The result from the HRXCT scan of the dorsal skin of *Tarentola annularis* showed ODs in greater detail than the X-ray plate image, and afforded a three-dimensional view (Fig. 5.13). The results from this technique showed that the ODs are regularly spaced, in defined rows and columns across the whole sample. ODs were not seen to be associated with the keratinised scale above, with each scale presenting multiple ODs below it.
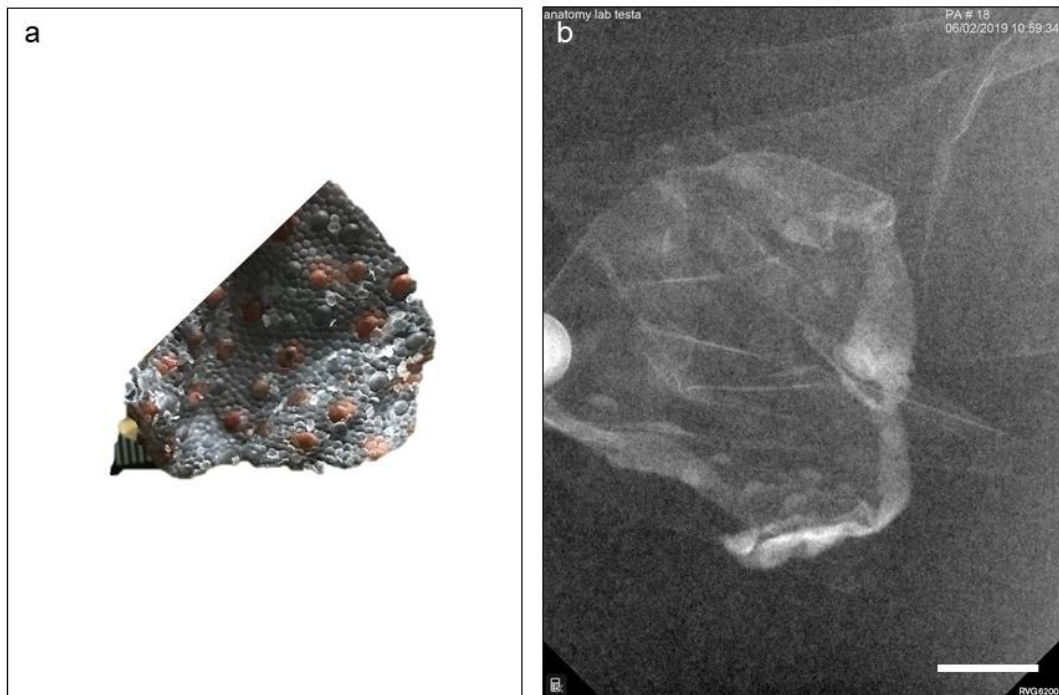
Figure 5.14: (a) photograph of adult *Gekko gecko* dorsal skin and (b) corresponding x-ray plate image.

Scale bars: (b) = 5mm.

Gekko gecko is the second target species of gecko, in which no ODs were observed in the dorsal skin in either the X-ray plate imaging (Fig 5.14) or the histological sections (Fig. 5.15), a collection of ODs were seen in the HRXCT scan from the same region (Fig. 5.16) where they appeared as roughly shaped lozenges, arranged in a vague ring around a single scale.
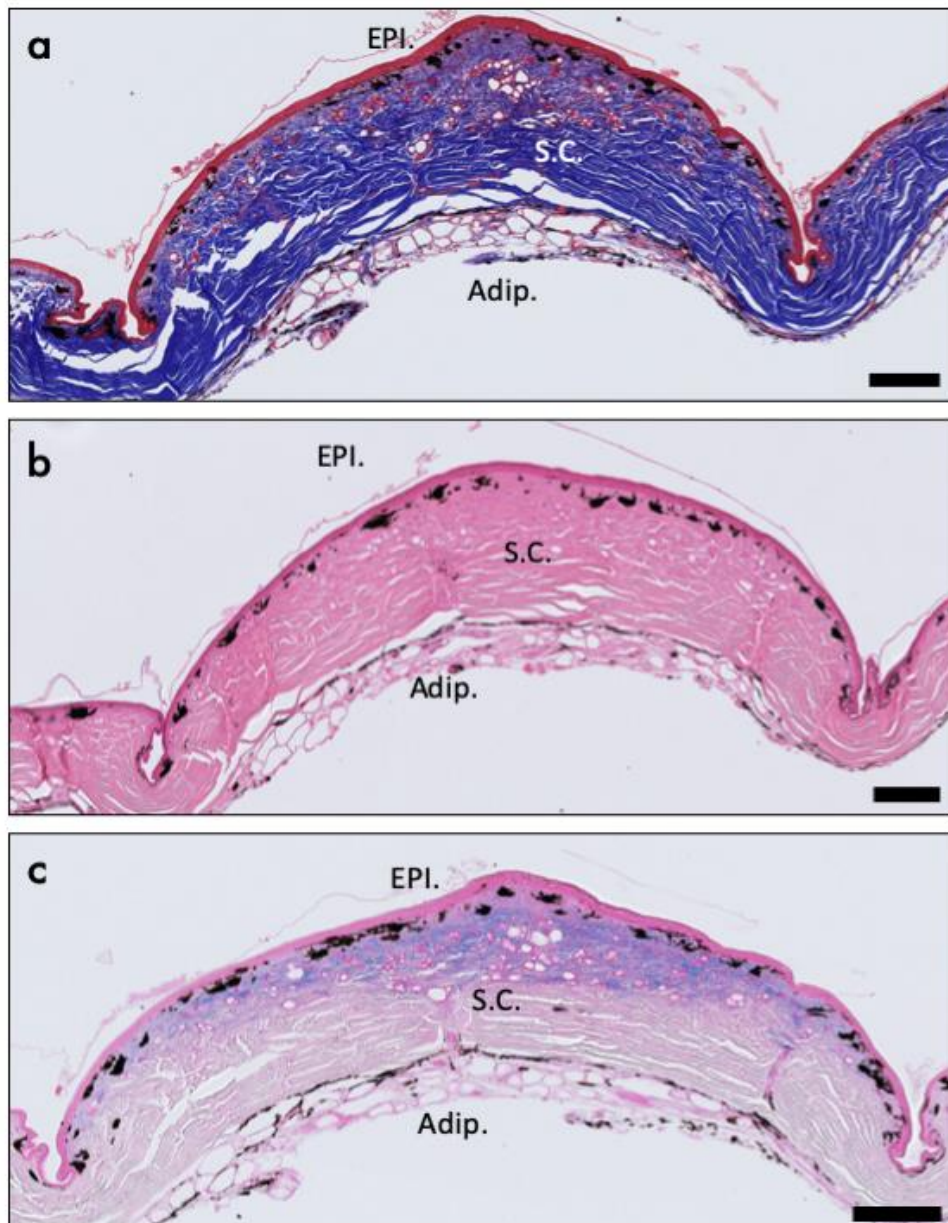
Figure 5.15: Histological staining of *Gekko gecko* dorsal skin sample, parasagittal sections stained with (a) Masson's trichrome (b) H&E, and (c) Alcian blue. Adip. = adipose tissue, Epi. = epidermis, S.C. = stratum compactum.

Scale bars: (a) = 100µm, (b) = 100µm, (c) = 100µm.
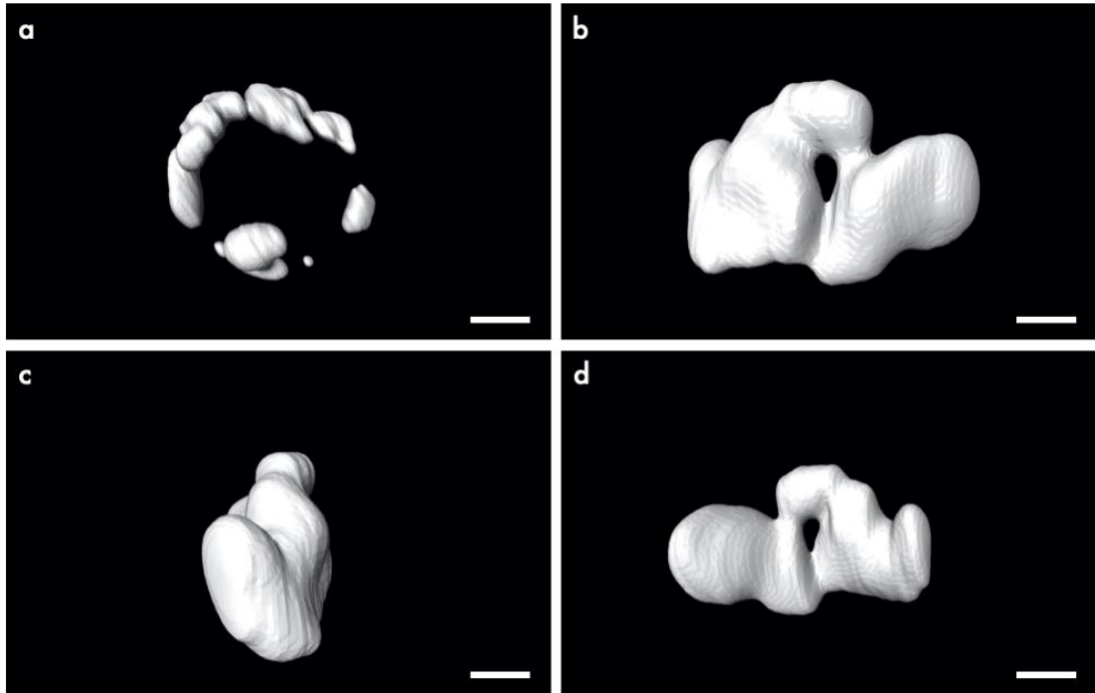
Figure 5.16: Three-dimensional, false colour surface reconstruction of OD mesh, segmented from HRXCT data of post-cranial, dorsal, adult *Gekko gecko* skin in (a) dorsal view and single osteoderm in (b) anterior view, (c) lateral view, (d) posterior view.

Scale bars: (a) = 320µm, (b) = 100µm, (c) = 150µm, (d) = 125µm.

5-6 ODs of varying size were observed to be roughly 750-1mm in length. The largest OD was segmented out as a single OD to view the three-dimensional arrangement.
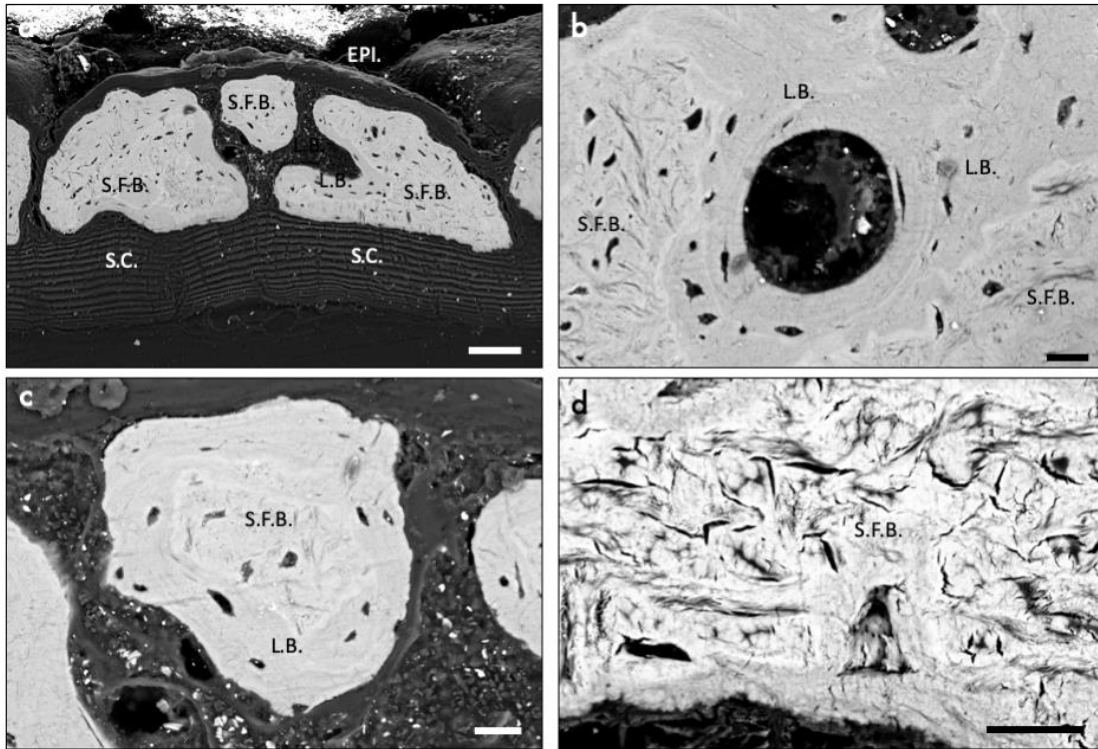
Figure 5.17: BSE-SEM imaging of *Gekko gecko* OD (a-d) parasagittal sections, resin embedded, ground and polished. EPI. = epidermis, L.B. = lamellar bone, S.C. = stratum compactum, S.F.B. = Sharpey-fibred bone.

Scale bars: (a) = 100 μm, (b) = 20 μm, (c) = 20 μm, (d) = 15 μm.

BSE-SEM results of the *Gekko gecko* skin sample showed that when present, ODs are composed of S.F.B. with L.B. lining the endosteal surfaces of secondary osteons following vascularisation and remodelling (Fig. 5.17). It was not possible to identify Sharpey's fibres that penetrate the apical surface, although they are observed expressed on the lateral and basal surfaces, thus this tissue resembles S.F.B.. Unfortunately, although attempted, polarised light microscopy was not successful on the *Gekko gecko* skin sample due to the sporadic expression of ODs, as in the histological staining.

5.2.3 Varanoidea

The group Varanoidea includes the extant Varanidae (the monitor lizards), the extant Lanthanotidae (earless monitor lizards), and the extinct Palaeovaranidae (Georgalis, 2017). The only living species in the Lanthanotidae is the earless monitor lizard (*Lanthanotus borneensis*). These semi-aquatic lizards are endemic to Borneo and are extremely rare. A HRXCT dataset of the cranium of *Lanthanotus borneensis* was made available via collaboration between the Evans lab and a lab in Japan, and is included for reference despite the lack of availability of a skin sample. Skin samples were available for this study from *Varanus komodoensis* and *Varanus ornatus*.

The Komodo Dragon (*Varanus komodoensis*) is the largest extant species of lizard, reaching up to 3 meters in length in its natural habitat on Indonesian islands and can live up to 30 years (Auffenberg, 1981). Komodo Dragons are known for their aggression and their venom, having attacked and killed humans (Walpole and Goodwin, 2000). Adult Komodo dragons live in tropical savannah forests and prefer open lowland areas with tall grasses and bushes, but can also be found in other habitats, such as beaches, and dry riverbeds where they feed on carrion, goats, deer, boar, buffalo, and smaller Komodo dragons (Wikramanayake, 1997).

The Nile monitor (*Varanus niloticus*) is a monitor lizard native to Sub-Saharan Africa and Egypt. Although not as large as the Komodo dragon (reaching up to 2.5m), they also have powerful legs, strong jaws and sharp teeth and are still formidable predators. Highly aquatic, excellent climbers and quick runners, Nile monitors feed on fish, snakes, insects, small mammals and other reptiles such as young crocodiles, crocodile eggs, snakes and birds. They are the second largest reptile to inhabit the Nile river, after the Nile crocodile (Bayless, 2002).

The ODs of Varanidae were recently described as vermiform cylinders, but also shown to be expressed in up to 4 different arrangements including rosette and dendrite shaped, as well meshing into an arrangement that is more like 'chain mail' (Maisano et al., 2019).

Varanus komodoensis ODs resemble smooth, slightly bent cylinders, roughly 2-4mm in length and partially overlapping one another (Fig. 5.18). ODs *of Varanus komodoensis* were recently shown to be expressed in up to 4 different morphologies (Maisano et al., 2019).

HRXCT of *Varanus komodoensis* skin afforded a high-resolution, three-dimensional view of the ODs present (Fig. 5.19). Although some ODs are very small compared to the majority, all of the ODs displayed a structure of vermiform, elongate and slightly bent cylinders. A slight overlap on the anterior and posterior ends of each OD was observed in lateral view (Fig. 5.19b).
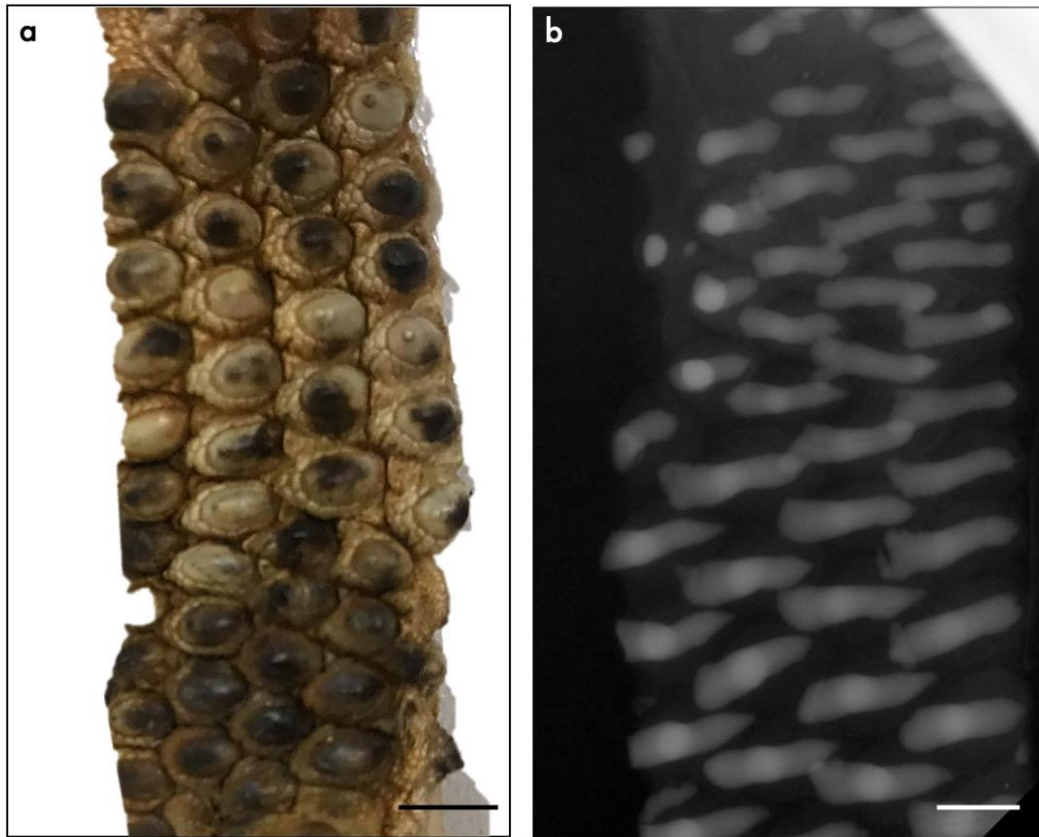
Figure 5.18: (a) photograph of adult *Varanus komodoensis* dorsal skin and (b) corresponding x-ray plate image.

Scale bars: (b) = 5mm.

A single OD was digitally segmented out of the OD mesh (Fig. 5.20) for greater clarity of the OD modular unit. Histology showed that *V. komodoensis* ODs were invested within the deep dermis (stratum compactum) (Fig. 5.21a) and did not reside close to the epidermis at any location along each OD. In addition, *Varanus komodoensis* ODs lacked S.F.B. and OST.. Instead, they were primarily composed of: (1) W.B (2) L.B. and (3) P.F.B.. In section, *V. komodoensis* ODs had a conspicuous concentric arrangement of outer rings and an inner core (Fig 5.19). The inner core region was composed of W.B, exhibiting a densely packed arrangement of interlacing, randomly arranged mineralised collagen fibres. The outer rings were composed of P.F.B., with

closely packed and regularly arranged collagen fibres. Evidence of remodelling was also observed, with deposits of L.B. contributing to the formation of an osteon (Fig 5.21e), as well as concentric lines of growth (Fig. 5.21f, Asterisks).
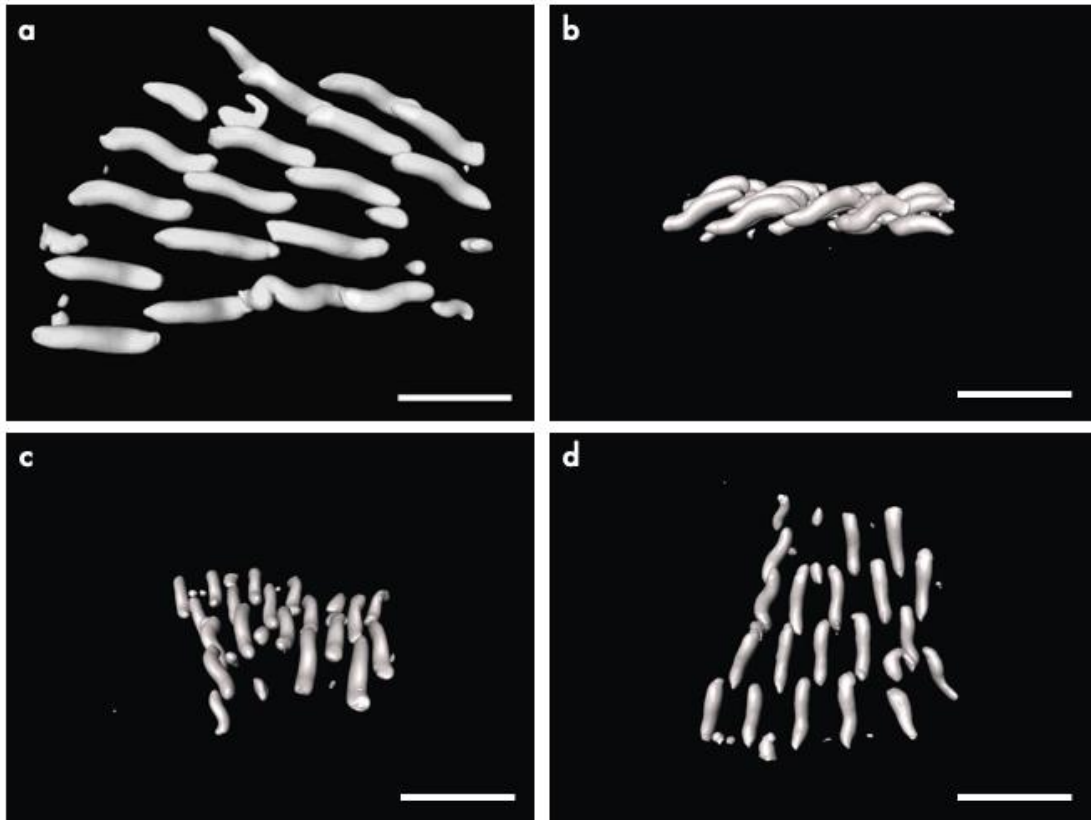
Figure 5.19: Three-dimensional false-colour surface reconstruction of OD mesh, segmented from HRXCT data of post-cranial, dorsal *Varanus komodoensis* dorsal skin in (a) dorsal view, (b) lateral view, (c) posterior view, (d) ventral view.

Scale bars: (a)= 2mm, (b) = 3mm, (c) = 5mm, (d) = 5mm.
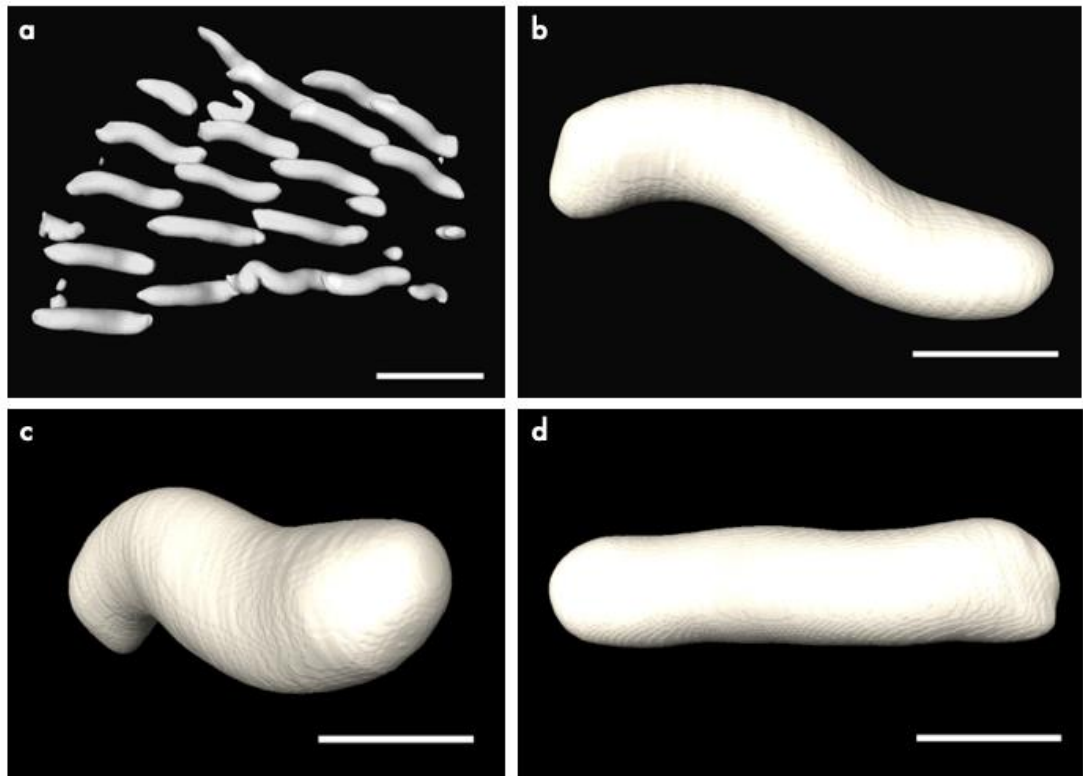
Figure 5.20: Three-dimensional false-colour surface reconstruction of (a) OD mesh in dorsal view, segmented from HRXCT data of adult *Varanus komodoensis* dorsal skin and single osteoderm in (b) lateral view, (c) posterior view, (d) ventral view.

Scale bars: (a) = 5mm, (b) = 500μm, (c) = 500μm, (d) = 500μm.
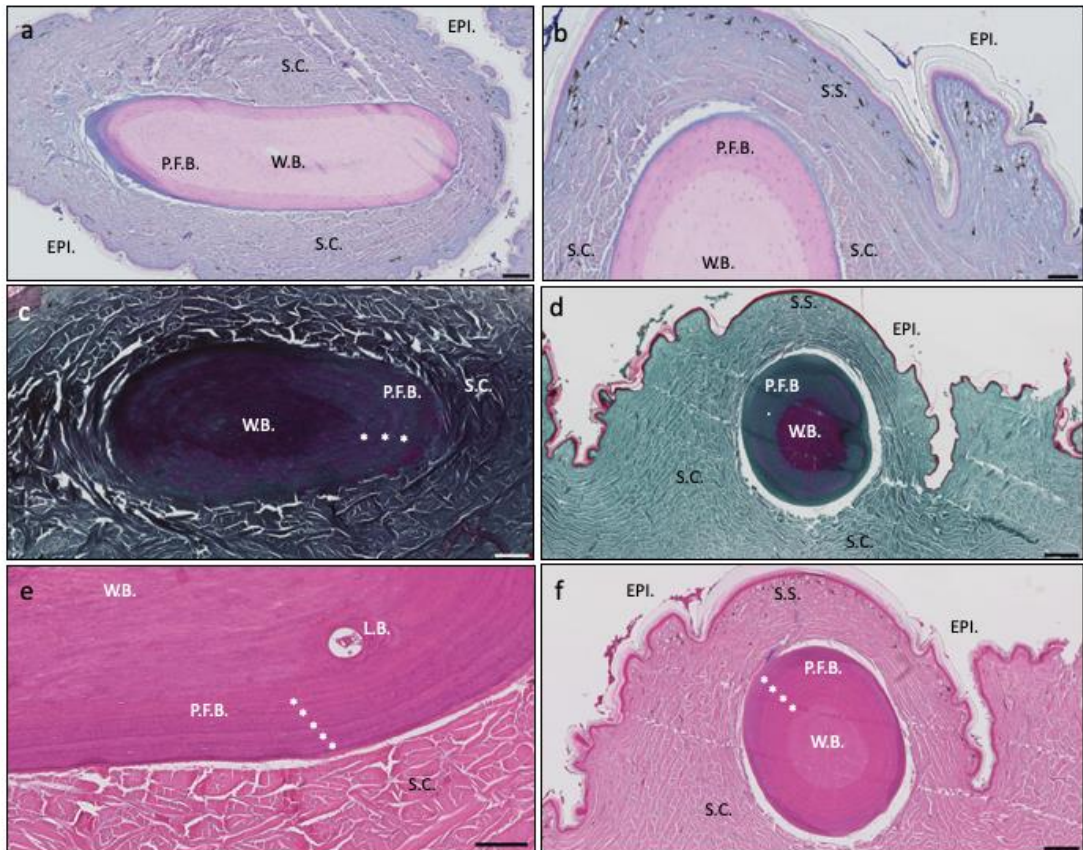
Figure 5.21: Histological staining of *Varanus komodoensis* dorsal skin sample stained with Alcian blue in (a) parasagittal and (b) coronal section, stained with Masson's trichrome in (c) parasagittal and (d) coronal section; and stained with Haematoxylin and Eosin in (e) parasagittal section and (f) coronal section. Asterisks = lines of arrested growth, EPI. = epidermis, L.B. = lamellar bone, P.F.B. = parallel-fibred bone, S.C. = stratum compactum, S.S. = stratum superficiale, W.B. = woven bone.

Scale bars: (a) = 200μm, (b and c) = 100μm, (d) = 200μm, (e) = 100μm, (f) = 200μm.

Multi-rotation polarised light microscopy (Fig. 5.22) revealed that *Varanus komodoensis* differ from those of *Heloderma* in exhibiting a sharp boundary between bone and dermis, with only occasional Sharpey's fibres anchoring the skeletal element into the surrounding skin (Fig. 5.22b, white arrows). The same morphology was observed in coronal sections (Fig. 5.22c, d). The microstructural appearance of the bone of *Varanus komodoensis* (lacking S.F.B.), is seemingly an unusual trait, given the observations of S.F.B. in all other lizards sampled in this study.

BSE-SEM imaging of the ODs from Varanus komodoensis (Fig. 5.23) complemented the histological staining and multi-rotation polarised light results, confirming the presence of a W.B core, P.F.B. in the external cortices and L.B. lining the endosteal surfaces of secondary osteons following remodelling.
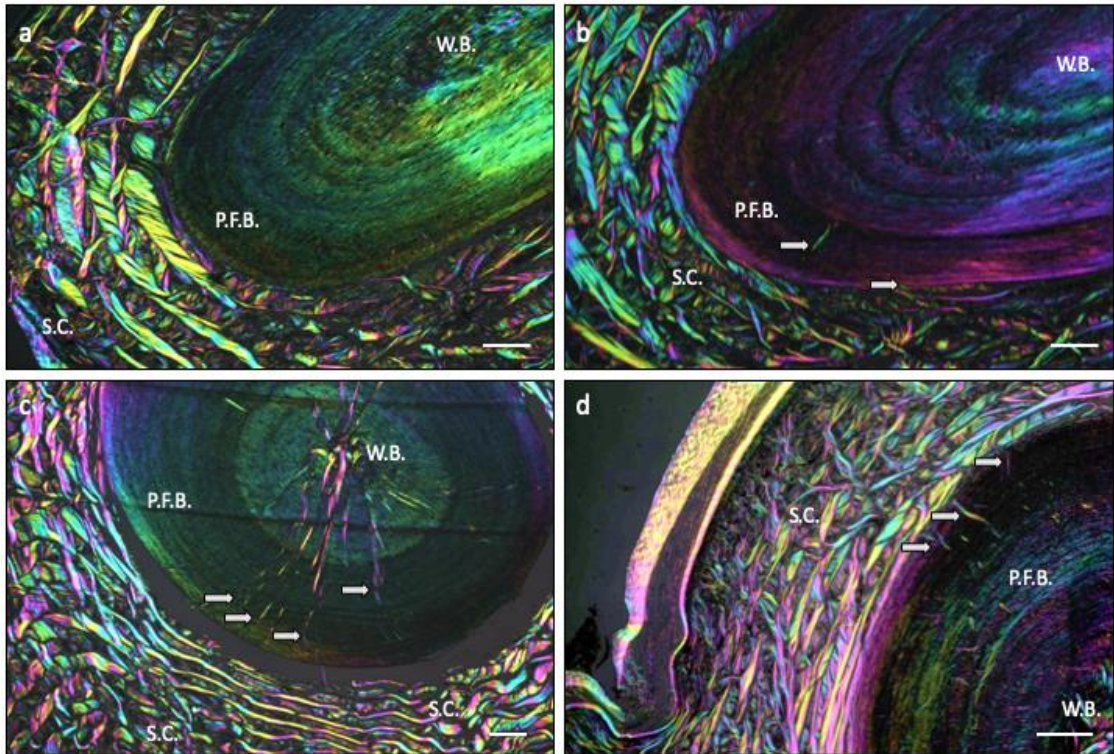
Figure 5.22: *Varanus komodoensis* OD stained with H&E and visualised with multi-rotation polarised light microscopy in (a and b) parasagittal section and (c and d) coronal section. P.F.B. = parallel-fibred bone, S.C. = stratum compactum, White arrows = Sharpey's fibres, W.B. = woven bone.

Scale bars: all 50μm.

The results from the adult specimen of *Varanus komodoensis* can be compared to the juvenile specimen, in X-ray plate imaging the ODs appear much thinner and needle-shaped than the adult counterpart (Fig. 5.24). Some ODs are well formed needles, others seem less developed and were observed as shorter spicules, with mineralisation appearing to originate on the anterior side of the scale (Fig. 5.24b, right side). Histological staining of the juvenile specimen of *Varanus komodoensis* showed that the immature ODs consist mainly of a knot of W.B that stains with the same

affinity as the surrounding connective tissue apart from some basophilic staining at the periphery of the mineralisation front (Fig. 5.25a). Some of the more well-developed ODs appeared to mirror the adult expression of P.F.B. in the periphery (Fig. 5.25b, c), but no L.B. was observed in any sections. These materials stained in the same way as in the adult specimen, but no collagen under tension was observed.
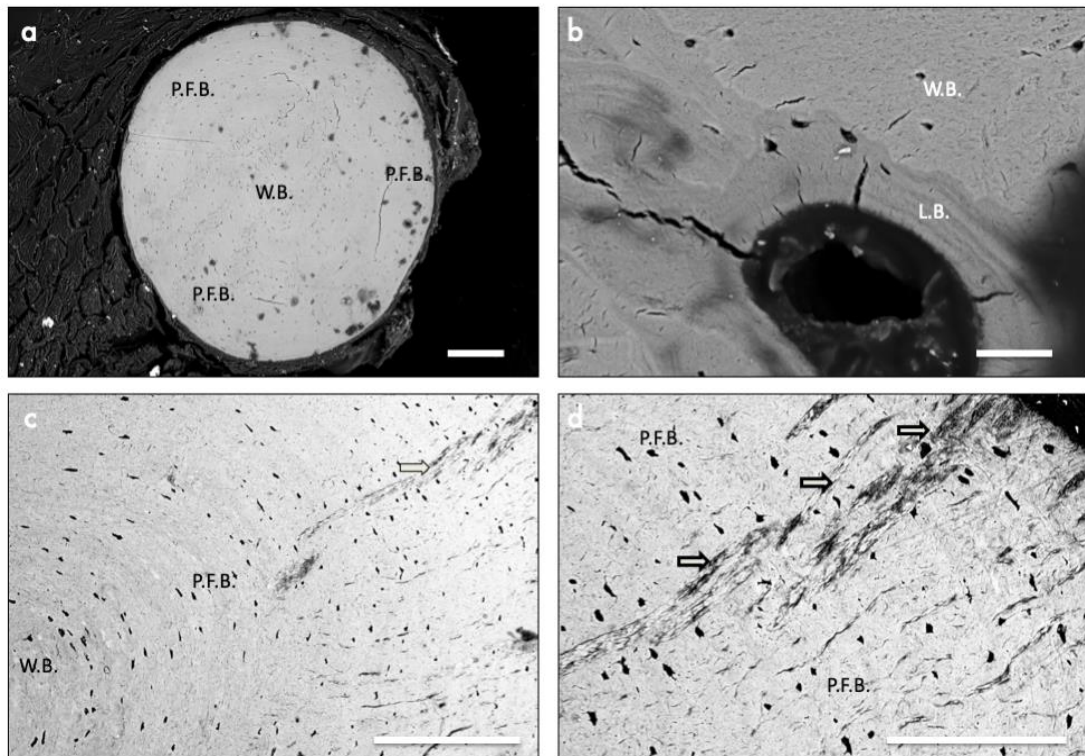
Figure 5.23: BSE-SEM imaging of adult *Varanus komodoensis* OD (a-d) coronal sections, resin embedded, ground and polished. P.F.B. = parallel-fibred bone, L.B. = lamellar bone, W.B. = woven bone, White arrows = Sharpey's fibres.

Scale bars: (a) = 200µm, (b) = 40µm, (c) = 200µm, (d) = 100µm.
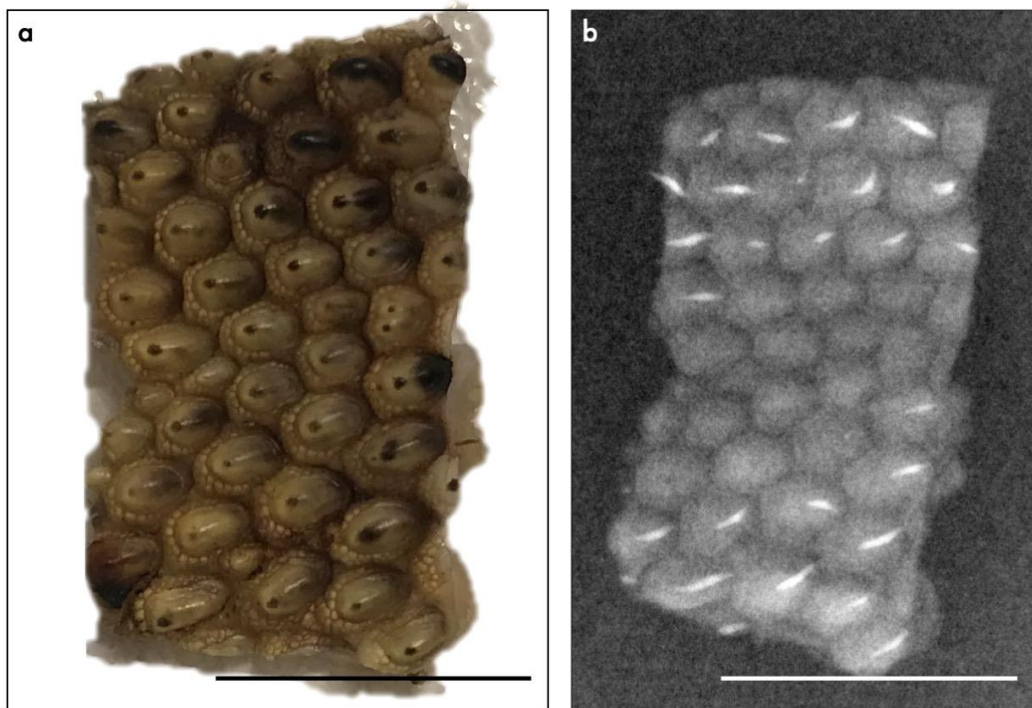
Figure 5.24: (a) photograph of juvenile *Varanus komodoensis* dorsal skin sample and (b) corresponding x-ray plate image, mineralised elements appear as white needle-shaped spicules, whereas the ovoid structures are non-mineralised, keratinised scales.

Scale bars: (b) = 5mm.

Another sampled *Varanus* species, *Varanus niloticus*, did not appear to express ODs in the dorsal skin, when using X-ray plate imaging (Fig. 5.26), histological staining (Fig. 5.27) or multi-rotation polarised light microscopy (Fig. 5.28). The stratum compactum of the dermis showed the standard layered arrangement and it was possible to observe extensive black specs just below the epidermis, which would correspond to melanocytes (Fig. 5.27, Mela.).
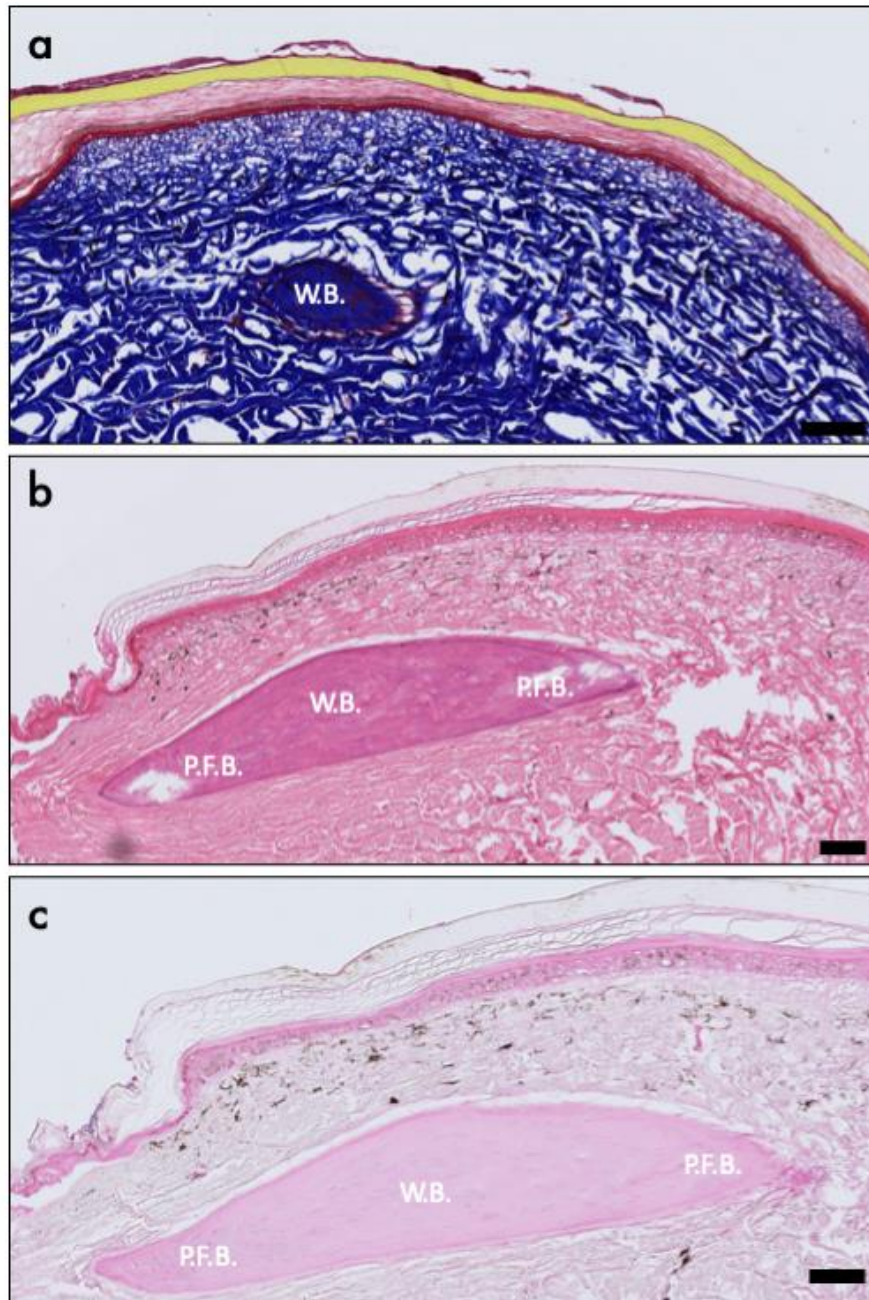
Figure 5.25: Histological staining of juvenile *V. komodoensis* OD stained with (a) Masson's trichrome in coronal section, (b) Haematoxylin and Eosin in parasagittal section and (c) stained with Alcian blue in parasagittal section. EPI. = epidermis, P.F.B. = parallel-fibred bone, W.B. = woven bone.

Scale bars: (a) = 100µm, (b) = 100µm, (c) = 100µm.
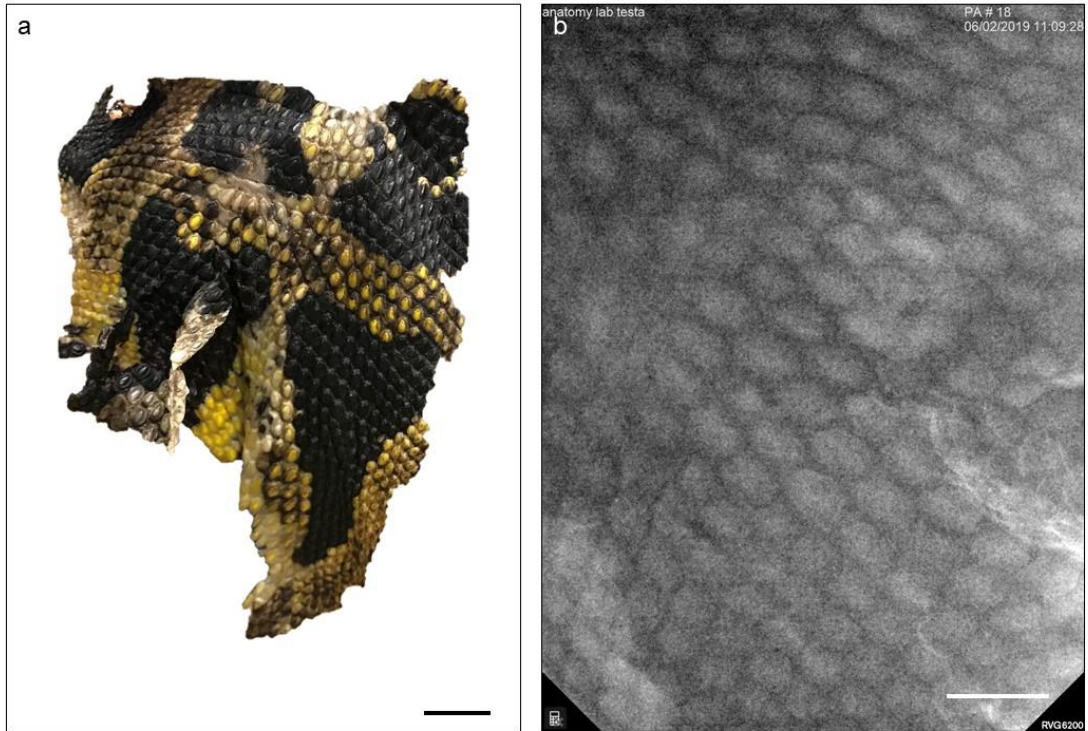
Figure 5.26: (a) photograph of adult *Varanus niloticus* dorsal skin sample and (b) corresponding x-ray plate image.
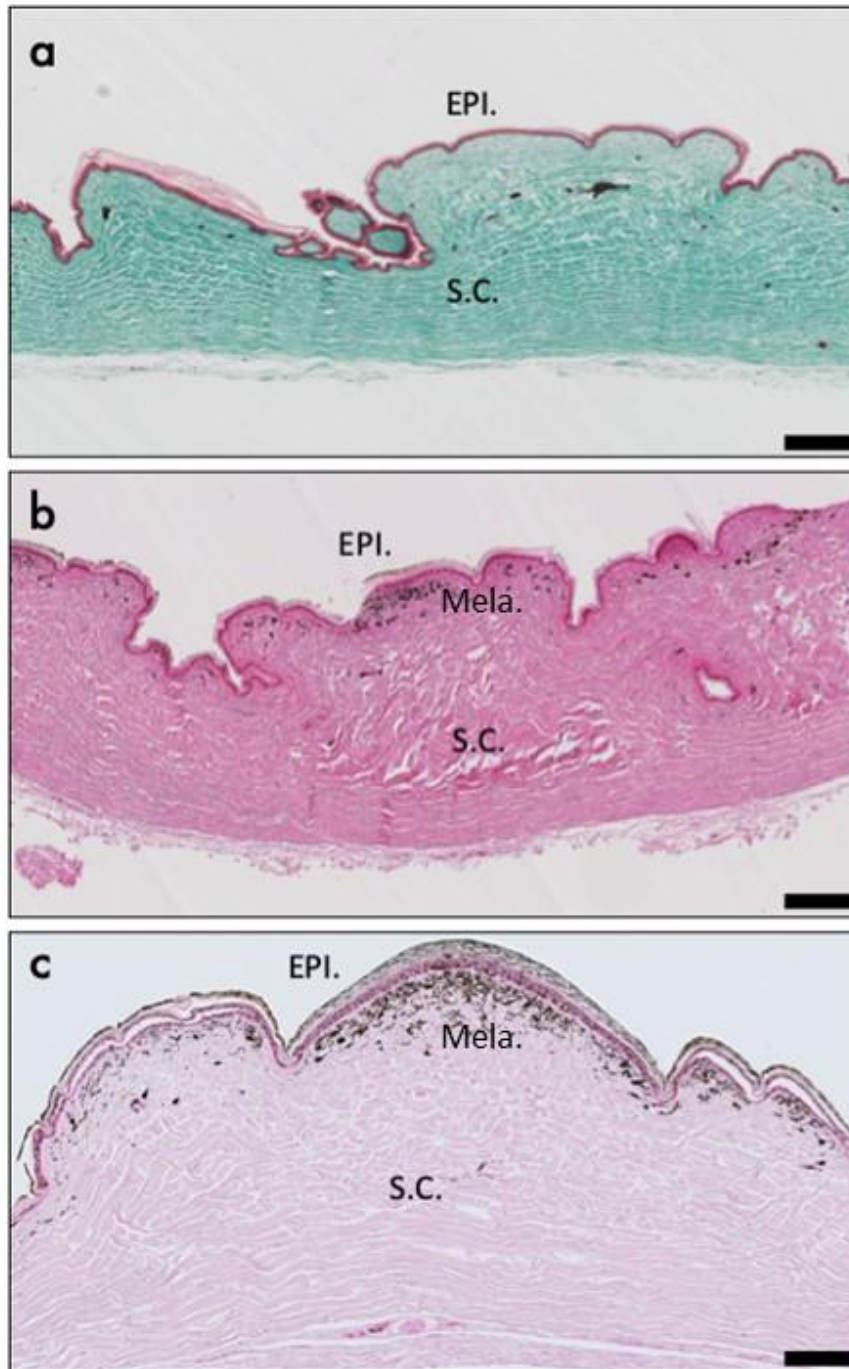
Scale bars: (b) = 5mm.

Figure 5.27: Histological staining of *Varanus niloticus* dorsal skin, parasagittal section stained with (a) Masson's Trichrome, (b) H&E, and (c) Alcian blue. EPI. = epidermis, Mela. = melanocytes, S.C. = stratum compactum

Scale bars: (a) = 200µm, (b) = 200µm, (c) = 100µm.
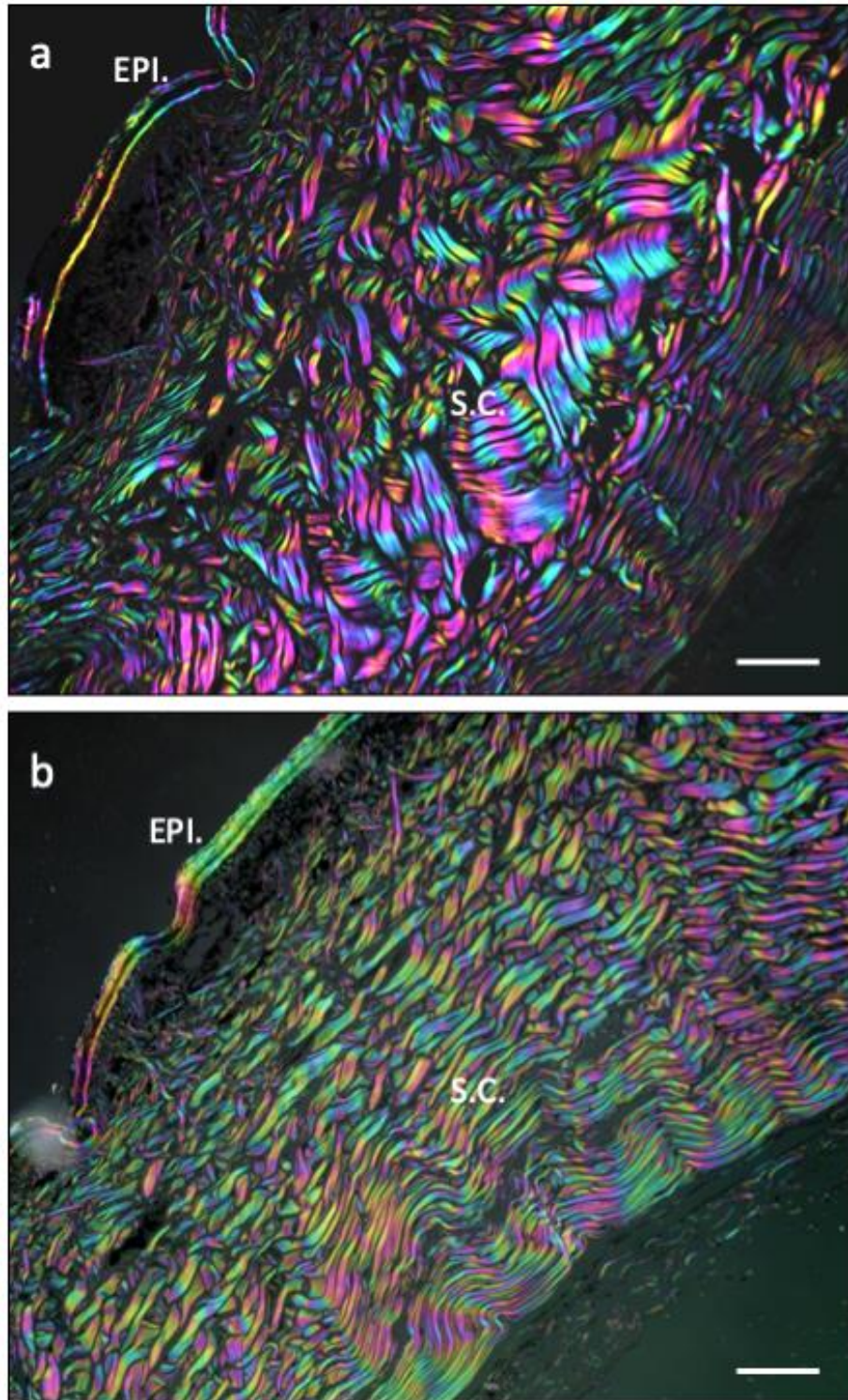
Figure 5.28: (a and b) parasagittal section of *Varanus niloticus* dorsal skin, stained with Masson's Trichrome and visualised with multi-rotation polarised light microscopy. EPI. = epidermis, S.C. = stratum compactum.

Scale bars: (a) = 120µm, (b) = 120µm.

Although no dermal skin samples were available for *Lanthanotus*, a HRXCT scan of *Lanthanotus borneensis* cranium is included for reference (Fig 5.63). ODs are clearly visible covering the whole cranium. These resemble the vermiform cylinders of Varanus komodoensis on the ventral part of the cranium, but on the right, left and dorsal sides, are observed as thicker and more bead-like in appearance. They also do not seem to overlap as much as *Varanus komodoensis ODs*.
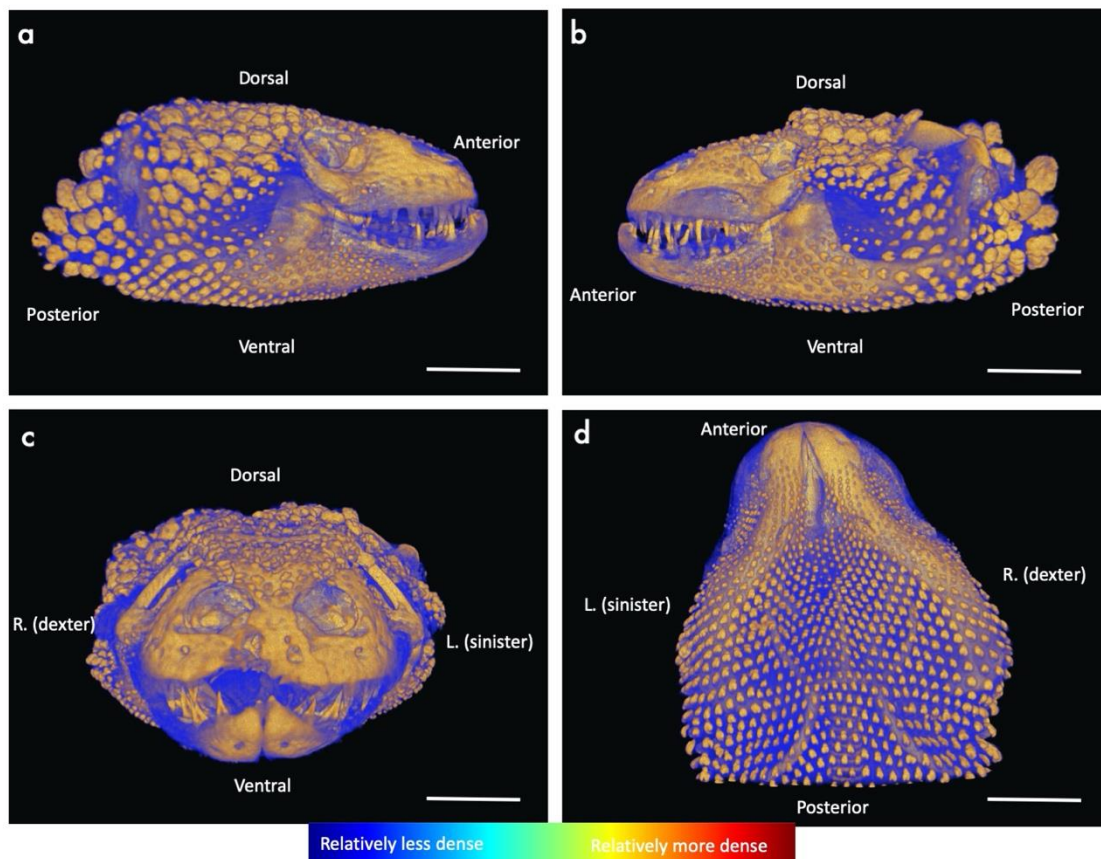
Figure 5.29: Volume rendering of HRXCT data of *Lanthanotus borneensis* cranium. Density dependent false-colour where blue indicates less dense material, orange indicates denser material, right lateral view (a), left lateral view (b), anterior view (c) and dorsal view (d)

Scale bars: (a-d) = 25 mm

5.2.4 Anguidae

Anguidae are a family of lizards native to the Northern Hemisphere, known for a lateral fold in the skin, for being carnivorous and for widespread OD expression (Gauthier, 1982). These lizards are known to inhabit a wide range of different habitats, from

tropical to temperate regions. There are three subfamilies, Anguinae, Diploglossinae and Gerrhonotinae. The two sampled species are *Ophisaurus ventralis* and *Elgaria multicarinata*.

Ophisaurus ventralis, commonly known as the Eastern glass lizard, is a species of limbless lizard endemic to the South-eastern United States. It belongs to the subfamily Anguinae. *O. ventralis* forages for insects, arachnids and small rodents both above ground and underground in burrows and can grow up to 1m in head-tail length (Uetz et al., 2018).

Elgaria multicarinata, commonly known as the Southern alligator lizard, is a small (reaching up to 30cm in head-tail length), limbed lizard that as the name suggests, resembles a miniature alligator and exhibits scales that are reinforced by bony ODs, as in alligators. It is commonly found along the Pacific coast of North America and belongs to the subfamily Gerrhonotinae. Carnivorous, it eats non-selectively, consuming a wide variety of prey, including insects, arthropods and other reptiles including other lizards. *Elgaria* species, like *Ophisaurus* species, have the ability to drop and subsequently regrow their tail (Uetz et al., 2018).

Two distinct types of anguid ODs have been described (Hoffstetter, 1962). The first type, reported in the Gerrhonotinae, are depicted as strongly linked to each other, bevelled along their lateral edges to increase the articular (contact) surface area between them (Hoffstetter, 1962; Meszoely, 1970). The second type of ODs is encountered in Diploglossinae, formed of rounded, non-bevelled ODs allowing shield flexibility (Hoffstetter, 1962; Meszoely, 1970; Bochaton, 2015). This last condition was proposed to be apomorphic within Anguidae (Meszoely, 1970). In addition, OD morphology in the three diploglossine genera *Diploglossus, Celestus* and *Wetmorena* was well described and studied by Strahm and Schwartz (1977). These authors proposed that the ODs of *Diploglossus* and *Celestus* could be distinguished by the occurrence of a cloud-like radix system of nutritive canals under the gliding surface of the ODs. As a consequence, ODs have commonly been used in the characterisation of anguids (Hoffstetter, 1962; Strahm and Schwartz, 1977; Gauthier, 1982). However, only the gross overall shape of the OD has been discussed and not the micromaterial composition. *Elgaria* ODs have been analysed using CT but only cranial ODs in relation to the skull bones (Ledesma and Scarpetta, 2008).

In the anguid lizard, *Ophisaurus ventralis*, extensive mineralisation was observed in all of the dorsal skin, apart from the lateral folds along the sides of the animal. The ODs appeared as large (roughly 5mm in length and 5mm in width) rectangular polygons with extensive internal vascularisation and/or surface ornamentation that was readily identifiable in X-ray plate imaging as vermiculate channels and patterning on every OD (Fig. 5.30b). They were laterally and anteriorly imbricate.
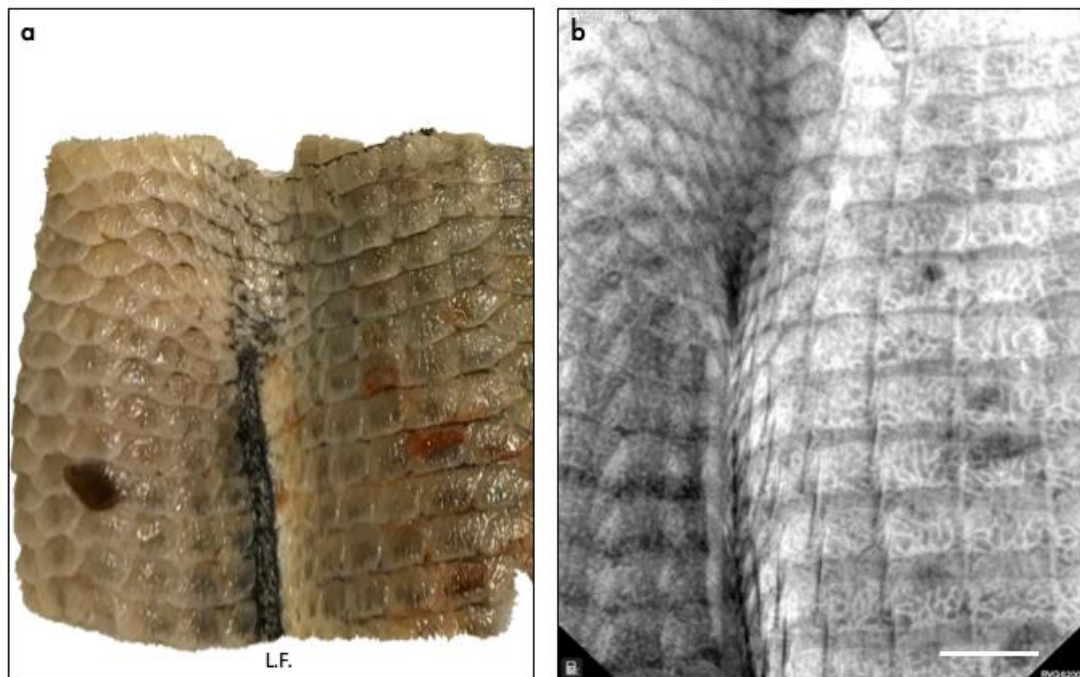
Figure 5.30: (a) Photograph of adult *Ophisaurus ventralis* post-cranial skin sample *ventralis* skin sample cut in the ventral midline, with dark pigmentation corresponding to the dorsal side (right), and pale pigmentation corresponding to the ventral side (left) and (b) corresponding x-ray plate image. L.F. = Lateral Fold.

Scale bars: (b) = 5mm.

HRXCT of the same *Ophisaurus ventralis* dorsal skin sample allowed visualisation of the OD mesh in greater detail than the X-ray plate imaging, and in three dimensions (Fig. 5.31). The results complemented the X-ray plate imaging, displaying a regularly overlapping mesh of laterally and posteriorly imbricating rectangular, polygonal ODs. No OD expression was present in either the left or right lateral folds. ODs were arranged in rows and columns and rarely deviated from this strict location patterning. The lines between columns of the ODs were almost always straight, but sometimes

appeared as a zig-zag pattern, for example, as was seen at the line between the most dorsal ODs (Fig. 5.31b, above the dissection nick indicating the posterior edge).
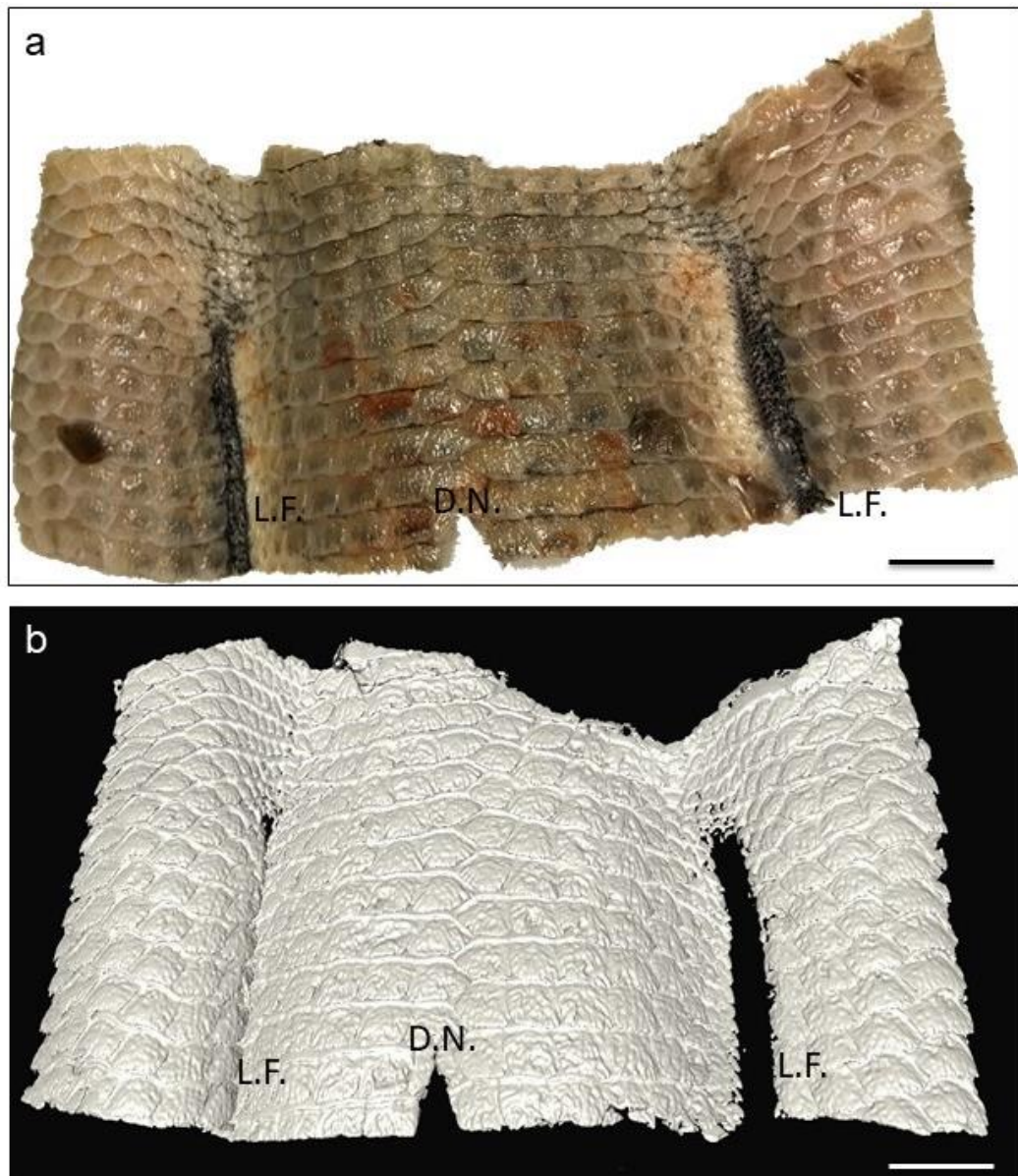
Figure 5.31: (a) photograph of adult *Ophisaurus* ventralis post-cranial skin sample cut in the ventral midline, with dark pigmentation corresponding to the dorsal side, and pale pigmentation corresponding to the ventral side. (b) corresponding three-dimensional false-colour surface reconstruction of OD mesh, in dorsal view, segmented from HRXCT data of the same sample. D.N. = Dissection nick, L.F. = Lateral fold.

Scale bars: (b) = 1.5cm.

A single OD was digitally segmented out of the OD mesh (Fig. 5.32) for greater clarity of the OD modular unit. This showed that the apical surface of each OD displays both a smooth gliding surface on the anterior side and a rough, ornamented surface on the posterior side. The rough, ornamented surface displayed multiple foramina, and extensive tubercles in a vermiform pattern (Fig. 5.32b). The gliding surface is the articular surface that overlaps with neighbouring ODs. The lateral edges of each OD are also smooth and bevelled towards the basal surface, which is smooth and perforated by foramina (Fig. 5.32c, d).
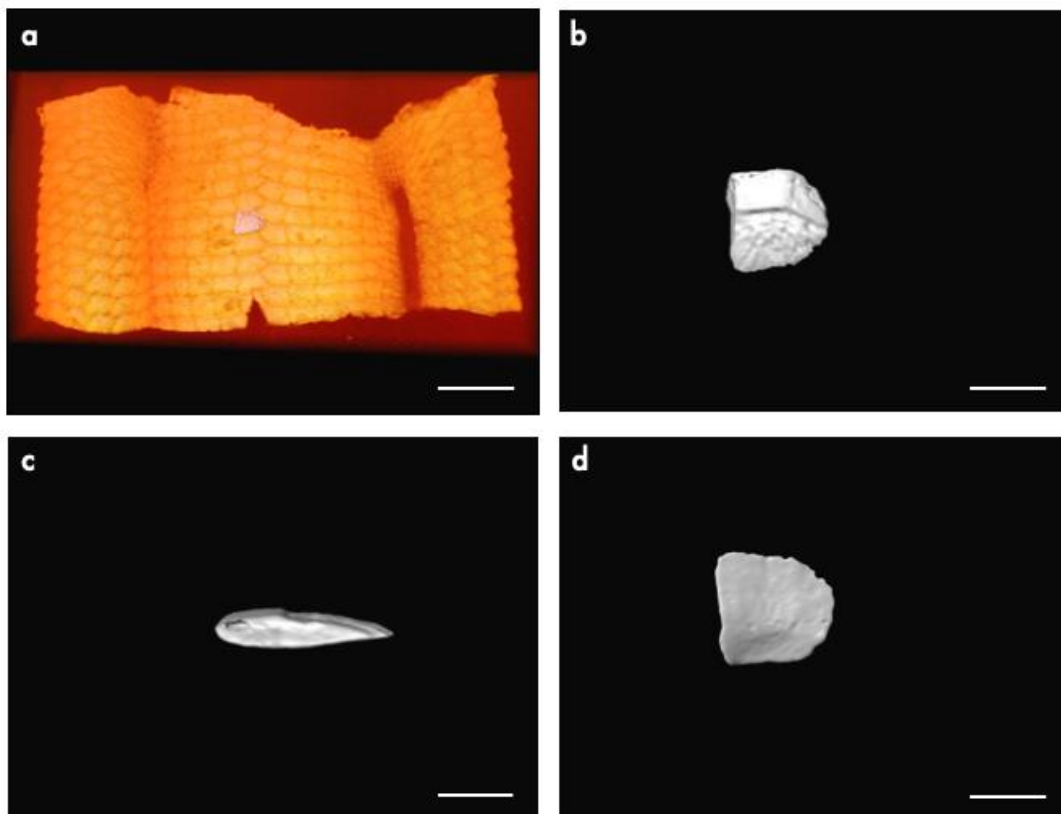
Figure 5.32: Three-dimensional false-colour volume rendering of OD mesh, generated from HRXCT data of adult *Ophisaurus ventralis* post-cranial, skin sample (a) in dorsal view. (b) Three-dimensional false-colour surface reconstruction of single OD, generated from HRXCT data of the same sample in dorsal view, (c) in lateral view and (d) in ventral view.

Scale bars: (a) = 1000µm, (b) = 100µm, (c) = 100µm, (d) = 100µm.

The histological sections showed the ODs as overlapping plates, up to three ODs thick in places (Fig. 5.33c and e), with extensive vascularisation and remodelling, and with a sculptured apical surface where the OD meets the lower layer of the epidermis. It is in this region, just below the epidermis, that OST. was identified on the apical surface of the most superficial part of each OD, staining colourless in Masson's trichrome, purple in H&E and strongly blue in Alcian blue (Fig. 5.33a, b, d, f), with evidence of successive generations of growth in the form of multiple growth lines and superimposed tubercles (Fig. 5.33d). The part of the OD located in the deepest part
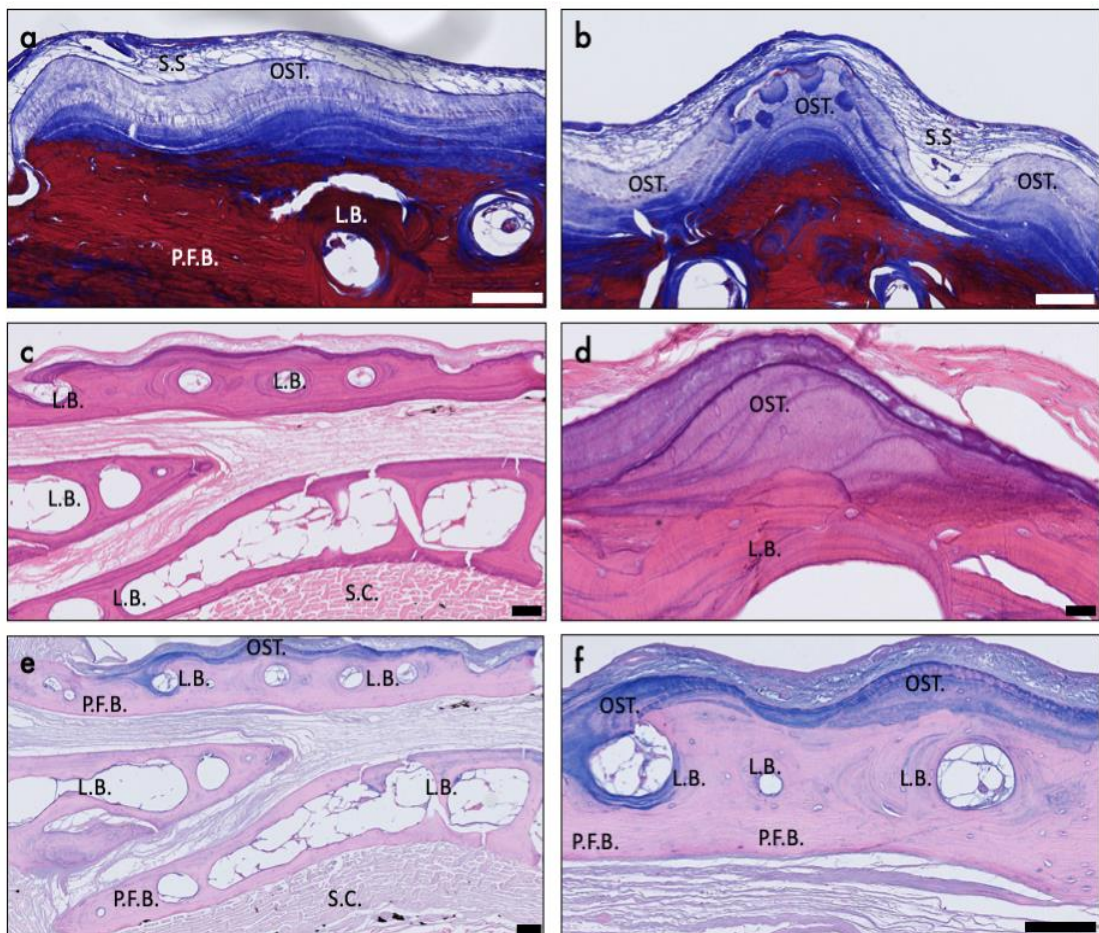
Figure 5.33: Histological staining of adult *Ophisaurus ventralis* dorsal skin sample sectioned parasagittally, (a) stained with Masson's trichrome, (b) stained with Masson's trichrome visualised at higher magnification, (c) stained with H&E, (d) stained with H&E visualised at higher magnification, (e) stained with Alcian blue and (f), stained with Alcian blue visualised at higher magnification. L.B. = lamellar bone, OST. = osteodermine, P.F.B. = parallel-fibred bone, S.C. = stratum compactum, S.S. = stratum superficiale.

Scale bars: (a) = 100µm, (b) = 100µm, (c) = 100µm, (d) = 20µm, (e) = 100µm, (f) = 100µm.

of the dermis is composed of P.F.B., with L.B. surrounding extensive vasculature. Such was the extent of this vascularisation, that a majority of ODs located in this deep location appeared essentially hollow (Fig. 5.33c, e). Multi-rotation polarised light microscopy confirmed these findings, with the most superficial surface of each ODs appearing black and thus displaying a lack of birefringence (a lack of a collagen matrix), apart from parallel Sharpey's fibres oriented perpendicular to the apical surface (Fig. 5.34, c, d). A section taken through the basal surface of each OD located deep in the dermis displayed a structure that resembled S.F.B., with extensive, regularly repeating thick collagen fibres that travel through the mineralised bone as well as soft tissue surroundings. (Fig. 5.34b, white arrows, S.F.B.).
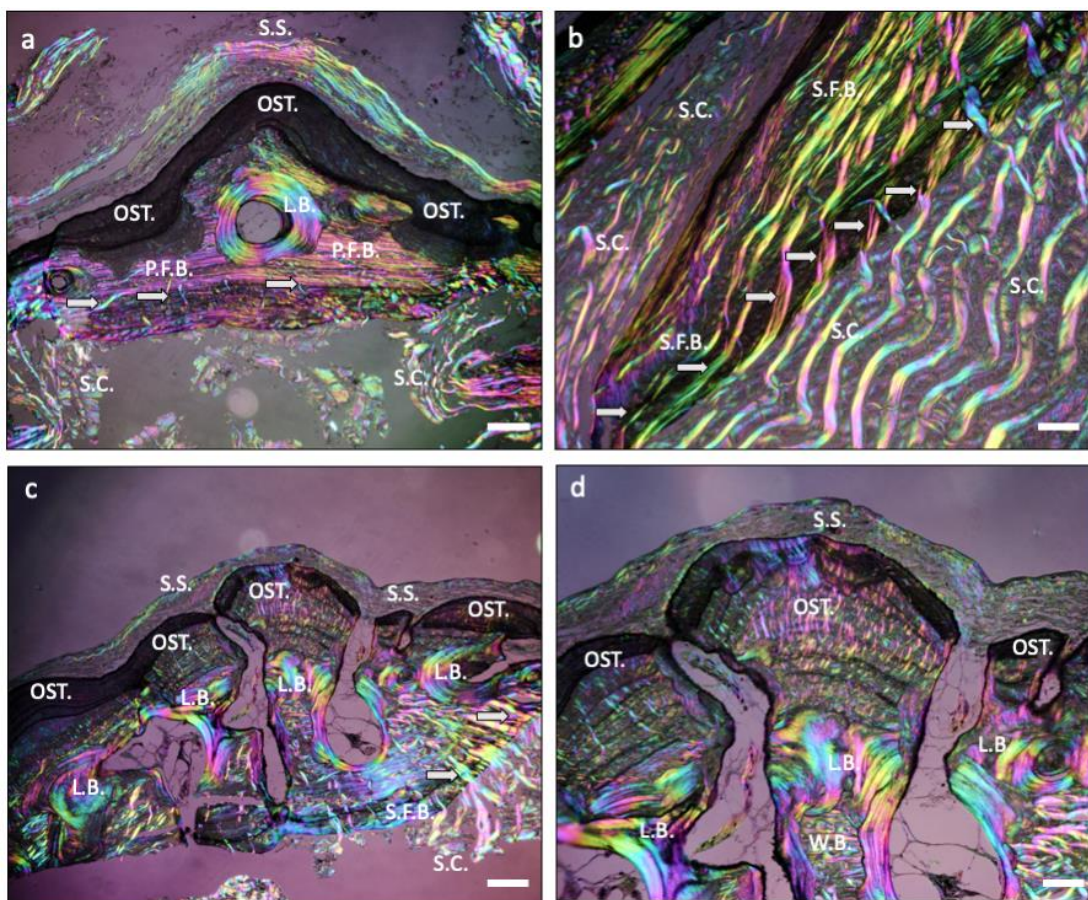
Figure 5.34: (a-d) parasagittal sections of adult *Ophisaurus ventralis* post-cranial dorsal skin stained with Alcian blue and visualised with multi-rotation polarised light microscopy. L.B. = lamellar bone, OST. = osteodermine, P.F.B. = parallel-fibred bone, S.C. = stratum compactum, S.F.B. = Sharpey-fibred bone, S.S. = stratum superficiale, white arrows = Sharpey's fibres

Scale bars: (a) = 120μm, (b) = 60μm, (c) = 120μm, (d) = 60μm.

The results from the adult specimen of *Ophisaurus ventralis* are easily compared to the juvenile specimen – the scales in the skin sample are much smaller (Fig. 5.35a), there was less surface patterning visible, and the ODs have roughly half the overall surface area of the adult ODs as seen in X-ray plate imaging (Fig. 5.35b).
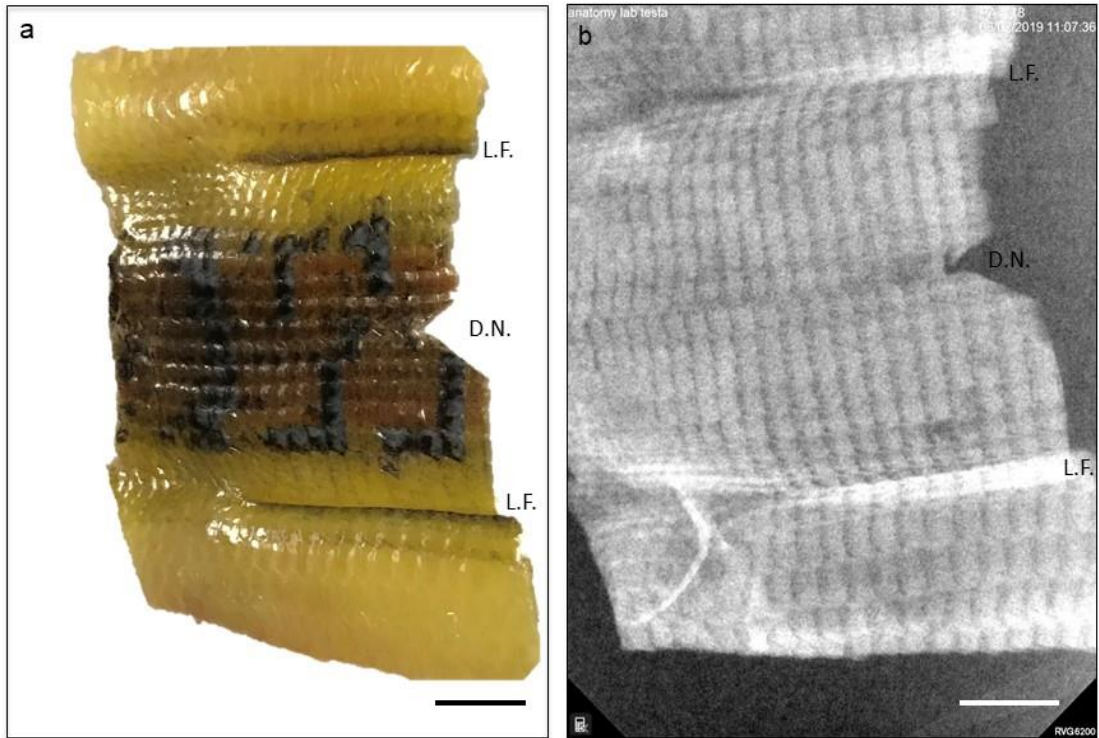
Figure 5.35: (a) photograph of juvenile *Ophisaurus ventralis* post-cranial skin sample cut in the ventral midline, with dark pigmentation corresponding to the dorsal side, and pale pigmentation corresponding to the ventral side. (b) corresponding x-ray plate image. D. N.= dissection nick (posterior margin), L. F. = lateral fold

Scale bars: (b) = 5mm.
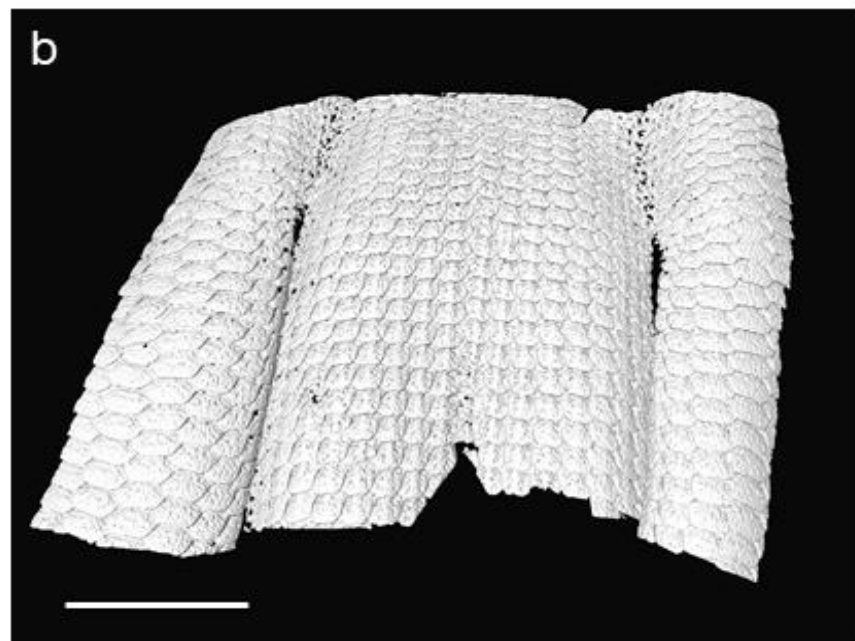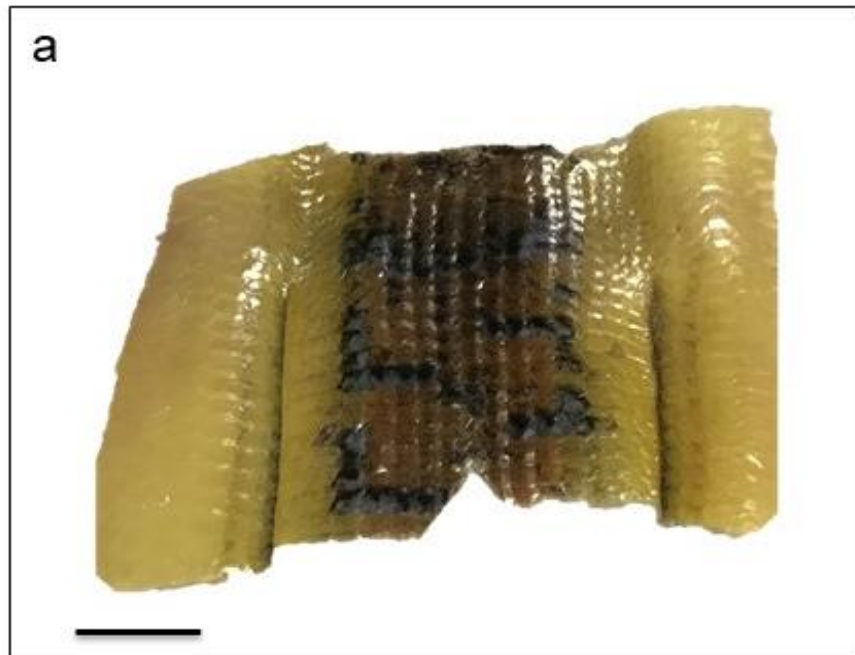
Figure 5.36: (a) photograph of juvenile *Ophisaurus ventralis* post-cranial skin sample cut in the ventral midline and (b) corresponding three-dimensional false-colour surface reconstruction of OD mesh, in dorsal view, segmented from HRXCT data of the same sample.

Scale bars: (b) = 1000µm.

HRXCT results mirrored that of the adult specimen at the level of overall anatomy of the ODs (Fig. 5.36) but ODs are roughly half the size. As expected, no OD expression was present in either the left or right lateral folds. There was also less surface patterning visible in the x-ray plate results, but this was confirmed as a resolution-based artefact due to the smaller size of the ODs, as demonstrated by the HRXCT scans of the same specimen.

As in the adult, a single OD was digitally segmented out of the OD mesh (Fig. 5.37) of the juvenile specimen for greater clarity of the OD modular unit. The OD from the juvenile specimen was very similar to that of the adult but slightly narrower (Fig. 5.37a), slightly thinner (Fig. 5.37b), less well formed with gaps on the anterior edge (Fig. 5.37a, d), and displayed the same divide of an anterior smooth gliding surface and a posterior rough, ornamented surface as that of the adult.
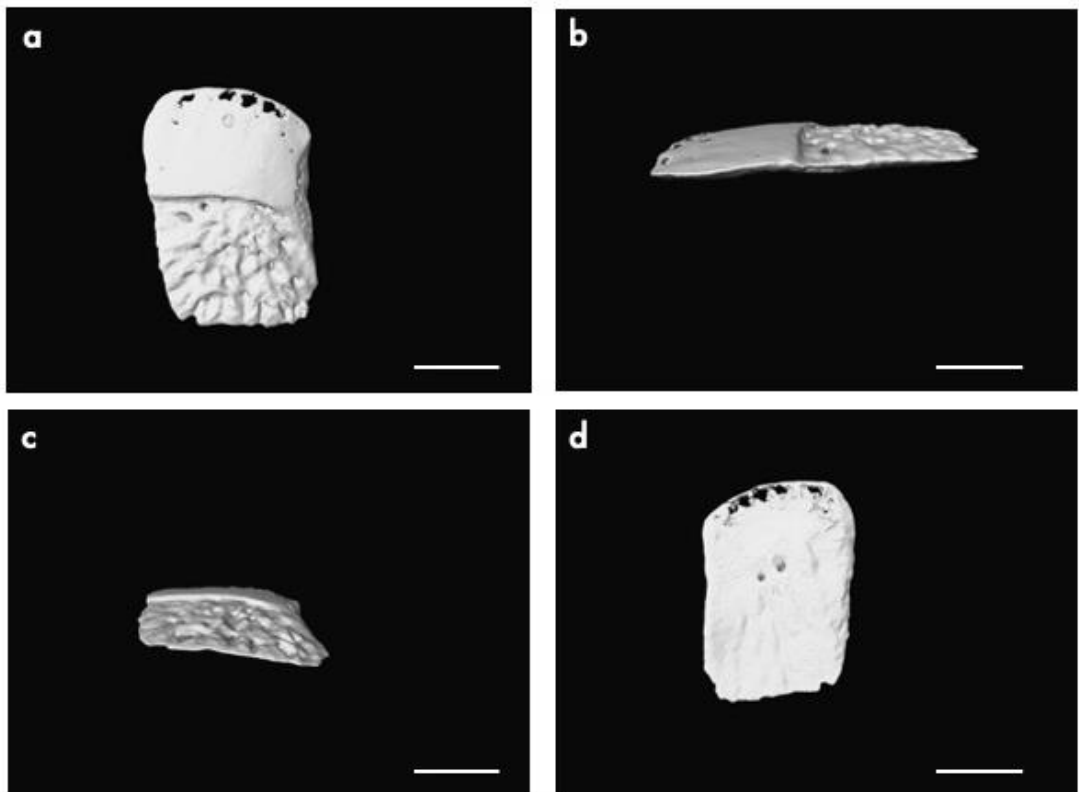
Figure 5.37: Three-dimensional false-colour surface reconstruction of single OD, segmented from HRXCT data of juvenile *Ophisaurus ventralis* post-cranial dorsal skin (a) in dorsal view, (b) in lateral view, (c) in posterior view and (d) in ventral view.

Scale bars: (a) = 100µm. (b) = 100µm. (c) = 100µm. (d) = 100µm.

Histological staining of the juvenile specimen of *Ophisaurus ventralis* showed that the immature ODs consist mainly of P.F.B. (parallel-orientated intrinsic collagen fibres in the base of the OD that do not extend out of the basal surface as is the case in S.F.B.) or L.B. (concentric lamellae with a scalloped border lining the endosteal surfaces of secondary osteons), with some increased basophilic staining on the apical surface of the most superficial ODs (Fig. 5.38b, d, f). Less extensive remodelling and vascularisation was observed in the juvenile than in the adult specimen. The
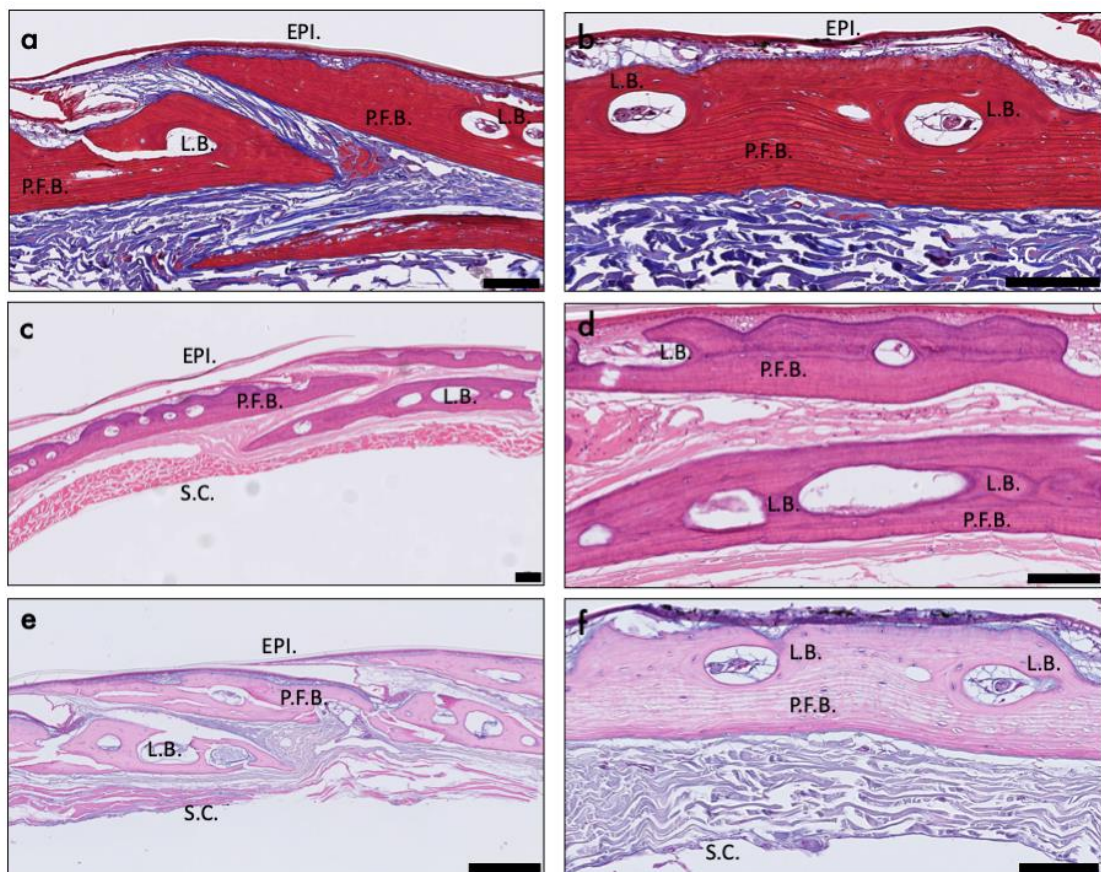
Figure 5.38: Histological staining of juvenile *Ophisaurus ventralis* dorsal skin, sectioned parasagittally and (a) stained with Masson's trichrome, (b) stained with Masson's trichrome visualised at higher magnification, (c) stained with H&E, (d) stained with H&E visualised at higher magnification, (e) stained with Alcian blue and (f), stained with Alcian blue visualised at higher magnification. EPI. = epidermis, L.B. = lamellar bone, P.F.B. = parallel-fibred bone, S.C. = stratum compactum.

Scale bars: (a) = 100µm, (b) = 100µm, (c) = 100µm, (d) = 20µm, (e) = 100µm, (f) = 100µm.
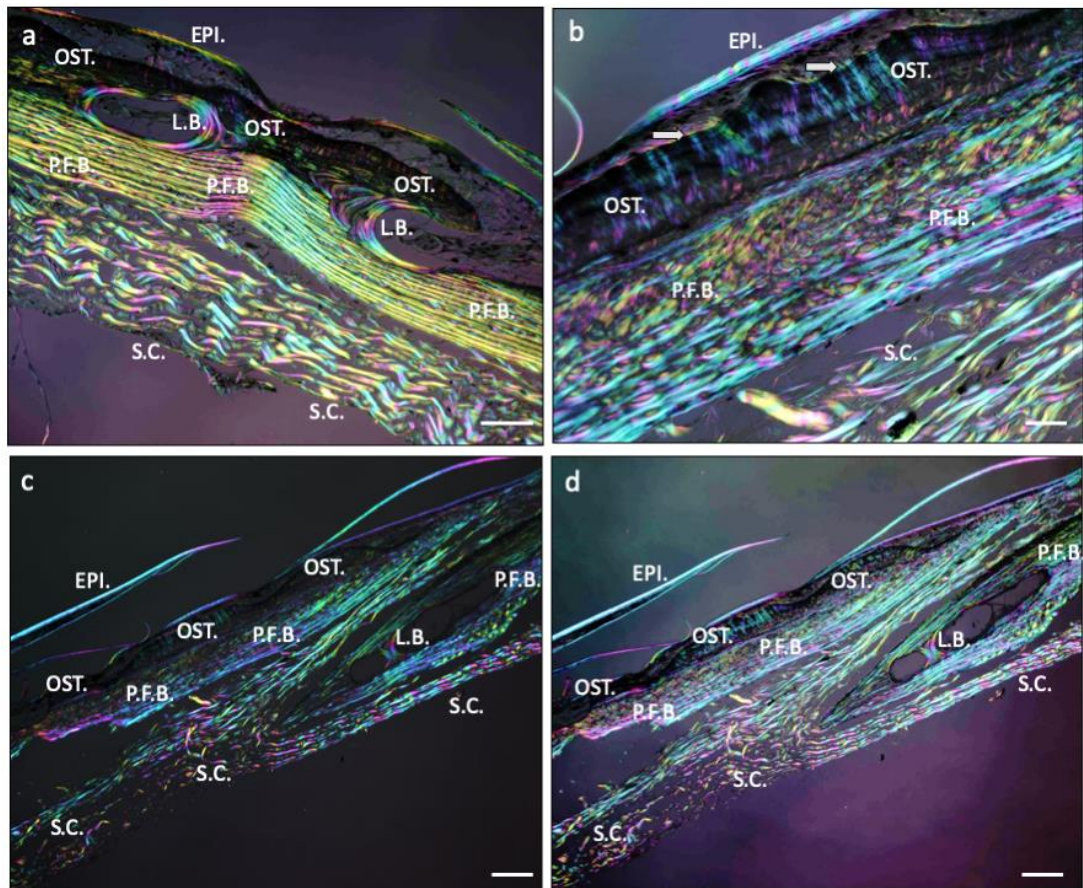
Figure 5.39: (a-d) parasagittal sections of juvenile *Ophisaurus ventralis* dorsal skin stained with Alcian blue and visualised with multi-rotation polarised light microscopy. The same result is shown in (c and d) however the contrast histogram is equalised in (d) for greater clarity. EPI. = epidermis, L.B. = lamellar bone, OST. = osteodermine, P.F.B. = parallel-fibred bone, S.C. = stratum compactum, White arrows = Sharpey's fibres.

Scale bars: (a) = 30µm, (b) = 60µm, (c) = 120µm, (d) = 120µm.

component materials stained in the same way as in the adult specimen, but no areas that completely lacked a collagen matrix were observed, no growth lines could be seen and the basophilic staining was not strong enough to make an accurate observation of OST.. The multi-rotation polarised light microscopy results for the juvenile specimen of *Ophisaurus ventralis* (Fig. 5.39) did show some lack of birefringence and thus a lack of collagen matrix on the apical surface, and parallel orientated Sharpey's fibres, with some evidence of successive growth with 1 or 2 growth lines. This area is thus labelled as OST. (Fig. 5.39b) but should be regarded as immature given the thinness, lack of extensive basophilic histological staining, presence of collagen and fewer growth lines.

As a representative of a different anguid subfamily (i.e. Gerrhonotidae), *Elgaria multicarinata* presented a very different OD anatomy to that of *Ophisaurus ventralis* when viewed using X-ray plate imaging (Fig 5.40). ODs were much smaller than in Ophisaurus ventralis, and did not appear on the X-ray plate imaging, as the resolution was not sufficient to make them out clearly, however alternate lines of increasing and decreasing pixel brightness were seen, indicating overlapping mineralisations.
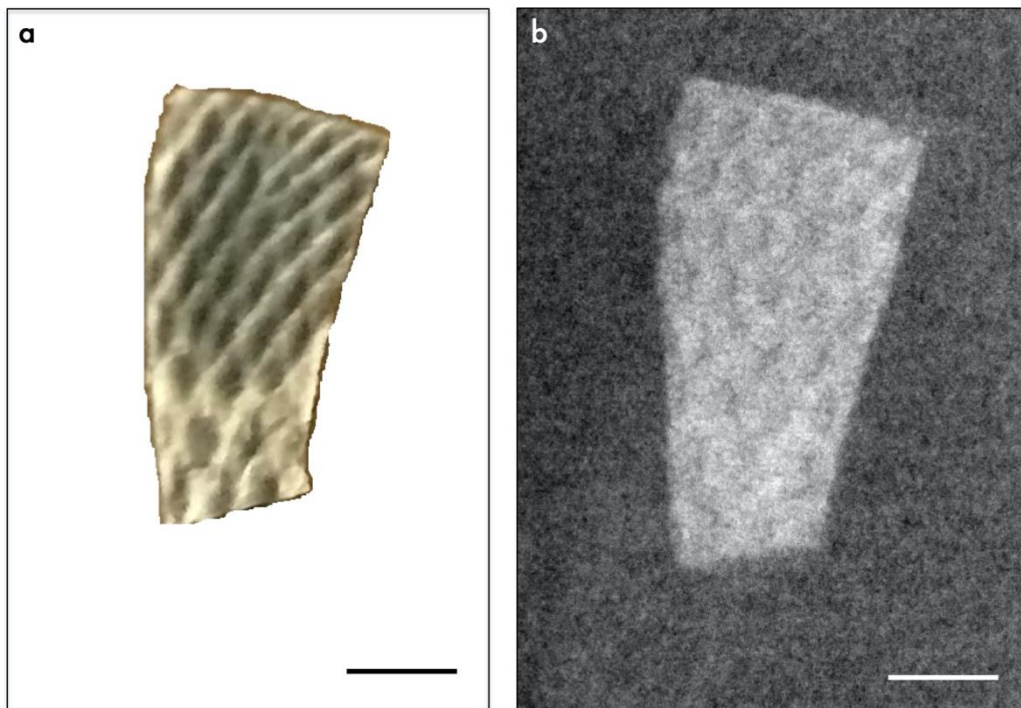
Figure 5.40: (a) photograph of *Elgaria multicarinata* dorsal skin sample at time of imaging and (b) corresponding x-ray plate image.

Scale bars: (b) = 0.5mm.
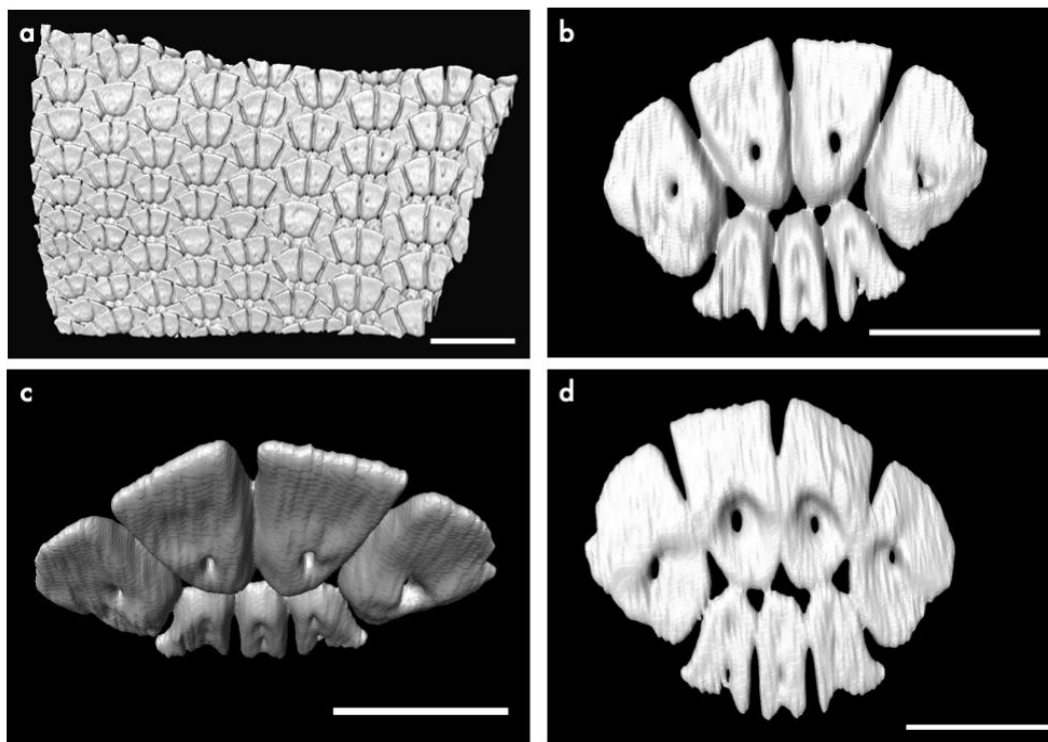
Figure 5.41: Three-dimensional, false colour surface reconstruction, segmented from HRXCT data of post-cranial, dorsal *Elgaria multicarinata* skin. (a) Osteoderm mesh in ventral view, (b) segmented single osteoderm ventral view, (c) anterior view, (d) dorsal view.

Scale bars: (a) = 200μm, (b) = 100μm (c) = 100μm, (d) = 100μm.

HRXCT results showed that each *Elgaria multicarinata* OD was circular, consisting of a system of seven small osteodermites (with four osteodermites on the anterior edge and three on the posterior edge) that fuse together to create the whole OD plate. Each of these OD plates is overlapped in a tiled pattern, both anteriorly and laterally (Fig. 5.41a) i.e. the anterior and lateral edges of one OD overlap the posterior and lateral edges of the OD in front of it. This imbrication results in a symmetric mesh of ODs, with only four osteodermites visible from a ventral view of each OD. These four osteodermites on the anterior edge are larger than the three on the posterior edge (Fig. 5.41b). All four of these osteodermites exhibited a large foramen in the centre, whilst the three located at the posterior edge did not (Fig. 5.41).

Histological staining revealed that the ODs of *Elgaria multicarinata* do overlap up to 3 ODs thick, becoming very thin in sections that show the edge of the scale, but can appear as thick and individually spaced in other sections (Fig. 5.42c, d). They are made of S.F.B. and OST.. S.F.B. stains blue to red in Masson's trichrome, (indicating collagen under tension) pink in H&E (indicating collagen) and pink in Alcian blue (indicating no acid mucosubstances) (Fig. 5.42, S.F.B.). No L.B. is recorded, and vascular penetration is very rare, perhaps due to the small size of the ODs. A
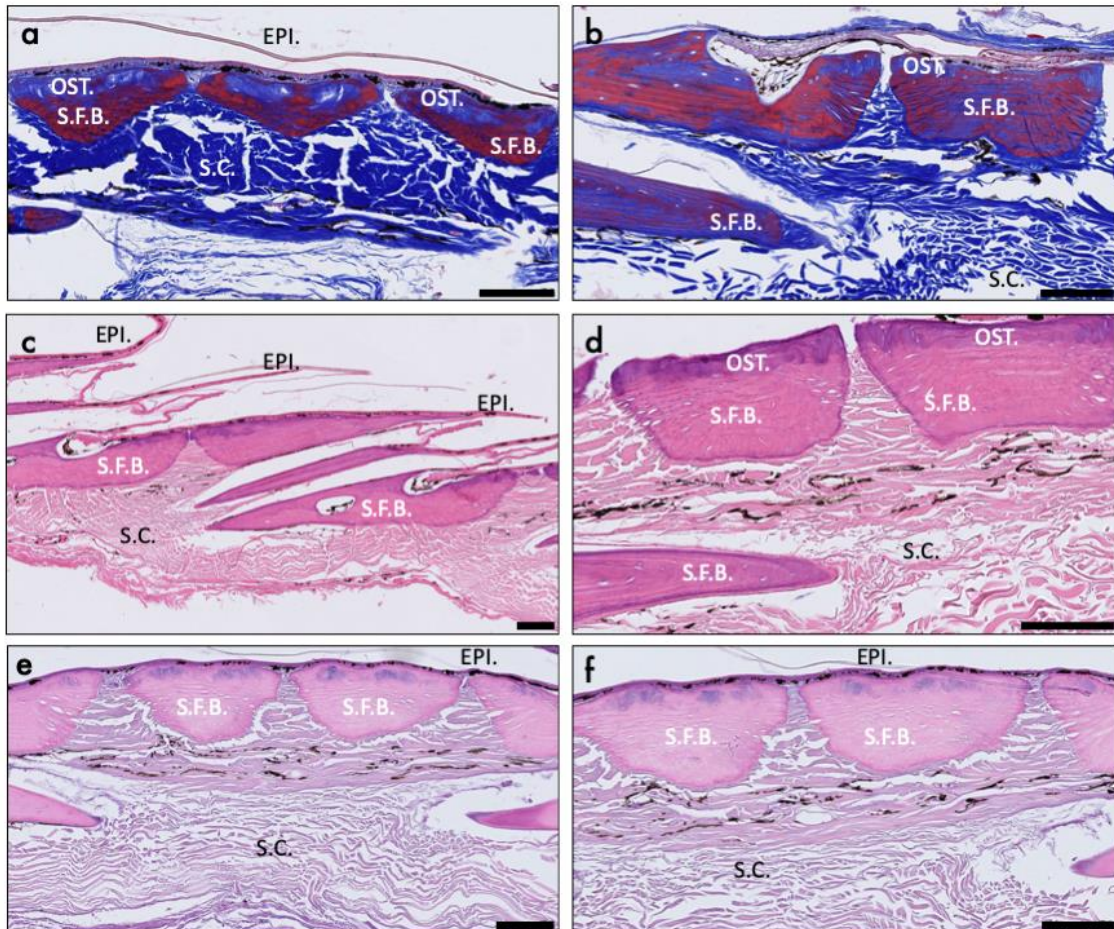
Figure 5.42: Histological staining of *Elgaria multicarinata* skin, parasagittal sections (a) stained with Masson's trichrome, (b) stained with Masson's trichrome visualised at higher magnification, (c) stained with H&E, (d) stained with H&E visualised at higher magnification, (e) stained with Alcian blue and (f), stained with Alcian blue visualised at higher magnification. EPI. = epidermis, OST. = Osteodermine, S.C. = stratum compactum, S.F.B. = Sharpey-fibred bone.

Scale bars: (a) = 100µm, (b) = 100µm, (c) = 100µm, (d) = 100µm, (e) = 100µm, (f) = 100µm.

reduction in collagen expression, combined with purple staining in H&E and blue staining in Alcian blue, (Fig. 5.42, OST.), led to the identification of a thin and sporadic deposit of OST. on the apical surfaces of the parts of ODs that lie directly below the epidermis. OST. in *Elgaria multicarinata* stained blue to colourless in Masson's trichrome, purple in H&E and blue in Alcian blue, matching staining of OST. in other taxa.

Multi-rotation polarised light microscopy results confirmed these findings, with the apical surface displaying a lack of birefringence and thus a lack of collagen matrix beneath the epidermis (Fig. 5.43, OST., EPI.). No growth lines or Sharpey's fibres could be identified in the OST. region, however the S.F.B. is anchored to the dermis with extensive Sharpey's fibres (Fig. 5.43, S.F.B., white arrows). The lack of attributes
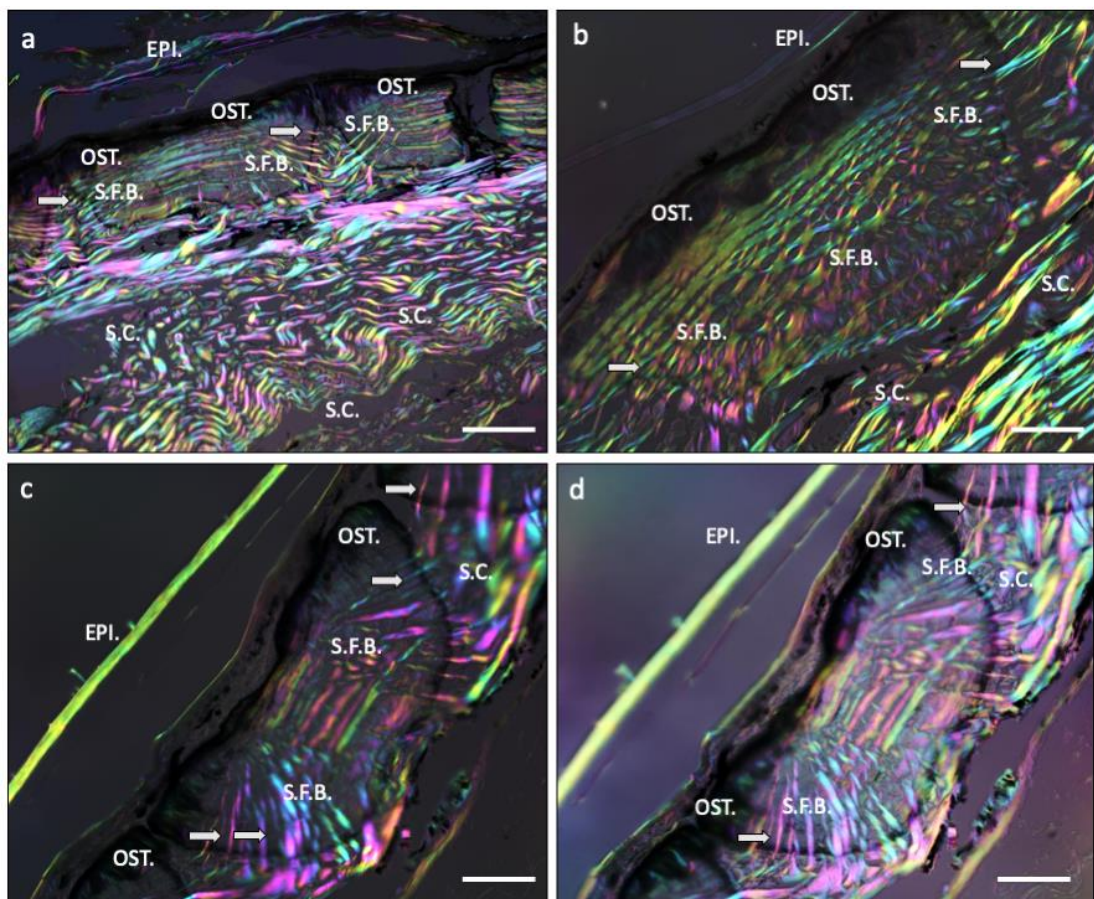
Figure 5.43: Parasagittal section of *Elgaria multicarinata* dorsal skin, stained with Masson's Trichrome and visualised with multi-rotation polarised light microscopy. EPI. = epidermis, OST. = Osteodermine, S.C. = stratum compactum, S.F.B. = Sharpey-fibred bone, White arrows = Sharpey's fibres.

Scale bars: (a) = 60µm, (b) = 30µm, (c) = 30µm, (d) = 30µm.

commonly seen in OST. might be explained by the thin layer and sporadic expression of OST. in the ODs of this species.

BSE-SEM imaging of the ODs from *Elgaria multicarinata* (Fig. 5.44) complemented the histological staining and multi-rotation polarised light results, confirming the presence of S.F.B. in the basal area and small deposits of OST. on the apical surface. It was also possible to identify L.B. on the internal surfaces of vascular channels in two of the figured sections (Fig. 5.44c, d).
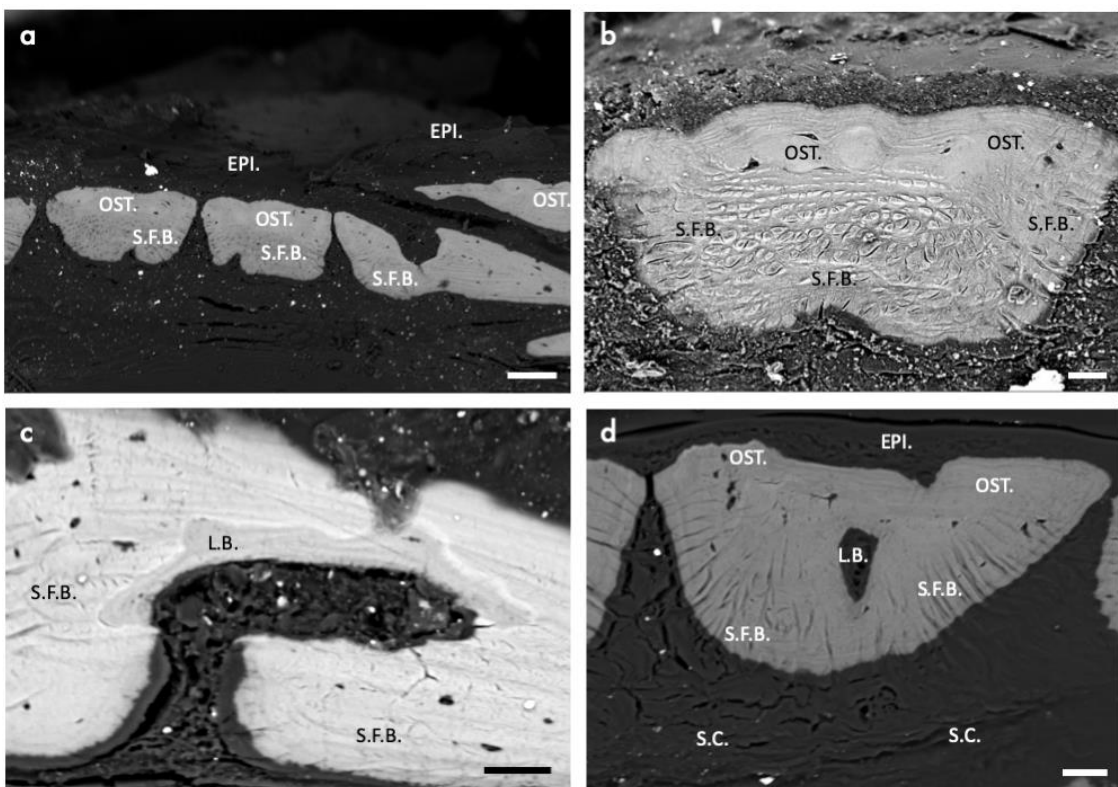
Figure 5.44: BSE-SEM imaging of *Elgaria multicarinata* OD (a-d) coronal sections, resin embedded, ground and polished. EPI. = Epidermis, L.B. = lamellar bone, OST. = Osteodermine, S.C. = stratum compactum, S.F.B. = Sharpey-fibred bone.

Scale bars: (a) =100µm, (b) = 20µm, (c) = 30µm, (d) = 30µm.

5.2.5 Scincidae

The family Scincidae is one of the most diverse families of lizards, with more than 1,500 species recorded. Most scincid species have no pronounced neck, and their legs are relatively small. Nearly all skinks dig and burrow underground, or enjoy habitats with lots of cover, such as rocky outcrops. They are carnivorous and insectivorous, often consuming their prey whole (Greer, 2007).

In the Scincidae, Otto (1909) studied scales from *Scincus, Gongylus, Seps, Lygosoma, Mabuya and Acontias.* In all of these, the ODs were found beneath each scale and were described as being composed of a mosaic-like structure of many plates. This type of OD is described as compound (, meaning the modular unit of the overlapping OD is formed from the fusion of more than one smaller modular units. Otto found that bony plates in different genera resembled one another, as long as they were sampled from the same anatomical region. In different anatomical regions, he observed considerable differences in the shape and morphology of the scales and underlying ODs (i.e. in *Scincus* and *Mabuya*) He also found that the number of plates in an individual OD varied on different parts of the body of the same species and on the same part of the body in different species but did not completely analyse this finding.

Three scincid species were sampled in this study, *Tiliqua rugosa, Corucia zebrata* and *Egernia stokesii.*

The bobtail skink or shingleback skink (*Tiliqua rugosa*) is a slow moving, heavily armoured, blue-tongued skink native to semi-arid regions of Australia (Uetz et al., 2018). This species is known for having a short, stumpy tail that contains fat reserves, much like *Heloderma*. They are omnivorous and have been known to live for 50 years in the wild (Greer, 2007).

The largest extant species of skink, *Corucia zebrata,* is more commonly known as the Solomon Islands skink, the prehensile-tailed skink, the giant skink, or the monkey skink (Adler et al., 1995). *Corucia* is completely herbivorous and live amongst a social group (McCoy, 2006).

Gidgee skinks (*Egernia stokesii*) are endemic to Western Australia and enjoy basking in large social groups around rocky areas. They are omnivorous, catching invertebrates and insects but feed predominately on vegetation (Cogger, 2000).

Tiliqua rugosa ODs have not been described to date apart from one X-ray plate image of the whole animal that is not sufficiently detailed to make out the compound nature of the ODs (Barten and Simpson, 2019). *Egernia spp.* have been shown to express ODs as compound, overlapping structures, characteristic of skinks, but only with simple alizarin red staining of whole mount specimens and microstructural details have not been explored (Vickaryous and Sire, 2009).

X-ray plate imaging of *Tiliqua rugosa* showed that a single adult OD is roughly 1.5mm-2mm in size. The ODs of this species are therefore the largest of those analysed in this study. Three large non-mineralised lines are visible in the X-ray image (Fig. 5.45b). These are interpreted to be natural boundaries between the osteodermites that comprise the compound OD. Extensive rough ornamentation across the entire apical surface of the OD is visible in the photograph as well as on the X-ray plate image. The brightest pixels, therefore the densest and/or thickest part of the OD, are seen along the anterior edge (Fig. 5.45b, left side).
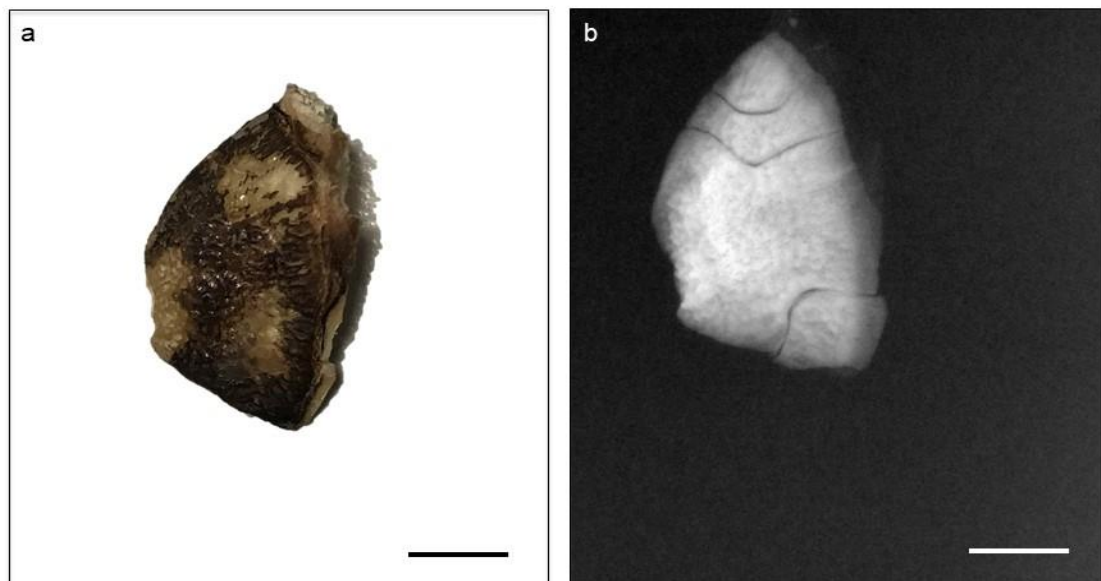
Figure 5.45: Photograph of *Tiliqua rugosa* dorsal single OD (a) and corresponding x-ray plate image (b).

Scale bars: (b) = 5mm.

HRXCT results of multiple ODs from *Tiliqua rugosa* dorsal skin demonstrated a slight anterior-posterior overlap, with the posterior edge of each OD residing beneath the anterior edge of the one following, with the anterior edge of one OD overlapping that in front of it (Fig. 5.46a). When segmented from the mesh, a single OD appeared with a thin aspect ratio, plate-shaped, roughly circular in dorsal view, with extensive ornamentation on the apical surface, and with a relatively smooth basal surface. Multiple foramina were readily observed on both the apical and the basal surface (Fig. 5.46c, d), which confirms the mosaic structure seen in the x-ray plate image.
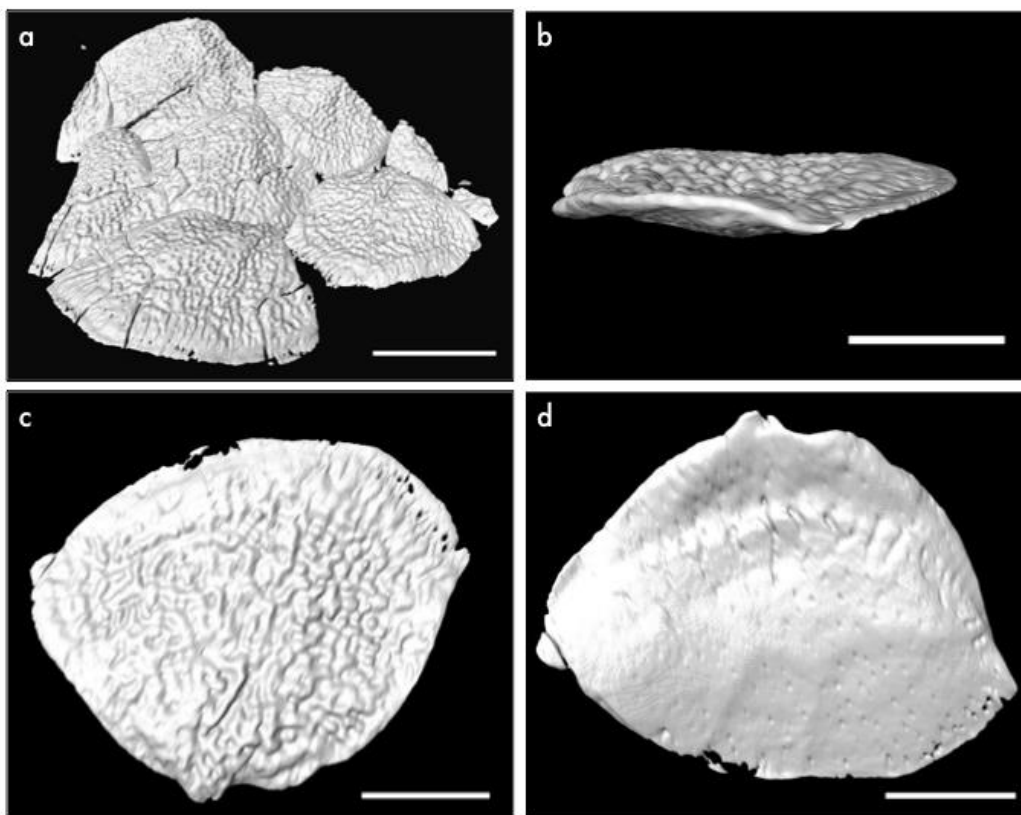
Figure 5.46: Three-dimensional, false colour surface reconstructions, segmented from HRXCT data of post-cranial, dorsal *Tiliqua rugosa* skin. (a) Osteoderm mesh in dorsal view, (b) segmented single osteoderm lateral view, (c) dorsal view, (d) ventral view.

Scale bars: (a) = 10mm, (b) = 5mm, (c) = 5mm, (d) = 5mm.

Histology of the OD revealed a core of W.B and a periphery of P.F.B. (Fig. 5.47, W.B., P.F.B.) and in one section, a secondary osteon with a lining of L.B. was identified. A lack of collagen matrix, successive growth lines and strong basophilic staining on the apical surface close to the lower layers of the epidermis were identified in some sections which led to the identification of OST. tubercles capping some areas of the apical surface. (Fig. 5.47b, f, OST.). The OST. tubercle expression varied due to the ornamentation of the surface and thus each tubercle appeared as an isolated semi-circular shaped mound in parasagittal section (Fig. 5.47d, OST.), located within the stratum superficiale. The OST. was also very brittle and it was hard to source an image that did not display extensive tearing of the sample in this location. The rest of
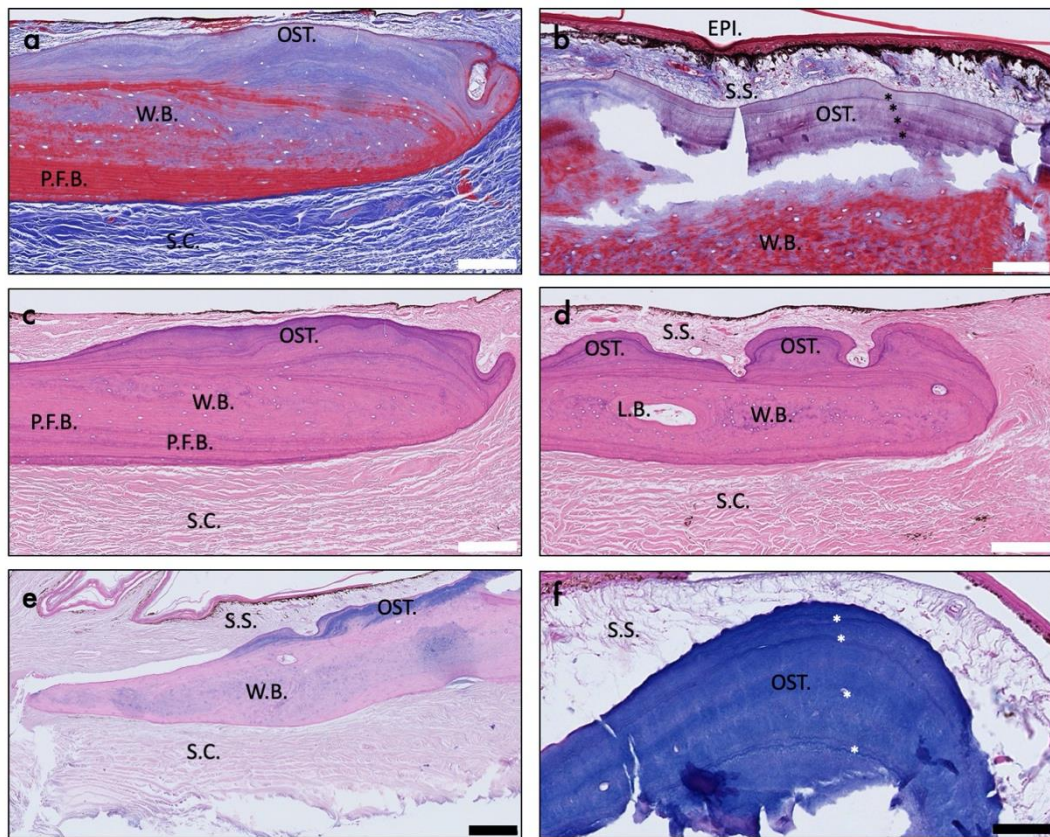
Figure 5.47: Histological staining of *Tiliqua rugosa* skin sample sectioned parasagittally (a) stained with Masson's trichrome, (b) stained with Masson's trichrome visualised at higher magnification, (c) stained with H&E, (d) stained with H&E visualised at higher magnification, (e) stained with Alcian blue and (f), stained with Alcian blue visualised at higher magnification. L.B. = lamellar bone, OST. = Osteodermine, P.F.B. = parallel-fibred bone, S.C. = stratum compactum, S.S. = stratum superficiale, W.B. = woven bone.

Scale bars: (a) = 100µm, (b) = 100µm, (c) = 100µm, (d) = 100µm, (e) = 100µm, (f) = 40µm.

the OD, composed of different types of bone, did not tear excessively across any sections.

Multi-rotation polarised light microscopy results confirmed these findings, with the apical surface displaying a lack of birefringence and thus a lack of collagen matrix beneath the epidermis (Fig. 5.48, OST., EPI.). Successive growth lines are also identified in the OST. region (Fig. 5.48, asterisks.) and occasional Sharpey's fibres were observed in the basal portion of the OD, which led to the identification of S.F.B. in this region, which was not possible to identify in histological staining without polarised light.
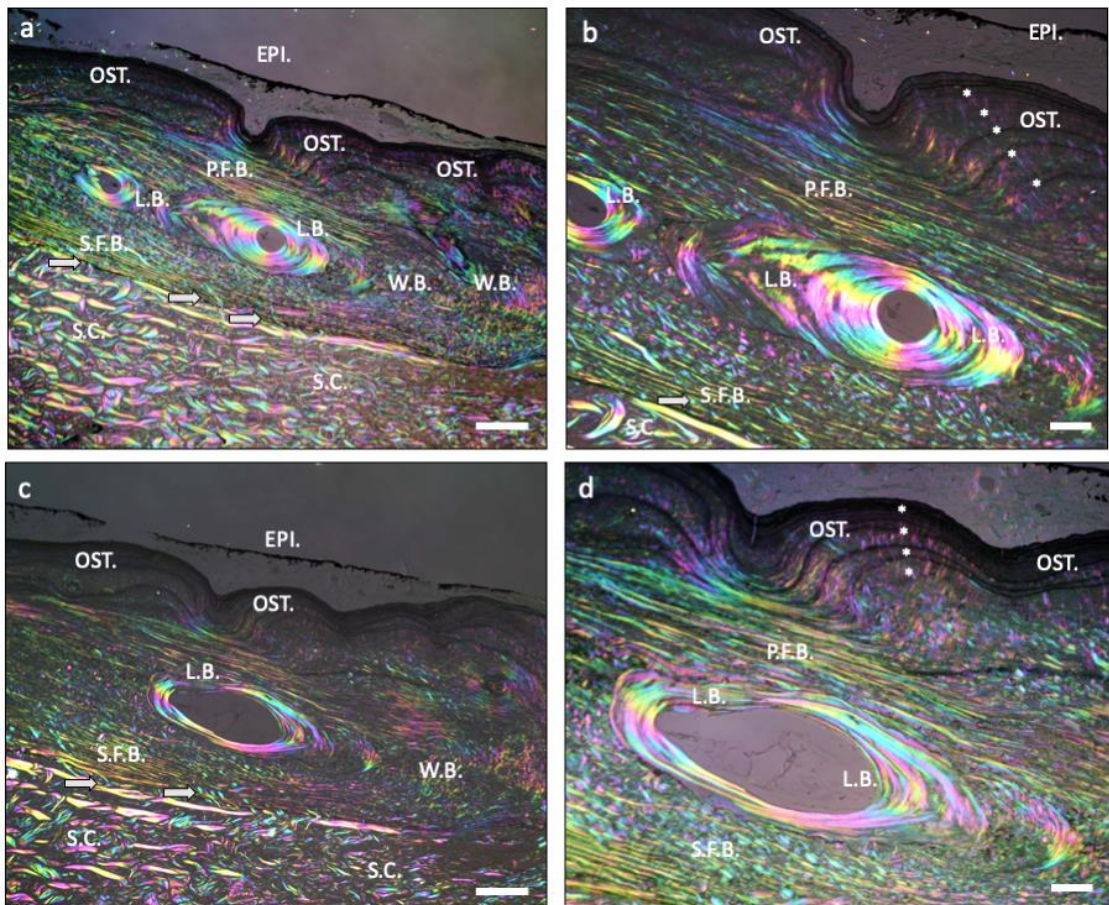
Figure 5.48: Parasagittal sections of *Tiliqua rugosa* dorsal skin, stained with Masson's Trichrome and visualised with multi-rotation polarised light microscopy. Asterisks = growth lines, EPI. = Epidermis, L.B. = lamellar bone, OST. = Osteodermine, P.F.B. = parallel-fibred bone, S.C. = stratum compactum, S.F.B. = Sharpey-fibred bone, White arrows = Sharpey's fibres, W.B. = woven bone.

Scale bars: (a) = 120μm, (b) = 60μm, (c) = 120μm, (d) = 60μm.

BSE-SEM results harmonised with histological staining and polarised light microscopy results in that it was possible to identify L.B., S.F.B., and OST. as a thick, dense, collagen-poor and cell-poor cap on the apical surface of the OD (Fig. 5.49a, b, OST.). A close up of the OST. region (Fig. 5.49c) showed a highly mineralised material with an almost complete lack of cellular lacunae.
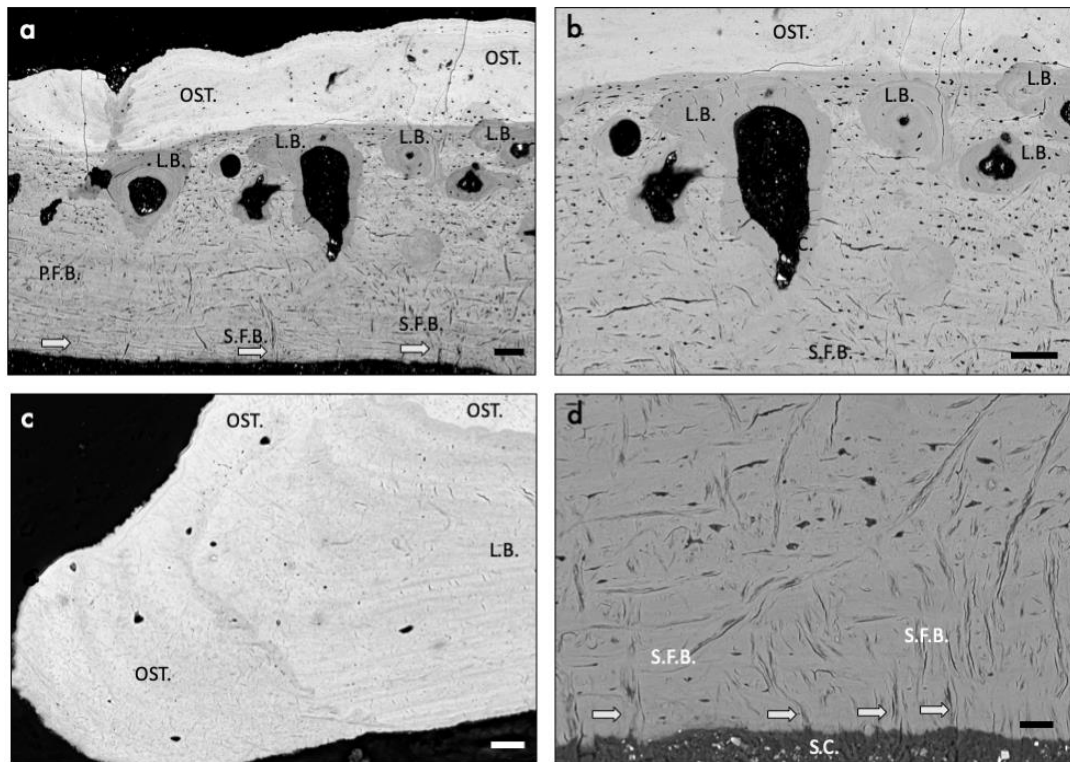
Figure 5.49: BSE-SEM imaging of *Tiliqua rugosa* OD (a-d) parasagittal sections, resin embedded, ground and polished. L.B. = lamellar bone, OST. = Osteodermine, P.F.B. = Parallel-fibred bone, S.C. = stratum compactum, S.F.B. = Sharpey-fibred bone, White arrows = Sharpey's fibres.

Scale bars: (a) = 100 μm, (b) = 100 μm, (c) = 20 μm, (d) = 40 μm.

The second species of skink examined was *Corucia zebrata.* An initial X-ray plate image of the dorsal skin sample (Fig 5.50) showed that the ODs as a whole were much smaller than those of *Tiliqua rugosa* and were composed of smaller still osteodermites, but each was larger than the resolution of the X-ray plate sensor. Alternating lines of increasing and decreasing pixel brightness were also seen, indicating overlapping mineralisations.
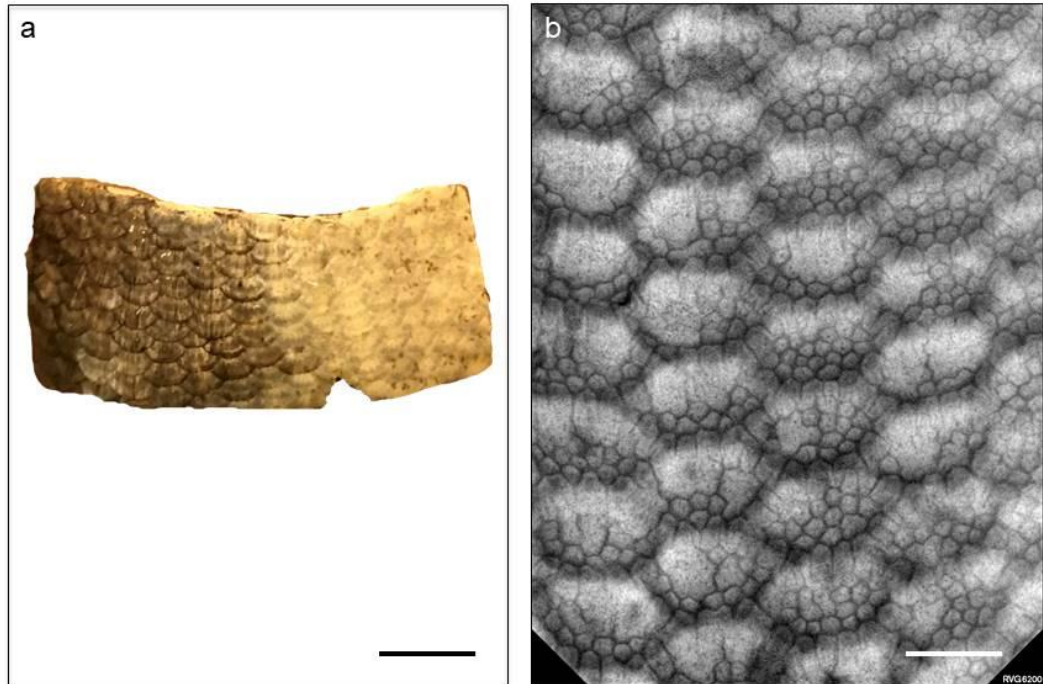
Figure 5.50: (a) photograph of *Corucia zebrata* dorsal skin sample at time of imaging and (b) corresponding x-ray plate image.

Scale bars: (b) = 5mm.

HRXCT results showed the dorsal surface of the OD mesh was almost uninterrupted and had a very rough surface (Fig. 5.51a). From this view, each OD resembled a single unit, but in ventral view (Fig. 5.51b, d), it became clear that each *Corucia zebrata* OD consisted of a system of sixteen small osteodermites (with five osteodermites on the anterior edge and three on the posterior edge) that fuse together to create the thin, oval, plate-like OD. An average OD was observed as roughly 600-700μm wide and around 400-500μm long. Each ODs overlapped in a tiled pattern, both anteriorly and laterally (Fig. 5.51b, d) such that the posterior and lateral edge of each OD was overlapped by the anterior and lateral edge of the following OD. This results in a symmetric mesh of ODs, with around half of the osteodermites visible from a ventral view of each OD. When a single OD unit was segmented from the mesh, it was clear that the OD unit consists of large, elongate and rectangular osteodermites

on the lateral edges of the plate, with smaller bead-shaped osteodermites in the centre (Fig 5.52).
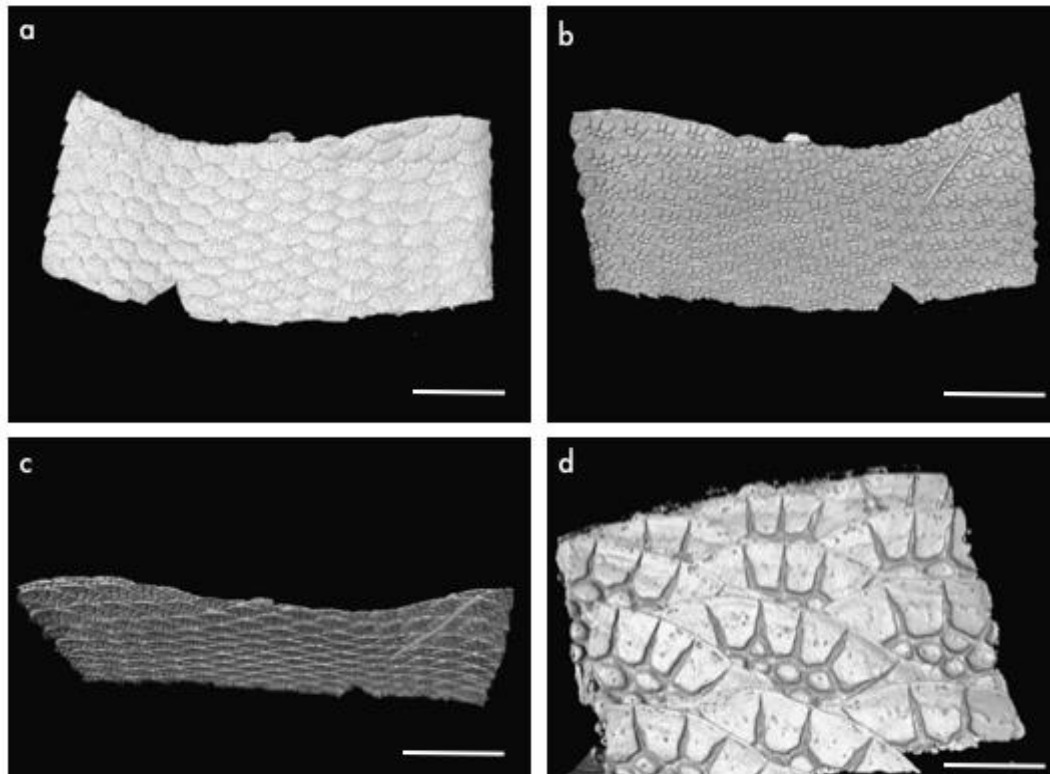
Figure 5.51: Three-dimensional, false colour surface reconstructions of OD mesh, segmented from HRXCT data of post-cranial, dorsal *Corucia zebrata* dorsal skin sample, (a) dorsal view, (b) ventral view, (c) posterior view, (d) ventral view at higher magnification.

Scale bars: (a) = 10mm, (b) = 10mm, (c) = 10mm, (d) = 500µm.

The five osteodermites on the anterior lateral edge were larger than the five on the posterior lateral edge (Fig. 5.52a, b). Almost all of the osteodermites exhibited foramina, with many foramina in the largest osteodermites (Fig. 5.52a, b). Interestingly, there is no continuous boundary to the outer edges of the external osteodermites, the mineralisations become thinner, sparser and eventually breakdown into individual, discontinuous pieces (Fig. 5.52c, d) which would explain the rough surface seen in dorsal view of the OD mesh (Fig. 5.51a). This is not just a resolution artefact as the histological staining results also show very small, discontinuous mineralisations in the superficial part of the OD.
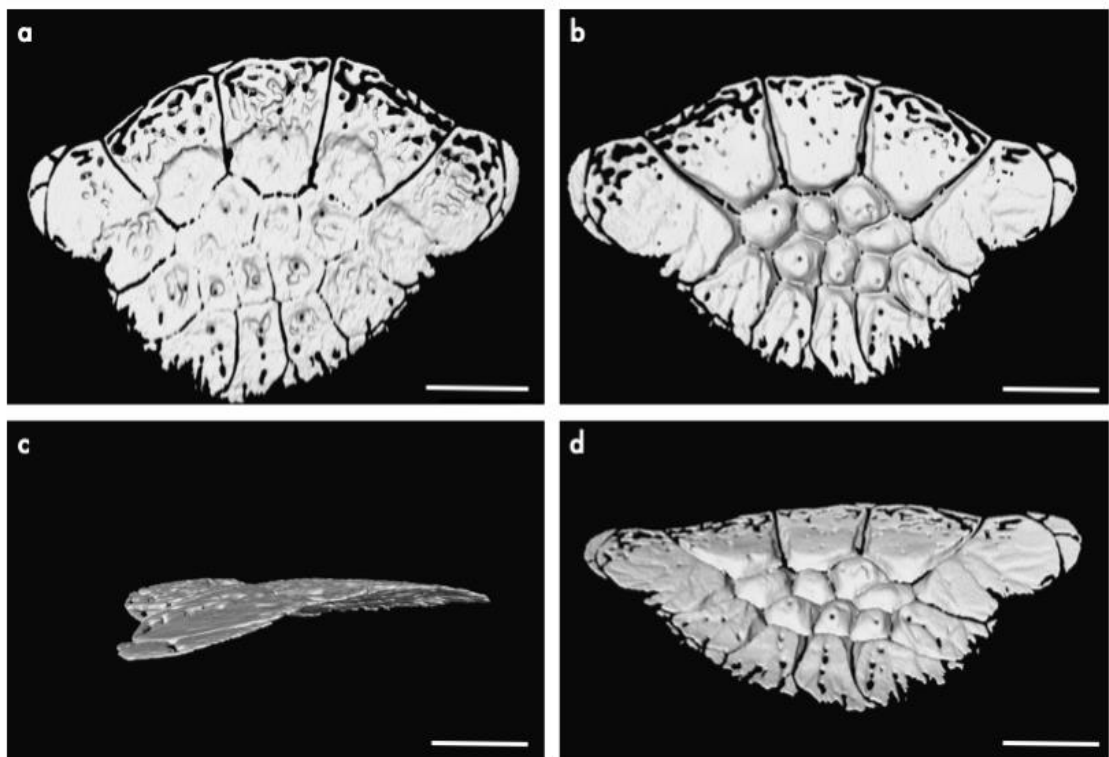
Figure 5.52: Three-dimensional, false colour surface reconstruction of single OD, segmented from HRXCT data of post-cranial, dorsal *Corucia zebrata* skin in (a) dorsal view, (b) ventral view, (c) lateral view (d) ventral, posterior view.

Scale bars: (a) = 150µm. (b) = 150µm. (c) = 120µm. (d) = 150µm.

Histological staining confirmed that ODs of *Corucia zebrata* do overlap up to 3 ODs thick (Fig. 5.53c), being primarily composed of S.F.B.. The deeper ODs were shown to be vascularised, containing L.B. on the surfaces of medullary cavities, however, close to the epidermis, the superficial parts of the ODs did not contain L.B. in any sections. The S.F.B. stained red in Masson's trichrome, pink with a purple periphery in H&E and pink in Alcian blue (Fig. 5.53, S.F.B.). A reduction in collagen expression, occasional lines of growth, combined with differential staining in the apical region led to the identification of a thin and sporadic deposit of OST. on the apical surfaces of the parts of each ODs that lie directly below the epidermis, residing within the stratum
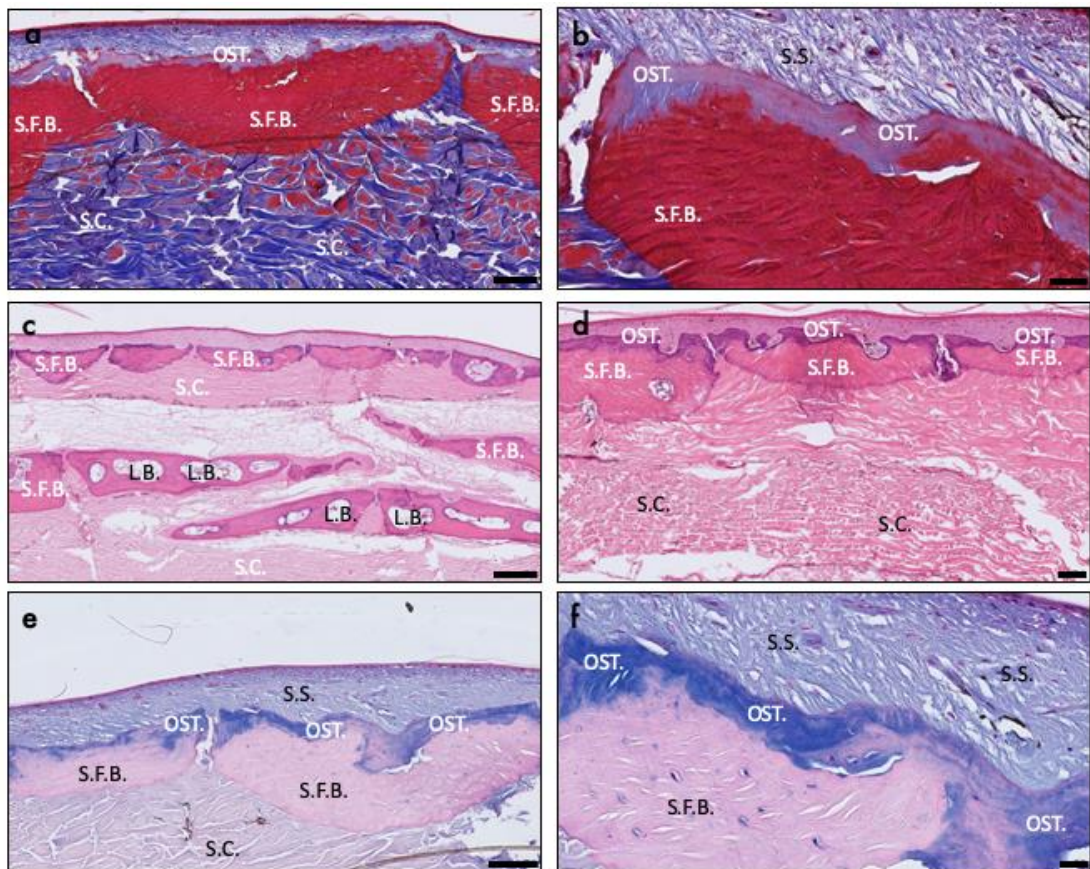
Figure 5.53: Histological staining of *Corucia zebrata* dorsal skin sample sectioned parasagittally (a) stained with Masson's trichrome, (b) stained with Masson's trichrome visualised at higher magnification, (c) stained with H&E, (d) stained with H&E visualised at higher magnification, (e) stained with Alcian blue and (f), stained with Alcian blue visualised at higher magnification. EPI. = epidermis, L.B. = lamellar bone, OST. = osteodermine, S.C. = stratum compactum, S.F.B. = Sharpey-fibre bone, S.S. = stratum superficiale.

Scale bars: (a) = 100μm, (b) = 20μm, (c) = 200μm, (d) = 100μm, (e) = 100μm, (f) = 20μm.

superficiale (Fig. 5.53, OST.). OST. is only seen in the superficial osteodermites, in close proximity to the epidermis. OST. in *Corucia zebrata* stained blue to colourless in Masson's trichrome, purple in H&E and blue in Alcian blue, matching staining of OST. in other taxa. The different parts of the OD that comprise the compound OD can be clearly seen in Fig 5.53. Each OD has a part close to the epidermis and a part that is deeper.
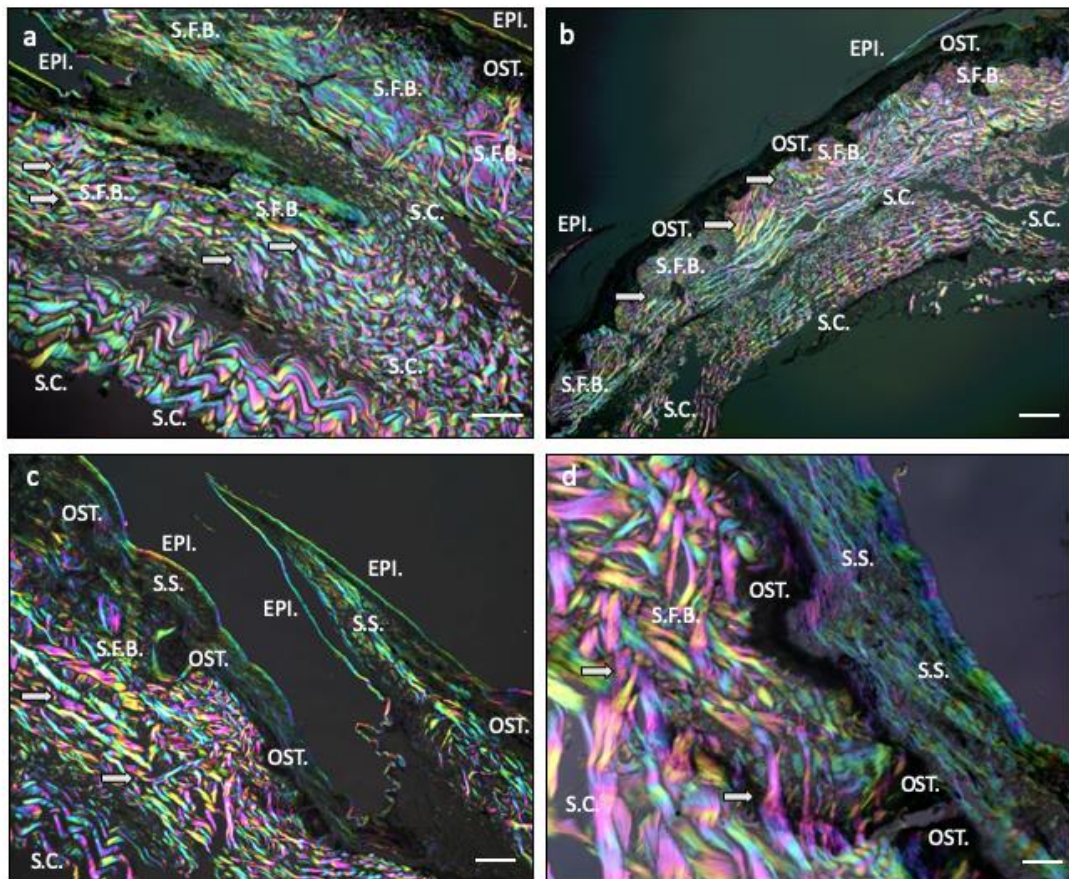
Figure 5.54: Parasagittal sections of *Corucia zebrata* dorsal skin, stained with Masson's Trichrome and visualised with multi-rotation polarised light microscopy. EPI. = epidermis, S.C. = stratum compactum, S.F.B. = Sharpey-fibre bone, OST. = osteodermine, S.S. = stratum superficiale.

Scale bars: (a) = 120µm, (b) = 300µm, (c) = 120µm, (d) = 30µm.

Multi-rotation polarised light microscopy results confirmed these findings, with the apical surface residing beneath the epidermis, in the stratum superficiale, displaying a lack of birefringence and thus a lack of collagen matrix (Fig. 5.54, OST., EPI.). No growth lines or Sharpey's fibres could be identified in the OST. region, however the

S.F.B. is anchored to the dermis with extensive Sharpey's fibres (Fig. 5.54, S.F.B., white arrows). The lack of attributes commonly seen in OST. might again be explained by the thin layer and sporadic expression of OST. in the ODs of this species.

Egernia stokesii was the third scincid species examined. X-ray plate imaging of the post-cranial dorsal skin revealed no mineralisation (Fig. 5.55).
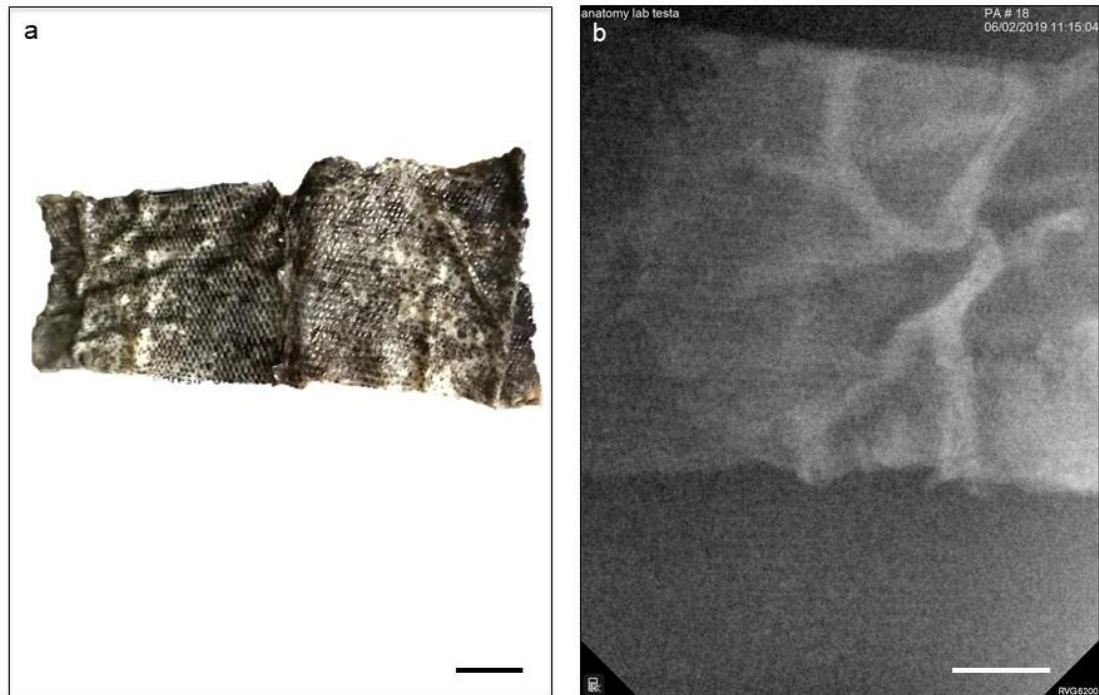
Figure 5.55: (a) photograph of *Egernia stokesii* dorsal skin sample at time of imaging and (b) corresponding x-ray plate image.

Scale bars: (b) = 5mm.

Histological staining (Fig. 5.56) confirmed the absence of ODs in this section but beneath the stratum compactum and above the layer of musculature was a thick layer of adipose tissue.
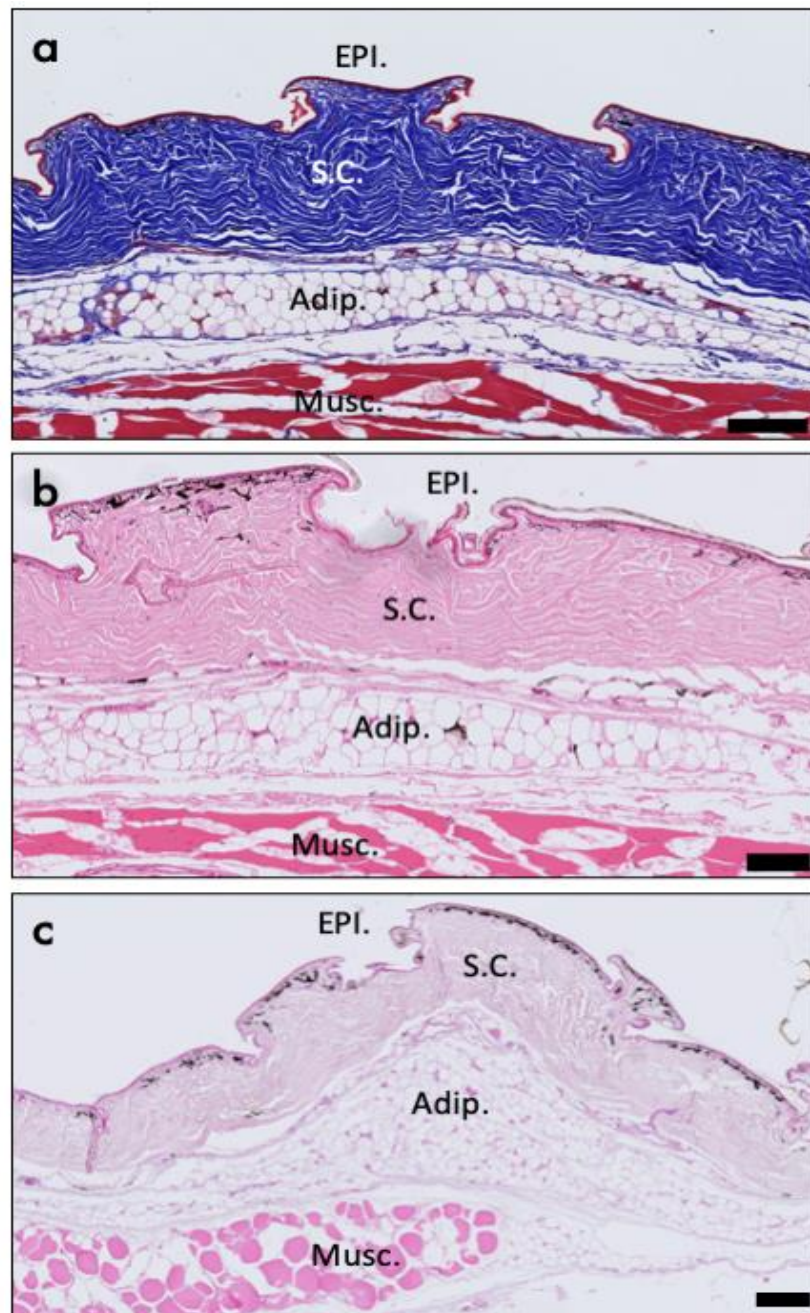
Figure 5.56: Histological staining of *Egernia stokesii* dorsal skin sectioned parasagittally, (a) stained with Masson's trichrome, (b) stained with H&E and (c) stained with Alcian blue. Adip. = Adipose tissue, EPI. = epidermis, Musc. = musculature, S.C. = stratum compactum.

Scale bars: (a) = 200μm, (b) = 100μm, (c) = 200μm.

To investigate if any mineralisation could be identified in the spiny tail of the same specimen, a strip of skin from the dorsal portion of the tail was also analysed in the same way. The results from the X-ray plate imaging showed that there was no mineralisation present in this anatomical location either (Fig. 5.57). The histological staining results also showed there were no ODs in the sampled sections of the tail (Fig. 5.58). Polarised light microscopy (Fig. 5.59) for both the post-cranial dorsal skin (Fig. 5.59a), and the tail skin (Fig. 5.59b) confirmed this but the stratum compactum in the tail appeared much thicker and with a different collagen fibre orientation to that of the post-cranial dorsal skin (Fig. 5.59, S.C.).
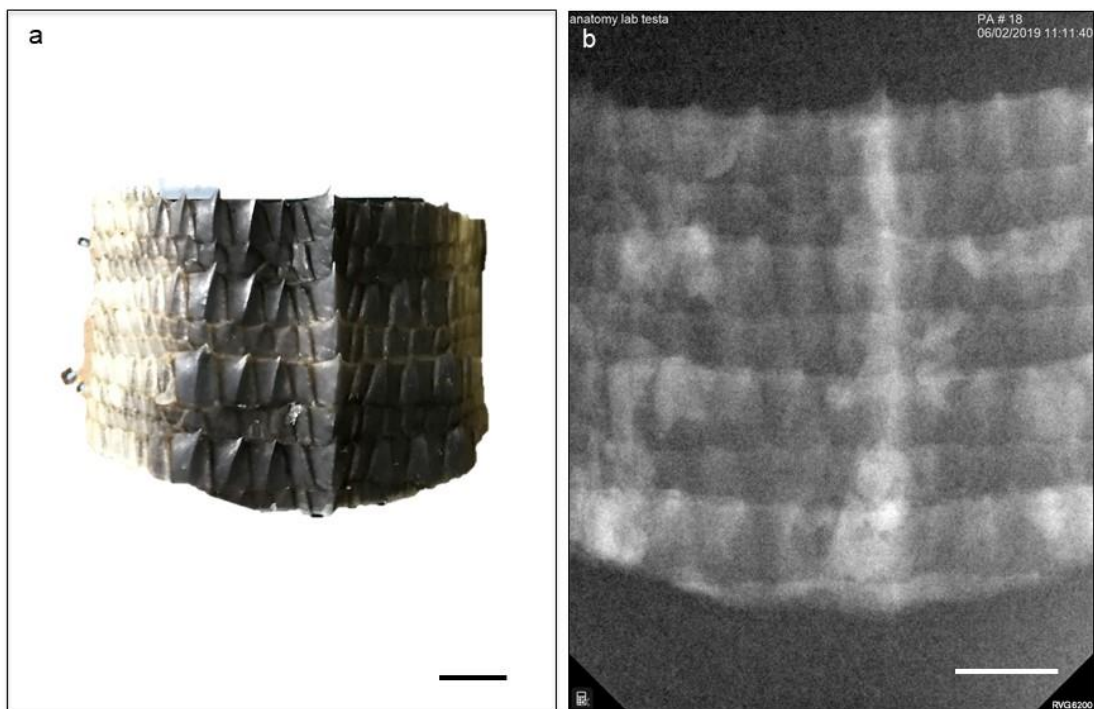
Figure 5.57: (a) photograph of *Egernia stokesii* tail skin sample at time of imaging and (b) corresponding x-ray plate image.
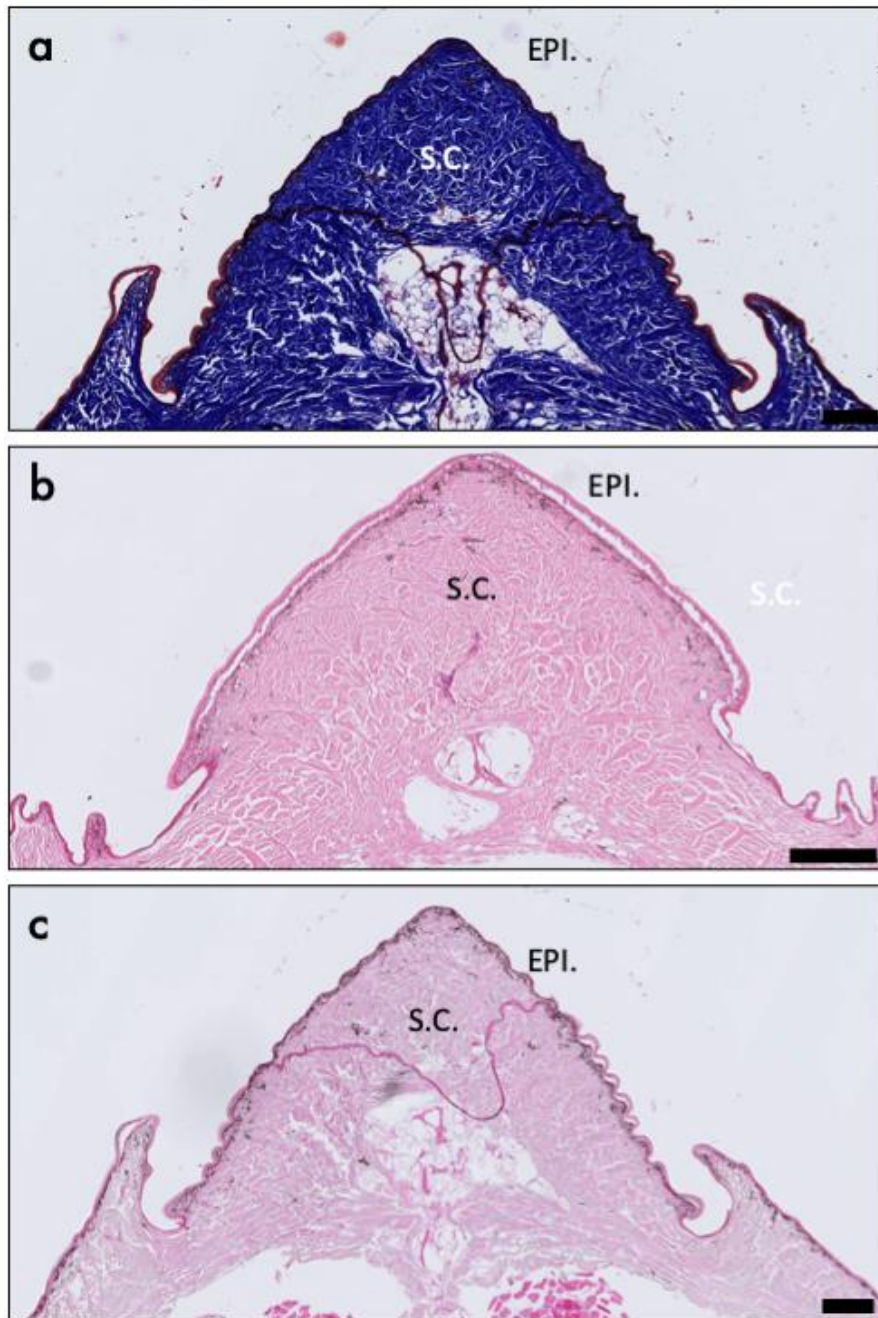
Scale bars: (b) = 5mm.

Figure 5.58: Histological staining of *Egernia stokesii* tail skin sectioned transversely, (a) stained with Masson's trichrome, (b) stained with H&E and (c) stained with Alcian blue. EPI. = epidermis, S.C. = stratum compactum.

Scale bars: (a) = 200μm, (b) = 200μm, (c) = 200μm.
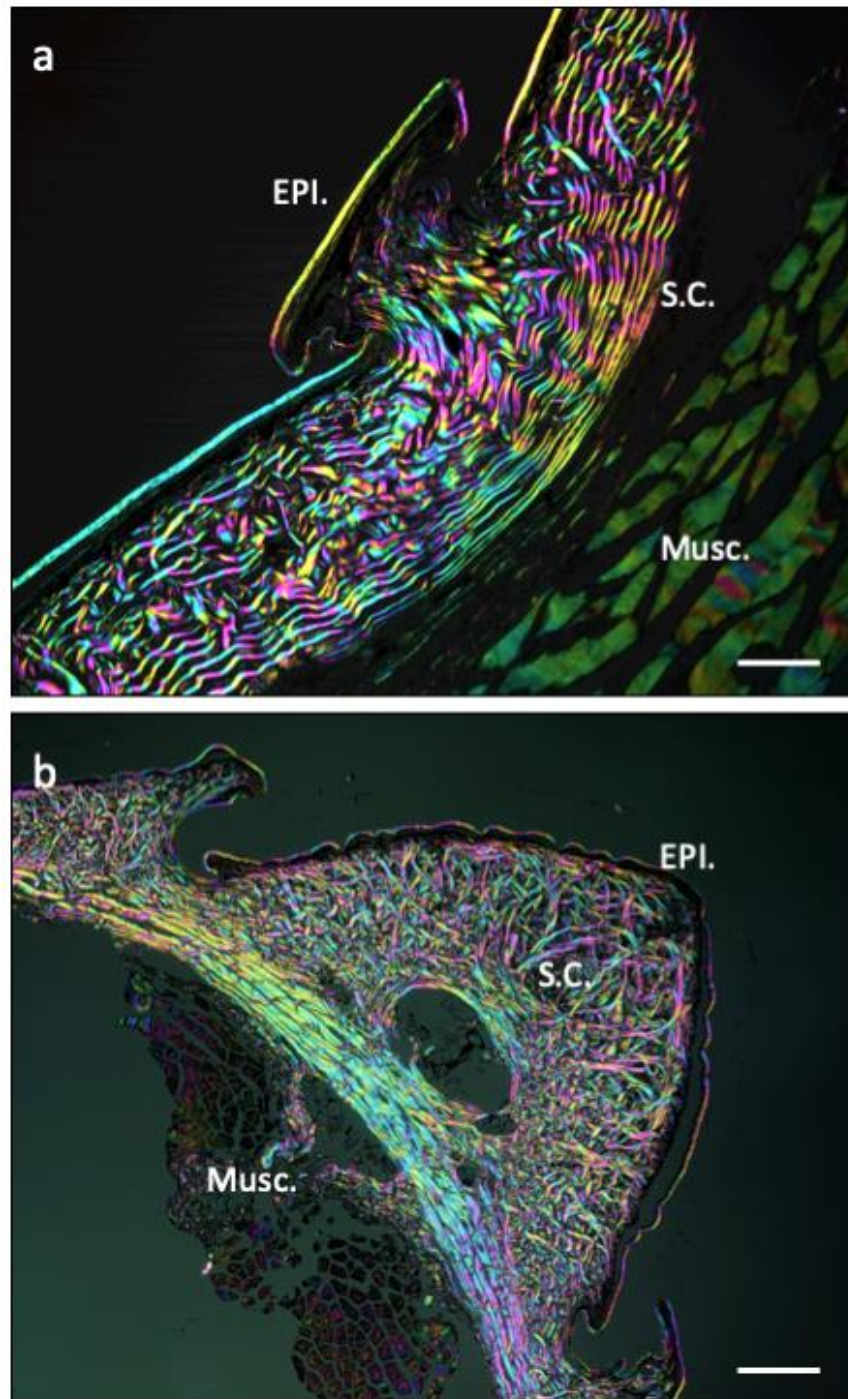
Figure 5.59: Parasagittal sections of *Egernia stokesii* (a) post-cranial dorsal skin, and (b) tail skin, stained with Masson's Trichrome and visualised with multi-rotation polarised light microscopy. EPI. = epidermis, Musc. = musculature, S.C. = stratum compactum.

Scale bars: (a) = 120μm, (b) = 300μm.

5.2.6 Lacertidae

The Lacertidae are members of the larger group Lacertoidea, along with tegus and racerunners (Teiidae), and the South American Gymnophthalmidae. Where present, in larger members of the family, lacertid ODs are restricted to the head (Camp, 1923; Arnold et al. 2007)

Lacertidae includes the wall lizards or true lizards, native to Europe, Africa and Asia. The sampled species *Timon lepidus*, is also known as the Ocellated lizard or Jewelled lizard, and is native to southwestern Europe, including Spain, Portugal, southern France and north-west Italy. This lizard is known for an abnormally large cranium. It prefers dry, bushy areas, such as open woodland and scrub, old olive groves and vineyards, and is sometimes found on more open, rocky or sandy areas. The lizard usually stays on the ground, but climbs well on rocks and in trees and burrows occasionally. It is said to be the largest European lizard, as it can reach up to 90cm in body length and can grow to a mass of more than 500grams (Arnold et al., 2007).

In *Timon lepidus*, ODs are found in the skin of the upper eyelid and on the sides of the head behind the eye. A skin sample was taken from the left side of the cranium of *Timon lepidus*, anterior to the ear (Fig.5.60a). When viewed with X-ray plate imaging, it was evident that an OD resides beneath every scale (Fig. 5.60b).
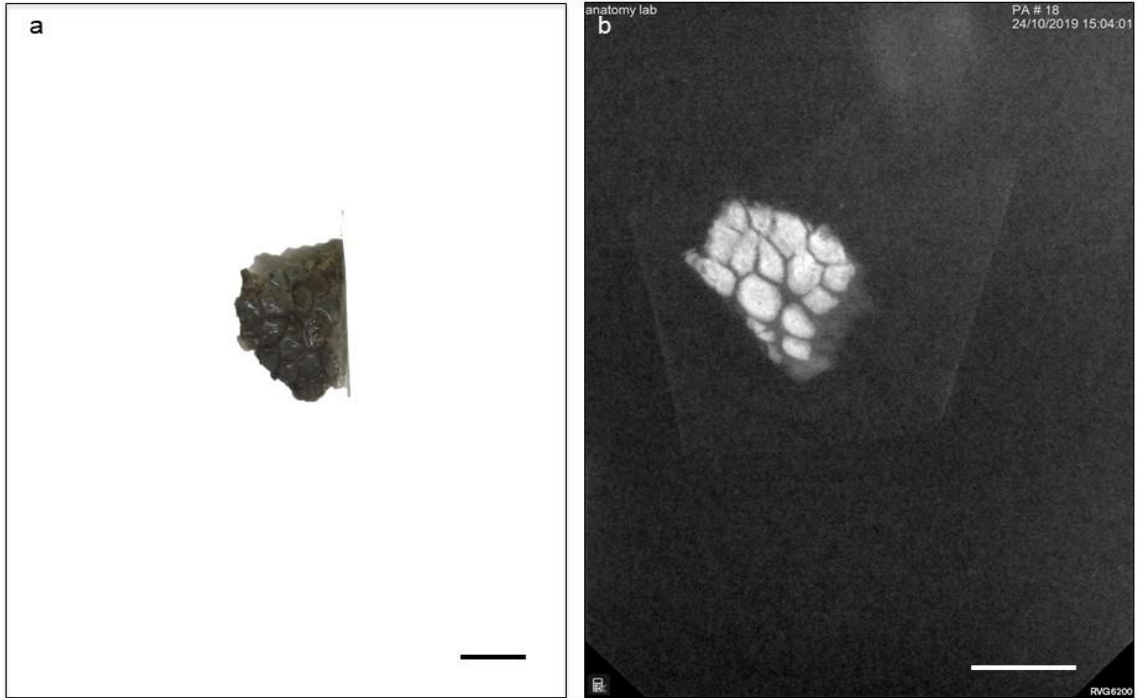
Figure 5.60: (a) photograph of *Timon lepidus* cranial skin sample at time of imaging and (b) corresponding x-ray plate image.

Scale bars: (b) = 5mm.
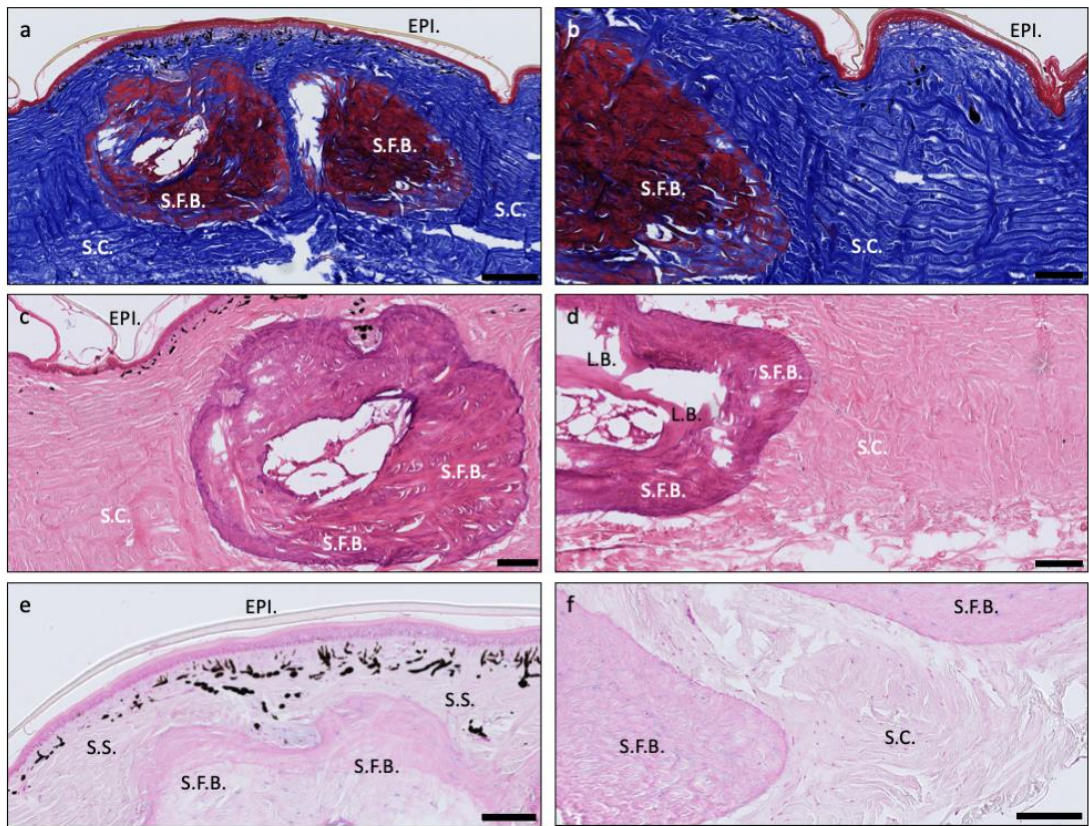
Figure 5.61: Histological staining of *Timon lepidus* cranial skin, sectioned parasagittally, (a and b) stained with Masson's trichrome, (c and d) stained with H&E and (e and f) stained with Alcian blue. EPI. = Epidermis, L.B. = lamellar bone, S.C. = stratum compactum, S.F.B. = Sharpey-fibered bone.

Scale bars: (a) = 200µm, (b) = 100µm, (c) = 100µm, (d) = 100µm, (e) = 100µm, (f) = 100µm.

Histological staining (Fig. 5.61) revealed that the ODs in *Timon lepidus* are primarily composed of S.F.B., with the structure of the regularly repeating collagen mesh of the soft tissue dermis echoed in the mineralised OD component. Additional L.B. was observed, presumably following remodelling of the S.F.B. base. OST. was not observed to be present in any of the sections analysed.

5.2.7 Teiidae

Teiidae is a family native to North and South America, consisting of around 150 species in 18 genera. These sometimes large (up to 1m head-tail length) lizards can run quickly and even sometimes bipedally, and inhabit a wide range of habitats including savannah, rain forest and semi-desert (Harvey et al., 2012), where they are thought to occupy the same ecological niche as the varanid lizards of the 'Old World'. Here the sampled species is *Salvator merianae*, also known as the Argentine Black and White tegu. These lizards have not been documented as containing ODs in the dermis, but were sampled so as to provide a control and comparison with OD bearing species.

In the Teiidae, the sampled species was *Salvator merianae*. The portion of the dermis sampled did not display any mineralisations in X-ray plate imaging (Fig. 5.62).
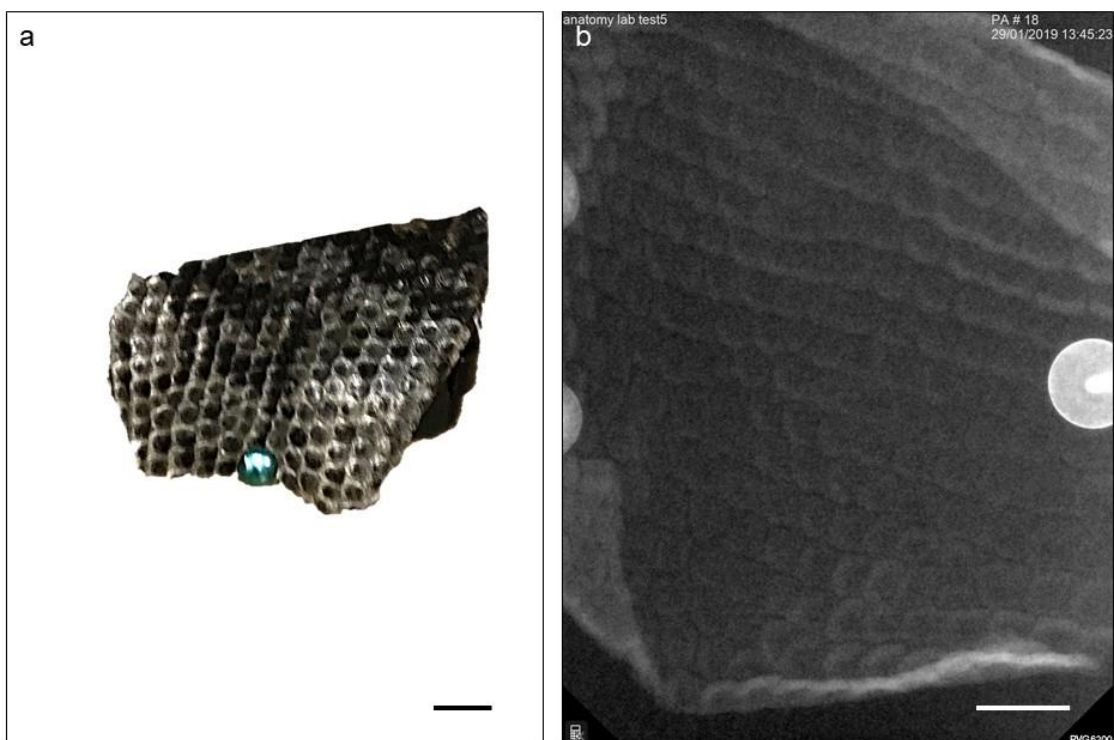
Figure 5.62: (a) photograph of *Salvator merianae* dorsal skin sample and (b) corresponding x-ray plate image.

Scale bars: (b) = 5mm.
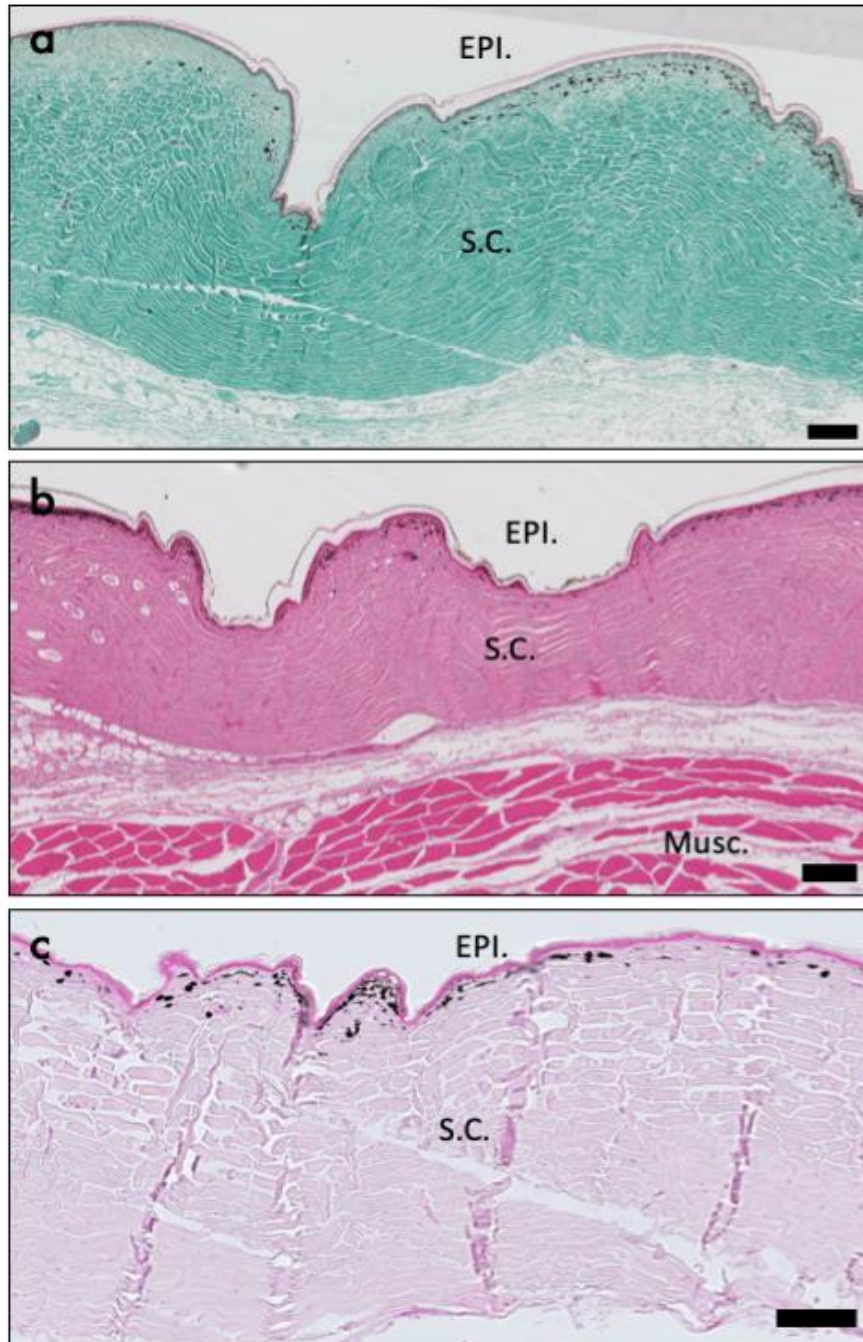
Figure 5.63: Histological staining of *Salvator merianae* dorsal skin sample sectioned parasagittally (a) stained with Masson's trichrome, (b) stained with H&E and (c) stained with Alcian blue. EPI. = epidermis, Musc. = musculature, S.C. = stratum compactum.

Histological staining (Fig. 5.63) confirmed this lack of ODs, but the stratum compactum of the dermis was observed to be very thick (Fig. 5.63, S.C.). Multi-rotation polarised light microscopy confirmed a lack of mineralisation and the unusually thick S.C. (Fig. 5.64).
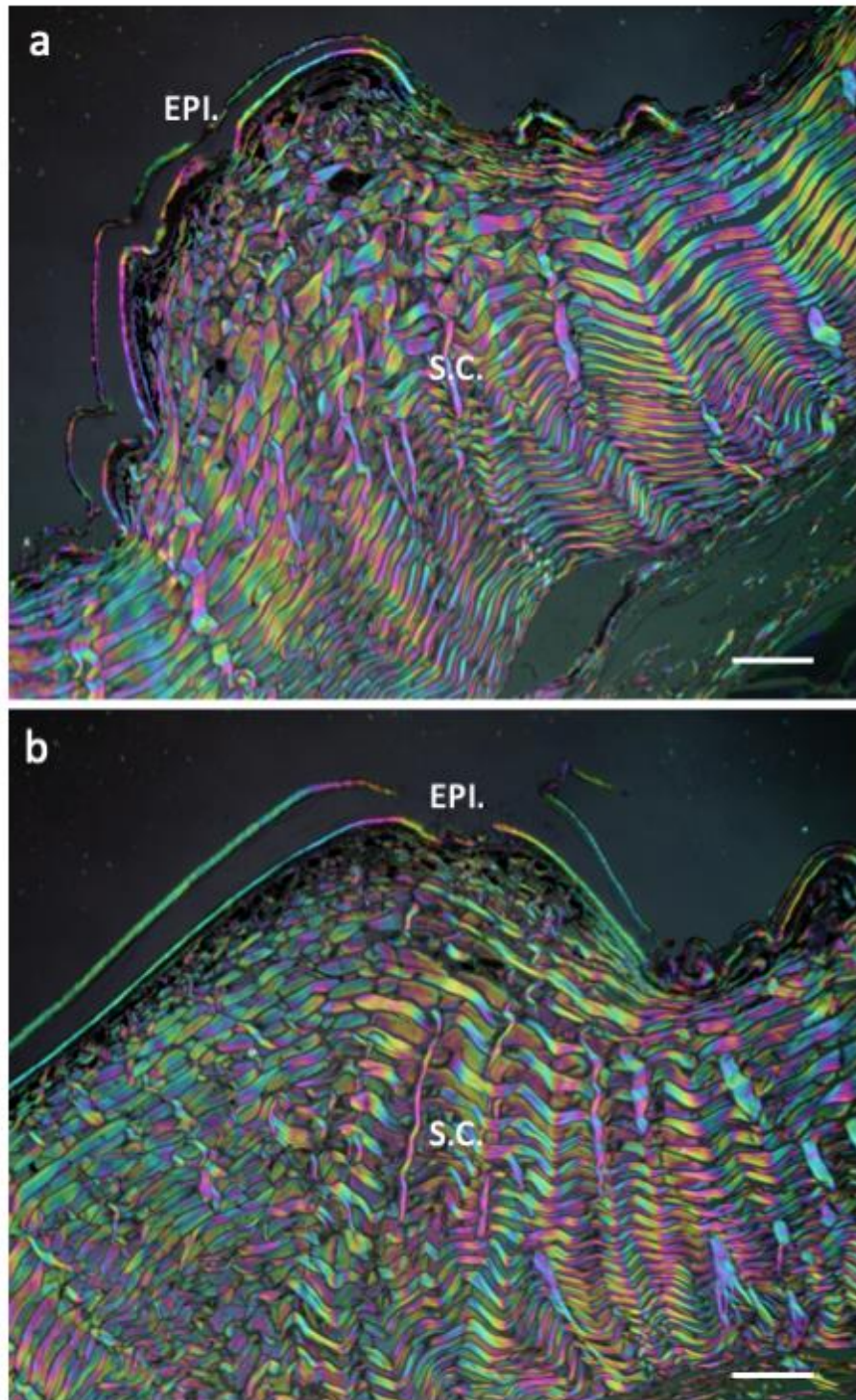
Figure 5.64: (a and b) Parasagittal sections of *Salvator merianae* dorsal skin, stained with Masson's Trichrome and visualised with multi-rotation polarised light microscopy. EPI. = epidermis, S.C. = stratum compactum.

Scale bars: (a) = 120μm, (b) = 120μm.

5.2.8 Archosauria

Although this study aims to analyse the dermal skeleton of squamates, archosaurs have been included for outgroup comparison. The archosaurs include the most recent common ancestor of living birds and crocodilians and all of the descendants of this ancestor. Two main subgroups of Archosauria exist, the Pseudosuchia (containing crocodilians and their extinct relatives and Avemetatarsalia (containing birds and their extinct relatives). The Pseudosuchia express extensive ODs covering almost the entire body, and given their large size and common appearance, these ODs have been extensively documented and characterised (Vickaryous and Hall, 2008). The most recent study that employed microstructural and histological analysis of archosaur ODs concludes that they are comprised of W.B, L.B. and mineralised dense connective tissue consistent with previous hypothesis of bone formation via metaplasia (Vickaryous and Hall, 2008). From this clade the sampled species is *Crocodylus niloticus*.

The X-ray plate results from the archosaur outgroup show that *Crocodylus niloticus* ventral skin ODs are large, roughly 2cm wide, rectangular, with extensive ornamentation, numerous foramina and connected by unmineralised zig-zag sutures (Fig. 5.65). No keel is observed in these ODs as they are ventrally located. Histological staining (Fig. 5.66) as well as multi-rotation polarised light microscopy (Fig. 5.67) showed that the internal structure of the ODs is comprised primarily of S.F.B. with L.B. deposited following remodelling. There was no OST. identified here, which would support a hypothesis that this material can only be found in ODs of squamates.
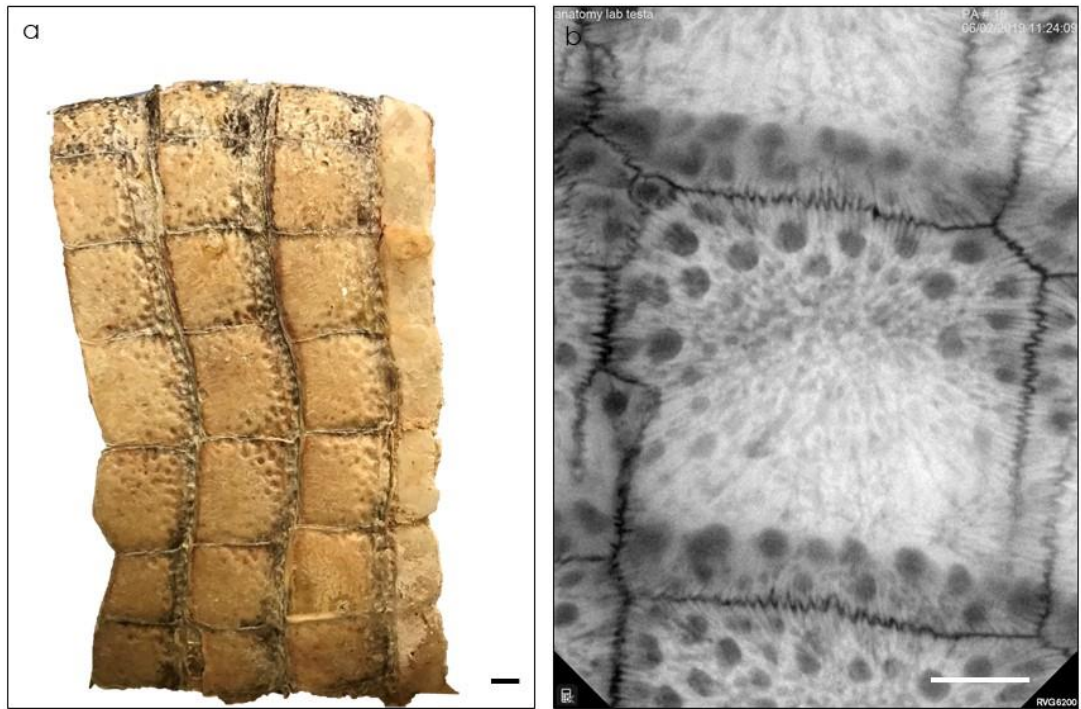
Figure 5.65: (a) photograph of *Crocodylus niloticus* ventral skin sample and (b) corresponding x-ray plate image.

Scale bars: (b) = 5mm.
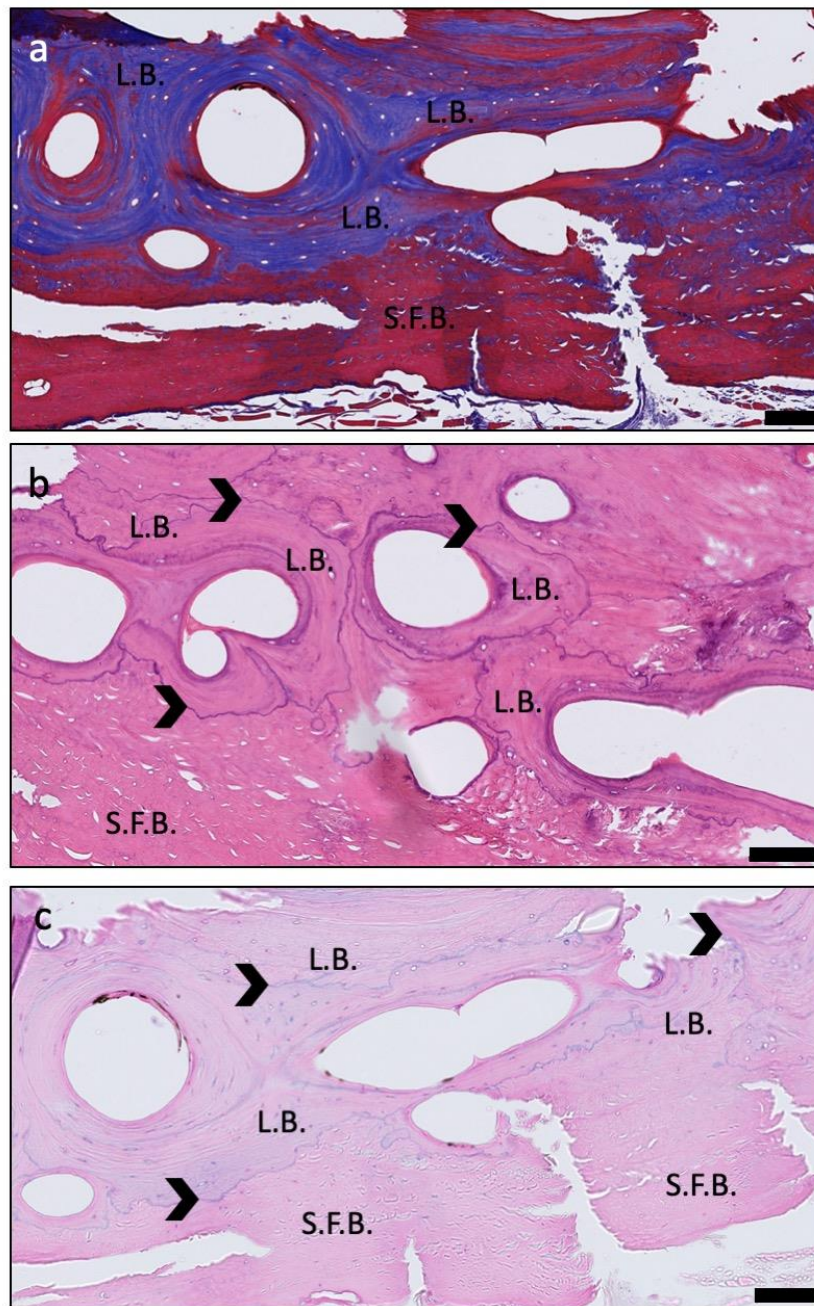
Figure 5.66: Histological staining of *Crocodylus niloticus* ventral skin sectioned parasagittally (a) stained with Masson's trichrome, (b) stained with H&E and (c) stained with Alcian blue. Chevrons = cement lines, L.B. = lamellar bone, S.F.B. = Sharpey-fibred bone.

Scale bars: (a) = 100μm, (b) = 100μm, (c) = 100μm.
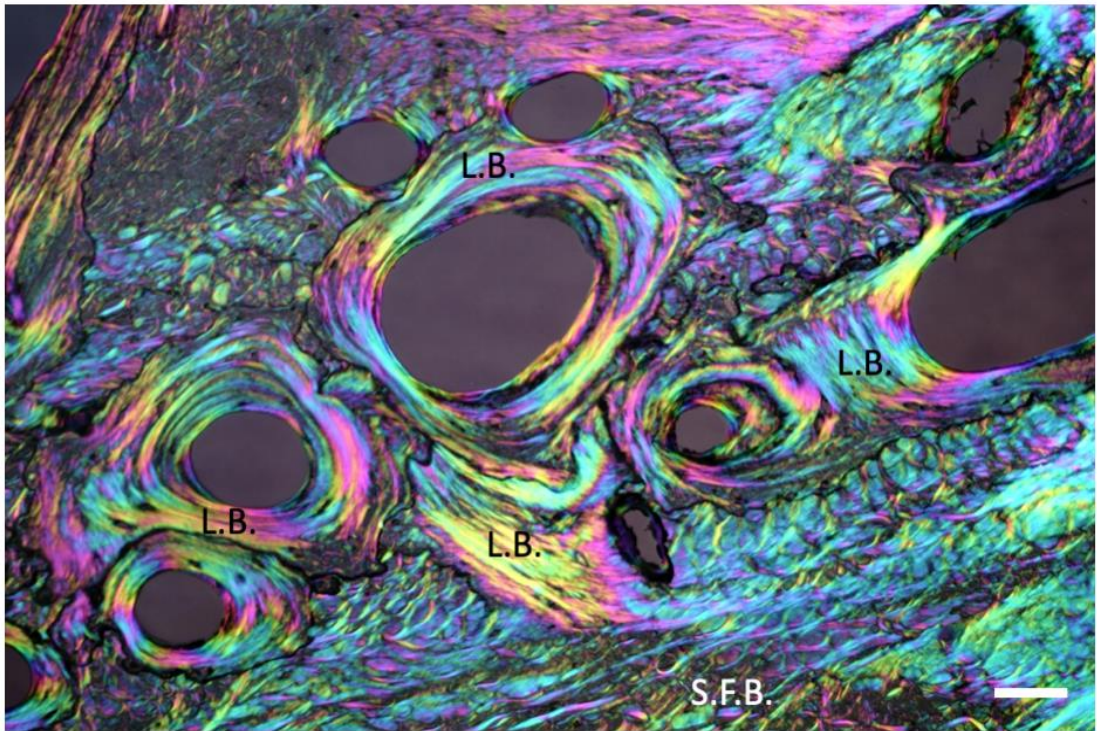
Figure 5.67: Parasagittal section of *Crocodylus niloticus* ventral skin, stained with Masson's Trichrome and visualised with multi-rotation polarised light microscopy. S.F.B. = Sharpey-fibre bone, L.B. = lamellar bone.

Scale bar: 120µm.
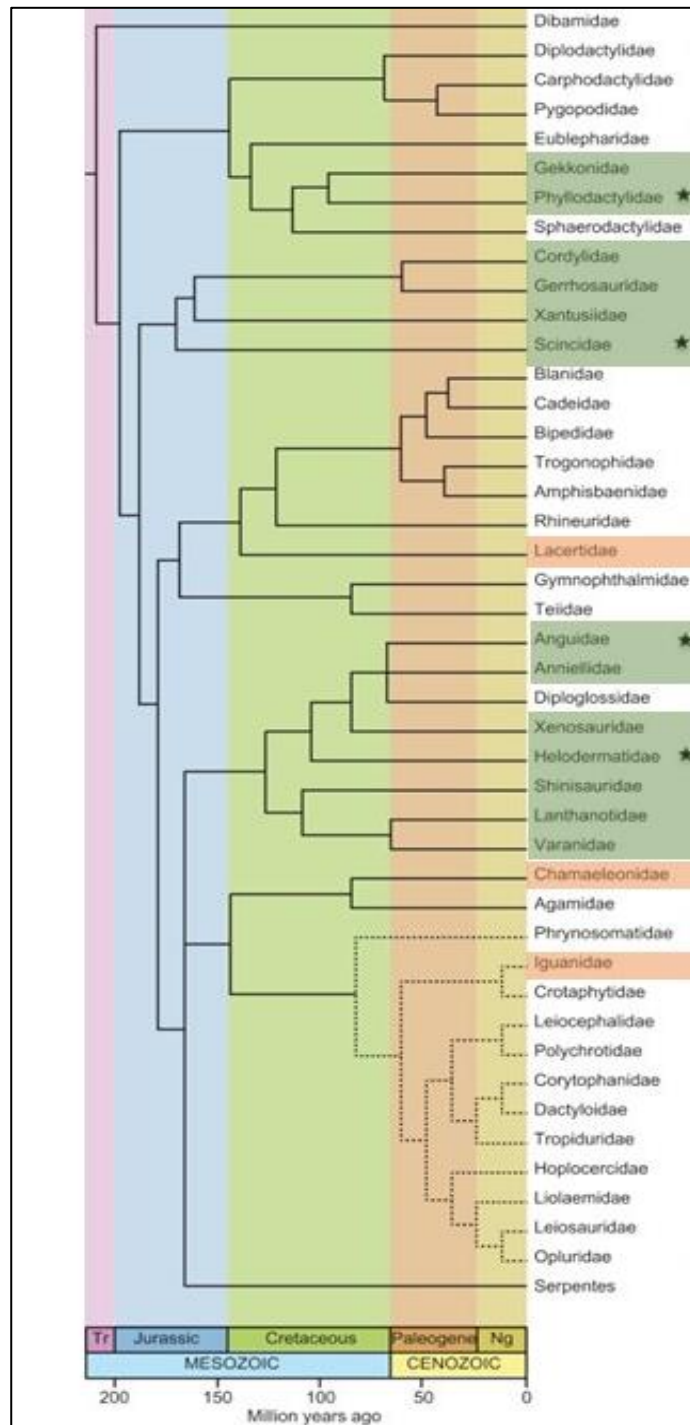
Figure 5.68: Timetree of lizard relationships (based on a molecular phylogeny) among clades as understood at time of writing. A five-pointed star indicates where osteodermine expression has been confirmed in this study. Taxa in green express ODs in multiple species and around the body, taxa in orange express ODs sporadically, only in a single species, or only on the head. Taxa with no colour have not yet been shown to express ODs. timing of divergences should be taken as estimates only. Dashed lines denote clades where the timing of divergences is uncertain. Adapted from Vidal and Hedges, (2009).

Fig. 5.68 provides a summary showing where the presence of OST. has been confirmed in many quite distantly related species. This figure provides a guide to the included taxa and not a point of discussion in its own right, rather, so that the expression of osteoderms and OST. can be compared to lizard relationships across geological timescales. OST. is seen, for example, expressed on the osteoderms of lizards that share a last common ancestor in the Jurassic period.

5.3   Discussion

5.3.1   Comparison with previous work

This chapter has provided the first observations on ODs of several lizard species (e.g. *Timon lepidus*) and new data on other species described previously, but with less detail such as *Tarentola annularis* (Vickaryous et al., 2015), *Gekko gecko* (Laver et al., 2019) and *Corucia zebrata* (Moss, 1969). Moss (1969) also examined *Egernia* and *Ophisaurus*, but sampled different species - *Egernia kingii* rather than *E. stokesii* (herein) and *Ophisaurus apodus* (vs *O. ventralis*, herein). Moreover, Moss's study covered only basic histology and, due to the early date of publication, presented only low resolution, black and white images.

HRXCT was the most useful technique for displaying the gross anatomy of ODs in three dimensions, in high resolution and high magnification. The most recent studies concerning ODs nearly always make use of HRXCT data sets (Maisano et al., 2002; Bever et al., 2005; Greenbaum et al., 2012; Stanley et al., 2016), polarised light microscopy (de Buffrénil et al., 2011) and SEM (Levrat-Calviac and Zylberberg, 1986) for visualising the anatomy of squamate osteoderms. These new techniques will likely prove to be very popular in future studies that require three-dimensional visualisation of OD expression and interactions between ODs.

Gekkotan ODs have received more attention in recent years, with recently published HRXCT datasets of *Geckolepis maculata* (Paluh et al., 2017), *Tarentola mauritanica* (Avallone, 2018) and *Gekko gecko* (Laver et al., 2019) ODs. The description made here of the gross anatomy of *Tarentola annularis* ODs matches that of previous authors (Otto, 1909; Bauer and Russell, 1989; Vickaryous et al., 2015) in that ODs appear as an organised mesh of regularly spaced, non-overlapping beads that do not correspond well to the epidermal scalation.

The micromaterials found present in *Tarentola annularis* ODs such as S.F.B. and OST. match those described by previous authors, including Vickaryous et al., (2015)

and Levrat-Calviac and Zylberberg, (1986) who described long, parallel and densely-packed Sharpey's fibres that deeply enter the peripheral (equatorial) regions of the ODs and make a strong bond between neighbouring elements, but in a second species *Tarentola mauritanica*. My study has added polarised light microscopy and HRXCT for the first time in the study of the ODs from *T. annularis*. The results published by these authors match the results presented in this chapter for *Tarentola annularis* and *Gekko gecko,* with no discrepancies in OD gross anatomy or micromaterial composition. S.F.B. and OST. were observed in *Tarentola*, which were so small that they did not feature any foramina and had no evidence of internal remodelling.

Results presented here for the anguid lizards agreed with those of other authors, in that the OD are rectangular and imbricating, with the anterior end of the OD overlaid by the posterior end of the following one (Bochaton et al., 2015). However, these results are the first to identify OST. as a microstructural material component of living anguid ODs (in *Elgaria multicarinata* and *Ophisaurus ventralis*) as de Buffrénil et al., (2011) found in a fossil anguid. It was also the first to show that the ODs of *Elgaria* are compound. Almost all of the larger anguid ODs showed signs of erosion of the S.F.B. and deposition of new L.B., apart from the superficial parts of the OD, that were very thin and close to the superficial surface of the skin. As in *Tarentola* ODs, it is thought that the small volume of these most-superficial ODs and ODites is sufficient to allow perfusion of essential nutrients to the living bone tissue without requiring internal vascularisation through remodelling.

Previous authors have commented on the presence of compound ODs in scincoid lizards (Camp, 1923; Estes et al., 1988), but I have shown scincoid ODs in high resolution for the first time, using modern techniques. The failure to record ODs in *Egernia stokesii* was a surprise as they are known to occur in at least some species (e.g. *E. striolata* where they completely cover the body). OST. was shown to present on the superficial surface of ODs from *Tiliqua rugosa* and *Corucia zebrata* for the first time.

Results presented for *Varanus komodoensis* OD gross anatomy match reports from other authors (Maisano et al., 2019), however, MRPLM was used to describe the OD micromaterial composition for the first time. Although *Varanus niloticus* has previously been described as having ODs present (Erickson et al., 2003), the techniques employed in this study revealed no expression in the sampled specimen from this species. The lack of ODs in *V. niloticus* is odd considering they were previously noted,

this may be due to the anatomical location studied, ontogenetic stage or previous misidentification of hardened epidermis. This highlights the uncertain expression of ODs and the variability between specimens and between species of the same genus. In the lacertid, teiid and lanthanotid lizards, less data was produced for these, but the OD gross anatomy matched previous authors in all, which was the same for the Archosaur out group, where no OST. was found, rather a mass of remodelled S.F.B., matching previous reports (Vickaryous and Hall, 2008).

5.3.2 Function

An antipredator function fails to explain why ODs are so rare among some lizard families, including in geckos, where Vickaryous et al., (2015) suggested that reinforcing the dermis with ODs not only provides defence against predation, but also against dangerous prey and aggressive intraspecific behaviours. ODs have been shown to be effective at protecting against bites from predators (Broeckhoven et al., 2015). The absence of OD expression in some lizard taxa has been associated with burrowing (Camp, 1923). However, this explanation is countered by the presence of substantial ossification of the dermis of other lizards that are habitual burrow-dwellers (for example, in helodermatids). ODs may also function to aid wedge rock/bark dwellers into cracks, forming a more rigid and rough surface compared to skin that lacks ODs (Cooper et al., 2000). Small rock-dwelling lizards include *Tarentola* and in this chapter, these were found to express many small osteoderms almost completely around the body, which may aid this hypothesis.

Another possibility relates to aggressive intraspecific interactions. *Tarentola* is often found in high densities, yet displays strong territoriality and is known to be cannibalistic (Loveridge, 1947). The diet of *Tarentola* includes large and combative animals including small mammals, other geckos, and large arthropods such as scorpions (Loveridge, 1947; Hoofien, 1962; Vickaryous et al., 2015). These authors relate the possibility of ODs functioning as defence from prey to greater OD expression on the head and jaws. A similar combination of combative prey and intraspecific aggression is observed in *G. gecko*. These large geckos are voracious feeders, known to eat relatively large and potentially formidable prey, including other lizards, young birds, and mammals. Also, like *Tarentola spp.*, *Gekko gecko* males are territorial, and males and females will vigorously defend their eggs and young (Laver et al., 2019). The comparatively restricted distribution of *G. gecko* ODs (primarily to the dorsal regions of the head and trunk) may relate to these violent behaviours as fighting animals usually deliver bites to the head. In *Geckolepis*, the OD expression

is different, so they are unlikely to share the same function as *Gekko* ODs. In *Timon lepidus*, the same cranial expression of ODs was observed. This may relate to a similar function, with the cranium requiring protection from other members of the same species. *Varanus komodoensis* is another agonistic lizard species where violent clawing and biting are common behaviours (Erickson et al., 2003). Their ODs coalesce and fuse together to form stunning 'chainmail' helmets over the snout and supraorbital regions in older specimens, which is presumed to be an adaptation to protect against aggressive intraspecific behaviours.

Microanatomical variation may also reflect the gender and reproductive status of the sampled individuals (Broeckhoven et al., 2017). In ODs of extant crocodiles, internal remodelling has been found to be more intensive in breeding females, in which large amounts of minerals must be mobilized for the formation of eggshells (Dacke et al., 2015). The internal vascular anatomy of titanosaur ODs from the Upper Cretaceous of Spain has also been shown to be compatible with a role in egg shell formation (Vidal et al., 2017). Gender and reproductive status were not controlled in this study, a limitation of the results presented here. Although it was not possible to determine functional aspects of the ODs described here, it is hoped that these data will contribute toward future studies that aim to elucidate the function of ODs in these taxa.

5.3.3   Phylogenetic information

OD gross anatomy has previously been the most commonly used taxonomically informative character (Camp, 1923; Estes et al., 1988; Read, 1986; Conrad, 2008). Gross anatomy of ODs typically centres around single (being composed of one single element) or compound types, (multiple fused osteodermites), overlapping (imbricating) or non-overlapping (non-imbricating) types, and keeled (ridged along the anteroposterior axis) or non-keeled. As more descriptions of OD expression are published, we will be able to more accurately define which families can express various OD gross anatomies. *Gekko gecko* and *Tarentola spp.* have previously been described as possessing granular ODs and this was also confirmed in this chapter, but the ODs of *Geckolepis maculata* are morphologically similar to the imbricating, squamous form observed in scincids and cordyliforms (Paluh et al., 2017). This recent discovery proves that gross anatomy of ODs within a family of lizards is much more complex than previously thought. Furthermore, sporadic expression of ODs within a family, and the unexpected findings in this study, for example, the discovery of compound ODs in an anguid, *Elgaria multicarinata*, which were previously thought to only express single ODs, proves that the real situation is likely to be more complicated

than first thought and broad conclusions about family links to OD gross and micromaterial anatomy should be avoided until more data is made available.

Family	Genus + species	S.F.B.	P.F.B.	W.B.	L.B.	OST.
Helodermatidae	*Heloderma suspectum*	✓	X	X	✓	✓
Phyllodactylidae	*Tarentola annularis*	✓	X	X	X	✓
Gekkonidae	*Gekko gecko*	✓	X	X	✓	X
Varanidae	*Varanus komodoensis*	X	✓	✓	✓	X
Varanidae	*Varanus komodoensis* juvenile	X	✓	✓	X	X
Varanidae	*Varanus niloticus*	N/A	N/A	N/A	N/A	N/A
Anguidae	*Ophisaurus ventralis*	✓	✓	X	✓	✓
Anguidae	*Ophisaurus ventralis* juvenile	✓	✓	X	✓	X
Anguidae	*Elgaria multicarinata*	✓	X	X	✓	✓
Scincidae	*Tiliqua rugosa*	✓	✓	✓	✓	✓
Scincidae	*Corucia zebrata*	✓	X	X	✓	✓
Scincidae	*Egernia stokesii*	N/A	N/A	N/A	N/A	N/A
Lacertidae	*Timon lepidus*	✓	X	X	✓	X
Teiidae	*Salvator merianae*	N/A	N/A	N/A	N/A	N/A
Lanthanotidae	*Lanthanotus borneensis*	?	?	?	?	?
Crocodylidae	*Crocodylus niloticus*	✓	X	X	✓	X

Table 5.1: Table of results for each family, genus and species of reptile and a summary of the micromaterials that were identified in each. S.F.B. = Sharpey-fibred bone, P.F.B. = parallel-fibred bone, W.B. = woven bone, L.B. = lamellar bone, OST. = osteodermine, N/A = no ODs were observed, ? = unknown due to lack of sample.

Despite the diversity in gross anatomies observed, the ODs are often composed of different combinations of the same microstructural tissues (Table 5.1)., For example, the OST. capping tissue is present in a greater ratio, as a thicker cap, in *Heloderma suspectum, Tarentola annularis, Ophisaurus ventralis* and *Tiliqua rugosa* than in *Corucia zebrata or Elgaria multicarinata*, in which only thin deposits of an OST. cap were seen.

The first colour histological staining results of OST. were published in 2015 by Vickaryous et al. Comparing these results to the results presented here, basophilic staining at the apical surface of the ODs of *Tarentola annularis Ophisaurus ventralis, Elgaria multicarinata, Tiliqua rugosa and Corucia zebrata* was observed in the histological sectioning. This is interpreted as OST. given the definitions of OST. used for *Heloderma suspectum* ODs (Chapters 3 and 4) and the definitions of OST. of *Tarentola* ODs (Vickaryous et al., 2015). Given the fact that this chapter identified OST. for the first time in the Scincidae and Anguidae, this means that my results confirm that the ability to produce non-osseous, hyper-mineralised tissues in the integument is shared by multiple families of lizards.

Apart from lizards, hyper-mineralised tissues such as OST. have not been reported in other tetrapod ODs including those of lissamphibians (Ruibal and Shoemaker, 1984), pareiasaurs (Scheyer and Sander, 2009), chelonians (Scheyer and Sanchez-Villagra, 2007), crocodilians (Vickaryous and Hall, 2008), dinosaurs (de Buffrénil et al., 1986), or mammals (Hill, 2006; Vickaryous and Hall, 2006). Lizards are, for now, seemingly unique in their ability to produce this tissue. Given OST. expression was observed in families that share a common ancestor estimated to live around the time of the Jurassic (Fig. 5.68), this indicates that the potential to express OST. is likely a shared trait among many extant taxa but not all exploit this ability. The scales of basal tetrapods such as *Tiktaalik* are cosmoid scales (Richter et al., 2011) Cosmine consists of a layer of dentine covered by a thin sheet of enamel (Daeschler et al., 2006). No evidence of dentine tubules or pulp cavities were found in OST., thus *Tiktaalik* contained scales more similar to modern day fish than modern day lizards. In comparison, ganoid scales exhibit a thicker, multi-layered layer of ganoine, which bears somewhat more resemblance to OST. (Schultze, 2016). Further analysis of OST. expression in families that have not yet been sampled with the techniques used in this study would be welcome to elucidate the full expression across squamates. Comparisons of osteoderms of lizards to living and extinct fish scales are welcomed

in an attempt to relate OST. to hyper-mineralised tissues such as ganoine and cosmine.

OST. expression can be further tested by a) examining fossil material of early squamate ODs and b) examining the microstructure of the ODs in the only OD bearing rhynchocephalian, the fossil *Pamizinsaurus*, to determine whether OST. might be a lepidosaurian rather than a squamate trait. Nonetheless, it is also clear that there is a disparity between lizards in the presence or absence of OST. (Vickaryous et al., 2015) suggests it may have been lost independently in some groups, such as the Varanidae. This means that OST. may eventually prove to be a phylogenetically useful character.

The recorded microanatomical variation may also reflect the gender and reproductive status of the sampled individuals (Broeckhoven et al., 2017). In ODs of extant crocodiles, internal remodelling has been found to be more intensive in breeding females, in which large amounts of minerals must be mobilized for the formation of eggshells (Dacke et al., 2015). The internal vascular anatomy of titanosaur ODs from the Upper Cretaceous of Spain has also been shown to be compatible with a role in egg shell formation (Vidal et al., 2017). Gender and reproductive status were not controlled in this study, a limitation of the results presented here. Given that ODs have previously been documented as having varied morphology around the body, another limitation was that this study examined ODs in one anatomical location: the post-cranial dorsum. In some samples, such as in *Egernia stokesii* and in *Timon lepidus,* skin was sampled from other locations. This was because in *Egernia stokesii* no ODs were observed in the dorsal skin and thus another anatomical location, the tail, was sampled to confirm this. In *Timon lepidus*, ODs are confined to the cranial skin, so the skin of the temporal region was sampled for this taxon. The failure to record ODs in *Egernia stokesii* was a surprise as they are known to occur in at least some species (e.g. *E. striolata* where they completely cover the body). This may have been an unusual specimen as it is a domesticated (zoo) specimen.

5.3.4 Development

The histological evidence suggests that OST. is only formed on OD surfaces in close proximity to the basal layer of cells of the epidermis (the stratum germinativum). In lizards with overlapping ODs, L.B. remodelling was observed to occur more in the deeper parts of the ODs than in the superficial ones. As mentioned in the introduction to Chapter 1, section 1.1, the scientific consensus is that fish express hyper-mineralised tissues such as ganoine and enamel in their integument. These tissues result from epidermal-dermal interactions, with an ultimate contribution of the

epidermal basal layer cells in the deposition of material at the scale surface (Sire et al., 2009). The location of the OD (or part of an OD) within the dermis is seemingly a better predictor of OST. expression than ecology or phylogeny – in every species that OST. was observed, it was only found on the apical surface when the superficial surface of the OD is in close proximity to the overlying epidermis. No evidence of osteodermine remodelling was observed.

OD overall size and micromaterial ratios appear to be subject to ontogenetic change in *Ophisaurus ventralis* ODs, which mirrors the findings of Scheyer et al., (2014) in basal archosauriform ODs and Hayashi (2009) in the dinosaur *Stegosaurus* ODs. When comparing the juvenile to the adult specimen of *Ophisaurus ventralis*, the juvenile specimen was shown to express all of the materials that were found within the adult OD, except for OST.. Additionally, the ODs seemed less remodelled in the juvenile, appearing less hollow and with less expression of secondary L.B. on the endosteal surfaces of hollow cavities. These results add weight to a hypothesis that OST. is the final material to be formed within the OD, and that L.B. is deposited following the remodelling process, which starts soon after the OD is formed and increases into adulthood. This hypothesis is further reinforced with the results presented here in *Varanus komodoensis* - despite the lack of OST. in the adult ODs, it was also possible to observe the same materials in both specimens regardless of age, apart from L.B. No L.B. was observed in any sections of ODs from the juvenile specimen, suggesting that no remodelling had occurred in this young specimen, at least in the ODs that were sectioned and analysed. There is a distinct lack of ontogenetic series of lizards due to a lack of breeding programmes; these are encouraged in future work to elucidate the relationship between OD expression and ontogenetic variation.

The only squamate for which S.F.B. was not observed in the OD was *Varanus komodoensis*, which exhibited much smaller collagen fibres in a parallel-fibred external cortex surrounding a core of woven fibred bone. The lack of S.F.B. and the presence of woven and P.F.B. tissue in *Varanus komodoensis* ODs described in this chapter are interpreted as potential evidence of intramembranous ossification. The other squamate ODs described herein were shown to be composed of S.F.B., and may thus follow a metaplastic development pattern, homologous to the development of *Heloderma suspectum* ODs, as proposed in earlier chapters.

The P.F.B. observed in the basal portions of ODs in *Tiliqua rugosa* and *Ophisaurus ventralis* would correspond to "the basal lamellar layer" documented in *Anguis fragilis*

ODs (Zylberberg and Castanet, 1985; Levrat-Calviac and Zylberberg, 1986) and glyptosaurine ODs (de Buffrénil et al., 2010). It is not known how or why this layer appears in some ODs but not others, and further investigation into this was outside of the scope of this study. Because these ODs also contained S.F.B., they are also believed to follow a metaplastic development pattern, at least at one stage of ontogeny. The term "parallel-fibred bone" as used by Vickaryous et al., (2015) to describe the parallel orientation of Sharpey's fibres in *Tarentola* ODs is synonymous with S.F.B. used here. P.F.B. is a term used here to describe the parallel-fibred cortex of ODs only where these fibres do not constitute Sharpey's fibres (cannot be traced from the external soft tissue into the mineralised OD). S.F.B. was only identified in the basal and peripheral portions of ODs composed of this tissue, due to the deep location of dermal collagen fibres of the stratum compactum that comprise it. The microstructural nature of S.F.B. is such that it would afford a strong anchor to the dermis, yet would remain quite flexible due to the large diameter of the collagen fibres.

5.3.5 Ecology

Large animals such as *Varanus komodoensis* were shown to express ODs of a smaller overall volume and surface area than that of smaller animals, for example, *Heloderma suspectum* or *Tarentola annularis.* The rest of the results compared well to this finding, for example, the results presented for skinks indicated that OD size was not related to the overall snout-vent length or head-tail length of the specimen. *Corucia zebrata* is the largest extant species of skink, but the ODs were much smaller than that of another large skink *Tiliqua rugosa.* Therefore, the results suggest that there is no correlation between OD expression and body size. The fact that *Corucia zebrata* is herbivorous, yet *Tiliqua rugosa* is omnivorous may indicate that larger ODs are required to protect against dangerous prey in skinks, as has been hypothesised for geckos (Vickaryous and Sire, 2009, Laver et al., 2019). However, both species were found to have the same overall gross anatomy of compound ODs that overlap in an anterior-posterior orientation using HRXCT. This idea is countered by the fact that *Corucia zebrata* lives in trees and climbs actively, hunted by birds of prey. This may mean it would require the flexibility of smaller ODs, but this is clearly not the case. Further information is therefore required to truly elucidate a relationship, if any, between OD size, expression and anatomy to ecology. Micromaterial composition appeared not to relate to ecology either, as similar materials (e.g. OST. and S.F.B., see Table 5.1) were observed in lizards that occupy drastically different ecological niches. The only species of aquatic lizard, the Marine Iguana *Amblyrhynchus cristatus* (Avery and Tanner, 1971) is the one of only two members of Iguania to exhibit

osteoderms on the head, the other member being *Brookesia perarmata* (Schucht et al., 2020). This likely means that ODs do not inhibit aquatic lifestyles, contrary to the lack of ODs seen in the extinct metriorhynchid crocodiles (Fraas, 1902). This may aid a hypothesis of ODs functioning in aquatic taxa as protection against acidosis (Janis et al., 2012).

It is not known if there is any relation between ODs and nocturnal or diurnal lifestyles, or arboreal v terrestrial lifestyles. No nocturnal lizards were sampled, and only one arboreal lizard (*Corucia zebrata*), so the sample numbers were not sufficient. This study did not explore these areas and a large sample size would be required for any study that attempts to elucidate the relationship between ecological lifestyles and OD expression.

5.3.6 Future work

A major limitation of this study is that due to limited sample material, only one specimen was used to sample each species and many other species belonging to the same families were not investigated. Future studies should use multiple specimens from multiple species across all families, both closely related and distantly related. Ideally, one would sample as many specimens as possible from as many species as possible, but realistically this is very difficult due to practical restraints. The more data that is collected and published (particularly on open source data sharing sites such as Digimorph™ for CT scan datasets), the easier it will become to find concrete relationships between OD morphology, ecology and phylogeny.

Future work that focuses on OST. would be particularly useful, in order to structurally and developmentally compare this tissue to other hyper-mineralised materials (enamel, enameloid, ganoine, etc.).

5.4 Conclusions

The key findings of this chapter are that:

- despite major differences in gross anatomy, most squamate ODs are composed of the same set of microstructural materials, in different combinations.
- In most of the lizards sampled, OD development is more likely to be due to metaplastic formation than to intramembranous ossification, due to the presence of S.F.B..

- OST., previously only described in *Tarentola* species and *Heloderma*, is shown to be a more widespread material within squamate ODs. It was identified in dorsal ODs from adult specimens of the anguid lizards *Elgaria multicarinata* and *Ophisaurus ventralis* as well as the scincids *Tiliqua rugosa* and *Corucia zebrata.* Moreover, it is found on OD surfaces in close proximity to the epidermis. OST. has not been recorded in non-squamate reptiles and may therefore be a derived character of the group.
- In terms of gross anatomy, a loose relationship was demonstrated between phylogenetic position and OD expression., For example, all skinks exhibited compound osteoderms, as previously recorded (e.g. Camp 1923), but the anguid lizard *Elgaria multicarinata* was also shown to exhibit this type of OD despite other anguids (including *Ophisaurus ventralis)* having non-compound osteoderms.
- Some lizards that are usually documented as having ODs (e.g. *Egernia*) were found not to express them in the specimen analysed.
- *Varanus komodoensis* ODs contained neither S.F.B. nor OST., and may therefore have developed in a dissimilar way.

These findings highlight the need for further sampling both within and between species and genera. Furthermore, more data is also required to understand how the microstructural composition of ODs might be related to lizard function and ecology, and how ODs develop in different lizard groups.

5.5 References

Adler G. H, Austin C. C. and Dudley R. (1995) Dispersal and speciation of skinks among archipelagos in the tropical Pacific Ocean. *Evolutionary Ecology* **9:**529-541.

Arnold E. N., Arribas O. and Carranza S. (2007) Systematics of the palaearctic and oriental lizard tribe Lacertini (Squamata: Lacertidae: Lacertinae), with descriptions of eight new genera *Zootaxa* **1430**:1–86.

Auffenberg W. (1981) *The behavioral ecology of the komodo monitor. Publisher: University Presses of Florida,* Gainesville, FL: University Press. Pp. 406.

Avallone B., Tizzano M., Cerciello R., Buglione M. and Fulgione D. (2018) Gross anatomy and ultrastructure of Moorish Gecko, *Tarentola mauritanica* skin. *Tissue and Cell* **51**:62–67.

Barten S. and Simpson S. (2019) 9 - Lizard taxonomy, anatomy, and physiology. In: *Mader's Reptile and Amphibian Medicine and Surgery* Editor(s): Divers S. J. and Stahl S. J. Publisher: Elsevier, Amsterdam, NL. Pp. 63-74.

Bauer A. M. and Russell A. P. (1989) Supraorbital ossifications in geckos (Reptilia: Gekkonidae). *Canadian Journal of Zoology* **67**:678–684.

Bayless M. K. (2002) Monitor lizards: a pan-African check-list of their zoogeography (Sauria: Varanidae: Polydaedalus) *Journal of Biogeography* **29**:1643-1701.

Bever G. S., Bell C. J. and Maisano J. A. (2005) The ossified braincase and cephalic ODs of *Shinisaurus crocodilurus* (Squamata, Shinisauridae). *Palaeontologia Electronica* **8**:1–36.

Bhullar B-A. S. and Bell C. J. (2008) Osteoderms of the California legless lizard *Anniella* (Squamata: Anguidae) and their relevance for considerations of miniaturization. *Copeia* **4**:785–793.

Bochaton C., de Buffrénil V., Lemoine M., Bailon S. and Ineich Y. (2015) Body location and tail regeneration effects on osteoderms morphology—are they useful tools for systematic, paleontology, and skeletochronology in diploglossine lizards (Squamata, Anguidae)? *Journal of Morphology* **276**:1333–1344.

Borsuk-Białynicka M., Lubka M. and Böhme W. (1999) A lizard from Baltic amber (Eocene) and the ancestry of the crown group lacertids. *Acta Palaeontol Polonica* **44**:349-382.

Broeckhoven C., Diedericks G. and Mouton P.L.F.N. (2015) What doesn't kill you might make you stronger: Functional basis for variation in body armour. *Journal of Animal Ecology* **84**:1213–1221.

Broeckhoven C, de Kock C. and Mouton P.L.F.N. (2017) Sexual dimorphism in osteoderm expression and the role of male intrasexual aggression. *Biological Journal of the Linnean Society* **122**:329-339.

Camp C. L. (1923) Classification of the Lizards. Bulletin of the American Museum of Natural History **48:**289-481.

Cogger H. G. (2000) Reptiles and Amphibians of Australia (6th edition). Reed New Holland, Sydney, Australia. Pp. 808.

Conrad J. L. (2008) Phylogeny and systematics of Squamata (Reptilia) based on morphology. *Bulletin of the American Museum of Natural History* **310**:1–182.

Cooper W. Jr., Van Wyk J. H., Mouton P. Le F. N., Al-Johany A. M., Lemos-Espinal J. A., Paulissen M. A. and Flowers M. (2000). Lizard antipredatory behaviors preventing extraction from crevices. *Herpetologica* **56**:394-401.

Dacke C. G., Elsey R. M., Trosclair P. L., Sugiyama T., Nevarez J.G. and Schweitzer M. H. (2015) Alligator osteoderms as a source of labile calcium for eggshell formation. *Journal of Zoology* **297**:255-264.

Daeschler E. B., Shubin N. H. and Jenkins F. A. (2006) Devonian tetrapod-like fish and the evolution of the tetrapod body plan *Nature* **440**:757–763.

De Buffrénil V., Farlow J. O. and de Ricqlès A. (1986) Growth and function of *Stegosaurus* plates: evidence from bone histology. *Paleobiology* **12**:459-473.

De Buffrénil V., Sire J-Y., and Rage J. C. (2010) The histological structure of glyptosaurine osteoderms (Squamata: Anguidae), and the problem of osteoderm development in squamates. *Journal of Morphology* **271**:729–737.

De Buffrénil V., Dauphin Y., Rage J-C. and Sire J-Y. (2011) An enamel-like tissue, osteodermine, on the osteoderms of a fossil anguid (Glyptosaurinae) lizard. *Comptes Rendus de l'Academie des Sciences Palevol* **10:**427-437.

de Queiroz K. (1987) Phylogenetic systematics of iguanian lizards: a comparative osteological study*. University of California Publications in Zoology* **118:**1–203.

Estes R., De Queiroz K. and Gauthier J. (1988) Phylogenetic relationships within Squamata. In: *Phylogenetic Relationships of the Lizard Families: Essays Commemorating Charles L. Camp.* Editors: R. Estes, G. Pregill, Publisher: Stanford University Press, Redwood City, CA, USA. Pp. 119-281.

Erickson G. M., Ricqlès A. de, Buffrénil V. de, Molnar R.E. and Bayless M.K. (2003) Vermiform bones and the evolution of gigantism in *Megalania* — How a reptilian fox became a lion. *Journal of Vertebrate Palaeontology* **23**:966-970.

Fraas E. (1902) Die Meer-Krocodilier (Thalattosuchia) des oberen Jura unter specieller Berücksichtigung von *Dacosaurus* und *Geosaurus. Palaeontographica.* **49**:1–72.

Farlow J. O., Hayashi S. and Tattersall G. J. (2010) Internal vascularity of the dermal plates of Stegosaurus (Ornithischia, Thyreophora). *Swiss Journal of Geosciences* **103**:173-185.

Gamble T., Bauer A. M., Greenbaum E. and Jackman T. R. (2008) Out of the blue: a novel, trans-Atlantic clade of geckos (Gekkota, Squamata). *Zoologica Scripta* **37**:355-366.

Gao K. and Norell M. A. (1998) Taxonomic revision of *Carusia* (Reptilia: Squamata) from the Late Cretaceous of the Gobi Desert and phylogenetic relationships of anguinomorphan lizards. *American Museum Novitates* **3230**:1–55.

Gauthier J. A. (1982) Fossil xenosaurid and anguid lizards from the early Eocene of Wyoming, and a revision of the Anguioidea. *Contributions to Geology, University of Wyoming* **21**:7-54.

Georgalis G. L. (2017) *Necrosaurus* or *Palaeovaranus*? Appropriate nomenclature and taxonomic content of an enigmatic fossil lizard clade (Squamata). *Annales de Paléontologie* **103**:293-303.

Greer A. (2007) The Biology and Evolution of Scincid Lizards. Online at: https://www.academia.edu/35305801/The_Biology_and_Evolution_of_Scincid_Lizards.doc Accessed: 02/05/2020.

Greenbaum E., Stanley E. L., Kusamba C., Moninga W. M., Goldberg S. R. and Bursey C. R. (2012) A new species of *Cordylus* (Squamata: Cordylidae) from the Marungu Plateau of south-eastern Democratic Republic of the Congo. *African Journal of Herpetology* **61**:14–39.

Harvey M. B., Ugueto G. N. and Gutberlet Jr. R. L. (2012) Review of Teiid Morphology with a Revised Taxonomy and Phylogeny of the Teiidae (Lepidosauria: Squamata). *Zootaxa* **3459**:1.

Hayashi S., Carpenter K., Scheyer T.M., Watabe M. and Suzuki D. (2010) Function and evolution of ankylosaur dermal armor. *Acta Palaeontologica Polonica*, **55**:213–228.

Hill R. V. (2006) Comparative anatomy and histology of xenarthran osteoderms. *Journal of Morphology* **267**:1441-1460.

Hoffstetter R. (1962) Observations sur les ostéodermes et la classification des anguidés actuels et fossiles (Reptiles. Sauriens). *Bulletin of the American Museum of Natural History* **34**:149-157.

Hoofien J. H. (1962) An unusual congregation of the gekkonid lizard *Tarentola annularis* (Geoffroy) *Herpetologica* **18**:54-56.

Laver R. J., Morales C. H., Heinicke M. P., Gamble T., Longoria K., Bauer A. M. and Daza J. D. (2019) The development of cephalic armor in the tokay gecko (Squamata: Gekkonidae: *Gekko gecko*). *Journal of Morphology* **281**:213-228.

Levrat-Calviac V. and Zylberberg L. (1986) The structure of the osteoderms in the gekko: *Tarentola mauritanica. American Journal of Anatomy* **446**:437–446.

Ledesma D. T. and Scarpetta S. G. (2018) The skull of the gerrhonotine *lizard Elgaria panamintina* (Squamata: Anguidae). PLoS ONE **13**:e0199584.

Loveridge A. (1947) Revision of the African lizards of the family Gekkondiae. *Bulletin of the Museum of Comparative Zoology at Harvard College* **98**:1-469.

Maisano J. A., Bell C. J., Gauthier J. A. and Rowe T. (2002) The ODs and palpebral in *Lanthanotus borneensis* (Squamata: Anguimorpha). *Journal of Herpetology* **36**:678–682.

Maisano J. A., Laduc T. J., Bell C. J. and Barber D. (2019) The cephalic osteoderms of *Varanus komodoensis* as revealed by high-resolution X-ray computed tomography. *The Anatomical Record* **302**:1675–1680.

McCoy M. (2006) Reptiles of the Solomon Islands. *Pensoft Series Faunistica* **57**:212.

McDowell S. M. Jr and Bogert C. M. (1954) The systematic position of *Lanthanotus* and the affinities of the anguinomorphan lizards. *Bulletin of the American Museum of Natural History* **105**:1–142.

Meszoely C. A. M. (1970) North American fossil anguid lizards. *Bulletin Museum of Comparative Zoology*, Harvard University **139**:87-149.

Moss M. L. (1969) Comparative histology of dermal sclerifications in reptiles. *Acta Anatomica* **73**:510–533.

Otto H. (1909) Die Beschuppung der Brevilinguier und Ascalaboten. *Jena Z Naturwiss* **44**:193–252.

Paluh D. J., Griffing A. H. and Bauer A. M. (2017) Sheddable armour: identification of osteoderms in the integument of *Geckolepis maculata* (Gekkota). *African Journal of Herpetology* **66**:12-24

Read R. (1986) Osteoderms in the Lacertilia: an investigation into the structure and phylogenetic implications of dermal bone found under the skin of lizards. PhD Thesis, Department of Biological Sciences, California State University, Fullerton, CA. Pp. 142.

Reynoso V. H. (1997) A "beaded" sphenodontian (Diapsida: Lepidosauria) from the Early Cretaceous of central Mexico. *Journal of Vertebrate Palaeontology* **17**:52–59.

Richter M., Daeschler T., Samson I., Shubin N. (2011) The dermal scales of *Tiktaalik roseae*. *Journal of Vertebrate Paleontology* **31**:178–179.

Ruibal R. and Shoemaker V. (1984) Osteoderms in anurans. *Journal of Herpetology* **18**:313–328

Scherz M. D., Daza J. D., Köhler J., Vences M. and Glaw F. (2017) Off the scale: a new species of fish-scale gecko (Squamata: Gekkonidae: Geckolepis) with exceptionally large scales. *PeerJ* **5**:2955

Scheyer T.M. and Sánchez−Villagra M.R. (2007) Carapace bone histology in the giant pleurodiran turtle Stupendemysgeographicus: Phylogeny and function. *Acta Palaeontologica Polonica* **52**:137–154.

Scheyer T. M. and Sander P. M. (2009) Bone microstructures and mode of skeletogenesis in osteoderms of three pareiasaur taxa from the Permian of South Africa. *Journal of Evolutionary Biology* **22:**1153-1162.

Schucht P. J., Rühr P. T., Geier B., Glaw F. and Lambertz M. (2020) Armored with skin and bone: The integumentary morphology of the Antsingy leaf chameleon *Brookesia perarmata* (Iguania: Chamaeleonidae). *Journal of Morphology* **280**:214–244.

Schultze H.-P. (2016) Scales, enamel, cosmine, ganoine, and early osteichthyans *Comptes Rendus Palevol* **15**:83-102

Sire J-Y., Donoghue C. J., Vickaryous M. K. (2009). Origin and evolution of the integumentary skeleton in non-tetrapod vertebrates. *Journal of Anatomy* **214**:409–440.

Strahm M. H. and Schwartz A. (1977) Osteoderms in the anguid lizard subfamily Diploglossinae and their taxonomic importance. *Biotropica* **9**:58-72.

Stanley E., Ceríaco L., Bandeira S., Valerio H., Bates M. and Branch W. (2016) A review of *Cordylus machadoi* (Squamata: Cordylidae) in southwestern Angola, with the description of a new species from the Pro-Namib desert. *Zootaxa* **4061**:201–226.

Sun C-Y. and Chen P-Y. (2013) Structural design and mechanical behavior of Alligator (*Alligator mississippiensis*) osteoderms. *Acta Biomaterialia* **9**:9049–64.

Uetz P., Freed P., and Hosek J. (2018) *The Reptile Database.* Accessed: 02/02/2020 URL: http://reptile-database.reptarium.cz/

Vickaryous M. K. and Hall B. K. (2006) Osteoderm morphology and development in the nine-banded armadillo, *Dasypus novemcinctus* (Mammalia, Xenarthra, Cingulata). *Journal of Morphology* **267**:1273-1283.

Vickaryous M. K. and Hall B. K. (2008) Development of the dermal skeleton in *Alligator mississippiensis* (Archosauria, Crocodylia) with comments on the homology of osteoderms. *Journal of Morphology* **269**:398–422.

Vickaryous M. K. and Sire J.-Y. (2009) The integumentary skeleton of tetrapods: origin, evolution, and development. *Journal of Anatomy* **214**:441–464.

Vickaryous M. K., Meldrum G. and Russell A. P. (2015) Armored geckos: A histological investigation of osteoderm development in *Tarentola* (Phyllodactylidae) and *Gekko* (Gekkonidae) with comments on their regeneration and inferred function. *Journal of Morphology* **276**:1345–1357.

Vidal N. and Hedges S.B. (2009*)* The molecular evolutionary tree of lizards, snakes, and amphisbaenians. *Comptes Rendus – Biologies* **332**:129-139.

Vidal D., Ortega F., Gascó F., Serrano-Martínez A. and Sanz J. L. (2017) The internal anatomy of titanosaur osteoderms from the Upper Cretaceous of Spain is compatible with a role in oogenesis *Scientific Reports* **7**:42035.

Walpole M. J. and Goodwin H. J. (2000) Local economic impacts of dragon tourism in Indonesia. *Annals of Tourism Research* **27**:559–576.

Wikramanayake E. (1997) Everyone knows that the dragon is only a mythical beast. *Smithsonian* **28**:74-79.

Zylberberg L. and Castanet J. (1985) New data on the structure and the growth of the osteoderms in the reptile *Anguis fragilis* (Anguidae, Squamata). *Journal of Morphology* **186**:327–342.

6 CHAPTER 6 Histology of fossil osteoderms

6.1 Introduction to fossilised ODs

As mineralised elements, ODs are often the only part of the integument that survives fossilisation. Unfortunately, given their location within the dermis, at the external surface of the body, they are also likely to be one of the first parts of the body to be lost after the death of an animal.

Compared to extant taxa, some of the most diverse and impressive dermal mineralisations are found in the fossil record. Some notable examples include spiked ODs from the Late Cretaceous dinosaur *Ankylosaurus* (Hayashi et al., 2010; Arbour et al., 2014), or from the Late Jurassic dinosaur *Stegosaurus*, which is well known for expressing sail-like ODs along the dorsal midline (Main et al., 2005). The largest ODs currently known from any taxon are also found in the fossil record, from the titanosaur *Rapetosaurus krausei*, where each OD has been estimated to have a volume of 9600 cubic centimetres (Curry Rogers et al., 2011). As introduced in Chapter 1, the ability to form dermal mineralisations is probably an ancestral trait of vertebrates, and seems to be a trait that can be suppressed or enhanced in different ways in different groups. This makes fossilised ODs strong candidates for studies that require a wide examination of OD expression.

Some authors (e.g. Mead et al., 2012) have argued that gross morphological features of ODs, such as overall shape or superficial surface texture, are difficult to interpret or score as characters. Others disagree and the gross anatomy of fossil ODs has been used to identify many fossil reptile taxa (Richter, 1994), through comparison with ODs from both extinct and living members of the same group. For example, ODs have been shown to be useful in diagnosing aetosaurs, an extinct order of Late Triassic (~210 million years ago [mya]) herbivorous archosaurs. Aetosaur species can often be identified from individual ODs based on their ornamentation pattern (Long and Ballew, 1985). Scheyer et al., (2014) also suggested that histological features of aetosaur ODs were potentially apomorphic (=derived) at species/genus level. Additionally, Hill (2010) demonstrated it was possible to locate the anatomical region from which ODs of the fossil crocodylomorph *Simosuchus clarki* originated through comparison with the morphology and histology of ODs from articulated fossils of this

and other taxa. In helodermatids, OD gross anatomy was used to identify fossilised forms, through comparison with extant species of *Heloderma* spp. (Mead et al., 2012).

As introduced in Chapter 1, most fossil ODs have been characterised purely by their gross anatomical appearance – studies that attempt to characterise ODs based on microstructure are rare and implications for variation in microstructure have not been discussed. This hole in our knowledge is what this chapter aims to begin to address.

6.2   Introduction to the Hampshire Basin

The Hampshire Basin, located in the southern U.K., is a rich site for fossils, with the only continuous sequence spanning the Eocene-Oligocene boundary (27-38 million years ago (mya)) in Western Europe. Two formations are sampled in this chapter; the Headon Hill Formation and the Bembridge Limestone Formation. These are shown on the map in figure 6.1, coloured pale pink.

The British Geological Survey (BGS) describes the Headon Hill Formation (within the parent unit of the Solent Group) as being up to 90m thick, found throughout the Isle of Wight, spanning the Priabonian stage of the late Eocene (34-38 mya)) (Melville and Freshnay,1982; Klembara and Green, 2010). There are nine members comprising interbedded clay, silt and sand with several limestone and lignite beds. The lower boundary of the formation is defined as an erosion surface overlying the fine- to medium cross-bedded sands of the Becton Sand Formation. The upper boundary of the formation is defined as an erosive contact into the various lithologies at the base of the Bembridge Limestone Formation. The stratotype sections are various localities at which the constituent members are exposed throughout the Isle of Wight.

The BGS defines the Bembridge Limestone Formation (within the parent unit of the Solent Group) as being up to 9m thick, found throughout the northern part of the Isle of Wight, spanning an age range between the Priabonian to the Rupelian stage of the Early Oligocene (27-34 mya) (Melville and Freshnay,1982; Insole and Daley, 1985; Daley and Edwards, 1990). The lithology comprises limestones and clayey limestones intercalated with lime-rich muds and clays. The lower boundary of the formation is defined as a contact with the underlying Headon Hill Formation. The upper boundary of the formation is defined as contact with clays and silts of the Bembridge Marls Member (the Bouldnor Formation). The stratotype section is an 8.5m cliff section at Whitecliff Bay, Isle of Wight, UK with pale brown to white fossiliferous limestones and lime-rich mudstone.

Eight fossil ODs were sampled from the Headon Hill Formation. Four fossil ODs were sampled from layer fifteen of the Bembridge Limestone formation, while three fossilised ODs were sampled from layer seventeen. Layers are numbered in ascending order (layer 1 being oldest), thus layer fifteen is older than layer seventeen. The samples were labelled as formation.layer.number.sample number, e.g. BL.15.1 corresponds to Bembridge Limestone, layer fifteen, OD number one. All of the sampled ODs were provided on loan from the collections of the Natural History Museum, London, UK, courtesy of Dr Jerry Hooker.
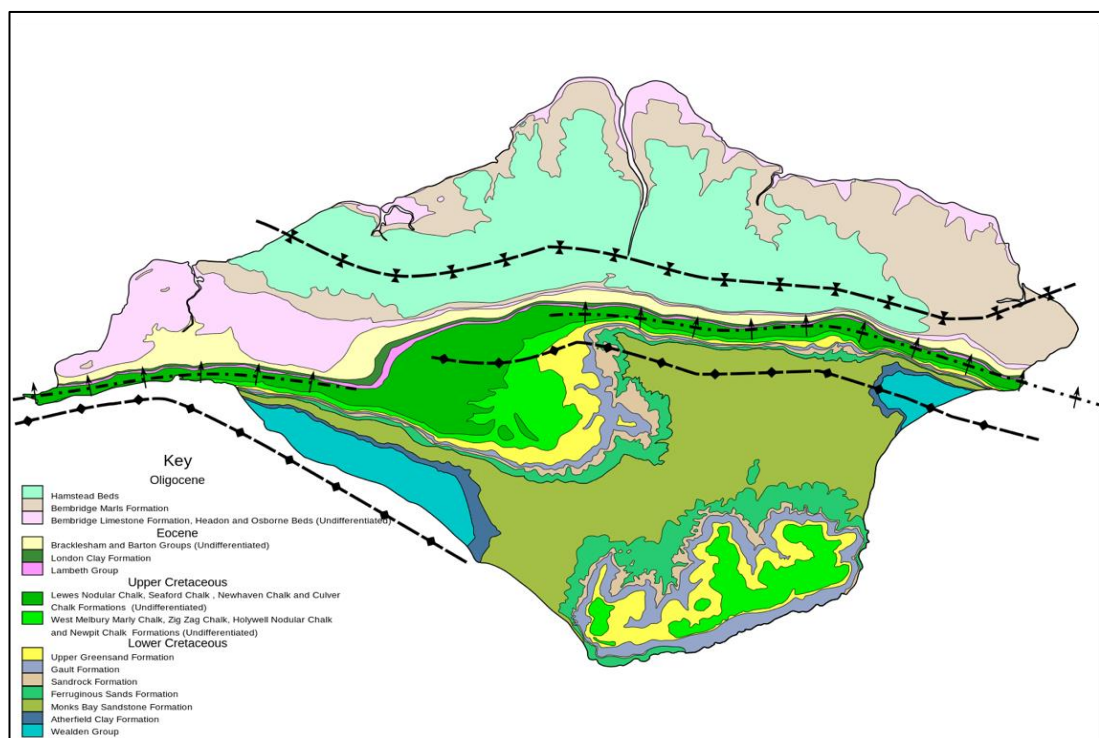
Figure 6.1: Geological stratifications of the Isle of Wight, U.K. The sampled locations from this chapter are the Bembridge Limestone formation and the Headon Hill formation (Pale pink). (Adapted from Insole and Daley, 1985; Klembara and Green 2010).

The aim was to characterise these ODs, using the same techniques applied to the ODs of extant lizards as detailed in previous chapters, so as to record both their gross anatomy and their microstructural composition. These features would then be assessed to see whether these parameters matched those of living taxa, and could therefore be used to identify to which taxon they may have belonged, as well as any other information, such as the body location from which the ODs originated.

6.3   Results

6.3.1   Gross morphology

6.3.1.1   Bembridge Limestone specimens

The ODs from layer 15 of the Bembridge Limestone (BL.15.1-BL.15.4) were observed as irregularly shaped with dark brown to black shiny dorsal surfaces (Fig. 6.3.1a, c, e, g), ornamented with granular raised tubercles. The dorsal or superficial surfaces did not appear to feature vascular pits. The ventral (deep) surfaces were brown flat, smooth, dull and often featured small vascular pits (foramina) (Fig. 6.3.1b, d, f, h). The edges appeared rounded, suggesting some erosion via transport of the sediment. Given the irregular outline of the ODs, and the fact that no articular surface could be observed, it was possible to reasonably conclude that the majority of these ODs were incomplete, featuring broken, rough edges.
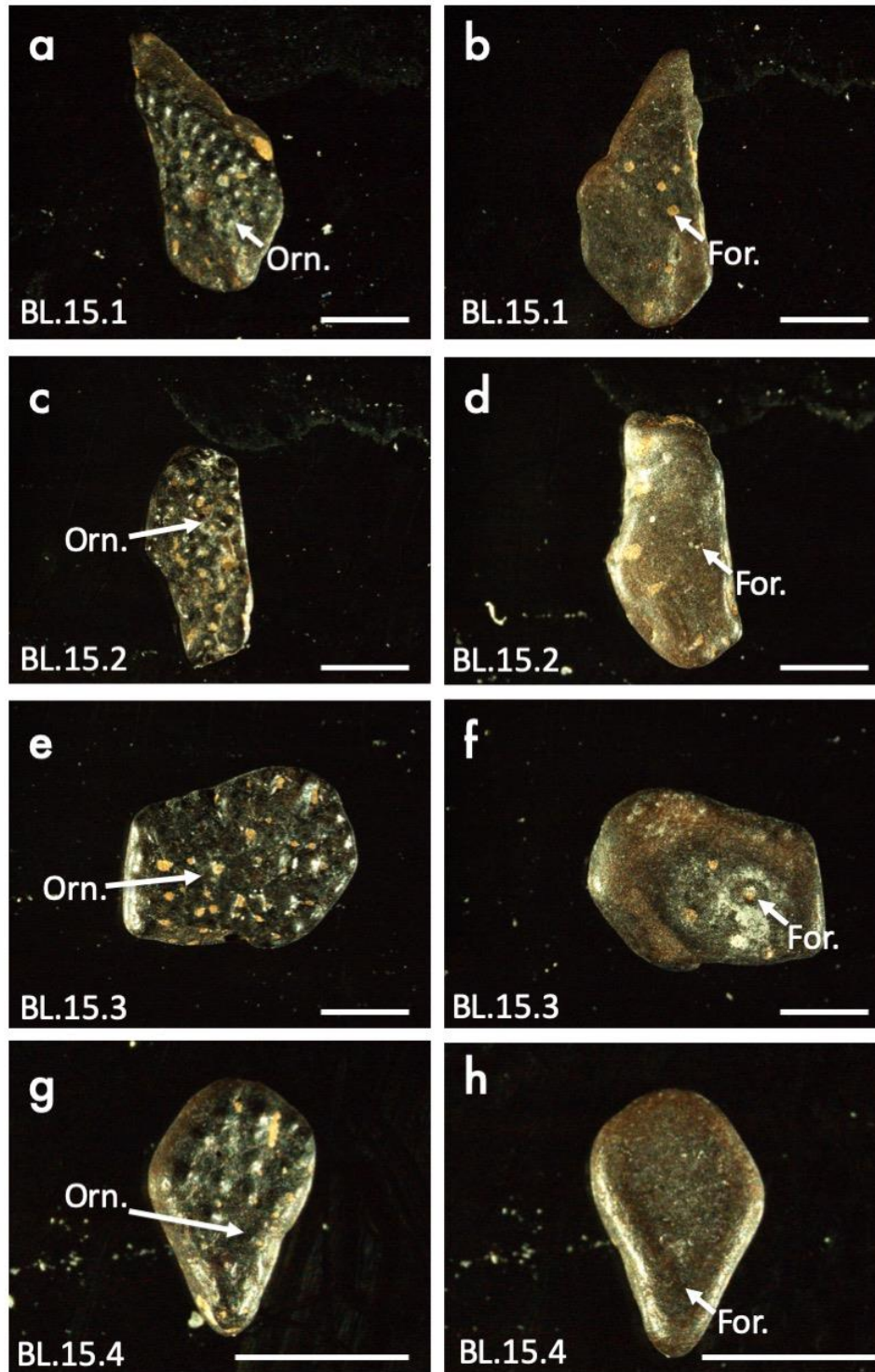
Figure 6.3.1: Morphotype 1 ODs from layer 15 of the Bembridge Limestone Formation visualised with light microscopy. (a) BL.15.1 in dorsal view, (b) BL.15.1 in ventral view, (c) BL.15.2 in dorsal view, (d) BL.15.2 in ventral view, (e) BL.15.3 in dorsal view, (f) BL.15.3 in ventral view, (g) BL.15.4 in dorsal view, (h) BL.15.4 in ventral view. For. = foramen, Orn. = ornamented surface.

Scale bars: (a-h) = 1000µm.

The ODs from layer 17 of the Bembridge Limestone (BL.17.1-BL.17.3) were also irregularly shaped with shiny black dorsal surfaces ornamented on one edge of the dorsal surface with granular raised tubercles (Fig. 6.3.2a, c, e, labelled Orn.) and on the other edge of the dorsal surface with smooth gliding or articular surfaces (Fig. 6.3.2a, c, e, labelled Artic.). Between the ornamented surface and the articular/glide surface was a clear line or ridge of separation. The ventral surfaces were similar to those of Fig 6.3.1 and appeared flat, smooth, dull and often featured small foramina (Fig. 6.3.1b, d, f, h). The edges were rounded, suggesting some erosion via transport of the sediment. These ODs were also assumed to be incomplete, given the irregular outline of the ODs, whereas BL.167.2 appeared to be the most complete sample.
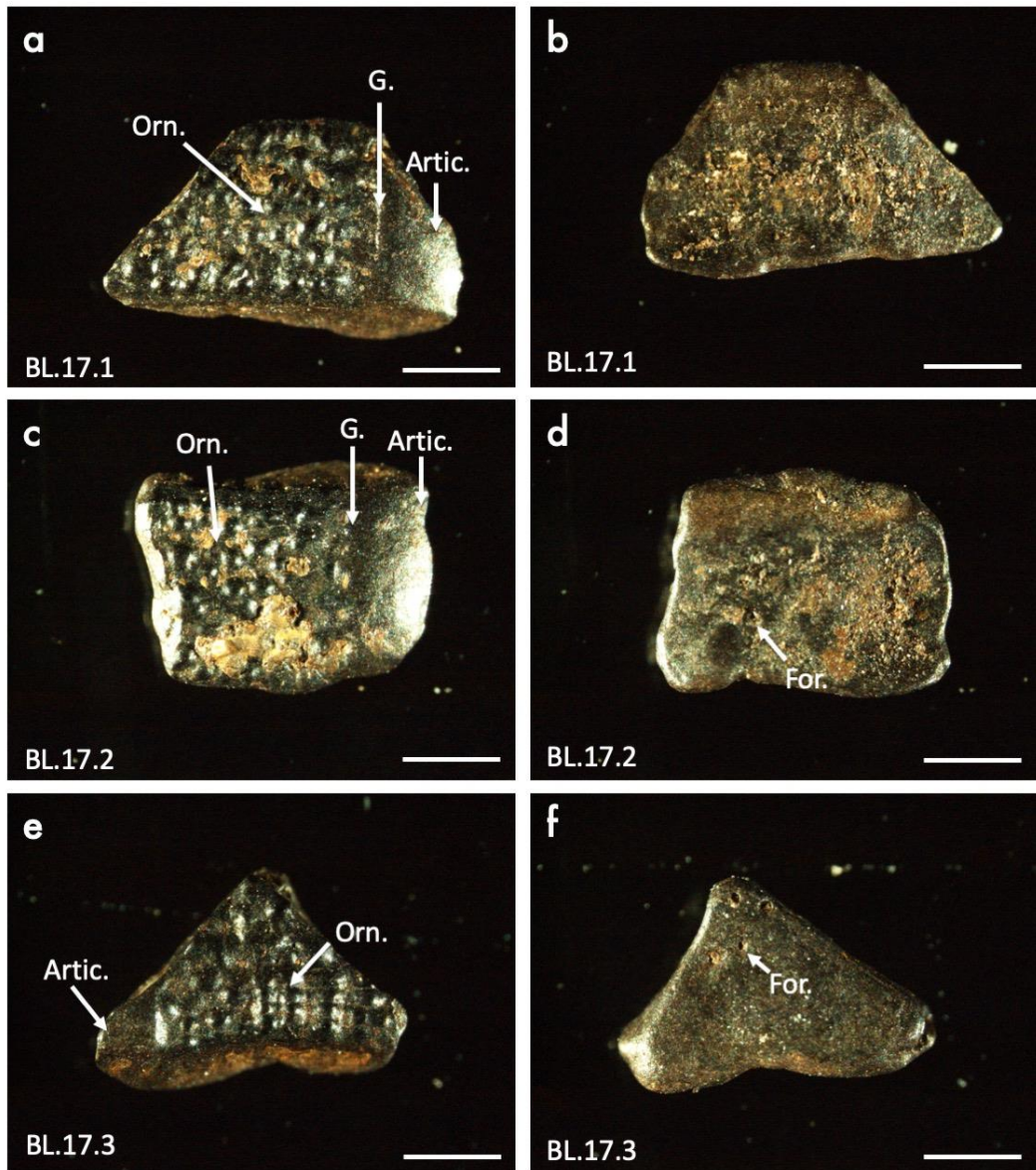
Figure 6.3.2: Morphotype 1 ODs from layer 16/17 of the Bembridge Limestone Formation visualised with light microscopy (a) BL.17.1 in dorsal view, (b) BL.17.1 in ventral view, (c) BL.17.2 in dorsal view, (d) BL.17.2 in ventral view, (e) BL.17.3 in dorsal view, (f) BL.17.3 in ventral view. Artic. = articular surface, For. = foramen, G. = groove, Orn. = ornamented surface.

Scale bars: (a-f) = 1000µm.

6.3.1.2 Headon Hill specimens

The ODs from layer 1 of the Headon Hill Formation vary in shape from ovoid, square or irregularly shaped, and many appeared to be incomplete. The incomplete specimens featured rough breaks, for example HH.1.4 (Fig 6.3.3g) featured a break perpendicular the midline keel. The Headon Hill ODs could be assigned to one of two discrete morphotypes - either featuring a pronounced keel on the dorsal surface, with a vermiculate surface texture surrounding the keel (HH.1.1, HH.1.4, HH.1.5, HH.1.7), or having a similar morphology to those from the Bembridge Limestone (Figures 6.3.1 and 6.3.2) with both ornamented and non-ornamented articular surfaces dorsally. The ventral surface appeared smooth in both morphotypes, occasionally concave, and featured many small vascular pits (Fig 6.3.1b, d, f, h and Fig 6.3.2b, d, f).

Unlike the ODs from the Bembridge Limestone Formation, the colour acquired by the ODs during fossilisation varied in the ODs from the Headon Hill Formation. Under white light microscopy, some ODs appeared pale brown in colour (Fig. 6.3.3a), whereas others appeared dark brown (Figure 6.3.3c) to black (Figure 6.3.3k). This indicated that the environments in which they had fossilised contained varying proportions of minerals.
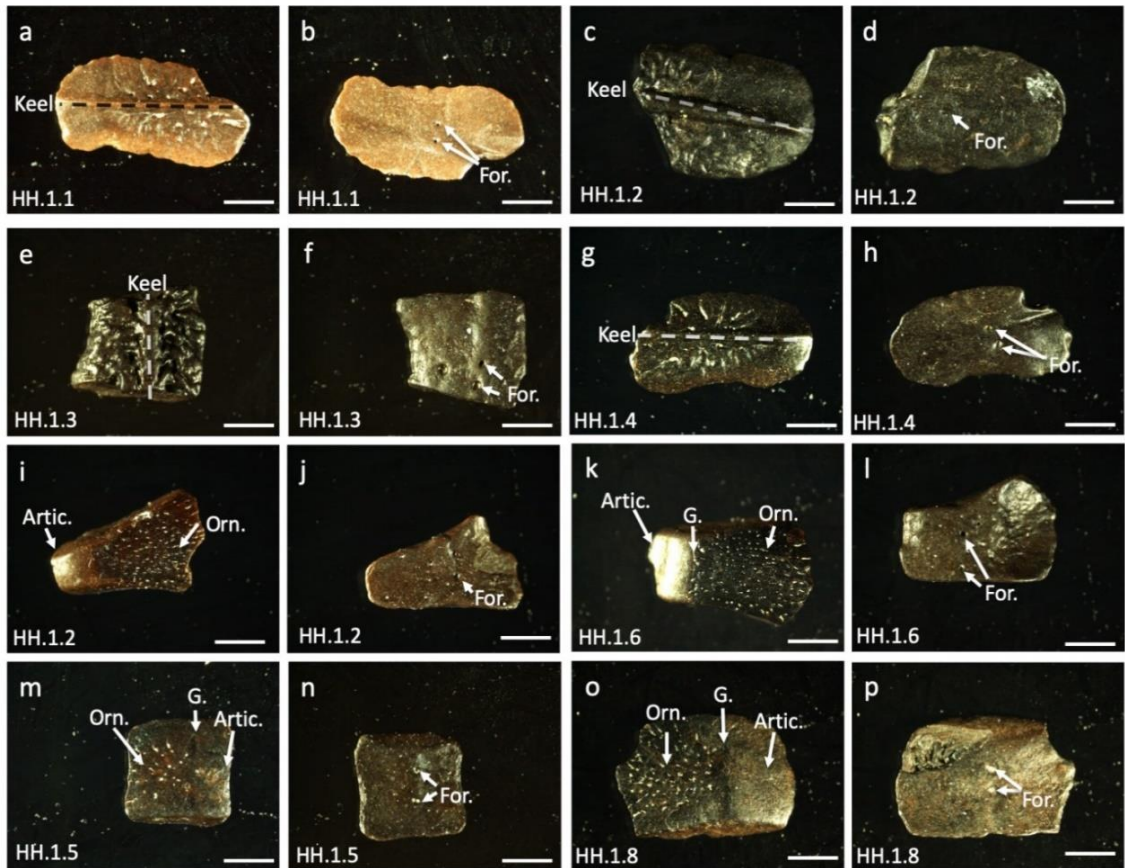
Figure 6.3.3: Morphotype 2 (a-h) and Morphotype 1 (i-p) ODs from layer 1 of the Headon Hill Formation visualised with light microscopy. (a) HH.1.1 in dorsal view, (b) HH.1.1 in ventral view, (c) HH.1.2 in dorsal view, (d) HH.1.2 in ventral view, (e) HH.1.3 in dorsal view, (f) HH.1.3 in ventral view, (g) HH.1.4 in dorsal view, (h) HH.1.4 in ventral view, (i) HH.1.5 in dorsal view, (j) HH.1.5 in ventral view, (k) HH.1.6 in dorsal view, (l) HH.1.6 in ventral view, (m) HH.1.7 in dorsal view, (n) HH.1.7 in ventral view, (o) HH.1.8 in dorsal view, (p) HH.1.8 in ventral view. Artic. = articular surface, For. = foramen, G. = groove, Keel and dashed lines = keel, Orn. = ornamented surface.

Scale bars: (a-p) = 1000µm.

6.3.2 HRXCT scanning

The corresponding HRXCT data for each OD is shown in figures 6.3.4-6.3.6. µ-CT scanning of ODs revealed surface topology that was obscured by debris in the light microscopy. For example, it was difficult to observe some of the tubercles on the dorsal surfaces of the ODs from the Bembridge Limestone formation using transmitted light, due to the shiny surface and dust or particulate debris. However, after reconstructing the surface topology of the OD from HRXCT data, the tubercles can be readily identified, as only material with the same density of the fossilised OD is shown. Additionally, it can be hard to deduce whether or not markings and specks on the basal surfaces of ODs are actually foramina, or just discoloration, when using light microscopy. After reconstructing the surface topology of the OD from HRXCT data, the resolution is sufficient to determine true foramina from false discolouration, as the true vascular channels appear as actual holes in the surface (Fig 6.3.4, For.). This unique technique affords the possibility of quantitative measurements of OD properties, for example, it became possible to count the individual tubercles and it became clear that there were foramina on the dorsal (superficial) surfaces of some of the Morphotype 2 ODs (Figure 6.3.6a, g, For.)
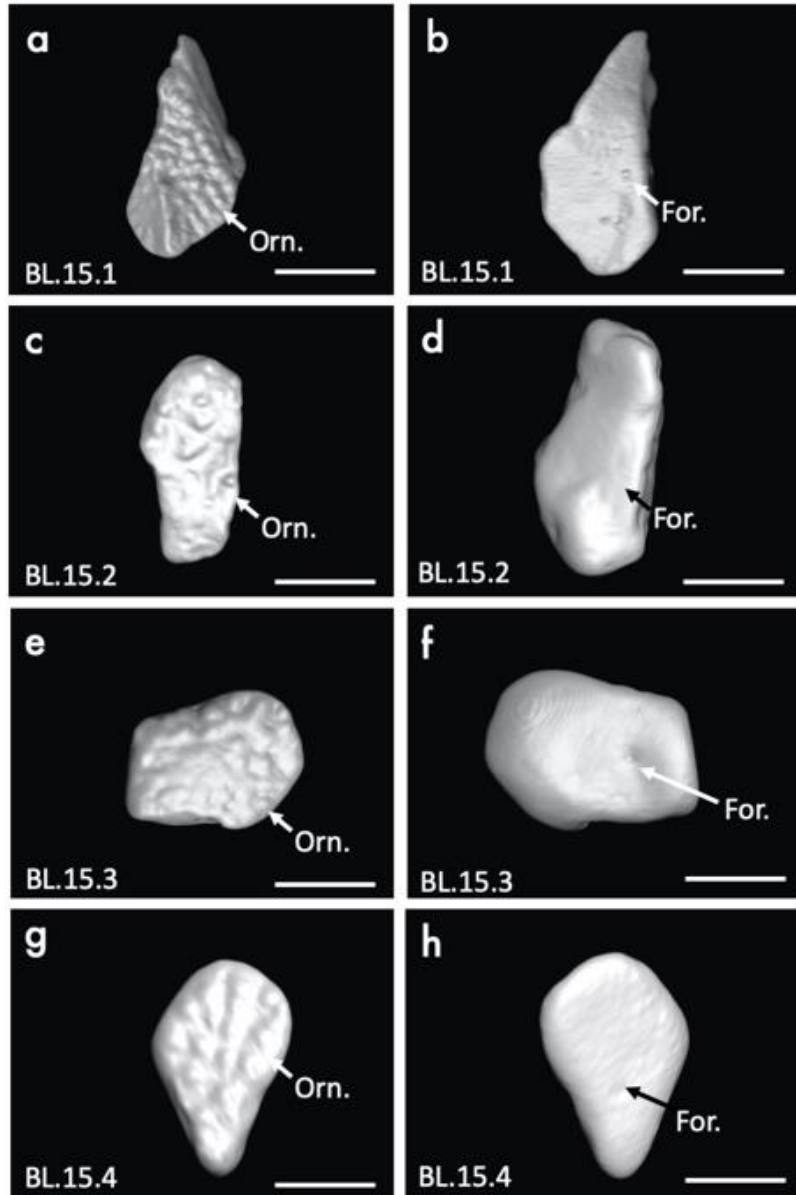
Figure 6.3.4: Three-dimensional, false colour surface reconstructions of Morphotype 1 ODs from layer 15 of the Bembridge Limestone Formation, segmented from HRXCT data. (a) BL.15.1 in dorsal view, (b) BL.15.1 in ventral view, (c) BL.15.2 in dorsal view, (d) BL.15.2 in ventral view, (e) BL.15.3 in dorsal view, (f) BL.15.3 in ventral view, (g) BL.15.4 in dorsal view, (h) BL.15.4 in ventral view. For. = foramen, Orn. = ornamented surface.

Scale bars: (a-h) = 1000µm.
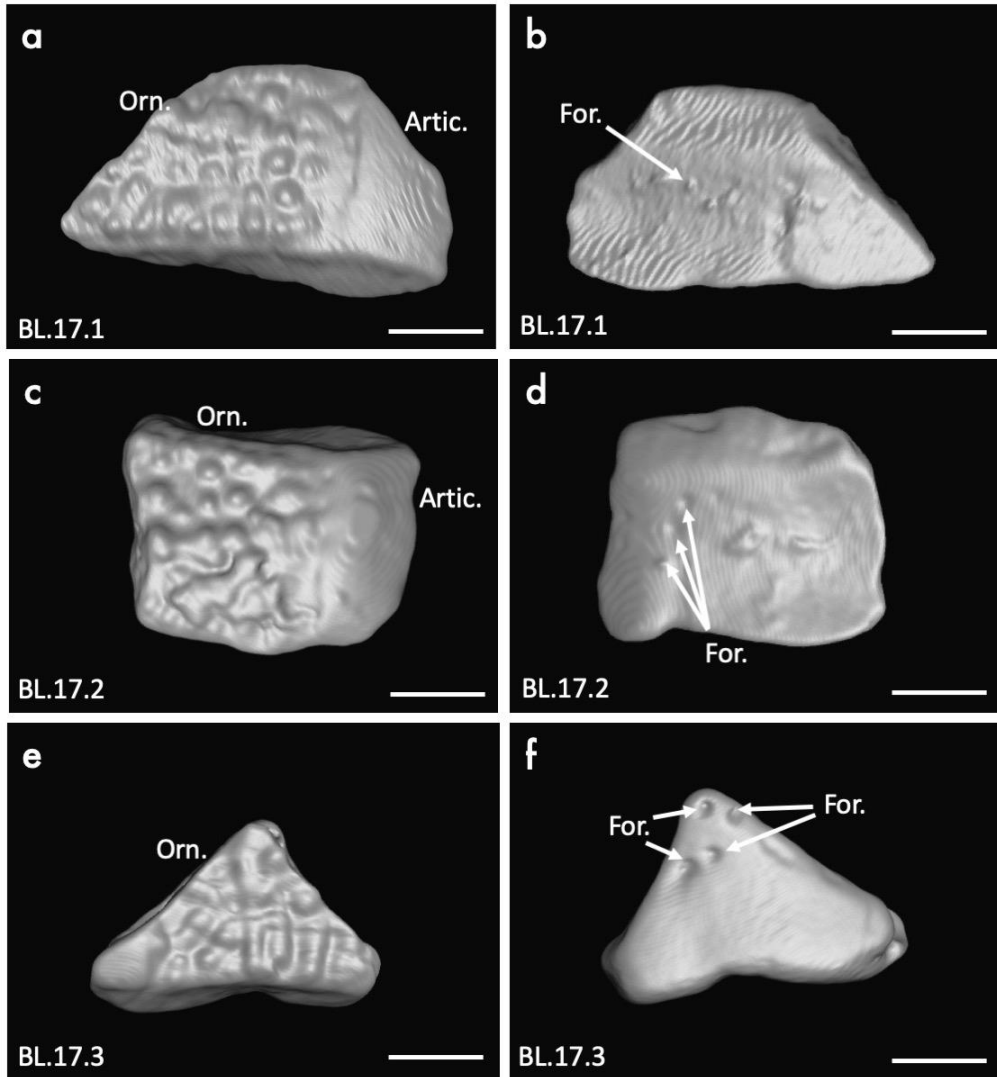
Figure 6.3.5: Three-dimensional, false colour surface reconstructions of Morphotype 1 ODs from layer 17 of the Bembridge Limestone Formation, segmented from HRXCT data. (a) BL.17.1 in dorsal view, (b) BL.17.1 in ventral view, (c) BL.17.2 in dorsal view, (d) BL.17.2 in ventral view, (e) BL.17.3 in dorsal view, (f) BL.17.3 in ventral view. Artic. = articular surface, For. = foramen, Orn. = ornamented surface.

Scale bars: (a-f) = 1000μm.
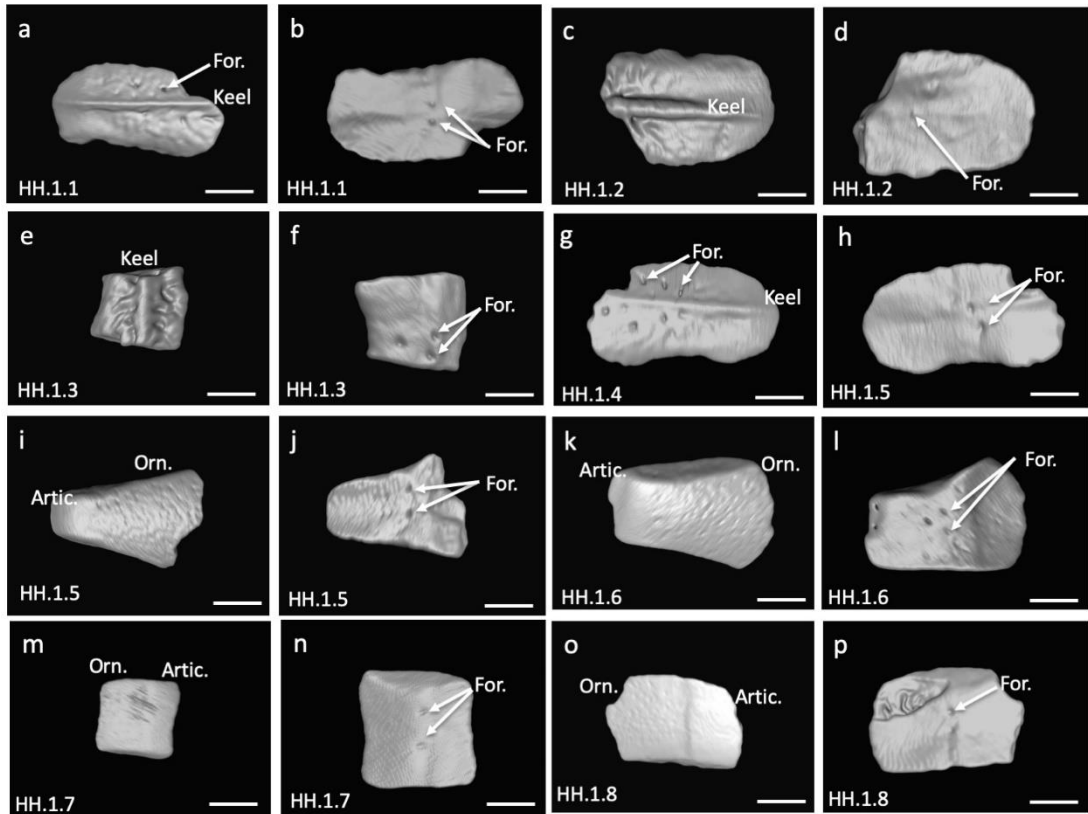
Figure 6.3.6: Three-dimensional, false colour surface reconstructions of Morphotype 2 (a-h) and Morphotype 1 (i-p) ODs from layer 1 of the Headon Hill Formation, segmented from HRXCT data. (a) HH.1.1 in dorsal view, (b) HH.1.1 in ventral view, (c) HH.1.2 in dorsal view, (d) HH.1.2 in ventral view, (e) HH.1.3 in dorsal view, (f) HH.1.3 in ventral view, (g) HH.1.4 in dorsal view, (h) HH.1.4 in ventral view, (i) HH.1.5 in dorsal view, (j) HH.1.5 in ventral view, (k) HH.1.6 in dorsal view, (l) HH.1.6 in ventral view, (m) HH.1.7 in dorsal view, (n) HH.1.7 in ventral view, (o) HH.1.8 in dorsal view, (p) HH.1.8 in ventral view. Artic. = articular surface, For. = foramen, Keel = keel, Orn. = ornamented surface.

Scale bars: (a-p) = 1000μm.

6.3.3   Multi-rotation polarised light microscopy

Sample ODs were sectioned using a diamond saw (Oxford University Earth Sciences). Multi-rotation polarised light microscopy was then employed in order to reveal the microstructure of the OD material components.

6.3.3.1   OD Morphotype 1 Bembridge Limestone:

Using this technique, it was possible to observe that the basal layer of BL.15.2 was composed of P.F.B., of a thickness around one third of total OD thickness (Fig. 6.3.7). This tissue is characterised by the alternation of very thin lamellae, appearing alternating light and dark. L.B. could be identified surrounding three holes that would have contained vasculature. The OST. capping layer appeared as a translucent, glassy capping tissue towards the dorsal surface of both ODs BL.15.2 and BL.17.3 in transverse section (Figs. 6.3.7 and 6.3.8, OST.). The basal layer of BL.17.3 was also composed of P.F.B., of a thickness up to half that of the total OD thickness (Fig. 6.3.8). This is named P.F.B. as it was not possible to determine if the fibres were in fact Sharpey's fibres (entering the mineralised OD from the surrounding soft tissue) due to the incomplete sample. L.B., with a distinctive scalloped border could also be identified surrounding one vascular channel. Despite both of these ODs appearing with a rough superficial surface in earlier figures, BL.15.2 has a smooth superficial surface in section, whereas BL.17.3 showed a rough superficial surface, although this is likely due to the section plane having been cut between tubercles, or close to the edge of the OD, where fewer tubercles are expressed. All the Morphotype 1 ODs examined herein showed a pattern of perivascular remodelling, i.e., the formation of secondary osteons and endosteal deposits of L.B. on the walls of broad resorption bays created by osteoclast activity (Figs 6.3.7 and 8, L.B.).
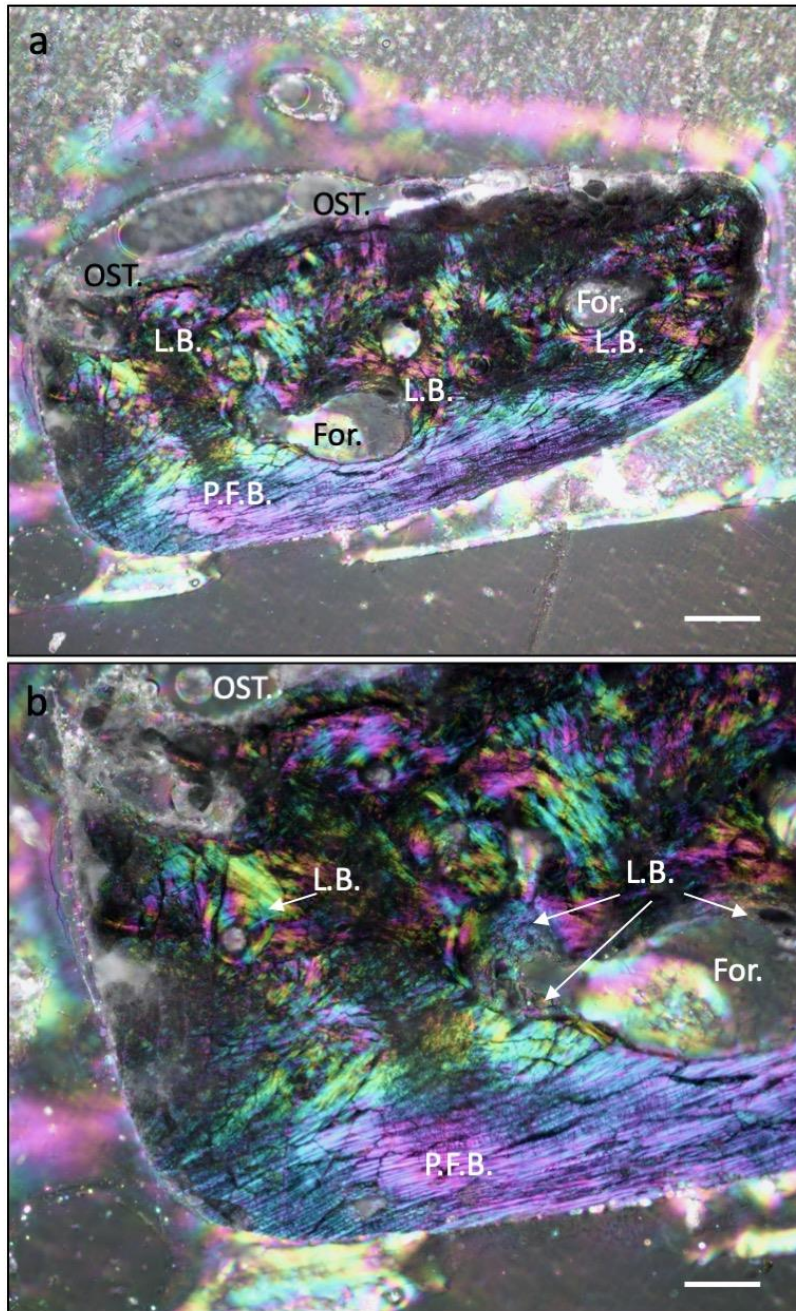
Figure 6.3.7: Transverse, ground section through a Morphotype 1 OD (BL.15.2), visualised with multi-rotation polarised light microscopy at (a) 10x magnification and (b) 20x magnification. For. = foramen, L.B. = lamellar bone, OST. = osteodermine, P.F.B. = parallel-fibred bone.

Scale bars: (a) = 120μm, (b) = 60μm.
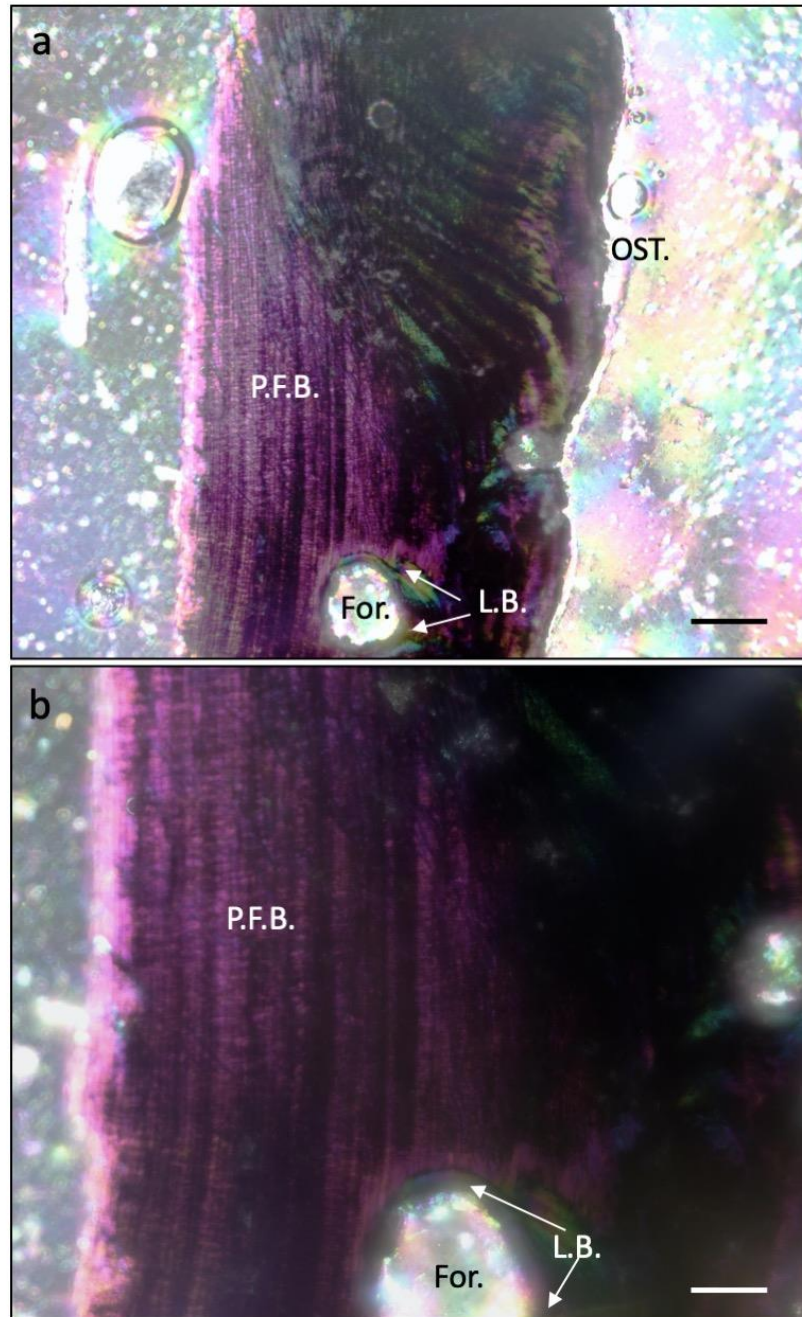
Figure 6.3.8: Transverse, ground section through a Morphotype 1 OD (BL.17.3), visualised with multi-rotation polarised light microscopy at (a) 20x magnification and (b) 40x magnification. For. = foramen, L.B. = lamellar bone, OST. = osteodermine, P.F.B. = parallel-fibred bone.

Scale bars: (a) = 60μm, (b) = 30μm.

6.3.3.2 OD Morphotype 2 Headon Hill:

The keel of HH.1.1 appeared as a raised protrusion in the centre of the superficial surface in transverse cross-section (Fig. 6.3.9). The keel did not seem to be composed of OST., as it was not translucent and glassy. Instead the superficial surface including the keel was composed of P.F.B, as in the basal surface. L.B., with a distinctive scalloped border could also be identified surrounding the internal surfaces of foramina or vascular channels (Fig. 6.3.9, For., L.B.). Thick fibres (much thicker than those of P.F.B. or L.B.) that seamlessly entered the periphery of the OD, perpendicular to the basal surface, originating from the surrounding soft tissue, could readily be observed in these areas, which lead to the identification of S.F.B. (Fig. 6.3.9, S.F.B. and white arrows).
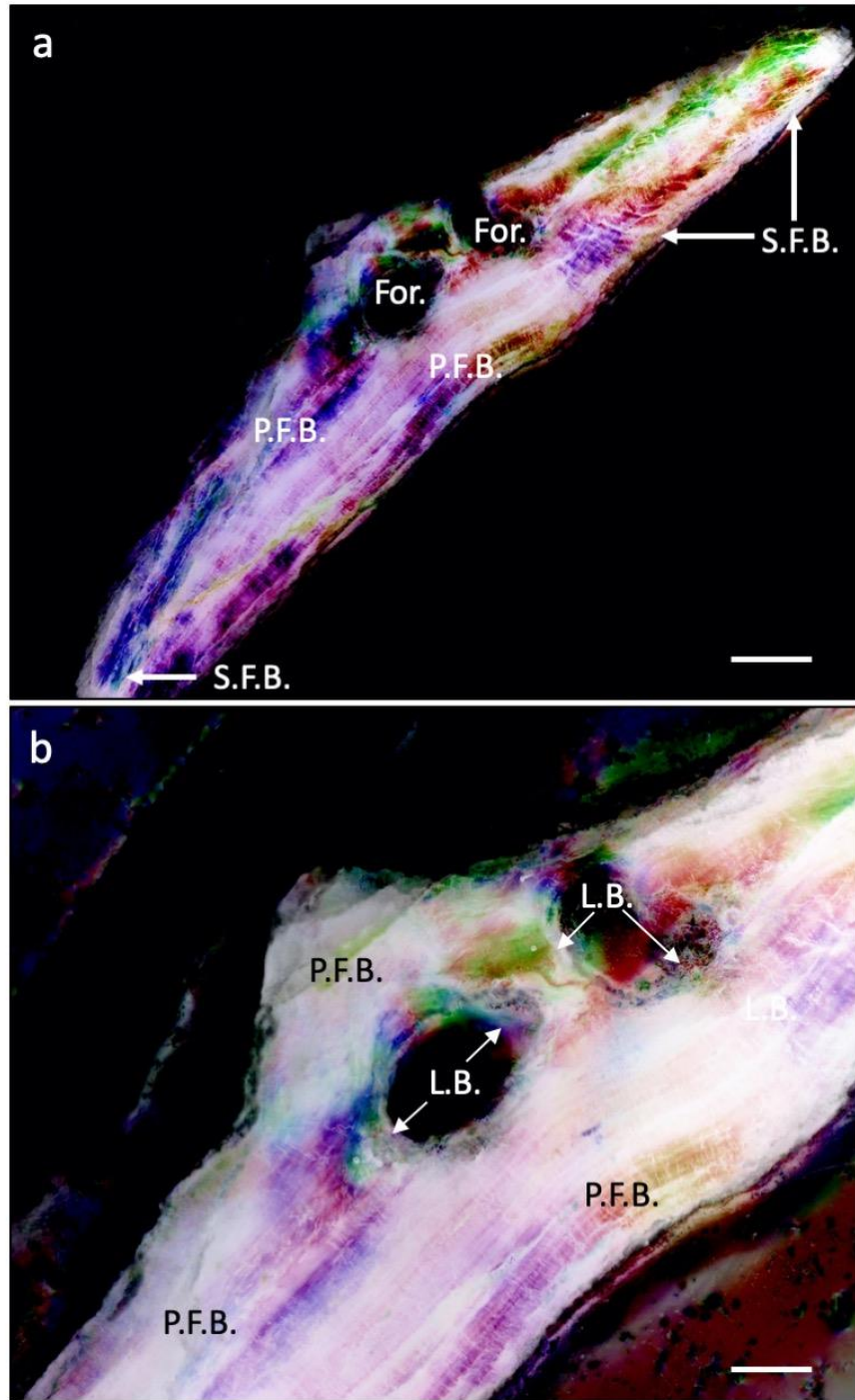
Figure 6.3.9: Transverse, ground section through a Morphotype 2 OD(HH.1.1) visualised with multi-rotation polarised light microscopy at (a) 10x magnification and (b) 20x magnification. The colour in this figure is inverted for better visualisation. For. = foramen, L.B. = lamellar bone, P.F.B. = parallel-fibred bone, S.F.B. = Sharpey-fibred bone .

Scale bars: (a) = 120µm, (b) = 60µm.

6.3.4 BSE-SEM imaging

BSE-SEM imaging complemented the findings of multi-rotation polarised light microscopy to reveal the microstructure of the OD material components.

6.3.4.1 OD Morphotype 1 Bembridge Limestone:

The same tissues, characterised by the same features, were observed in BL.15.2 (Fig 6.3.10) using BSE-SEM imaging as those seen under multi-rotation polarised light. BSE-SEM revealed the same alternating arrangement of light and dark lamellae in the basal layer of P.F.B. and a scalloped border at the edges of L.B. surrounding vascular channels. However, using this technique it was possible to observe increasing tissue density (increased pixel brightness), as well as a reduction in collagen content (fewer visible fibres and more mineral matrix), towards the superficial surface of BL.15.2, leading to the identification of OST. in this region. The tubercles identified using earlier techniques are formed from OST., appearing in the transverse
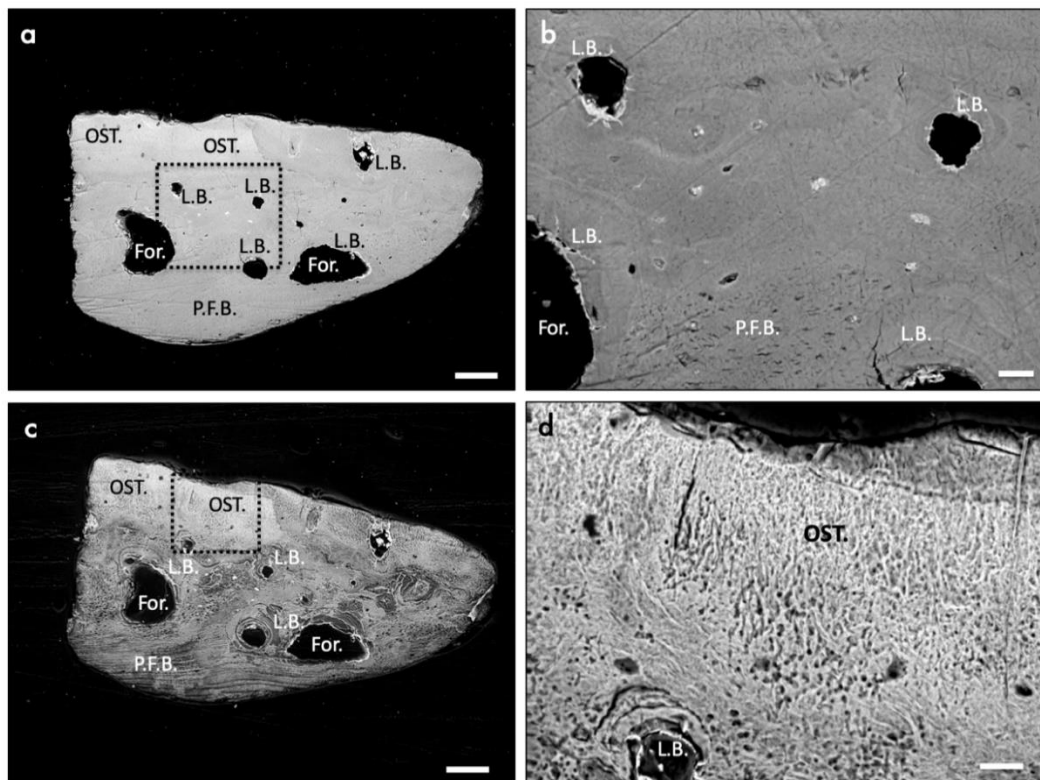
Figure 6.3.10: Ground, polished, transverse section of BL.15.2 imaged with BSE-SEM. (a) = Low magnification view of BL.15.2, (b) = higher magnification view, (c), = low magnification view of BL.15.2, with H_3PO_4 etching, (d) = higher magnification view of BL.15.2, with H_3PO_4 etching. For. = foramen, L.B. = lamellar bone, OST. = osteodermine, P.F.B. = parallel-fibred bone.

Scale bars: (a) = 100μm, (b) = 20μm, (c) = 100μm, (d) = 20μm.

section as the bumps and ridges of the superficial surface. Phosphoric acid etching of the surface revealed greater clarity of topology (compare Fig. 6.3.10a and b to c and d).

BSE-SEM imaging of BL.17.3 revealed long bundles of fibres, oriented in parallel and perpendicular to the surfaces of the extremities of the basal P.F.B. bone layer (Fig. 6.3.11), which confirmed the identification of S.F.B.. These could not be seen when using multi-rotation polarised light (Fig. 6.3.8) and BSE-SEM imaging also revealed
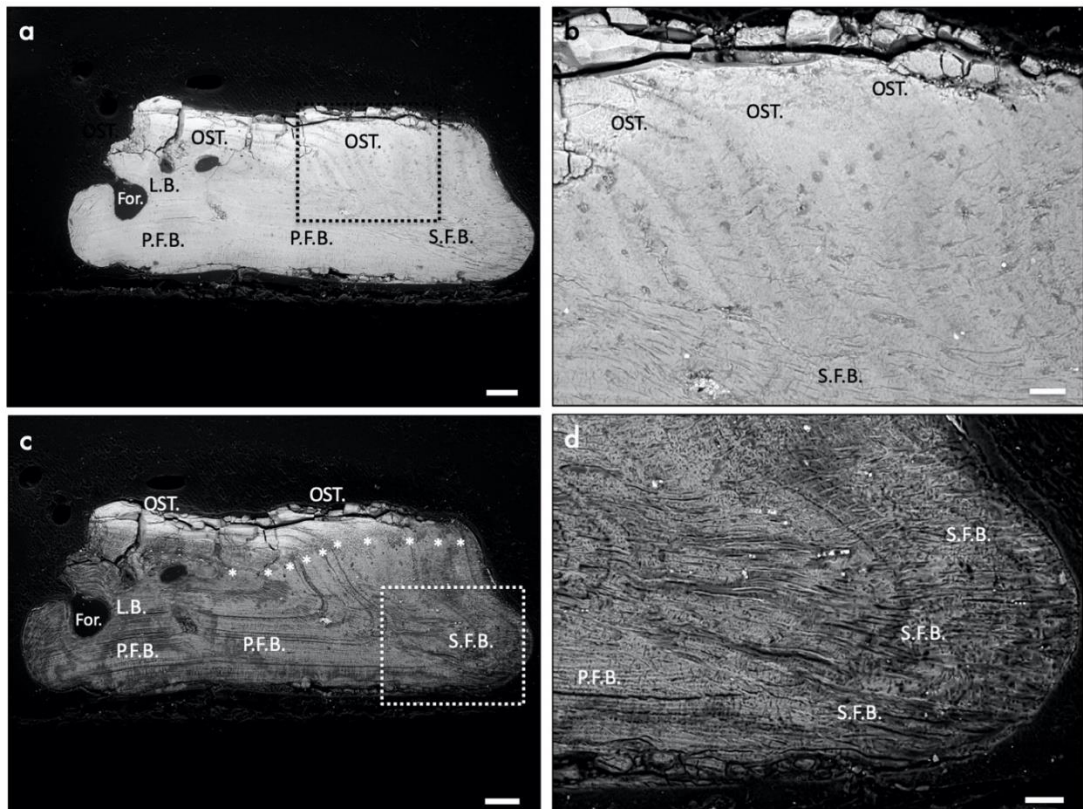
Figure 6.3.11: Ground, polished, transverse section of a Morphotype 1 OD (BL.17.3) imaged with BSE-SEM. (a) = Low magnification view of BL.17.3, (b) = higher magnification view, (c), = low magnification view of BL.17.3, with H_3PO_4 etching, (d) = higher magnification view of BL.17.3, with H_3PO_4 etching. Asterisks = growth lines, For. = foramen, L.B. = lamellar bone, OST. = osteodermine, P.F.B. = parallel fibred bone, S.F.B. = Sharpey-fibred bone.

Scale bars: (a) = 100µm, (b) = 40µm, (c) = 100µm, (d) = 40µm.

more than ten periodic growth lines throughout the basal lamellar layer of P.F.B., the superficial layers of OST. and the S.F.B. of the periphery (Fig. 6.3.11, Asterisks).

6.3.4.2   OD Morphotype 2: Headon Hill

In HH.1.1, BSE-SEM imaging (Fig. 6.3.12), revealed the same tissues that were seen in the earlier multi-rotation polarised light microscopy (Fig. 6.3.9). S.F.B. was located at the lateral margins of this OD, whereas toward the centre, L.B. surrounding vasculature was observed perforating P.F.B. In this sample, the superficial portion, which features a raised keel, was not found to be comprised of OST., as the density
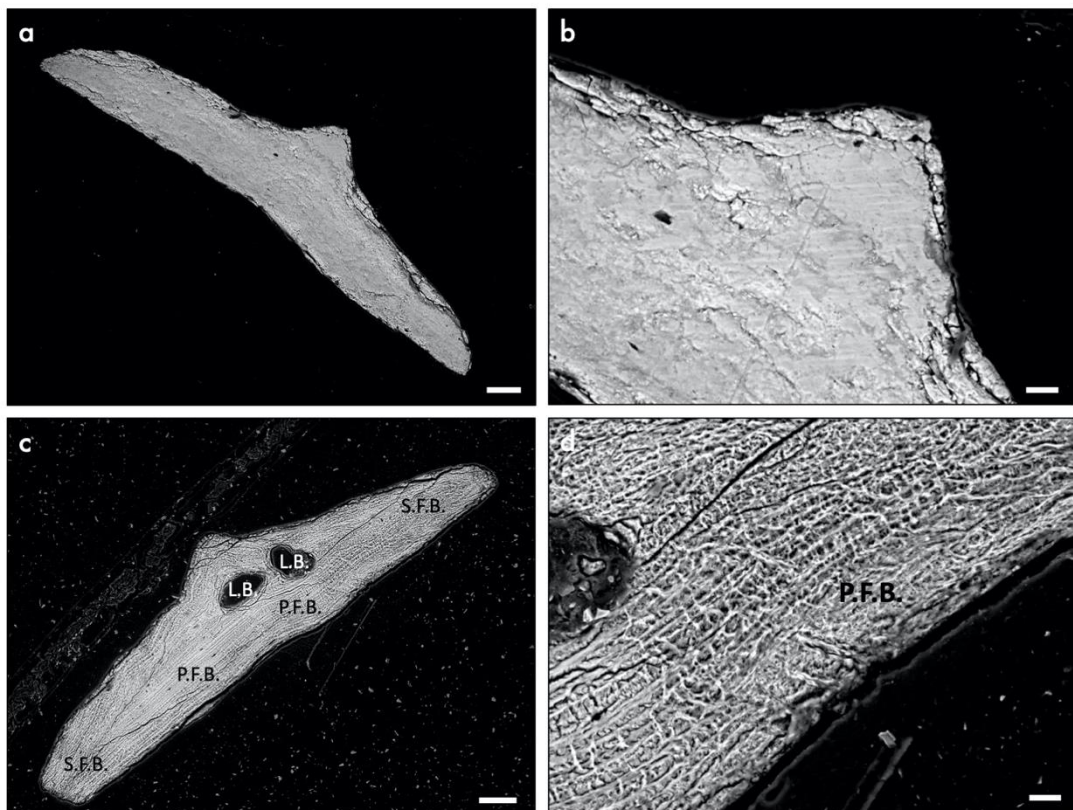
Figure 6.3.12: Ground, polished, transverse section of HH.1.1 imaged with BSE-SEM. (a) = Low magnification view of BL.17.3, (b) = higher magnification view, (c), = low magnification view of BL.17.3, with H_3PO_4 etching, (d) = higher magnification view of BL.17.3, with H_3PO_4 etching. L.B. = lamellar bone, P.F.B. = parallel-fibred bone, S.F.B. = Sharpey-fibred bone.

Scale bars: (a) = 100µm, (b) = 20µm, (c) = 100µm, (d) = 20µm.

of the superficial region matches that of the basal region, confirming the results using

multi-rotation polarised light microscopy. The keel was composed of a compact external cortex, matching findings using multi-rotation polarised light microscopy. L.B. was identified using the previous techniques and was also identified using this technique, BSE-SEM.

6.4 Discussion

6.4.1 Gross morphological anatomy

The ODs from the Bembridge Limestone and Headon Hill could be separated into two distinct morphologies. ODs of morphotype 1 are rectangular, with the dorsal surface divided into ornamented and non-ornamented (articular) regions. The ornamented surface displays glassy tubercles of OST.. ODs of morphotype 2 are lozenge-shaped with a midline keel, and lack tubercles of OST..

As discussed in Chapter 5, ODs can be compound (formed from many units fused together) or non-compound (formed from one unit). Scincids and gerrhosaurid cordyliforms possess compound ODs (Camp, 1923; Richter, 1994). In scincids, compound ODs are found dorsally and ventrally (Camp, 1923; Richter, 1994; Estes et al., 1988). In gerrhosaurids (Camp, 1923; Estes et al., 1988), they have been described as occurring only ventrally. As neither of the OD morphotypes described here were compound, this rules out the possibility of their being from either the ventral side of a gerrhosaurid or a scincid (Estes, 1983; Richter, 1994).

6.4.1.1 Morphotype 1 ODs

Given the presence of the glassy tubercles on the ornamented surface, which were found to be composed of OST., consideration was given to the possibility that these ODs originated from a monstersaur. The clade Monstersauria contains all taxa more closely related to *Heloderma* than *Varanus*. It includes *Heloderma*, as well as several extinct genera, such as *Estesia, Primaderma* and *Gobiderma* (Reeder et al., 2015). Helodermatid ODs are not compound, the texture of the superficial surface is ornamented with tubercles that are fused together and has been termed vermiculate (exhibiting worm-like lines), see Figure 3.6 in Chapter 3. However, the apical surface texture of Morphotype 1 ODs was not vermiculate; the tubercles were separate with no connecting ridges. Moreover, monstersaurian ODs do not imbricate and therefore do not bear articular glide surfaces. Morphotype 1 ODs also lack the hexagonal outline with a ring-extension in the base described for monstersaur ODs (Mead et al., 2012).

Among squamates, a granular ornamentation on the dorsal surface of ODs is restricted to anguid ODs, mainly those of Glyptosaurinae (Hoffstetter, 1962). All known glyptosaurines display rectangular body ODs and ODs from Paleogene glyptosaurine anguids have been described as thin plates, rectangular or hexagonal in outline, depending on the body location (Estes, 1983, Hoffstetter, 1962; Strahm and Schwartz, 1977; Richter, 1994).

The glyptosaurine *Melanosaurus* (from the Palaeogene) is a likely candidate for the Morphotype 1 ODs. The first record of melanosaurin ODs is restricted to a scientific illustration (Hoffstetter, 1962, Fig 3A, B, C), but that image closely resembles the ODs of the glyptosaurine anguid in which OST. was first reported (de Buffrénil, 2011) and also the Morphotype 1 ODs described here. *Melanosaurus* ODs are described as rectangular in outline, with dorsal surfaces bearing ornamented regions of discrete tubercles, and smooth articular surfaces that correspond to the positions of overlapping ODs. Klembara and Green (2010) previously described glyptosaurine *Melanosaurus* ODs from the Bembridge Limestone Formation.

A prominent groove between the gliding surface and the sculptured area of the body OD, first described in *Glyptosaurus* (Meszoely, 1970), is present in all members of the subfamily Glyptosaurinae and in some other anguid subfamilies (Sullivan, 1979). The same groove can be seen in some of the ODs imaged here, labelled "G.". Glyptosaurines and melanosaurines are defined by having characteristic hexagonal cranial and cheek ODs. Because the Morphotype 1 ODs were probably rectangular it is unlikely that they are cranial ODs, as glyptosaur cranial ODs have a unique hexagonal shape.

In glyptosaurs, the size, arrangement, and tubercular pattern of the granular ornamentation can be used in identification as it is different between the Glyptosaurini and the Melanosaurini (Sullivan, 1979). The tubercles of Morphotype 1 ODs were not patterned into concentric rings, making it unlikely that they originated from *Glyptosaurus*, *Paraglyptosaurus*, or *Placosaurus* (Sullivan, 1979). The cranial ODs of *Helodermoides* lack concentric rings of tubercles (Sullivan, 1979; Mead et al., 2012), but are also hexagonal, thus *Helodermoides* is an unlikely candidate.

In conclusion, an attribution to *Helodermoides* is ruled out. The Morphotype 1 ODs can be confidently attributed to the post-cranial ODs of the glyptosaurine *Melanosaurus* and are unlikely to have originated from *Glyptosaurus*, *Paraglyptosaurus*, or *Placosaurus.*

6.4.1.2 Morphotype 2 ODs

Imbricating anguine ODs are known to display well-defined keels (Gauthier 1982; Augé, 2005). Although Morphotype 2 ODs were keeled, their lack of obvious articular surfaces and their more rounded, lozenge shapes mean that they were unlikely to be imbricating, as an articular surface would have been required for smooth biomechanical movement. The presence of high-keeled ODs has been proposed to be a synapomorphy of 'necrosaurs' (Augé, 1986), as is an ovoid or lozenge outline (Augé, 2005). Thus, the lozenge shaped, high-keeled Morphotype 2 ODs probably belonged to a 'necrosaur'. Keeling is confined to the dorsal side of the lizard in necrosaurs and varies in prominence (Augé, 1986). These ODs therefore likely originated from the dorsal side of a 'necrosaur'. Klembara and Green (2010) previously described 'necrosaur' ODs from the Bembridge Limestone Formation using gross anatomical features. This adds weight to the identification of Morphotype 2 ODs as those of 'necrosaurs'. The terminology 'necrosaur' has now been superseded by "*Paleovaranus*" after uncertainty arose as to the monophyly (natural group status) of necrosaurs; they are probably a grade of lizard on the stem of varanoids (Georgalis, 2017).

6.4.2 Microanatomy

The histological structure of ODs has previously been used to classify dinosaurs such as ankylosaurs from incomplete remains (Scheyer and Sander, 2004; Hayashi, 2010). Both the proportions of different kinds of bone, as well as the overall types of bone present, have been used as classification tool (Vickaryous and Sire, 2009). Differences in bone histology of ODs in temnospondyl amphibians, i.e. *Plagiosuchus* compared to *Gerrothorax,* have been interpreted as suggestive of an iterative evolution of ODs (Witzmann and Soler-Gijón, 2010).

Both types of OD described herein show a similar structural arrangement of a strengthened external cortex, either with an OST. capping (Morphotype 1), or a compact bone tissue covering a thick cushion of cancellous (remodelled and spongy) bone (Morphotype 2). More specifically, the cancellous bone base is composed of P.F.B. (in the basal portion) and interspersed in this, are lumens of foramina, which are comprised of L.B.. This mirrors findings of structurally-optimised ODs in many extant squamate taxa (Chapter 5) and other fossilised ODs from non-squamate taxa, for example, as in ankylosaurid and polacanthid dinosaurs (Scheyer and Sander, 2004), rauisuchians (Cerda et al., 2013) and aetosaurs (Cerda and Desojo, 2010).

De Buffrénil et al., (2010) homologised the basal layer of bone in fossil glyptosaurine ODs to that in the extant slowworm *Anguis fragilis*. The same basal layer of bone was observed in the ODs described here and was labelled P.F.B., so as to not cause confusion with the L.B. identified surrounding the endosteal cavities of secondary reconstructions. The tissue L.B. was identified in all of the ODs described here, both from morphotype 1 and morphotype 2. The basal cortex in ODs of aetosaurs and phytosaurs was also found to be composed of P.F.B. (Scheyer et al., 2014), a condition mirroring that of the glyptosaurs. This finding reinforces the theme from earlier chapters that ODs, despite having different gross morphologies, are generally composed of similar micromaterials.

In the peripheral region of ODs of the arboreal scincid *Corucia zebrata*, Moss (1969) observed a "sclerification...intermediate between calcified tendon and bone". The same tissue was described in the gekkonid *Tarentola mauritanica,* for which Levrat-Calviac and Zylberberg (1986) described long, parallel and densely-packed Sharpey's fibres that deeply enter the peripheral (equatorial) regions of the ODs. In *Dasypus novemcinctus* (a xenarthran mammal, the armadillo), the bone occupying the peripheral regions of the ODs can also be regarded as homologous to this tissue (Vickaryous and Hall, 2006). The same tissue (S.F.B.) was identified in the basal regions of *Heloderma suspectum* ODs, and is interpreted as being formed from a process of metaplastic ossification (Chapter 5; Kirby et al., 2020). Due to the similarities of the fibre orientation and location of this material in the ODs sampled here (at the periphery of the basal layer), it was identified as S.F.B.. This adds weight to a hypothesis of metaplastic ossification in the formation of these ODs. The exact process by which the isolated tubercles of OST. are formed, rather than a single, smooth and homogenous layer of OST. as in extant species, is uncertain and elucidating the exact process of OST. tubercle formation will likely require many developmental studies, a rich morphological variety of ODs to analyse from many different localities and time periods and thus likely to require large-scale international collaboration.

When the ODs from extant *Varanus komodoensis* in the previous chapter are compared to the extinct 'necrosaur' ODs described in this chapter, similarities as well as clear differences arise. Neither of the two were found to contain the OST. capping tissue, despite the presence of this capping tissue in the Morphotype 1 ODs. Additionally, in the 'necrosaur' Morphotype 2 ODs, the orientation of the fibres of S.F.B in Fig 6.3.9 is perpendicular to the basal surface, hinting that they are entering

directly from the surrounding tissues. Thus S.F.B. could be identified in the extremities of the ODs, whereas the extant *Varanus* ODs lack S.F.B. *Varanus* ODs are slender, elongate cylinders, slightly bent dorsoventrally. This shape is drastically different to the ovoid, ridged, plate-like ODs of the extinct 'necrosaur' ODs. Because the extinct 'necrosaurs' are thought to be early relatives of the extant *Varanus* genus, these differences in both microstructure and gross anatomy highlight how ODs can change shape and probably development in relatively short periods of geological time. The description of these ODs provided here could represent an intermediate stage in the formation of the more deeply placed (forming within the stratum compactum) ODs of varanoids.

6.4.3 Development

All ODs examined herein by sectioning showed a pattern of perivascular remodelling, i.e., the formation of secondary osteons and endosteal deposits of L.B. on the walls of broad resorption bays created by osteoclast activity. In early growth stages, osseous metaplasia might also have been involved, due to the presence of S.F.B. in the periphery of one OD, but this is not substantiated by any other histological observations. It is likely that the growth of the basal layer of P.F.B. on the deep side of the ODs, and the L.B. surrounding the endosteal cavities of remodelled channels, were the result of the activity of osteoblasts (de Buffrénil et al., 2010). It is obviously impossible to view fossil ODs in the context of surrounding soft tissue. However, given the histological similarities shared by the fossil ODs sampled here to the extant lizard ODs described in earlier chapters (i.e. the presence of S.F.B.), and to accounts of fossilised ODs in the literature, it is likely that the Morphotype 1 glyptosaurine ODs analysed herein using PL and SEM, were formed through an initial stage of metaplastic ossification, followed by remodelling which was mediated with osteoblasts. The presence of mineralised structural fibres (S.F.B.) in both morphotypes sampled here supports the previous hypothesis of metaplastic development and not intramembranous ossification.

6.4.4 Limitations

Care must be taken to ensure that the absence of a tissue is not an artefact of sectioning. Further analysis of the ODs described here would include serial sectioning, to ensure that a good survey of the entire OD has been accomplished, so as to not miss any tissues that may be present in other regions of the OD that were not sectioned. Serial virtual sections can be done with high resolution CT, and a

synchrotron can afford even greater levels of resolution. These techniques were not employed in this work and future use of these techniques is encouraged.

It would have been useful to perform serial sections on all of the ODs and imaged these using polarised light microscopy and scanning electron microscopy, but logistical, economic and time-based restrictions prevented this. An extended study of histology of the different glyptosaurine ODs presented would probably identify the same materials and histological features in all, but differences in the local ratios of these materials might be expected, as the ODs likely originate from different individuals. Thus, care must be taken to control of any expected differences in material ratio and only significant changes in these ratios should be used to inform our understanding of material components.

Differences in the bone microstructure could be related to the age, ontogenetic change, sex and reproductive status of the sampled individuals (Chapter 5). Because these parameters are often difficult to controlled for, caution must be used when interpreting the results presented here.

6.5 Conclusions

The key findings of this chapter are that:

- Despite major differences in gross anatomy, the two morphotypes of fossil ODs analysed here are composed primarily of P.F.B. and L.B.

- Tubercles of OST. were shown to be present in the superficial regions of Morphotype 1 ODs sampled from Bembridge Limestone Formation and from the Headon Hill Formation, whereas this tissue could not be observed Morphotype 2 ODs from the Headon Hill Formation.

- Based on gross anatomy and microanatomical features, both OD Morphotypes were identified as belonging to members of squamate clade Anguimorpha, with Morphotype 1 attributed to glyptosaurines and Morphotype 2 to 'necrosaurs' – a grade group of extinct lizards that may lie on the stem of varanoids.

- A combination of metaplastic and intramembranous ossification is proposed as the developmental path for both types of ODs analysed, based on micromaterial features and a comparison with available literature.

- The Morphotype 1 ODs can be confidently attributed to the post-cranial ODs of the glyptosaurine *Melanosaurus* and the Morphotype 2 ODs are likely to have originated from *Paleovaranus*, a stem-varanoid.

- Overall, limited though this study is, it has shown there is a potential for the study of fossil ODs to contribute to our understanding of the evolution of squamate ODs. For example, an absence of OST. was identified in the ODs of extant *Varanus* species in Chapter 5, and the results from this chapter show that ancestors of modern varanoids also did not exhibit OST. in their osteoderms. The loss of OST. may have been a step in the evolution of a simplified OD but further sampling is required.

6.6   References

Arbour V. M., Burns M. E., Bell P. R. and Currie P. J. (2014) Epidermal and dermal integumentary structures of ankylosaurian dinosaurs. *Journal of Morphology* **275**:39-50.

Augé M. L. (1986) *Les Lacertiliens (Reptilia, Squamata) de l'Eocène supérieur et de l' Oligocène ouest européen.* Thesis: Université Pierre et Marie Curie, Paris, Pp. 218.

Augé M. L. (2005) Évolution des lézards du Paléogène en Europe. *Memoires du Museum national d'Histoire naturelle* 19. Publisher: Publications Scientifiques du Museum Paris. Pp. 369.

Camp C. L. (1923) Classification of the Lizards. *Bulletin of the American Museum of Natural History*, **48:**289-481.

Cerda I. A. and Desojo J. B. (2010) Dermal armour histology of aetosaurs (Archosauria: Pseudosuchia), from the Upper Triassic of Argentina and Brazil. *Lethaia*, **44**:417-428.

Cerda I. A., Desojo J. B, Scheyer T. M. and Schultz C. L. (2013) Osteoderm microstructure of "rauisuchian" archosaurs from South America. *GeoBios* **46**:273-283*.*

Curry Rogers K., D'Emic M., Rogers R., Vickaryous M. K. and Cagan, A. (2011) Sauropod dinosaur osteoderms from the Late Cretaceous of Madagascar. *Nature Communications* **2:**564.

Daley B. and Edwards N. (1990) The Bembridge Limestone (Late Eocene), Isle of Wight, southern England: a stratigraphical revision. *Tertiary Research* **12**:51-64.

De Buffrénil V., Sire J-Y. and Rage J-C. (2010) The histological structure of glyptosaurine osteoderms (Squamata: Anguidae), and the problem of osteoderm development in squamates. *Journal of Morphology* **271**:729-737.

De Buffrénil V., Dauphin Y., Rage J-C. and Sire J-Y. (2011) An enamel-like tissue, osteodermine, on the osteoderms of a fossil anguid (Glyptosaurinae) lizard. *Comptes Rendus de l'Academie des Sciences Palevol* **10:**427-437.

Estes R. (1983) Sauria Terrestria, Amphisbaenia. In: *Encyclopedia of Paleoherpetology*. Editor: Wellnhofer P. Publisher: Gustav Fischer Verlag, Stuttgart, Germany. Pp. 249.

Estes R., De Queiroz K. and Gauthier J. (1988) Phylogenetic relationships within Squamata. In: *Phylogenetic Relationships of the Lizard Families: Essays Commemorating Charles L. Camp*. Editors: Estes R. and Pregill G., Publisher: Stanford University Press, Redwood City, CA, USA. Pp. 119-281.

Gauthier J. A. (1982) Fossil xenosaurid and anguid lizards from the Early Eocene of Wyoming, and a revision of the Anguioidea. *Contributions to Geology, University of Wyoming* **21**:7-54.

Georgalis G. L. (2017) *Necrosaurus* or *Palaeovaranus*? Appropriate nomenclature and systematic content of an enigmatic clade of fossil lizards (Squamata). *Annales de Paléontologie* **103**:293-303

Hayashi S., Carpenter K., Scheyer T.M., Watabe M. and Suzuki D. (2010) Function and evolution of ankylosaur dermal armor. *Acta Palaeontologica Polonica*, **55**:213–228.

Hill R. V. (2010) Osteoderms of *Simosuchus clarki* (Crocodyliformes: Notosuchia) from the Late Cretaceous of Madagascar. *Journal of Vertebrate Paleontology* **30**:154-176

Hoffstetter R. (1962) Observations sur les ostéodermes et la classification des Anguidés actuels et fossiles (Reptiles, Sauriens). *Bulletin du Muséum national d'histoire naturelle*, **34**:149-157

Insole A. and Daley B. (1985) A revision of the lithostratigraphical nomenclature of the Late Eocene and Early Oligocene Strata of the Hampshire Basin, Southern England. *Tertiary Research* **7**:67-100.

Kirby A., Vickaryous M., Boyde A., Olivo A., Moazen M., Bertazzo S. and Evans S. (2020) A comparative histological study of the osteoderms in the lizards *Heloderma suspectum* (Squamata: Helodermatidae) and *Varanus komodoensis* (Squamata: Varanidae). *Journal of Anatomy* **236**:1035-1043.

Klembara J. and Green B. (2010) Anguimorph lizards (Squamata, Anguimorpha) from the Middle and Late Eocene of the Hampshire Basin of southern England. *Journal of Systematic Palaeontology* **8**:97-129.

Levrat-Calviac V. and Zylberberg L. (1986) The structure of the osteoderms in the gekko: *Tarentola mauritanica. American Journal of Anatomy* **446**:437–446.

Long R. A. and Ballew K. L. (1985). Aetosaur dermal armor from the late Triassic of southwestern North America, with special reference to material from the Chinle Formation of Petrified Forest National Park. *Museum of Northern Arizona Bulletin* **47**:45-68.

Main R. P., de Ricqlès A., Horner J. R. and Padian K. (2005) The evolution and function of thyreophoran dinosaur scutes: implications for plate function in stegosaurs. *Paleobiology* **31**:291-314.

Mead J. I., Schubert B. W., Wallace S. C. and Swift S. L. (2012) Helodermatid lizard from the Mio-Pliocene oak-hickory forest of Tennessee, Eastern USA, and a review of monstersaurian osteoderms. *Acta Palaeontologica Polonica* **57**:111-121.

Melville R. V. and Freshney E. C. (1982) *British regional geology: the Hampshire Basin and adjoining areas (4th Edition).* Publisher: HMSO for Institute of Geological Sciences, London, UK Pp. 146.

Meszoely C. A. M. (1970) North American fossil anguid lizards. *Bulletin Museum of Comparative Zoology*, Harvard University **139**:87-149.

Moss M. L. (1969) Comparative histology of dermal sclerifications in reptiles. *Acta Anatomica* **73**:510–533.

Reeder T. W., Townsend T. M., Mulcahy D. G., Noonan B. P., Wood P. L., Sites J. W. and Wiens J. J. (2015) Integrated analyses resolve conflicts over squamate reptile phylogeny and reveal unexpected placements for fossil taxa. *PLoS ONE* **10**: 0118199.

Richter A. (1994) Lacertilia aus der Unteren Kreide von Uña und Galve (Spanien) und Anoual (Marokko). *Berliner geowissenschaftliche Abhandlungen* **14**:1-147.

Scheyer T. M. and Sander P. M. (2004) Histology of ankylosaur osteoderms: implications for systematics and function. *Journal of Vertebrate Palaeontology* **24**: 874-893.

Scheyer T. M., Desojo J. B. and Cerda I. A., (2014) Bone histology of phytosaur, aetosaur, and other archosauriform osteoderms (Eureptilia, Archosauromorpha). *The Anatomical Record* **297**:240–260.

Strahm M. H. and Schwartz A. (1977) Osteoderms in the anguid lizard subfamily diploglossinae and their taxonomic importance. *Biotropica* **9**:58-72

Sullivan R. M. (1979) A revision of the Paleogene genus *Glyptosaurus* (Reptilia, Anguidae). *Bulletin of the American Museum of Natural History* **163**:1-72.

Witzmann F. and Soler-Gijón R. (2010) The bone histology of osteoderms in temnospondyl amphibians and in the chroniosuchian *Bystrowiella*. *Acta Zoologica* (Stockholm) **91**:96–114.

Vickaryous M. K. and Hall B. K. (2006) Osteoderm morphology and development in the nine-banded armadillo, *Dasypus novemcinctus* (Mammalia, Xenarthra, Cingulata). *Journal of Morphology* **267**:1273-1283.

Vickaryous M. K. and Sire J-Y. (2009) The integumentary skeleton of tetrapods: origin, evolution, and development. *Journal of Anatomy* **214**:441–464.

7 CHAPTER 7 Discussion

7.1 Discussion

Osteoderms (ODs) are mineralised organs present in the skin of many tetrapods, including amphibians (extinct fossil forms and some frogs), many reptiles, and a few mammals (e.g. armadillos). In some groups, like Chelonia (tortoises and turtles), ODs are present in all taxa, but in many groups the distribution of ODs is patchy, raising questions as to their functional role.

Squamates (lizards, snakes, and amphisbaenians) are a large and successful reptilian group with more than 10,000 species and a near global distribution. They show a diversity of size and morphology, occupy multiple ecological niches, and have a long evolutionary history (250 Ma+). Osteoderms (ODs) are not found in snakes, but they are found in several families of lizards including Scincidae, Cordylidae, Gerrhosauridae, Anguidae, Lacertidae, Helodermatidae, and Varanidae, where they show variation in expression. However, ODs are only rarely found in two major lizard clades, Iguania and Gekkota, and have not been reported in Teiidae, Gymnophthalmidae, or Amphisbaenia. Thus, squamates are an ideal group in which to study the evolution and function of ODs.

Prior to this study, it was already recognised that squamate ODs were morphologically varied (Moss, 1969; Erickson et al., 2003; de Buffrénil et al., 2010; Paluh et al., 2017). However, among the many major questions that remain about the biology of ODs, it became clear that there was limited knowledge regarding the microstructure of ODs. This is partly due to poor sampling across the wide range of lizard species, as well as past difficulties in imaging OD microstructure quickly, cheaply and efficiently. Moreover, accurate classification of OD micromaterial components was lacking. Consequently, earlier researchers recognised the need for more extensive datasets on the histology of ODs (Moss, 1969; de Buffrénil et al., 2010).

The primary aims and objectives of this thesis (Section 1.6 of Chapter 1) were therefore intended to address the gap in our knowledge of OD microstructure. Additionally, we can ask whether an improved knowledge of OD microstructure might impact on our understanding of OD distribution, development, and function, in the context of ecology and evolution (Vickaryous and Sire, 2009).

The use of different techniques ensured that the data gathered on the microstructure of ODs were replicable. For example, if the same micromaterial was visible within the OD sample using two different types of microscopy, then it is less likely that artefacts would be misinterpreted. Much of the previous work on OD anatomy has relied on the gross anatomy or on simple histological staining and light microscopy. Polarised light microscopy has occasionally been used before (de Buffrénil et al., 2011) but not multi-rotation polarised light and few modern techniques had been applied across a wide range of species in the same study. Some techniques afforded information that other techniques could not provide, for example, in the ODs of *Heloderma* and of fossil taxa, the use of BSE-SEM showed growth lines that were not visible using other techniques. Polarised light microscopy proved to be the best technique for visualising the orientation of collagen fibres, whereas SEM was useful for determining the relative density of a material and for situations requiring higher magnification of features smaller than the resolution of light microscopy.

7.1.1 Do all squamate osteoderms have the same microstructural composition?

The ODs of the American Gila Monster, *Heloderma suspectum*, were examined in order to provide a protocol and a basis for comparison with other lizard taxa. The ODs of *Heloderma suspectum* were examined using multiple techniques, including standard histological staining, BSE-SEM, μ-CT scanning and polarised light microscopy.

Heloderma suspectum ODs were found to be a composite of different materials, including a dense capping material (OST., see 7.1.2), S.F.B., and L.B. (Chapters 3 and 4). These OD materials matched those previously described in the literature (Vickaryous and Hall, 2006, 2008; de Buffrénil et al., 2011; Vickaryous et al., 2015), but with the use of more modern techniques it was possible to characterise them in greater detail. This should help future researchers to identify OD materials at higher resolutions.

The data presented in Chapters 3 and 5 showed that the ODs of all the sampled lizards were composites of P.F.B., W.B, L.B., and, in many cases, S.F.B. and OST.. In Chapter 6, the same tissues were found in the fossil ODs. None of the ODs sampled were formed from just one type of mineralised material.

All squamate ODs analysed here are formed as composite materials, but the type, relative distribution and ratios of materials differed dramatically between species.

7.1.2 Is OST. the dense capping tissue present in *Heloderma suspectum* ODs and is OST. a more widespread material than previously thought?

OST. is a dense, enamel-like tissue first described by de Buffrénil et al., (2011) from a fossil glyptosaur OD, and later described in the gekkotans *Tarentola* annularis and *Tarentola mauritanica* by Vickaryous et al., (2015). The first objectives of the thesis, addressed in Chapters 3 and 4, were to clearly characterise OST.; to determine whether the unusual dense tissue reported to be present in *Heloderma suspectum* ODs (Moss, 1969) is OST.; and then to assess whether OST. is present in all lizard osteoderms.

A combination of MRPLM and SEM confirmed the presence of a dense tissue capping the OD of Heloderma. This tissue matched that originally described (de Buffrénil et al., 2011) as OST., and μ-CT permitted this tissue to be characterised in greater resolution.

As noted above, OST. had only previously been reported on the outer surfaces of ODs from an extinct anguid (glyptosaur) lizard (de Buffrénil et al., 2011) and the gecko *Tarentola annularis* (Vickaryous et al., 2015). In addition to *Heloderma*, the analyses in Chapter 5 found OST. to be present as a capping material in the ODs, *Corucia zebrata* and *Tiliqua rugosa* (Scincidae)*, Elgaria multicarinata* and *Ophisaurus ventralis* (Anguidae)*,* and in *Tarentola annularis* (Gekkonidae), but it was absent in the ODs of *Varanus komodoensis* (Varanidae) and *Timon lepidus* (Lacertidae). As an outgroup comparison, ODs of *Crocodylus* were examined and OST. could not be identified, confirming the observations of previous authors (Vickaryous and Hall, 2008).

The results confirming OST. expression in the ODs of several lizard families challenge the theory that only non-tetrapods (i.e. 'fish') can express hyper-mineralised tissues in the skin (Vickaryous and Sire, 2009). The findings presented here may therefore provide insight into the evolution of mineralised tissues across tetrapods in the future. Observations of OST. tubercles in fossil anguid (glyptosaur) ODs (Chapter 6) as well as in several families of extant lizards (Chapter 5) afforded a comparison of OST. across geological timescales. In the fossil glyptosaur OST. is expressed in tubercles, an in extant taxa OST. varies in its expression from a relatively even thickness (as in *Tiliqua*), to a vermiculate, rough and ridged texture (as in *Heloderma*), and to discrete, small manifestation (in *Corucia*).

7.1.3 Does the macrostructure of ODs provide clues as to their function and/or development?

The most recent papers published on OD function focus (Broeckhoven et al., 2017; Schucht et al., 2020) on gross anatomy, size and shape of ODs, fluctuating asymmetry, or anatomical location of expression (e.g. cephalic, dorsal, ventral).

In terms of gross morphology, squamate ODs are known to vary, both in shape and in the density and pattern of their distribution across the body (Camp, 1923). The use of whole body HRXCT scanning provides a way to examine OD patterning, both in adults and juveniles, as well as detailed observation of individual ODs (as in Chapter 5). To date, this approach has been taken by relatively few authors (Stanley et al., 2016, Broeckhoven et al., 2017) but is clearly an area that requires further work as it has the potential to reveal patterns that may be developmentally, phylogenetically, or functionally significant, and may yield surprises (as in the case of simple vs compound ODs, see below).

From a developmental perspective, whole body scans of individual taxa from hatchling to full adult would provide important data as to where and when ODs are first expressed. Both *Ophisaurus* and *Varanus* were shown to express fully mature ODs relatively late in post-hatchling development (Chapter 5), and similar observations have been made by other authors (Laver et al., 2019). Similarly, a side project by the UCL group on OD regeneration in the autotomised tails of the gecko *Tarentola* found that although ODs regenerated fully, their patterning was different between original and regenerated tails – suggesting a role for the paraxial mesoderm in patterning. This matches findings by other authors (Vickaryous et al., 2015).

Gross morphology of ODs does appear to have a phylogenetic signal at several levels. The first is in the presence or absence of ODs. ODs are found in almost all scincoid and anguimorph lizards, and are found in the head but not body of many lacertids. However, they are unrecorded in any teiioids, and are known in only three genera of geckos and two of iguanians. The ODs of scincoids and many anguimorphs form a complete tile-like covering across the body (e.g. Figure 5.56) that must be protective in function, whereas in *Varanus* and the related *Lanthanotus*, these plates have been reduced to a mesh of spindles.

At the level of individual ODs, the HRXCT scanning analysis outlined in Chapter 5 also demonstrated the potential to overturn some current hypotheses. One such feature is the presence of compound versus simple ODs. Scincoid lizards have been

characterised by the possession of compound ODs (Camp, 1923), whereby a single OD plate (as related to one epidermal scale) is composed of a mosaic of smaller units. Unexpectedly, HRXCT analysis of *Elgaria multicarinata*, an anguid lizard from the subfamily Gerrhonotinae, showed that it also has compound ODs, although a second anguid lizard (*Ophisaurus*, subfamily Anguinae) did not. Similarly, HRXCT found the ODs under a single scale of the gekkotan *Tarentola* to be made up of clusters of smaller subunits. This further highlights the need for more data on the macroscopic as well as microscopic structure of ODs across squamates.

The most commonly hypothesised function of ODs is as defensive armour against predators (Moss, 1972; Seidel, 1979; Vickaryous and Sire, 2009; Vickaryous et al., 2015), so much so that the terms 'osteoderms' and 'armor' are sometimes used as synonyms (Yang et al., 2012). While it may be true that many ODs exist to reinforce the structural rigidity and mechanical toughness of the skin, restraint should be used when using the term armour to avoid any oversimplification that may be misleading. In crocodilians for example, the ODs are expressed ubiquitously in adults while being absent in hatchlings, despite the fact that adults rarely experience predation (Vickaryous and Sire, 2009; English, 2018). This might suggest that OD expression is inversely correlated to predation - exactly the opposite of what is expected if the function of ODs were to protect from predation. The same finding is alluded to by Maisano et al., (2019) in their study of *Varanus komodoensis* hatchlings compared to adults. However, this assumes that the only danger to an animal comes from predators. Adults are just as likely to need protection from conspecifics during territorial and other such encounters (e.g. *Crocodylus*, English, 2018; *Gekko*, Laver et al., 2019; *Varanus*, Maisano et al., 2019), or even from their prey (e.g. *Tarentola*; Vickaryous et al., 2015). Investigating the role of predation in shaping body armour is important because the possession of body armour has consequences. For instance, it greatly reduces the sprinting capacity in cordylid lizards (Losos et al., 2002). Evolutionary pressures on a slow moving insectivorous lizard (e.g. *Tiliqua rugosa*) would likely result in the expression of a heavy cover of ODs (as was observed in this study) to confer a function as protective armour, however a fast-moving predator that requires flexibility (e.g. *Varanus komodoensis*) would be handicapped by a thick cover of plate-like ODs and would be expected to show reduction in their expression (shown in this study and previous references e.g. Maisano et al., 2019).

The ODs of some taxa have been shown to be structurally inadequate to act as armour (de Buffrénil et al., 1986; Main et al., 2005; Marinho, 2007), even though this

might originally have been assumed. In crocodiles, ODs have been shown to reduce flexibility during locomotion (Frey 1988; Losos et al., 2002), although they may stabilise the vertebral column, alleviating some stress on muscles and joints during locomotion on land (Frey, 1988). The absence of OD expression, for example in the skull of *Lanthanotus*, has also been linked to greater cranial kinesis or auditory reception (Maisano et al., 2002). In *Gekko gecko*, Laver et al (2019) have argued that OD distribution, limited to the head with scattered small elements on the dorsum of the trunk (e.g. Fig. 5.16, Chapter 5), argues against any physiological role (thermoregulation, water loss). Instead, the OD layer forms a dorsal cephalic shield that may protect from agonistic behaviours (Vickaryous et al., 2015). Similarly, large lacertid lizards, such as *Timon Lepidus* (Fig. 5.59, Ch.5), has ODs limited to the sides of the skull. These too are more likely to provide protection during agonistic biting. A similar suggestion was made for the lateral cranial ODs described in *Hongshanxi*, a Jurassic lizard (~160 Ma) from China (Dong et al., 2019).

Paluh et al., (2017) proposed that lizard ODs might also function as additional reservoirs of calcium. It has also been proposed for alligators as a store of calcium for eggshell production (Dacke et al., 2015). ODs could store calcium during 'good times', but still provide a source of calcium during pregnancy.

7.1.4 Does the microstructure of ODs provide clues as to their function and/or development?

The results presented in Chapters 3-5 demonstrate that squamate ODs are constructed from several different tissue types: a dense external covering of OST., a variably distributed region of P.F.B., and a, usually deep, layer of S.F.B.. This raises questions as to how these components were formed and then came together during development, and the specific mechanisms by which ODs develop are hotly debated (Zylberberg and Castanet, 1985; Levrat-Calviac and Zylberberg,1986; de Buffrénil et al., 2010).

While a comprehensive answer to this question will likely require extensive developmental data, the results from Chapters 3 -5 provide some starting points.

S.F.B. is characterised as only appearing in mineralisations that directly incorporate fibres from the surrounding soft tissue. It is thus said to form metaplastically (Haines and Mohuiddin, 1968; de Buffrénil et al., 2010), and metaplastic ossification has been

proposed as one of the main mechanisms for OD formation (Vickaryous and Sire, 2009; Vickaryous et al., 2015). In sections of *Heloderma suspectum OD*, particularly those taken with multi-rotation polarised light (MRPLM), S.F.B. was clearly seen in the base and the periphery of OD sections. Individual fibres can be traced from the embedding soft tissue into the osteoderm, with a fairly sharp boundary between the hard and soft parts. Similar material was seen in almost all of the lizard ODs.

P.F.B. was observed in the *Varanus komodoensis* ODs analysed here. It is thought to result from remodelling of the S.F.B. (de Buffrénil et al., 2010) after an initial metaplastic formation. The use of MRPLM aided in this identification as it depicted the lamellar arrangement of collagen in this region very clearly (Fig. 5.20), compared to the S.F.B. of other lizards, for example, *Heloderma suspectum* (Fig. 4.2c) or *Tarentola annularis* (Fig. 5.12). The term P.F.B. was also used to describe the 'basal lamellar layer' of *Tiliqua rugosa* and *Ophisaurus ventralis* ODs as well as the basal layers of the fossil Morphotype 2 ODs, as there was no evidence that these fibres were Sharpey's fibres (in that they could not be observed to travel from soft tissue surroundings into the mineralised OD), yet displayed a regular repeating orientation.

W.B. was identified in the core of *Varanus komodoensis* ODs. This material is characterised by large fibres without any form of orientation (not lamellar rings surrounding a lumen, nor parallel large fibres). The core of the *Varanus komodoensis* ODs was the only area in which this tissue was located.

However, in a majority of the lizard ODs examined, these two fibrous bone components (S.F.B. or P.F.B.) were capped by a layer (continuous or discontinuous) of dense enamel-like OST.. It has been suggested that OST. formation requires an interaction with the epidermis, but there is currently little data as to when this occurs during development nor which cells are responsible for doing so (de Buffrénil, 2010, 2011).

Nonetheless, in another anguimorph lizard, *Varanus komodoensis*, neither OST. nor S.F.B. could be identified. Instead, the reduced, spindle-like ODs of *Varanus* were composed of P.F.B. surrounding W.B. (Kirby et al., 2020). This suggests that in these two relatively closely related lizards, *Heloderma* and *Varanus*, ODs develop in different ways. If OST. deposition requires close contact with the epidermis (de Buffrénil et al., 2011), then its absence in *Varanus* could be explained by the deeper position of these ODs within the skin. Why they also lack S.F.B., and thus lack the close connection with the surrounding fibrous soft tissue remains unclear, but it is

likely to be a secondary (derived) feature of *Varanus*. The presence of S.F.B. in the ODs of the fossil stem-varanid (Chapter 6) provides support for this. The same replication of the pre-existing collagen pattern was not seen in extant *Varanus komodoensis* ODs.

To explore this further, it would be necessary to sample ODs at regular time points throughout ontogeny, using a growth series of skin samples from each species. The same techniques outlined in this thesis could be applied to these samples, including histological staining and SEM to understand which materials are present and their order of appearance, as well as µ-CT scans to provide three-dimensional views of OD development in high resolution. To determine how the materials form and are patterned will ultimately require the application of techniques from molecular and cell biology such as immunohistochemistry to target proteins and techniques to target nucleic acids and gene targets. These include techniques such as qPCR and RNA sequencing, although the transcriptome of lizards is relatively poorly annotated - only in the last five years have studies been published that attempt to annotate the transcriptome (Trapanese et al., 2017; Maldonado et al., 2020). The gene control for ODs is currently not understood and further work on gene regulation of osteoderm expression is highly recommended. It may be that the same cellular population produces all the materials in the OD, but it is unlikely, given the difference in structures, and the hyper-mineralised nature and non-collagenous matrix of OST..

The use of multi-rotation polarised light microscopy (MRPLM), developed by Professor Alan Boyde at Queen Mary's, was particularly valuable in imaging the sections of osteoderms. It is a substantial improvement on previous black and white polarised light techniques (without rotation of the polarising filters) which were previously standard for studying OD histology (de Buffrénil, 2010). MRPLM enables rapid visualisation of the orientation of the collagen fibres within the OD section. With this novel technique, the colour of the collagen fibres in the final image was representative of the relative orientation. It allowed the direct observation, in one micrograph, of pre-existing patterns of collagen replicated in the mineralised portion of the *Heloderma suspectum* OD, affording an unprecedented view into the relationship between hard and soft tissues.

Heterotopic ossification (HO) is the abnormal, pathogenic formation of bone in soft tissues. There are several inherited forms of HO, including fibrodysplasia ossificans progressiva (FOP), progressive osseous heteroplasia (POH), and Albright's hereditary osteodystrophy. Several recent studies implicate altered bone

morphogenetic protein (BMP) signaling as a primary cause of FOP. In spite of this progress, the pathophysiology of HO remains unclear. In HO, the process of bone formation itself appears to be normal, but the temporal and spatial patterns of skeletogenesis are aberrant. Although the specific mode of OD ossification varies, all ODs develop from within connective tissues that possess latent skeletogenic potential. Whether the variation in OD morphology, expression and distribution in closely related lizard species involves the same genes implicated in human HO pathologies, or undiscovered genes, remains unknown (Albertson et al., 2009). The findings presented in Chapter 5, which indicate that the majority of extant lizards form ODs metaplastically from pre-existing collagen fibres of the dermis, increase our knowledge of OD development in these squamates and in turn, may help to provide a better model to understand the onset and progression of pathogenic diseases in humans (Dubansky and Dubansky, 2018).

The composite structure of most ODs raised questions about how ODs develop, but it also begs the question as to whether OD microstructure relates to function and whether or not the proportions of different tissues in the ODs of different lizards have any functional significance.

7.1.4.1 Finite element modelling of CT scan data

In order to explore why the ODs of *Heloderma* might be structured as they are, the UCL OD team (Iacoviello et al., 2020) developed a 3-D computer model of a single *Heloderma* OD from high resolution CT scans. Multiple mechanical loading scenarios were simulated by finite element modeling, with a uniform force (Fig. 7.1.1b) or a uniform displacement (Fig. 7.1.1c) applied to the superficial surface. In the first instance, the OD was simulated as being composed only of L.B.; in the second, as composed of a fibrous material akin to S.F.B.; in the third as composed entirely of osteodermine; and in the final scenario, the OD was simulated as it appears in nature – as a composite of all three materials (Fig 7.1.1). The results showed that if the ODs were formed out of a single tissue, they would not disperse forces as well as ODs formed out of a composite of tissues. The natural state was the best arrangement for dispersion of stresses and strains, with a composite structure being the most effective in avoiding mechanical failure of the OD (Iacoviello et al., 2020).
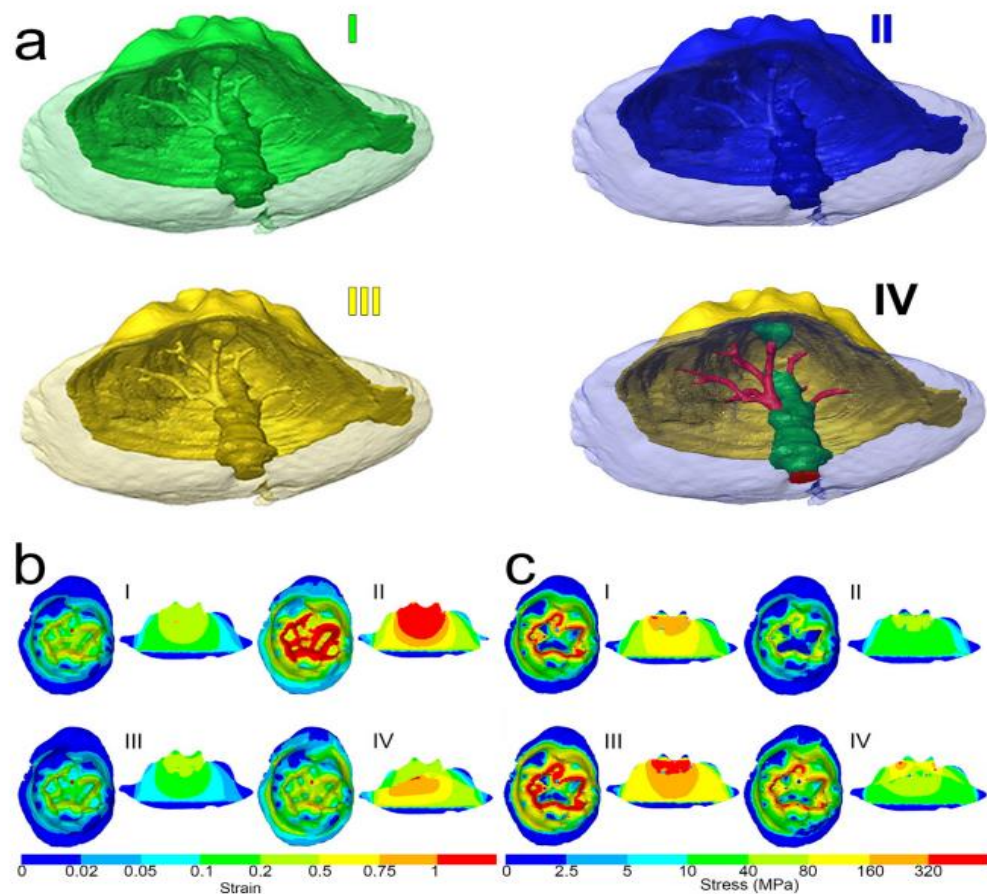
Figure 7.1.1: Finite-element simulations of four mechanical loading scenarios applied to a *Heloderma suspectum* OD, hypothetically composed of (aI) lamellar bone, (aII) Sharpey-fibred bone, (aIII) osteodermine, and (aIV) the actual composition. Stiffness values measured by atomic force microscopy (A.F.M.) were used to test distribution of strain and stress under application of force (b) or displacement (c) obtained by finite element analysis (Adapted from Iacoviello et al., 2020)

Therefore, the arrangement and proportions of the different materials may provide clues as to the function of the OD. Nano-indentation showed that S.F.B. was the most flexible, followed by L.B., then OST. *Heloderma suspectum* ODs contain a stiff capping tissue of OST as part of the composite material. In contrast, *Varanus komodoensis* ODs lack both of these attributes. Therefore, *Heloderma* ODs are proposed to have more of a protective function, better at dispersing forces in comparison to the *Varanus* ODs. This is likely to be due to the different ecological niches occupied by these lizards. *Varanus* is more of an apex predator, thus would require flexible integument for chasing prey, with *Heloderma* requiring strong, firmly embedded ODs as it is slow, sluggish and defensive. The results of Iacoviello et al.,

(2020) suggest that ODs made of a composite material are likely to confer a protective function, whereas those that are more homologous in their structure are less likely to. This would need to be tested using similar simulations for other ODs. The results of such simulations could inform the fabrication of flexible, yet strong and durable bio-inspired materials.

However, it is possible that ODs may also be providing an additional hematopoietic function (production of red blood cells, as in the bone marrow of the endoskeleton). In *Heloderma*, and several of the other lizards sampled, including the imbricating ODs of *Corucia* and *Ophisaurus*, the ODs were seen to contain neurovascular channels and/or where these channels became enlarged, a substance resembling bone marrow. A similar suggestion was made recently (Schucht et al., 2020) in a study of the miniaturised chameleon *Brookesia perarmata* in which ODs were described for the first time*.

7.1.5 Evolutionary history of ODs

This thesis focused mainly on OD microstructure rather than attempting a comprehensive survey of OD distribution and evolution. Nonetheless, it is clear that ODs are widely distributed across squamates and their occurrence in early diverging groups like the gekkotans (albeit rarely) and scincoids suggest that the potential to develop dermal mineralisations is a primitive trait within Squamata, with losses in snakes, amphisbaenians, teiioids, and most iguanians. This is supported by the finding of ODs in several Jurassic squamates (Conrad et al., 2013; Dong et al., 2019). Nonetheless, ODs are reported in only one representative (*Pamizinsaurus*) of Rhynchocephalia, the sister group of Squamata, Why ODs are common in squamates but rare in rhynchocephalians is unclear. One possibility would be that the potential to produce ODs arose in the stem of Squamata, with *Pamizinsaurus* being an exceptional case. The absence of ODs in any known stem lepidosaur (the group encompassing Rhynchocephalia and Squamata) might seem to support this. However, there are very few known examples of early lepidosaurs and, with a few exceptions, most are fragmentary.

A wider survey across reptiles shows that the ODs are widespread. They are found in many groups of archosauromorphs (the sister group to lepidosaurs and their stem), including crocodiles and many dinosaurs (but not birds), turtles, and many stem groups, and they are found in other parts of the reptilian tree (e.g. the parareptile parieasaurs and procolophonids), a few mammals, many several groups of amphibians. Fish also, of course, express many different types of mineralised tissue

in their skins. Thus, a tendency to form dermal mineralisations is considered to be primitive (Vickaryous and Sire, 2009) for vertebrates, but is clearly a trait that can be switched on and off in different lineages.

7.2 Major limitations and future outlook

For most species, only a single specimen was sampled for tissue analysis. Factors such as age, reproductive status or gender of the specimens were not controlled for, except in a few taxa (e.g. *Ophisaurus*) for which one juvenile and one adult were available. Although there has been some work on intraspecific variation of ODs (Broeckhoven et al., 2017), more work targeting multiple individuals (male/female; developmental stages; different ecologies) of the same species would help our understanding of variations in expression.

OD expression varies across anatomical locations on the body of lizards, and although time was taken to ensure that multiple body locations were sampled for *Heloderma suspectum*, in other taxa only the skin of the post-cranial dorsum was sampled. Therefore, the results are limited by the anatomical location sampled. Future studies should document the variation of micromaterial and gross anatomical features of ODs around the body.

Additionally, from the taxa sampled, fewer than ten sections were taken from each sample for imaging. This was the same for all the techniques used that required sectioning (MRPLM, BSE-SEM and standard histological staining). Serial sectioning was attempted but unsuccessful. This technique affords a 3D view of tissue by imaging multiple sections taken at the same distance apart and collating them into a series.

The study sampled, at most, two genera from any family and at most two species from any genus. Therefore, more taxon sampling is required to better understand the variation between genera in the same family. Further studies should consider the variation of OD expression around the body in different anatomical locations, any variations that exist between males and females, the variations that occur through ontogeny from juvenile to adult, as well as any variation in OD expression that might rise due to environmental conditions or individual differences.

Two morphotypes of relatively recent fossil squamate ODs were sampled, but further sampling of ODs from much earlier fossil taxa will also help to elucidate the evolutionary history of ODs.

Other modern physio-chemical techniques could be applied to the research of ODs and other mineralised tissues, such as X-ray photoelectron spectroscopy (XPS). This technique affords comparative, quantitative analysis of the elemental composition of a sample, which is likely to produce significant differences between the materials present, due to differences in collagen fibre content, mineral content and matrix composition. More datasets on the elemental composition of OD materials are welcomed in order to define these materials more specifically.

A contribution from the epidermis in the development of OST. was proposed by de Buffrénil et al., (2011), but further research is needed to establish which populations of cells are responsible for the development, and sculpturing of OST., as well as the molecular signaling mechanisms responsible for cell-mediated bone growth in the ODs of lizards, and the sequence of tissue deposition in these multi-layered structures.

Sampling of both OST. expressing taxa and non-OST. expressing taxa would be advised for the focus of further work. More modern methods yield the best results for the least time and resources, but older methods such as histological staining combined with more modern high-resolution slide scanning were also proven in this study to depict tissue contents clearly in digitised format, despite this technique being resource and time-intensive compared to modern techniques such as CT scanning.

To properly test the function of osteoderms, it would be highly important to sample wild species, which are exposed to natural prey, predators and environments. This study only sampled domesticated zoo animals. Thorough observation of both OD-expressing taxa and non-OD-expressing taxa in their natural environments, it may be possible to deduce the function of osteoderms in these taxa through comparison to their material components and overall gross anatomy.

This project was part of a larger study of ODs and many of the other questions (function, development, material properties) are being addressed in a wider project (Human Frontier Science Program, RGP0039/2019).

7.3   References

Albertson R. C., Cresko W., Detrich H. W., and Postlethwait J. H. (2009) Evolutionary mutant models for human disease. *Trends in Genetics* **25**:74-81.

Broeckhoven C., De Kock C. and Mouton P. (2017) Sexual dimorphism in osteoderm expression and the role of male intrasexual aggression. *Biological Journal of the Linnean Society* **122**:329-339.

Camp C. L. (1923) Classification of the Lizards. *Bulletin of the American Museum of Natural History* **48:**289-481.

Conrad J. L., Wang Y., Xu X., Pyron A. and Clark J. (2013) Skeleton of a heavily armored and long-legged Middle Jurassic lizard (Squamata, Reptilia). *Supplement to the online Journal of Vertebrate Paleontology* 73rd Annual Meeting, Abstracts. Pp. 108.

Dacke C. G., Elsey R. M., Trosclair P. L., Sugiyama T., Nevarez J.G. and Schweitzer M. H. (2015) Alligator osteoderms as a source of labile calcium for eggshell formation. *Journal of Zoology* **297**:255-264.

De Buffrénil V., Farlow J. O. and de Ricqlès A. (1986) Growth and function of *Stegosaurus* plates: evidence from bone histology. *Paleobiology* **12**:459-473.

De Buffrénil V., Sire J-Y. and Rage J-C. (2010) The histological structure of glyptosaurine osteoderms (Squamata: Anguidae), and the problem of osteoderm development in squamates. *Journal of Morphology* **271**:729-737.

De Buffrénil V., Dauphin, Y., Rage, J-C. and Sire, J-Y. (2011) An enamel-like tissue, osteodermine, on the osteoderms of a fossil anguid (Glyptosaurinae) lizard. *Comptes Rendus de l'Academie des Sciences Palevol* **10:**427-437.

Dong L. P., Wang Y., Mou L., Zhang G. and Evans S. E. (2019) A new Jurassic lizard from China. *Geodiversitas* **41**:16.

Dubansky B. H. and Dubansky B. D. (2018) Natural development of dermal ectopic bone in the american alligator (*Alligator mississippiensis*) resembles heterotopic ossification disorders in humans. *The Anatomical Record* **301**:56–76.

Erickson G. M., Ricqlès A., de Buffrénil, V. de, Molnar R. E. and Bayless M. K. (2003) Vermiform bones and the evolution of gigantism in *Megalania* — How a reptilian fox became a lion. *Journal of Vertebrate Paleontology* **23**:966-970.

English L. T. (2018) Variation in crocodilian dorsal scute organization and geometry with a discussion of possible functional implications. *Journal of Morphology* **279**:154-162.

Frey E. (1988) The crocodile support system - a biomechanical and phylogenetic analysis. *Stuttgart Contributions to Natural History Series A (Biology)* **426**:1-60.

Haines R. W. and Mohuiddin A. (1968) Metaplastic Bone. *Journal of Anatomy* **103**:527–38.

Iacoviello F., Kirby A.C., Javanmardi Y., Moeendarbary E., Shabanli M., Tsolaki E., Sharp A.C., Hayes M.J., Keevend K., Li J.H., Brett D.J., Shearing P.R., Olivo A., Herrmann I.K., Evans S.E., Moazen M. and Bertazzo S. (2020) The multiscale hierarchical structure of *Heloderma suspectum* osteoderms and their mechanical properties. *Acta Biomaterialia.* **197**:194-203.

Kirby A., Vickaryous M., Boyde A., Olivo A., Moazen M., Bertazzo S. and Evans S. (2020) A comparative histological study of the osteoderms in the lizards *Heloderma suspectum* (Squamata: Helodermatidae) and *Varanus komodoensis* (Squamata: Varanidae). *Journal of Anatomy* **236**:1035-1043.

Laver R. J., Morales C. H., Heinicke M. P., Gamble T., Longoria K., Bauer A. M. and Daza J. D. (2019) The development of cephalic armor in the tokay gecko (Squamata: Gekkonidae: *Gekko gecko*). *Journal of Morphology* **281**:213-228.

Levrat-Calviac V. and Zylberberg L. (1986) The structure of the osteoderms in the gekko: *Tarentola mauritanica* **446**:437–46.

Losos J. B., Mouton P. L. F. N., Bickel R., Cornelius I. and Ruddock L. (2002) The effect of body armature on escape behaviour in cordylid lizards. *Animal Behaviour* **64**:313-321.

Main R. P., de Ricqlès A., Horner J. R., Padian K. (2005) The evolution and function of thyreophoran dinosaur scutes: Implications for plate function in stegosaurs. *Paleobiology* **31**:291–314.

Maisano J. A., Bell C. J., Gauthier J. A. and Rowe T. (2002) The osteoderms and palpebral in *Lanthanotus borneensis* (Squamata: Anguimorpha). *Journal of Herpetology* **36**:678–682.

Maisano J. A., Laduc T. J., Bell C. J. and Barber D. (2019) The cephalic osteoderms of *Varanus komodoensis* as revealed by high-resolution X-ray computed tomography. *The Anatomical Record* **302**:1675–1680.

Maldonado J. A., Firneno T. J. Jr., Roelke C. E., Rains N. D., Mwgiri J. and Fujita M. K. (2020) Transcriptome sequencing reveals signatures of positive selection in the Spot-Tailed Earless Lizard. *PLoS ONE* **15**:e0234504

Marinho T. D. S. (2007) Functional aspects of titanosaur osteoderms. *Anuario Do Instituto de Geociencias* **30**.

Moss M. L. (1969) Comparative histology of dermal sclerifications in reptiles. *Acta Anatomica* **73**:510–533.

Moss M. L. (1972) The vertebrate dermis and the integumental skeleton. *American Zoologist* **12**:27–34.

Paluh D. J., Griffing A. H. and Bauer A. M. (2017) Sheddable armour: identification of osteoderms in the integument of *Geckolepis maculata* (Gekkota). *African Journal of Herpetology* **66**:12-24

Schucht P. J., Rühr P. T., Geier B., Glaw F. and Lambertz M. (2020) Armored with skin and bone: The integumentary morphology of the Antsingy leaf chameleon *Brookesia perarmata* (Iguania: Chamaeleonidae). *Journal of Morphology* **280**:214–244.

Seidel M. R. (1979) The osteoderms of the American alligator and their functional significance. *Herpetologica* **35**:375-380.

Stanley E., Ceríaco L., Bandeira S., Valerio H., Bates M. and Branch W. (2016) A review of *Cordylus machadoi* (Squamata: Cordylidae) in southwestern Angola, with the description of a new species from the Pro-Namib desert. *Zootaxa* **4061**:201–226.

Trapanese M., Buglione M., Maselli V., Petrelli S., Aceto S., Fulgione D. (2017) The first transcriptome of Italian wall lizard, a new tool to infer about the island syndrome. *PLoS ONE* **12**:e0185227.

Vickaryous M. K. and Hall B. K. (2006) Osteoderm morphology and development in the nine-banded armadillo, *Dasypus novemcinctus* (Mammalia, Xenarthra, Cingulata). *Journal of Morphology* **267**:1273-1283.

Vickaryous M. K. and Hall B. K. (2008) Development of the dermal skeleton in *Alligator mississippiensis* (Archosauria, Crocodylia) with comments on the homology of osteoderms. *Journal of Morphology* **269**:398–422.

Vickaryous M. K. and Sire J-Y. (2009) The integumentary skeleton of tetrapods: origin, evolution, and development. *Journal of Anatomy* **214**:441–464.

Vickaryous M. K., Meldrum, G. and Russell, A. P. (2015) Armored geckos: a histological investigation of osteoderm development in *Tarentola* (Phyllodactylidae) and *Gekko* (Gekkonidae) with comments on their regeneration and inferred function. *Journal of Morphology* **276**:1345–1357.

Yang W., Chen, I. H., McKittrick, J. and Meyers, M. A. (2012) Flexible dermal armor in nature. *Journal of Morphology* **64**:475-485.

Zylberberg L. and Castanet J. (1985) New data on the structure and the growth of the osteoderms in the reptile *Anguis fragilis* (Anguidae, Squamata). *Journal of Morphology* **186**:327–342.

7.4   Peer-reviewed Publications

Kirby A., Vickaryous M., Boyde A., Olivo A., Moazen M., Bertazzo S. and Evans S.E. (2019) Osteoderms of *Heloderma suspectum*: a new nano-micro hierarchical biomineralised structure in vertebrates. *International Congresses of Vertebrate Morphology,* Poster Presentation. Prague.

Kirby A., Vickaryous M., Boyde A., Olivo A., Moazen M., Bertazzo S. and Evans S. (2020) A comparative histological study of the osteoderms in the lizards *Heloderma* suspectum (Squamata: Helodermatidae) and *Varanus komodoensis* (Squamata: Varanidae). *Journal of Anatomy* **236**:1035-1043.

Iacoviello F., Kirby A., Javanmardi Y., Moeendarbary E., Shabanli M., Tsolaki E., Sharp A. C., Hayes M. J., Keevend K., Li J. H., Brett D. J., Shearing P. R., Olivo A., Herrmann I. K., Evans S. E., Moazen M. and Bertazzo S. (2020) The multiscale hierarchical structure of *Heloderma suspectum* osteoderms and their mechanical properties. *Acta Biomaterialia* **107**:194-203.

Loaiza S., Ferreira S. A., Chinn T. M., Kirby A., Tsolaki E., Dondi C., Parzych K., Strange A. P., Bozec L., Bertazzo S., Hedegaard M. A. B., Gentleman E. and Auner H. W. (2018) An engineered, quantifiable in vitro model for analysing the effect of proteostasis-targeting drugs on tissue physical properties. *Biomaterials* **183**:102-113.